SSC-353

ANALYSIS OF WAVE CHARACTERISTICS IN EXTREME SEAS

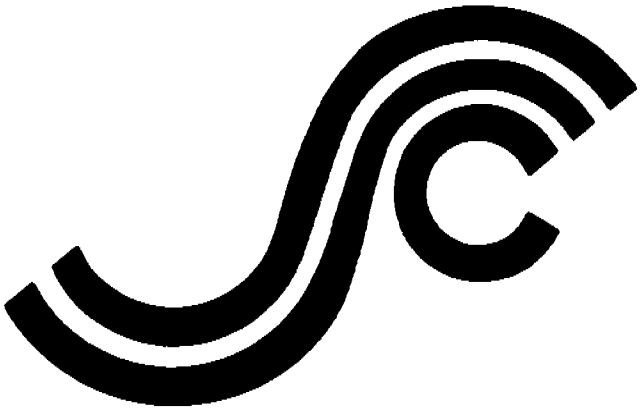

SHIP STRUCTURE COMMITTEE

1991

SHIP STRUCTURE COMMITTEE

The SHIP STRUCTURE COMMITTEE is constituted to prosecute a research program to improve the hull structures of ships and other marine structures by an extension of knowledge pertaining to design, materials, and methods of construction.

RADM J. D. Sipes, USCG, (Chairman)
Chief, Office of Marine Safety, Security and Environmental Protection
U. S. Coast Guard

Mr. Alexander Malakhoff
Director, Structural Integrity Subgroup (SEA 55Y)
Naval Sea Systems Command

Dr. Donald Liu
Senior Vice President
American Bureau of Shipping

Mr. H. T. Haller
Associate Administrator for Ship–building and Ship Operations
Maritime Administration

Mr. Thomas W. Allen
Engineering Officer (N7)
Military Sealift Command

CDR Michael K. Parmelee, USCG,
Secretary, Ship Structure Committee
U. S. Coast Guard

CONTRACTING OFFICER TECHNICAL REPRESENTATIVES

Mr. William J. Siekierka
SEA 55Y3
Naval Sea Systems Command

Mr. Greg D. Woods
SEA 55Y3
Naval Sea Systems Command

SHIP STRUCTURE SUBCOMMITTEE

The SHIP STRUCTURE SUBCOMMITTEE acts for the Ship Structure Committee on technical matters by providing technical coordination for determinating the goals and objectives of the program and by evaluating and interpreting the results in terms of structural design, construction, and operation.

AMERICAN BUREAU OF SHIPPING

Mr. Stephen G. Arntson (Chairman)
Mr. John F. Conlon
Dr. John S. Spencer
Mr. Glenn M. Ashe

MILITARY SEALIFT COMMAND

Mr. Albert J. Attermeyer
Mr. Michael W. Touma
Mr. Jeffery E. Beach

MARITIME ADMINISTRATION

Mr. Frederick Seibold
Mr. Norman O. Hammer
Mr. Chao H. Lin
Dr. Walter M. Maclean

NAVAL SEA SYSTEMS COMMAND

Mr. Robert A. Sielski
Mr. Charles L. Null
Mr. W. Thomas Packard
Mr. Allen H. Engle

U. S. COAST GUARD

CAPT T. E. Thompson
CAPT Donald S. Jensen
CDR Mark E. Noll

SHIP STRUCTURE SUBCOMMITTEE LIAISON MEMBERS

U. S. COAST GUARD ACADEMY

LT Bruce Mustain

U. S. MERCHANT MARINE ACADEMY

Dr. C. B. Kim

U. S. NAVAL ACADEMY

Dr. Ramswar Bhattacharyya

STATE UNIVERSITY OF NEW YORK MARITIME COLLEGE

Dr. W. R. Porter

WELDING RESEARCH COUNCIL

Dr. Martin Prager

NATIONAL ACADEMY OF SCIENCES – MARINE BOARD

Mr. Alexander B. Stavovy

NATIONAL ACADEMY OF SCIENCES – COMMITTEE ON MARINE STRUCTURES

Mr. Stanley G. Stiansen

SOCIETY OF NAVAL ARCHITECTS AND MARINE ENGINEERS – HYDRODYNAMICS COMMITTEE

Dr. William Sandberg

AMERICAN IRON AND STEEL INSTITUTE

Mr. Alexander D. Wilson

Member Agencies:

United States Coast Guard
Naval Sea Systems Command
Maritime Administration
American Bureau of Shipping
Military Sealift Command

Ship Structure Committee

An Interagency Advisory Committee
Dedicated to the Improvement of Marine Structures

Address Correspondence to:

Secretary, Ship Structure Committee
U.S. Coast Guard (G-MTH)
2100 Second Street S.W.
Washington, D.C. 20593-0001
PH: (202) 267-0003
FAX: (202) 267-0025

SSC-353
SR-1309

January 31, 1991

ANALYSIS OF WAVE CHARACTERISTICS IN EXTREME SEAS

It is important that we have the ability to characterize and model the nonlinear wave forms of extreme seas as we continue to develop advanced ship designs. This report presents the method used to analyze nonlinear time series data and includes results from towing tank experiments where nonlinear extreme wave spectra were replicated. This information should prove to be quite useful in assessing loads imposed on hull structures.

J. D. SIPES
Rear Admiral, U.S. Coast Guard
Chairman, Ship Structure Committee

Technical Report Documentation Page

1. Report No.	2. Government Accession No.	3. Recipient's Catalog No.
SSC-353		

4. Title and Subtitle	5. Report Date
Analysis of Wave Characteristics in Extreme Seas	AUGUST 1989
	6. Performing Organization Code
	8. Performing Organization Report No. SR-1309
7. Author(s) William H. Buckley	
9. Performing Organization Name and Address DAVID TAYLOR RESEARCH CENTER Code 1730.6 Bethesda, MD 20048-5000	10. Work Unit No. (TRAIS) 11. Contract or Grant No. DTCG23-87-F-10030
12. Sponsoring Agency Name and Address Commandant U.S. Coast Guard 2100 Second Street, SW Washington, DC 20593	13. Type of Report and Period Covered Final Report 14. Sponsoring Agency Code G-M

15. Supplementary Notes

Sponsored by the Ship Structure Committee and its member agencies.

16. Abstract

The results from three studies concerning identification and characterization of extreme waves in storm driven seaways are presented. Methods and results using time series wave height data from hurricane Camille are illustrated. Task 1 demonstrated the utility of the half-cycle matrix (HACYM) method in analyzing nonlinear time series data. Task 2 involved wave making experiments where the Camille nonlinear wave spectrum was replicated. Task 3, using second order wave-wave interaction theory, provided a nonlinear time domain wave height model conforming to the Camille nonlinear wave spectrum. In Task 1, the HACYM analysis of input and output realizations from Dalzell's nonlinear simulation model showed that this analysis method provides a clear indication of the nonlinearity of a time series random variable. In Task 2, the nonlinearity of waves generated in two different towing tanks approached that of the original Camille seaway when the wave spectrum was approximated by mechanically generated waves. In Task 3, while numerically modeled hurricane Camille time series waves showed somewhat less nonlinearity than the original time series data, the flattening of wave troughs and elevations of crests due to nonlinear wave-wave interaction was realistic.

17. Key Words	18. Distribution Statement
Wave Characteristics Extreme Seas Nonlinear Wave Spectrum Wave Modeling Half-Cycle Matrix Method	Available from: Nat'l Technical Information Service Springfield, VA 22161 or Marine Tech. Information Facility National Maritime Research Center Kings Point, NY 10024-1699

19. Security Classif. (of this report)	20. Security Classif. (of this page)	21. No. of Pages	22. Price
Unclassified	Unclassified		

Form DOT F 1700.7 (8-72) Reproduction of completed page authorized

METRIC CONVERSION FACTORS

Approximate Conversions to Metric Measures

Symbol	When You Know	Multiply by	To Find	Symbol
	LENGTH			
in	inches	*2.5	centimeters	cm
ft	feet	30	centimeters	cm
yd	yards	0.9	meters	m
mi	miles	1.6	kilometers	km
	AREA			
in^2	square inches	6.5	square centimeters	cm^2
ft^2	square feet	0.09	square meters	m^2
yd^2	square yards	0.8	square meters	m^2
mi^2	square miles	2.6	square kilometers	km^2
	acres	0.4	hectares	ha
	MASS (weight)			
oz	ounces	28	grams	g
lb	pounds	0.45	kilograms	kg
	short tons (2000 lb)	0.9	tonnes	t
	VOLUME			
tsp	teaspoons	5	milliliters	ml
Tbsp	tablespoons	15	milliliters	ml
fl oz	fluid ounces	30	milliliters	ml
c	cups	0.24	liters	l
pt	pints	0.47	liters	l
qt	quarts	0.95	liters	l
gal	gallons	3.8	liters	l
ft^3	cubic feet	0.03	cubic meters	m^3
yd^3	cubic yards	0.76	cubic meters	m^3
	TEMPERATURE (exact)			
°F	Fahrenheit temperature	5/9 (after subtracting 32)	Celsius temperature	°C

*1 in = 2.54 (exactly). For other exact conversions and more detailed tables, see NBS Misc. Publ. 286, Units of Weights and Measures, Price $2.25, SD Catalog No. C13.10:286.

Approximate Conversions from Metric Measures

Symbol	When You Know	Multiply by	To Find	Symbol
	LENGTH			
mm	millimeters	0.04	inches	in
cm	centimeters	0.4	inches	in
m	meters	3.3	feet	ft
m	meters	1.1	yards	yd
km	kilometers	0.6	miles	mi
	AREA			
cm^2	square centimeters	0.16	square inches	in^2
m^2	square meters	1.2	square yards	yd^2
km^2	square kilometers	0.4	square miles	mi^2
ha	hectares (10,000 m^2)	2.5	acres	
	MASS (weight)			
g	grams	0.035	ounces	oz
kg	kilograms	2.2	pounds	lb
t	tonnes (1000 kg)	1.1	short tons	
	VOLUME			
ml	milliliters	0.03	fluid ounces	fl oz
l	liters	2.1	pints	pt
l	liters	1.06	quarts	qt
l	liters	0.26	gallons	gal
m^3	cubic meters	35	cubic feet	ft^3
m^3	cubic meters	1.3	cubic yards	yd^3
	TEMPERATURE (exact)			
°C	Celsius temperature	9/5 (then add 32)	Fahrenheit temperature	°F

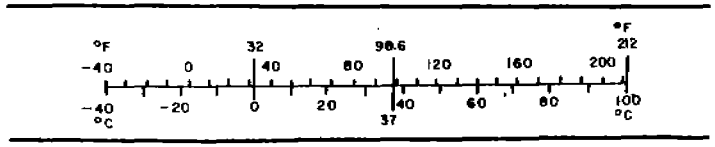

TABLE OF CONTENTS

LIST OF FIGURES

LIST OF FIGURES (CONTINUED)

LIST OF TABLES

NOTATION

e/a, elevation amplitude ratio defined as the mean value of a wave height half-cycle event divided by its amplitude; generally trough to peak.

fp, frequency at peak of a unimodal wave height spectrum.

Hm_0, significant wave height = $4[m_0]^{\frac{1}{2}}$.

Hmax, maximum trough to peak or peak to trough wave height in a particular realization.

Hd, trough to peak wave height.

H/L, ratio of wave height to length.

(L+Q), sum of linear and quadratic constituents in Dalzell's simulation.

(L+Q+C), sum of linear, quadratic and cubic constituents.

$S(f)$, wave spectrum energy density at frequency f.

T_{hd} , time duration of a trough to peak wave height event.

T_p , modal period corresponding to fp.

X(t), time series realization of Dalzell's input wave spectrum.

Y1(t), linear constituent of time series response in Dalzell's simulation.

Y2(t), quadratic constituent of time series response.

Y3(t), cubic constituent of time series response.

Y(t), sum of Y1(t) + Y2(t) + Y3(t).

ϵ, spectrum bandwidth parameter, $\left[\frac{m_0 m_4 - m_2}{m_0 m_4}\right]^{\frac{1}{2}}$

where $m_0 = \int_0^\infty S(f)\, df$

$m_4 = \int_0^\infty S(f)\, f^4\, df$

σ, standard deviation

σ_x = input excitation employed in Dalzell's simulation.

ABBREVIATIONS

AOC, Arctec offshore Corporation, Escondido, Calif.

DL, Davidson Laboratory of Stevens Institute of Technology, Hoboken, N.J.

DTRC, David Taylor Research Center, Bethesda, MD.

HACYM, half-cycle matrix; used to analyze successive peak/trough statistics of stochastic data.

MVDAE, mean value distribution of amplitude events in a HACYM.

ZUC, zero up-crossing method of analyzing trough to peak wave height events in time series data.

1.0 INTRODUCTION

The purpose of this study is best described by the prospectus from which it originated:

> "The present methods of simulating waves in the test tank and on the computer are based on the sea surface being normally distributed. In addition, linear structural analysis schemes are well suited to such wave input information inasmuch as the output is in the same Gaussian terms. These facts mean that extensive experimental understanding, computer software, and analytical competence exist in the profession in the use of Gaussian descriptions of the wave phenomena. On the other hand, there is evidence from the report SSC-320*[1], and other sources, that extreme waves exist and that their occurrence and characteristics may not be predicted by the Gaussian simulations. Of even greater importance is the evidence that these extreme waves produce significant damage to vessels.
>
> The design of fixed offshore structures already considers extreme waves having such nonlinear characteristics as elevated crests and nonlinear drag forces. If substantiated, these critical concerns can warrant extensive changes in design and simulation procedures.
>
> Recommendation
>
> Pursue the analysis of wave characteristics in extreme seas
>
> o Developing further the techniques for identifying the special characteristics of extreme waves from storm records, and
>
> o Developing alternative statistical or deterministic wave treatments which can be utilized expediently in testing, simulation, and analysis schemes."

With regard to the first recommendation, the half-cycle matrix (HACYM) method of time series data analysis was believed to be a suitable technique for the stated purpose. However, the relationship between the nonlinearity of the wave height variable and the distribution of peak-tough events in a half cycle matrix needed to be clearly identified to demonstrate its value in analyzing random field and test tank wave data. The second recommendation was believed to be appropriately addressed by assessing the existing state-of-the art of random wave generation in test tanks and computer simulations. In this regard development initiatives were deferred until the capabilities of existing methods could be assessed. Based upon this interpretation of the two recommendations contained in the prospectus, the following specific tasks were established:

1. Conduct a Half-Cycle Analysis of a Random Nonlinear Response Variable.

---

* A complete listing of references is given on page 71.

As discussed below this was accomplished using the results of an existing nonlinear simulation.

2. Compare Test Tank and Full-Scale Wave Characteristics for a Seaway of Limiting Steepness.

This comparison would employ a wave height spectrum derived from hurricane Camille time series data which gave evidence of substantial nonlinearity.

3. Investigate Computer Modeling of a Nonlinear, Random Seaway.

The third task was to be accomplished using a second order functional polynomial model where the quadratic term was derived from a second order Stokes expansion for progressive gravity waves. The combined linear plus quadratic constituents would be required to model the Camille wave spectrum of Task 2.

This report presents the results of each task in individual sections which contain both the immediate results and a discussion of them. Two additional sections are presented, one of which presents a re-analysis of hurricane Camille wave data in a HACYM format that evolved from Task 1 and a second which overviews the results of the three basic tasks so as to identify follow-on initiatives to this project.

Appendix A of the report outlines the basic methodology of half-cycle matrix analysis while Appendix B contains a synopsis of the nonlinear simulation whose time series realizations were analyzed in Task 1. Appendices C and D summarize test tank wave making procedures and resulting wave spectra associated with Task 2. Appendix E contains the mathematical development of the nonlinear wave simulation associated with Task 3.

2.0 BACKGROUND

The conduct of this study has been strongly influenced by developments associated on the one hand with the mechanics of HACYM Analysis and on the other with characteristics of extreme waves. As a result, certain aspects of these two subjects are reviewed before proceeding.

HACYM Analysis

The half-cycle matrix (HACYM) method of time series data analysis is used extensively in this report because of its ability to identify nonlinear behavior. The mechanics of the method and certain of its inherent characteristics are summarized in Appendix A. Those particular statistical summaries which have been utilized in this study are identified in Figure 1. The example HACYM distribution of events shown in Figure 1(a) is a normalized analysis of the input linear, Gaussian time series employed in the simulation of Task 1.*

*The summation of up-going half-cycle events (i.e. events to the right of the null diagonal) differs from the corresponding sum of down-going events due to the use of a dead band corresponding to ±10% of the bin width, or ±0.05σ in this case. See Appendix A.

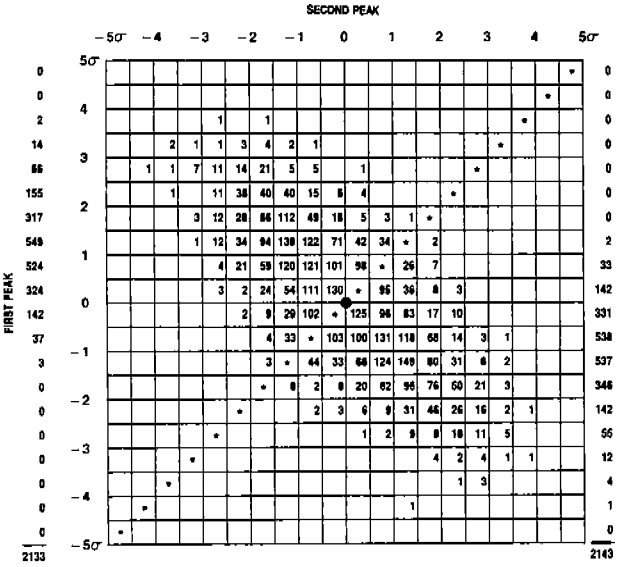

Fig. 1a. HACYM distribution (± 5σ, zero mean).

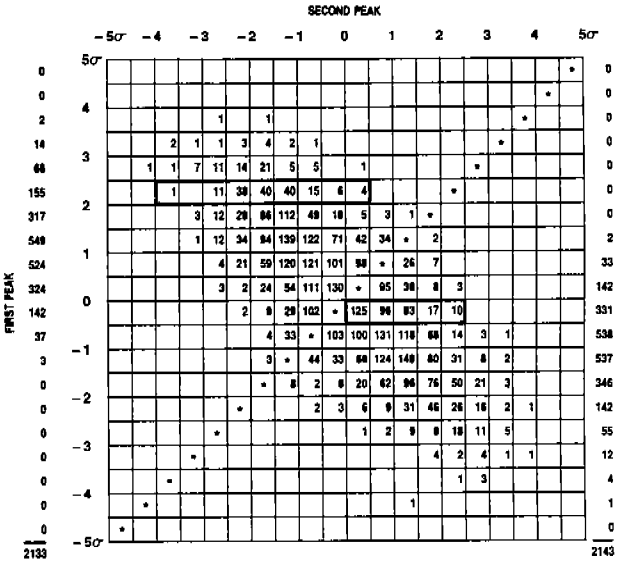

Fig. 1b. Marginal distributions (maxima & minima).

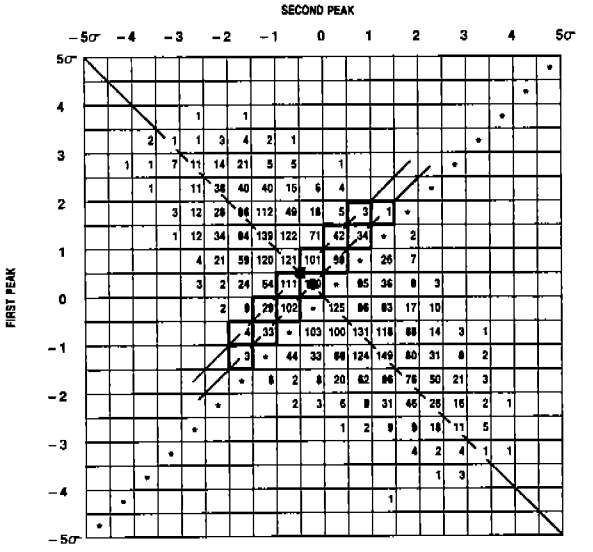

Fig. 1c. Mean values of diagonal distributions.

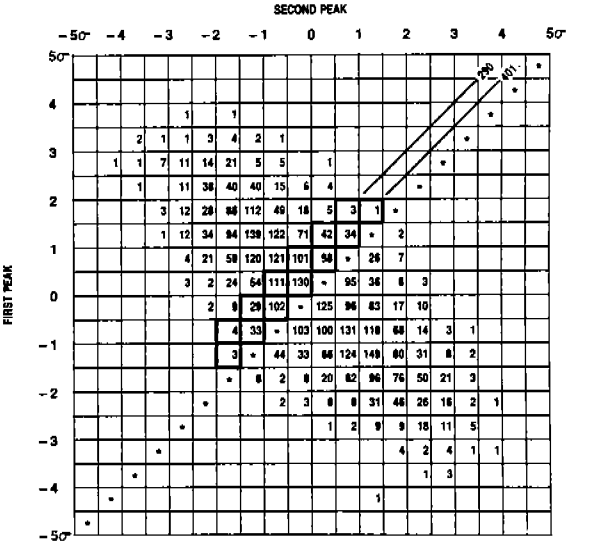

Fig. 1d. Diagonal distributions (amplitude events).

Fig. 1. Formation of Statistics Associated With HACYM Distributions.

Figure 1(b) depicts the summation of upward-going and downward-going half-cycle event sums to obtain the distribution of maxima and minima of the time series. Inasmuch as the first peaks of up-going events are minima, the summation of rows to the right of the null diagonal (i.e., the marginal distribution) leads to the percentage occurrence of minima for the associated class intervals.

In the highlighted row, 331 out of a total of 2143 events had negative peaks in the interval 0 to - 0.5σ (standard deviation). The summation of the highlighted row of first peaks of downward-going half cycle events shows that 155 out of a total of 2133 events had positive peaks in the interval 2σ to 2.5σ. The density distributions of maxima and minima presented in this study are also used as checks on the reprocessing of Dalzell's original nonlinear computer realizations, i.e., the measured density distributions of maxima and minima previously obtained by Dalzell should be found to be the same as those obtained from the HACYM Analysis. (The statistics of maxima and minima are also used in demonstrating that the analysis of only positive or only negative wave height peaks to investigate conformance to a Rayleigh distribution is inappropriate if the process itself is nonlinear (see Section 3.0)).

The statistics of Figures 1(c) and (d) are unique to HACYM Analysis. It is important to note (as explained in Appendix A) that the location of a half-cycle event with respect to the diagonals of the HACYM is a measure of the mean value and amplitude of a half-cycle event. The statistic identified in Figure 1(c) is the mean value of the distribution of half-cycle events along individual diagonals. As shown in each of the highlighted diagonals, the mean value is plotted at right angles to the reference level diagonal, i.e., the diagonal running from the upper left to lower right corner of the HACYM. In this instance the mean values are close to zero and hence fall on the diagonal. The curve formed by interconnecting the mean values is called the mean value distribution of amplitude events or MVDAE. This particular distribution is unique to the present study since it has not previously been formed. The plots of MVDAE which follow are drawn as dashed lines whenever one of the average values being interconnected is estimated from less than 5 half-cycle events, otherwise a solid line is shown.

The statistics used to define the estimated probability density distribution of amplitude events are formed by summing the number of events along each diagonal. In Figure 1(d) the highlighted data come from down-going half-cycle events. Because there are twice as many diagonal as row or column sums (actually 38 vs 20), the event totals for adjacent diagonals are added together to maintain the same class interval resolution as the marginal distributions. For the highlighted diagonals, a total of 691 events had amplitudes between 0 and 0.5σ out of a total of 2133 downward-going half-cycle events.

The probability distribution curves which are shown in subsequent figures are plotted as percentages of the total number of events per unit of the class interval employed. If the ordinate is percent per σ (in normalized format) the density is 1/100 times the value shown or alternatively if the ordinate is percent per 0.5σ the density is 2/100 times the value shown since in either case the unit of the abscissa is σ. With this transformation, the area under the plotted distribution curve should, of course, be close to unity.

The HACYM is also used here to select time series segments of data (or computer generated realizations) which correspond to extreme, or outlying amplitude events. The rationale for isolating and examining such events stems from the presumption that these events are most likely to exhibit the influence of nonlinearity in the associated process and further that continuous time series data are most appropriate for purposes of characterizing nonlinear behavior although certain parametric characterizations can also be useful.

A second methodology employed in this study is computer implemented Monte Carlo simulations whereby a statistical experiment is conducted under specified ground rules. The complexity of closed-form analysis of the expectation of half-cycle events in a HACYM has thus far precluded its determination for a random process having an arbitrary variance spectrum. One exception to this generalization applies to the linear, Gaussian, narrow-band process as discussed in Appendix A. In the absence of a general capability, recourse has been made to Monte Carlo methods which obviously do not have the generality of a closed-form solution. On the other hand because of its experimental nature the Monte Carlo method provides the scatter of events beyond expectation which in an investigation on nonlinear random processes can be useful, e.g., Buckley, et al[2]. A third element of methodology which is of basic importance to this study is the use of functional polynomials in the characterization of nonlinear random processes. The case for their use has previously stated by Dalzell[3]:

> "In general, when non-linear responses become of importance there is no agreed universal model for dealing with the irregular sea case. However, when the non-linearities may be considered 'weak' in some sense one of the conceptual approaches which have been proposed has considerable attraction. This is the functional series model. Among the attractions are that the model is suitable for any reasonably well-behaved wave input (regular, transient or random) and since the model contains the completely linear system as a special case it appears to be a logical extension of present practice. In addition, prediction methods for scalar response spectra are available and it appears that the statistics of maxima may be approximated. Finally, it is possible to closely relate the functions required by the model to deterministic hydromechanical analyses and experiment because the effects of hydrodynamic 'memory' which complicate the usual analysis are automatically accounted for."

With respect to the basic concepts of this methology, Chapter 4 of Marmarelis and Marmarelis[4] provides an excellent exposition except that a generic wave spectrum has been used here for input excitation because the physical significance of the nonlinear output is more apparent. An additional matter that should be noted (which is not particular to methodology) is that response of a nonlinear system is a nonlinear function of the excitation level. Characterization of system output in HACYM format necessarily suggests evaluation at more than one level of excitation.

Extreme Waves

As noted in the Introduction, concern for the existence of extreme waves is basic to the origin of this study and it is thus important that the types of extreme waves considered here be identified. Table 1 is an updated version of Table 2 of Buckley[1]. The designation "non-Gaussian" refers to large waves which would not be realized by the linear transformation of a scalar spectrum back to the time domain assuming the process to be Gaussian. Nonlinearity of the wave height process is implicit. The designation "episodic" here refers to the fact that most of these waves have been identified by visual means and that they clearly stood apart in appearance from the majority of the large waves in the seaway. Such waves could well be non-Gaussian and/or nonlinear, but the current lack of time series wave height measurements precludes such a categorization. Of immediate importance is the fact that this state of affairs also precludes their consideration in this study. It is only the non-Gaussian waves of hurricane Camille for which continuous time series measurements of wave height are available so that the nonlinear quality of the waves could be analyzed here in Section 4.0 and also used to investigate physical and numerical modeling in Sections 5.0 and 6.0.

Figure 2 is presented to help relate the hurricane Camille wave data used here to an empirically derived envelope of extreme combinations of measured significant wave heights (Hm_o) and modal frequencies (f_p), see Buckley[5]. The right hand boundary and circled datum of the crosshatched area were derived as explained in the reference while the dashed boundary shown here is entirely schematic. The diamond datum corresponds to the 1500-1530 hr. time interval when the Camille seaway was highly nonlinear. The associated wave energy spectrum has been employed in the test tank and computer simulations of this study.

3.0 HALF-CYCLE ANALYSIS OF A RANDOM NONLINEAR RESPONSE VARIABLE.

Although previous analyses of hurricane Camille wave data[2] and unpublished analyses of certain ship motion and component strain data had strongly suggested that a skewed distribution of half-cycle events in a HACYM was the result of nonlinear behavior of the variable in question, an explicit evaluation of this characteristic has not previously been undertaken. The availability of the output data files of Dalzell's nonlinear computer simulation[3] made an ad hoc investigation of this characteristic relatively simple and it has been under-taken in this study for two input excitation levels.

Dalzell's general methodology, input seaway excitation and selection of nonlinear response functions are discussed in Appendix B.* With respect to the HACYM analyses presented here it is important to note that:

(a) The input excitation was a linear, Gaussian realization of a model scale Bretschneider wave spectrum.

*The symbol σ as used here in connection with Dalzell's simulation refers to excitation level. The symbol σ is used elsewhere to designate standard deviation.

Table 1. An Initial Characterization of Large Nonlinear and Episodic Waves (Rev. A).

Type	Characterization	Basis for Characterization
I. Nonlinear: short crested, breaking waves	• Steep and elevated above mean water level. Short crested. • Elevation/amplitude ratio ≈ 0.5 • Produced by strong, rapidly increasing winds	• Time-series wave data from Hurricane Camille and associated wind velocity increase. • Casualty cases associated with strong rapidly increasing winds: — *SEA-LAND MARKET* — *LPD-12* — *CHESTER A. POLING* — *F/V FAIR WIND*
II. Episodic Waves:		
a. Steep Long-crested Waves	• Recurring as every 7th or 9th large wave in a storm driven seaway containing waves at least 20 ft high	• Observations by officers from ocean weather ships.
b. Large Grouped Waves	• Group of three large waves in seaway. Second wave frequently largest in group. • Occur in storm winds which are no longer increasing, or which have begun to decrease.	• Waves encountered by CV-62, SEA-LAND McLEAN, LST-1193 • Observations by officers from ocean weather ships.
c. Episodic Wave Packets	• "Three Sisters": group of three long-period waves intruding into existing seaway at angles of about 30° from principal wave direction. Generally occur in vicinity of storm with central winds of 60 kn or more.	• Observations by officers from ocean weather ships as well as ship masters of considerable at-sea experience
	• "Rogue" Wave: large breaking wave intruding into existing seaway at angles up to 50° from principal wave direction. Likely to occur in vicinity of upper altitude "TROF" as it overtakes an existing or developing low. High altitude comma shaped cloud usually associated with TROF.	• Rogue Wave encouters by U.S. *NAVY FRIGATE, CHU FUJINO, MUNCHEN*, and associated synoptic weather patterns.

Note: These characterizations do not necessarily apply to waves in Agulhas current (S.E. Coast of Africa).

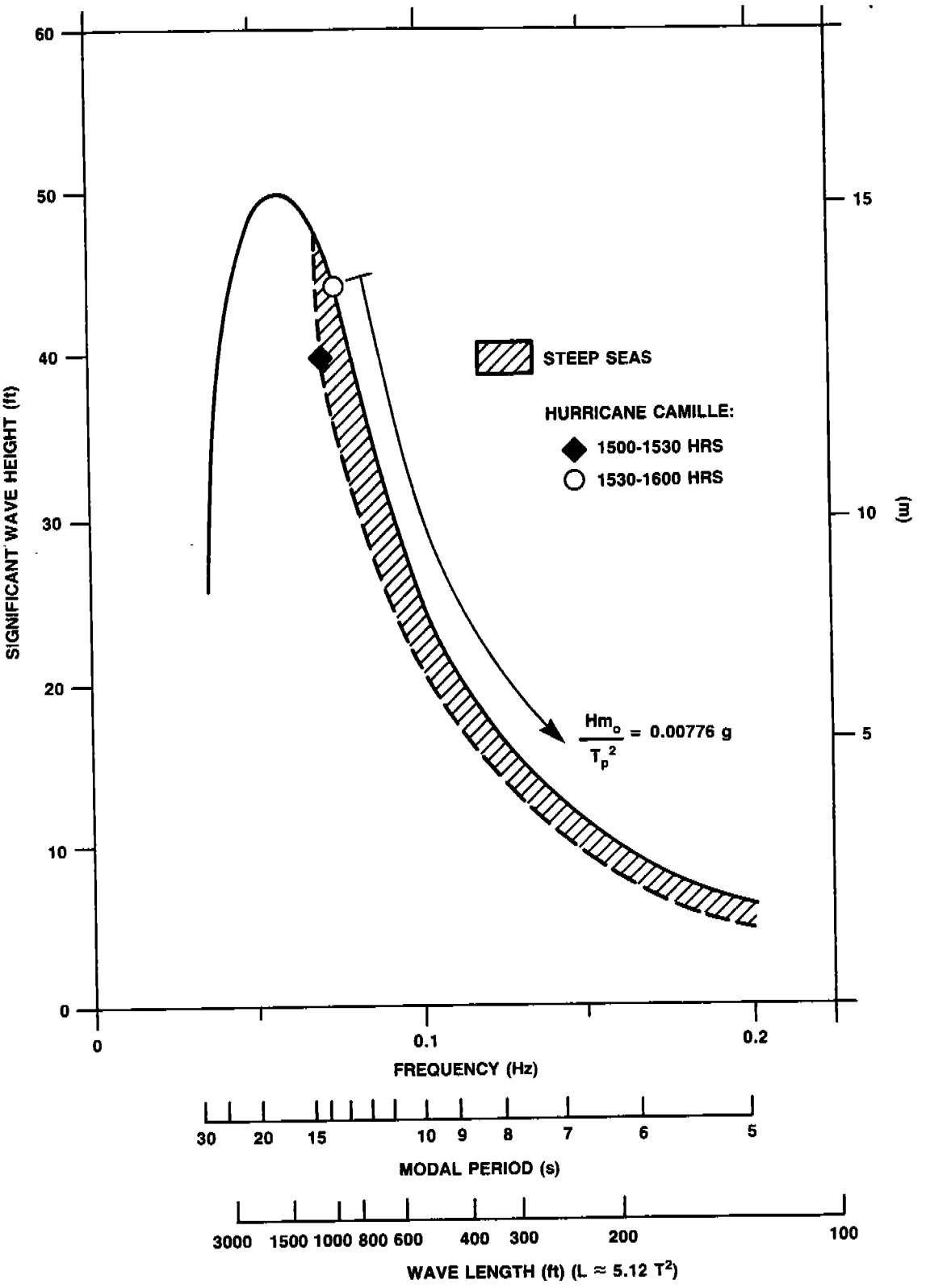

Fig. 2. Maximum Measured Significant Wave Heights vs Frequency Corresponding to Modal Frequency (from Reference 5).

(b) From among the various nonlinear output realizations, only those corresponding to $\sigma_x = 0.25$ (base line input) and $\sigma_x = 1.0$ (maximum input) wave spectra have been analyzed. While the significant wave height was increased by a factor of four, the modal frequency remained fixed at 1 hz.

(c) As discussed in Appendix B, the nonlinear response at all excitation levels beyond the baseline case are available by linear superposition of the factored time domain constituent outputs, i.e., C (Linear) $+C^2$ (Quadratic) $+C^3$ (Cubic) = Total response (L+Q+C) where for the baseline case ($\sigma_x = 0.25$) C = 1.0.

(d) In view of this homogeneity property, the constituent outputs were first analyzed separately in normalized HACYM format and then in combination, with the linear plus quadratic case (L+Q) being omitted in favor of the combined case (L+Q+C) at $\sigma_x = 0.25$ because the contribution of the cubic constituent was relatively small. The first of 10 sample output realizations at this excitation level is shown in Figure 3. The first set of HACYM analyses corresponds to the combined outputs (i.e., 10 sample realizations combined) for X(t), Y1(t), Y2(t), Y3(t) and Y(t). Since all of these were normalized by their respective time series standard deviations (with zero mean) only the combined output Y(t) changed as a result of changing the excitation level. Figure 4 presents the constituent results for $\sigma_x = 1.0$ (Sample 1) wherein Y1(t) increased by a factor of 4.0, Y2(t) by 4.0^2 and Y3(t) by 4.0^3. It is evident that only the combined output Y(t) will produce a different time series and HACYM result in normalized format at $\sigma_x = 1.0$.

(e) At $\sigma_x = 1.0$, HACYM analyses of Y(t) are presented for both (L+Q) and (L+Q+C) cases since important differences now exist between these combined outputs.

Figure 5 summarizes the results of HACYM analysis of the linear, Gaussian (model-scale) seaway input. The range of the half-cycle matrix in Figure 5(a) was chosen as $\pm 5\sigma$, there being 2142 half-cycle events with positive slope and 2133 with negative slopes which crossed from one data bin level to another and did not lie entirely within the deadband of $\pm 0.05\sigma$. (See Appendix A). Since the number of half-cycle events uncounted for failure to cross class interval levels with an amplitude greater than 0.05σ is not necessarily the same for up-going and down-going events, these totals will not necessarily be the same. The percentage difference should of course be small for a large data sample, in this case $100 \times 9/2132 = 0.42\%$. The distribution curves of maxima and minima are asymmetric in shape but symmetric in relation to each other as one would expect from the results of Cartwright and Longuet-Higgins[7]. Their bandwidth parameter in this case is approximately ($\varepsilon = 0.6$), see Figure A-7 of Appendix A. The mean value distribution of amplitude events of Figure 5(c) is linear out to the point where less than 20 events are averaged. Relatively large excursions occur where less than 5 events are averaged (see dashed lines in plot). The shape which the distribution curve of amplitude events Figure 5(d) should take is not known but the relatively large number of events lying below = $\pm 1\sigma$ is believed related to the high frequency, low energy portion of the input wave spectrum.

The linear constituent of the response is analyzed in Figure 6 where both Figures 6(a) and 6(b) reflect the more narrow-band character of the response spectrum as shown in Figure 13 of Dalzell[3] and as implied by the time-series of

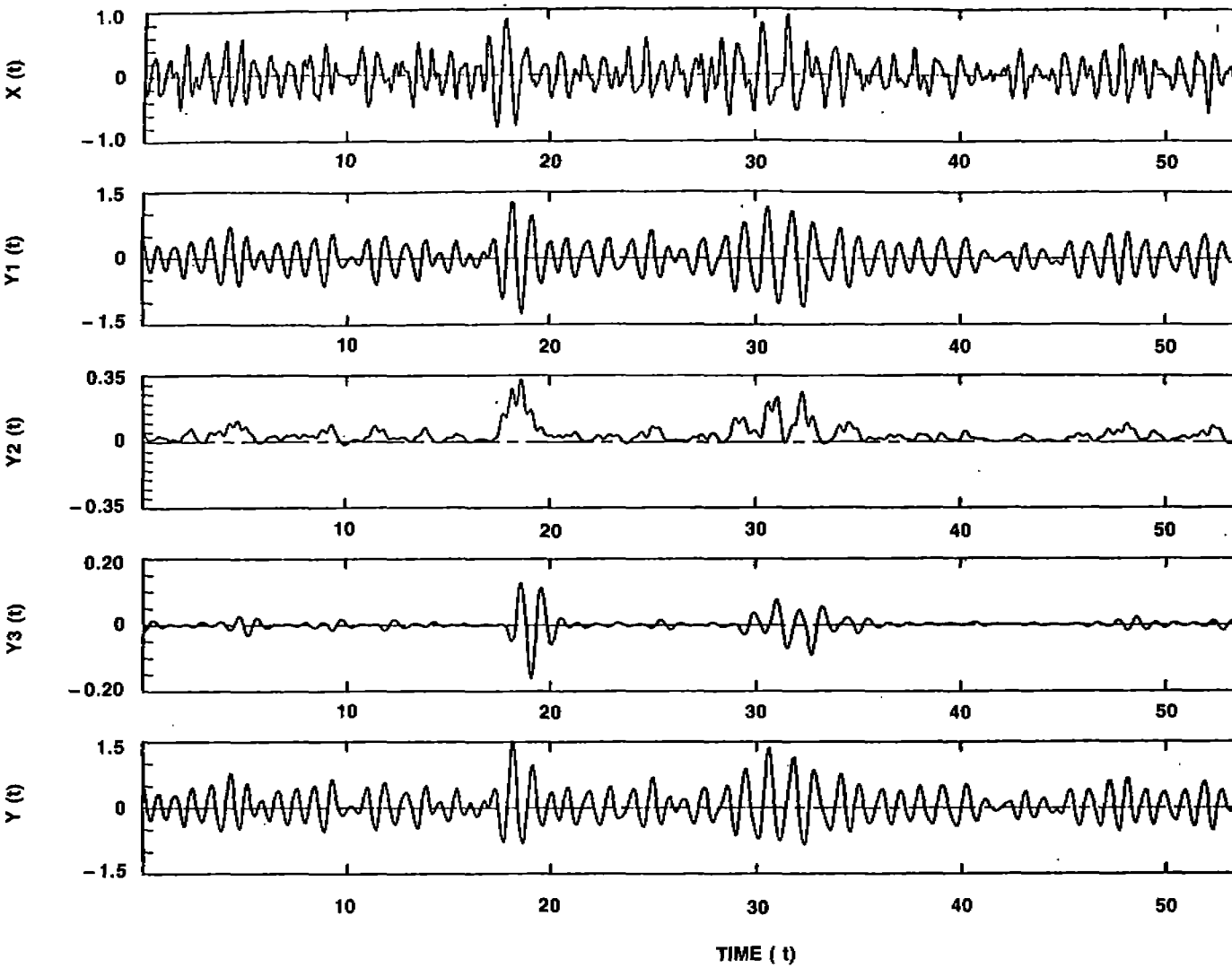

Fig. 3. Simulated Time Histories of Nonlinear Response to Random Excitation: Sample 1, σ_x =

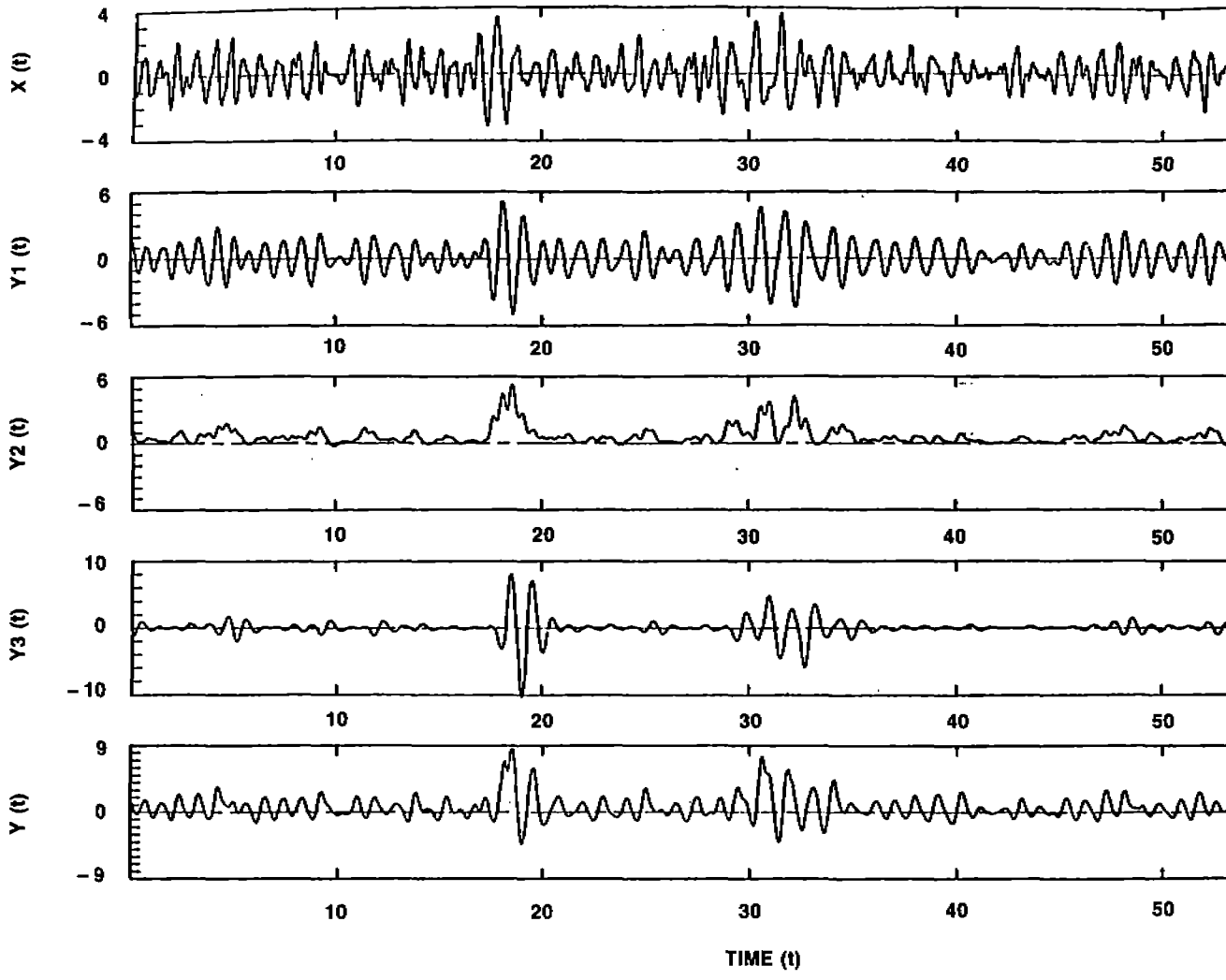

Fig. 4. Simulated Time Histories of Nonlinear Response to Random Excitation: Sample 1, σ_x

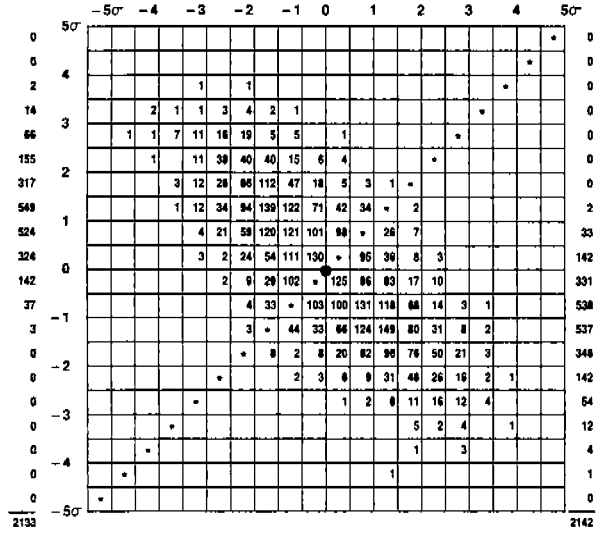

Fig. 5a. Half-cycle analysis of input time-series (± 5σ, zero mean, 10 samples combined).

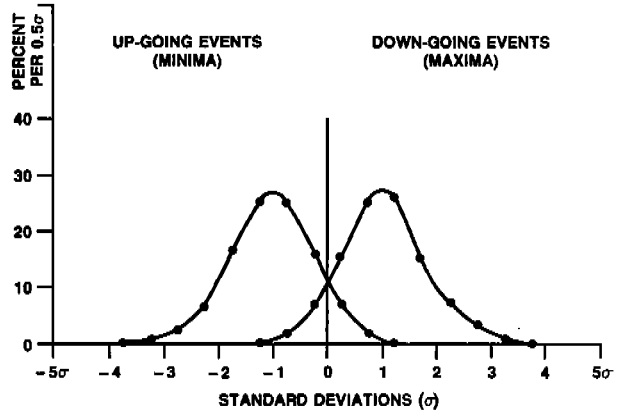

Fig. 5b. Probability density distribution of maxima and minima.

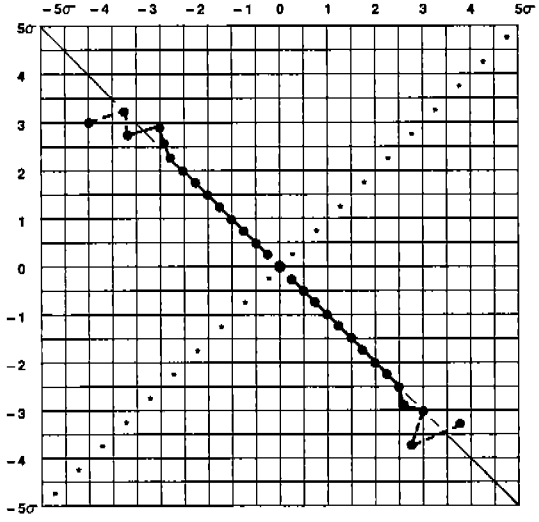

Fig. 5c. Mean value distribution of amplitude events.

[---DENOTES LESS THAN 5 EVENTS AVAILABLE TO DEFINE MEAN.]

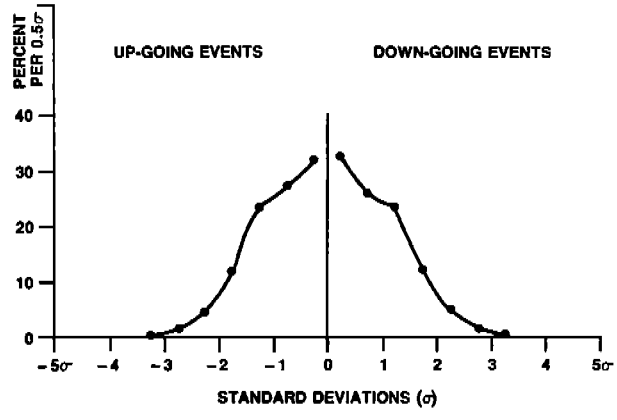

Fig. 5d. Probability density distribution of amplitude events.

Fig. 5. HACYM Analysis of Linear Gaussian Wave Input to Dalzell's Nonlinear Ship Response Simulation.

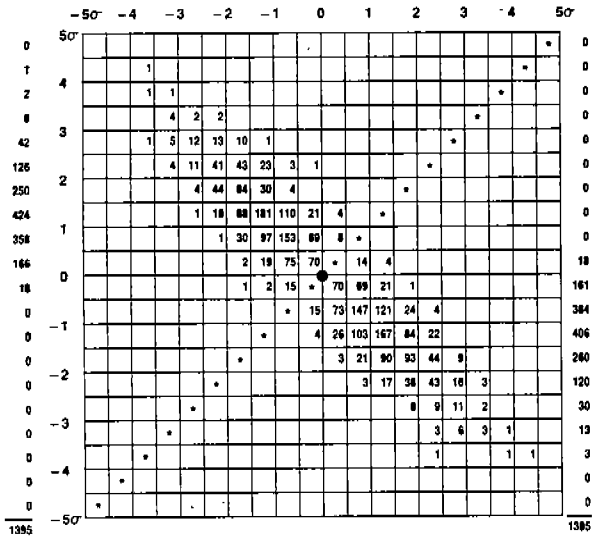

Fig. 6a. Half-cycle analysis of linear constituent of output (± 5σ, zero mean, 10 samples combined.

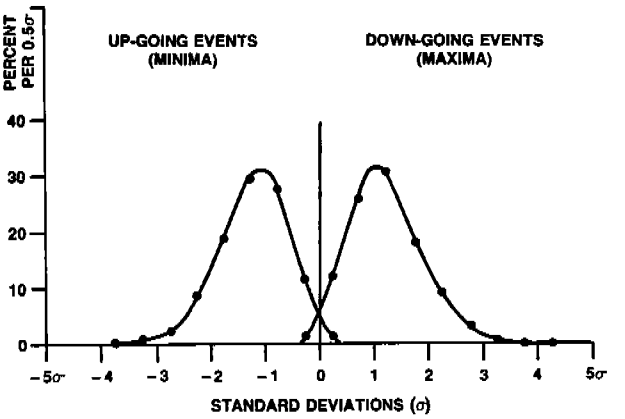

Fig. 6b. Probability density distribution of maxima and minima.

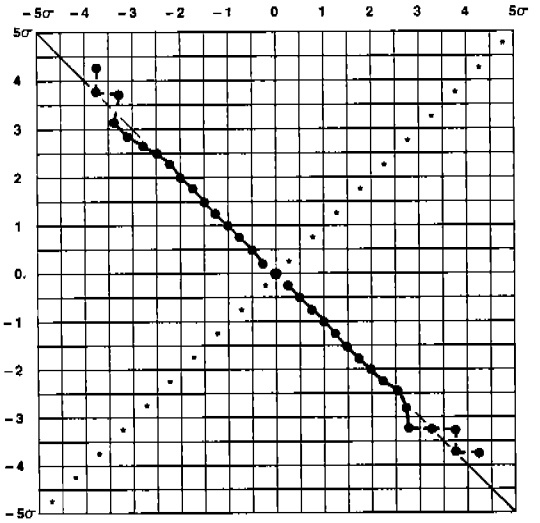

Fig. 6c. Mean value distribution of amplitude events.

[--- DENOTES LESS THAN 5 EVENTS AVAILABLE TO DEFINE MEAN.]

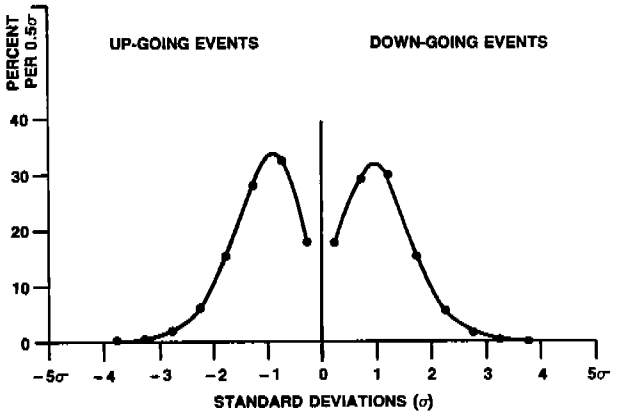

Fig. 6d. Probability density distribution of amplitude events.

Fig. 6. HACYM Analysis of Linear Constitutent of Output of Dalzell's Nonlinear Ship Response Simulation.

Figure 3. The bandwidth parameter inferred from the distribution curves of maxima and minima in 6(b) is approximately $\varepsilon = 0.2$ (where 0 would result in a Rayleigh distribution). Again the mean value distribution of amplitude events is linear out to a point where only about 20 events are averaged. In Figure 6(c) as in 5(c) the trend of the curve is still essentially linear over that part of the range in which sampling variability is an important factor. Roughly, the linear trend of the distribution curve is evident out to a point where about 5 events are being averaged even though the individual statistics are subject to appreciable variability. Beyond that point sampling variability is dominant. (It will be noted that this observation is made with respect to a random process which is effectively stationary). The shape of the amplitude distributioncurve of Figure 6(d) resembles that for the input variable above $\pm 1\sigma$. Below this value the distribution curves are quite different apparently due to virtual elimination of the high frequency portion of the wave spectrum by the filtering action of the relatively narrow-band response function (which incidentally peaks in this simulation at the modal frequency of the wave spectrum).

HACYM analysis of the quadratic constituent of the response is shown in Figure 7 while a sample of the original time-series variable is shown in Figure 3 as Y2(t). The half-cycle analysis of Figure 7(a) results in a highly skewed pattern of events and the need for a matrix range of = $\pm 10\sigma$ in contrast to the linear input and output variables of Figures 5 and 6. Figure 7(b) reveals that the distribution curves of maxima and minima are no longer symmetric with respect to one another and that the mean value distribution of amplitude events of 7(c) is highly nonlinear with only about half of the curve determined as the result of averaging more than 5 events. The distribution curves of amplitude events of 7(d) retain their symmetry about the null diagonal although the shape of the curves is unknown below 0.5σ. The requirement that the area under the probability density distribution curve be unity suggests that below 0.5σ the curves turn downward, but the local shape is unknown.

Figure 8 presents the results of HACYM analysis of the cubic constituent of the nonlinear response. The half-cycle analysis of Figure 8(a) reveals a generally symmetric distribution of half-cycle events in contrast to Figure 7(a) for the quadratic constituent. (Note that the scale of the matrix $\pm 10\sigma$ is the same in each case). The distributions of maxima and minima of Figure 8(b) are nearly symmetric reflecting the generally symmetric distribution of events in Figure 8(a). The mean value distribution of amplitude events of Figure 8(c) is essentially linear for the same reason. While the range of this curve is appreciably greater than that of Figure 7(c), it is apparent that here also a substantial proportion of the curve is defined by less than 5 events. This suggests that both constituents will tend to produce greater variability of the more extreme events in the composite time series and by implication more extreme values per se. (See also the time series samples of Figures 3 and 4, Y2(t) and Y3(t). One can reasonably anticipate that the extent to which this is true will be a strong function of the input excitation level and further that since the cubic constituent is increasing more rapidly than the quadratic by the value of C, its influence can become substantial depending upon the excitation level.

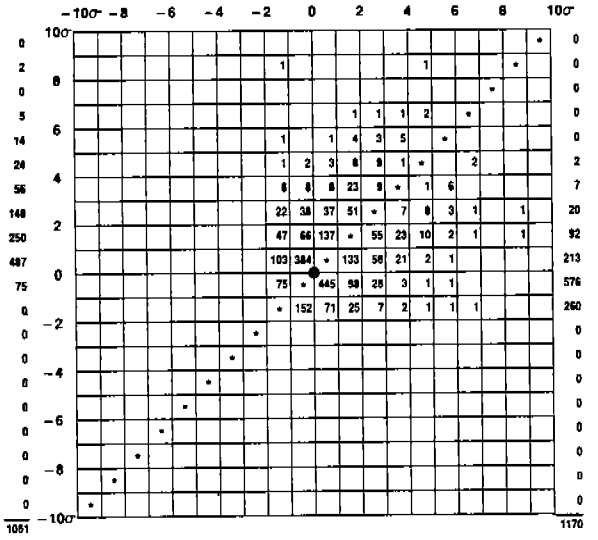

Fig. 7a. Half-cycle analysis of quadratic constituent of output (± 10σ, zero mean, 10 samples combined.

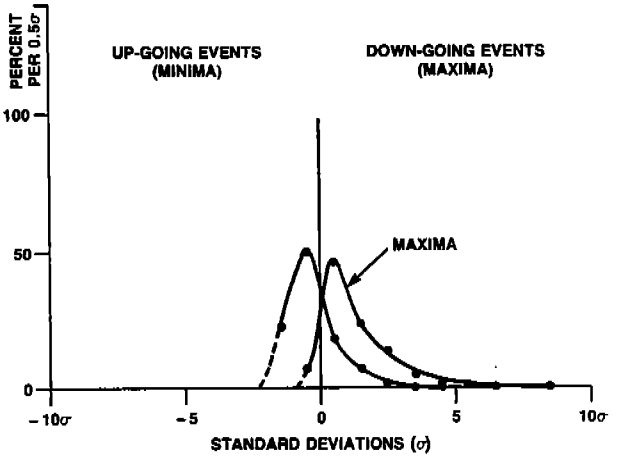

Fig. 7b. Probability density distribution of maxima and minima.

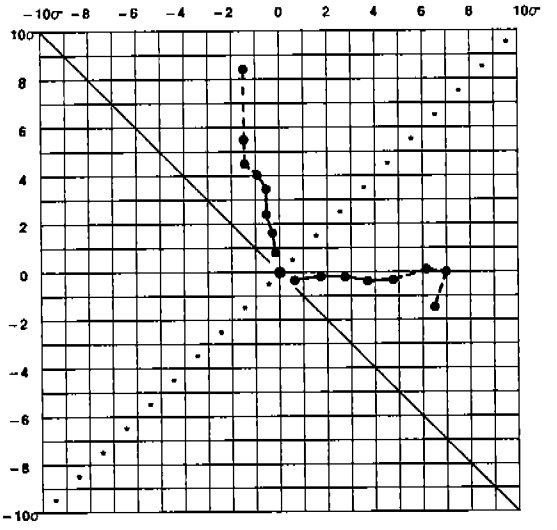

Fig. 7c. Mean value distribution of amplitude events.

[- - - DENOTES LESS THAN 5 EVENTS AVAILABLE TO DEFINE MEAN.]

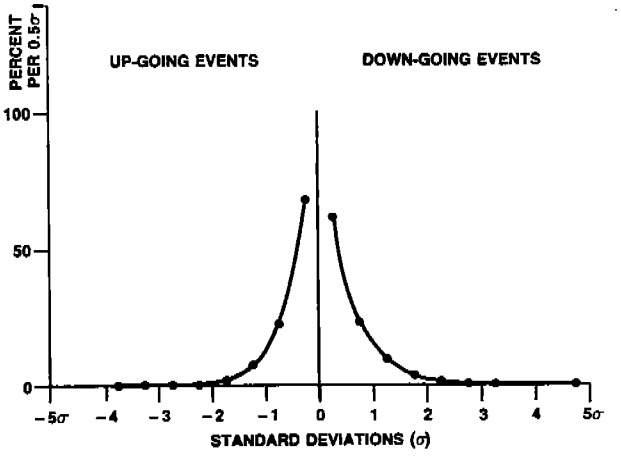

Fig. 7d. Probability density distribution of amplitude events.

Fig. 7. HACYM Analysis of Quadratic Constituent of Output of Dalzell's Nonlinear Response Simulation.

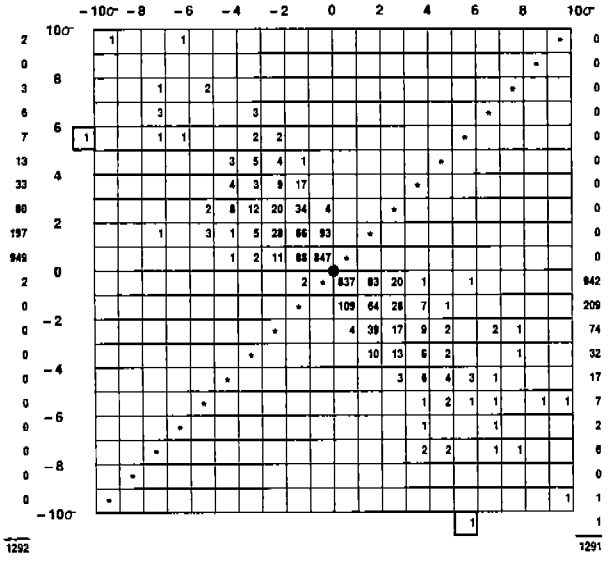

Fig. 8a. Half-cycle analysis of cubic constituent output (± 10σ, zero mean, 10 samples combined).

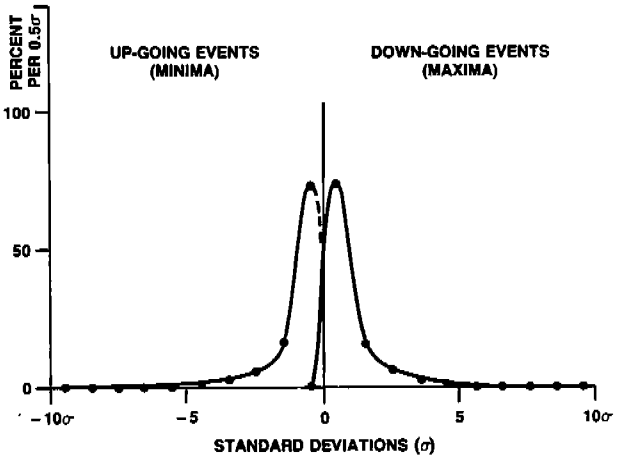

Fig. 8b. Probability density distribution of maxima and minima.

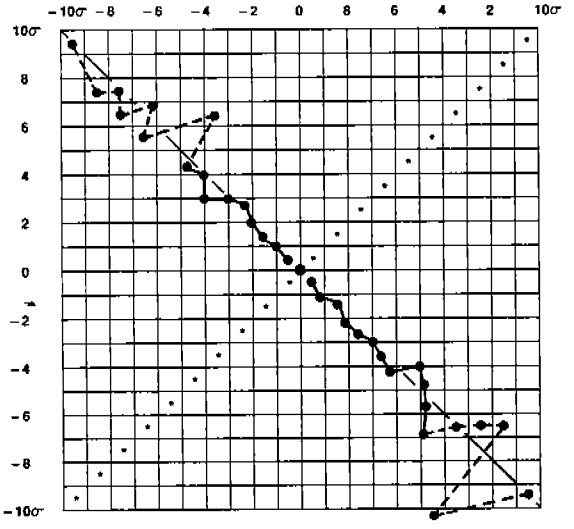

Fig. 8c. Mean value distribution of amplitude events.

[---DENOTES LESS THAN 5 EVENTS AVAILABLE TO DEFINE MEAN.]

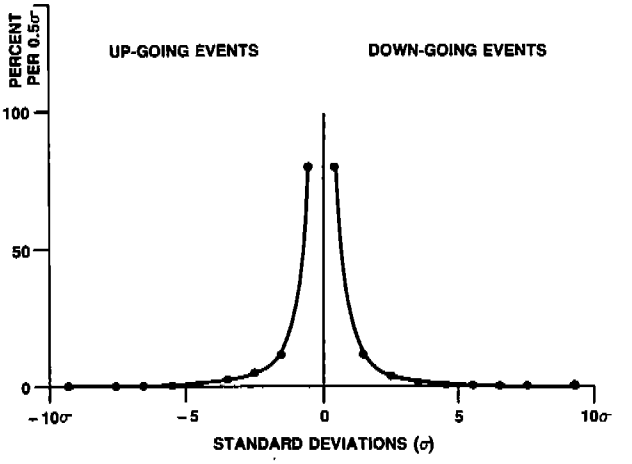

Fig. 8d. Probability density distribution of amplitude events.

Fig. 8. HACYM Analysis of Cubic Constituent of Output of Dalzell's Nonlinear Response Simulation.

The inherent ability of the cubic constituent to ultimately produce more extreme responses is reflected in the scale of the abscissas of Figure 8(d) and 7(d). The majority of the amplitude units in each figure fall within $\pm 1\sigma$ but to encompass the more extreme values of the cubic constituent it was necessary to increase the $\pm 5\sigma$ scale of 7(d) to $\pm 10\sigma$ in 8(d).

For the response model at hand, it is apparent that the nonlinearity of the MVDAE curve reflects the nonlinearity inherent in the quadratic constituent but not the cubic constituent.

The HACYM analysis of the combined ((L+Q+C) output at the $\sigma_x = 0.25$ excitation level is given in Figure 9. Inasmuch as the linear constituent and the combined output have been normalized, direct comparison of the respective figures is appropriate. The half-cycle analysis of Figure 9(a) contrasts with 6(a) in two obvious respects. First, the distribution of half-cycle events is obviously skewed in 9(a) whereas that of 6(a) is not. Second, with each HACYM scaled to $\pm 5\sigma$, the peak half-cycle events of the normalized linear case clearly fall within the bounds of the matrix whereas it is reached (and at one point exceeded) in the normalized nonlinear case. The nature of the nonlinear distribution of half-cycle events in the HACYM is quite apparent in the MVDAE curve of Figure 9(c) while the linearly of the MVDAE of the linear constituent is equally apparent in Figure 6(c). The change from linear to nonlinear response is also reflected as asymmetry in the distribution of maxima and minima, compare Figures 6(b) and 9(b). The influence on the distribution curves of amplitude events Figures 6(d) and 9(d) is minimal at the $\sigma_x = 0.25$ excitation level. This statistic in the case at hand is apparently influenced more by spectrum shape than by the nonlinearity of the process.

Dalzell[6] previously provided the distributions of maxima and minima for the combined output (L+Q+C) at both $\sigma_x = 0.25$ and $\sigma_x = 1.0$ which can now be compared to the corresponding distributions obtained by HACYM analysis. Figure 10(a) presents the comparison for $\sigma_x = 0.25$ from which it can be seen that except for a slight zero shift (about 0.2σ)*, the two distributions are in close agreement. At $\sigma_x = 1.0$ a similar zero shift exists. In this case the distribution of maxima are in close agreement but not the minima. It is believed that this difference is due primarily to a lack of resolution in the HACYM analysis since 94% of all minima fall in just two class intervals. The conclusion is drawn form these comparisons that, with the exception of a small zero shift, good agreement exists in these independent assessments of maxima and minima for the time-series simulations.

The HACYM analyses of combined output for the linear plus quadratic (L+Q) and linear plus quadratic plus cubic (L+Q+C) cases at an input excitation level of $\sigma_x = 1.0$ are presented in Figures 11 and 12. the half-cycle analysis of Figure 11(a) is distinctively skewed and contains two related half-cycle events which exceed the $\pm 7\sigma$ scale of the matrix. A correspondingly strong asymmetry exists in the distributions of maxima and minima of Figure 11(b). The MVDAE distribution of Figure 11(c) is strongly nonlinear as implied by the half-cycle count distribution of Figure 11(c) while the distribution of amplitude events of 11(d) remains symmetric.

---

* Due to differences in defining the mean value of the time series output.

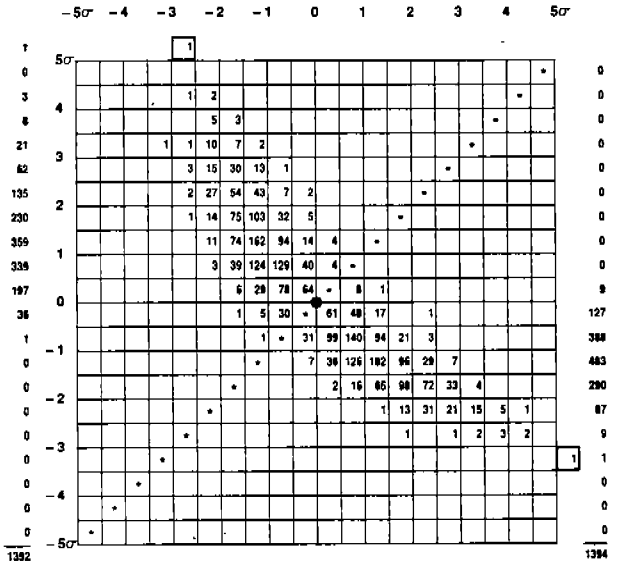

Fig. 9a. Half-cycle analysis of nonlinear output (L+Q+C), σ_x = 0.25 (± 5σ, zero mean, 10 samples combined).

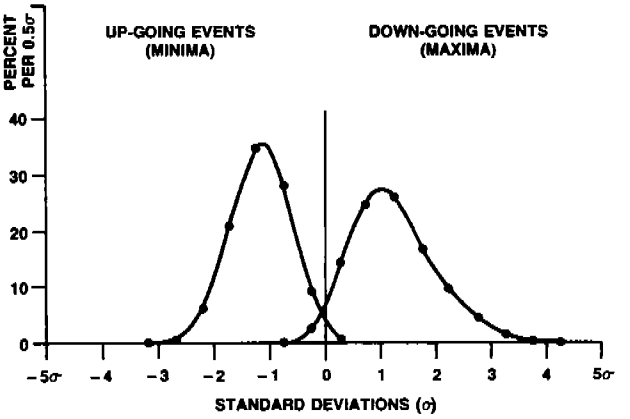

Fig. 9b. Probability density distribution of maxima and minima.

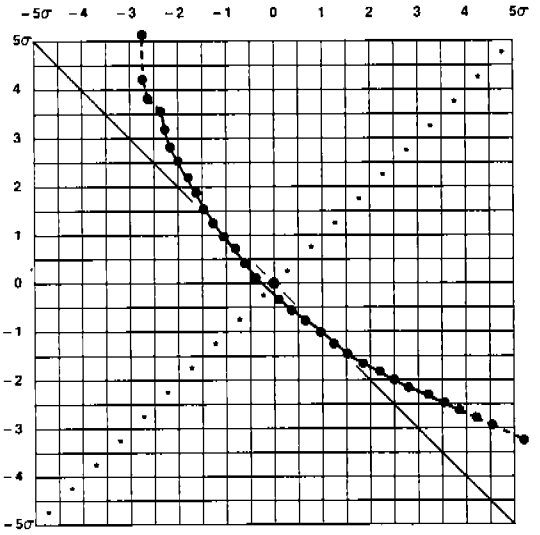

Fig. 9c. Mean value distribution of amplitude events.

[---DENOTES LESS THAN 5 EVENTS AVAILABLE TO DEFINE MEAN.]

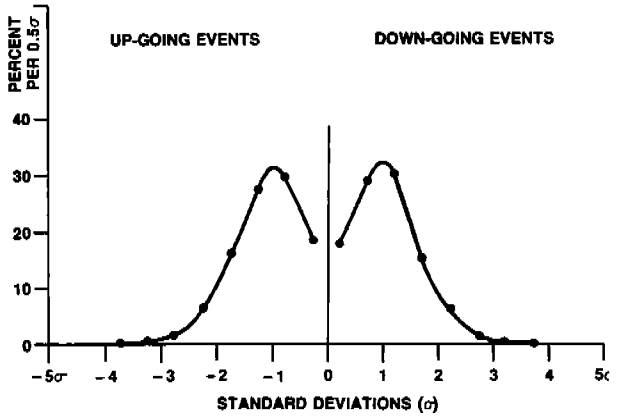

Fig. 9d. Probability density distribution of amplitude events.

Fig. 9. HACYM Analysis of Combined Output (L+Q+C) of Dalzell's Nonlinear Response Simulation, σ_x = 0.25.

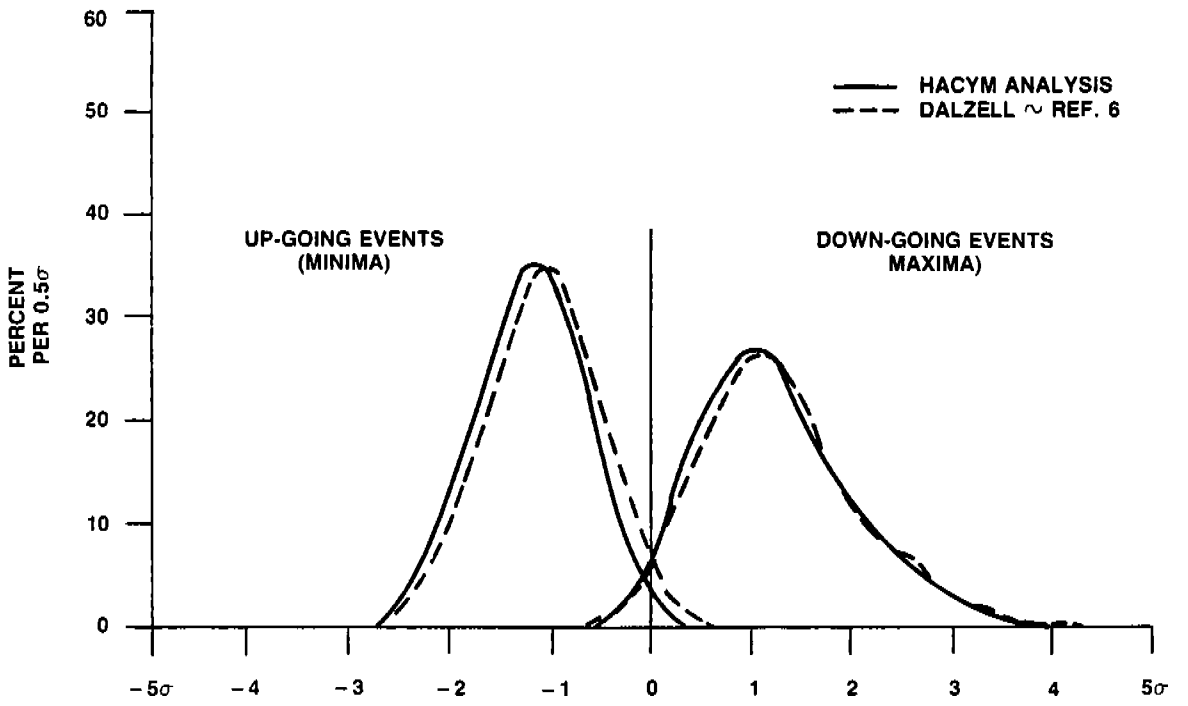

Fig. 10a. $\sigma_x = 0.25$.

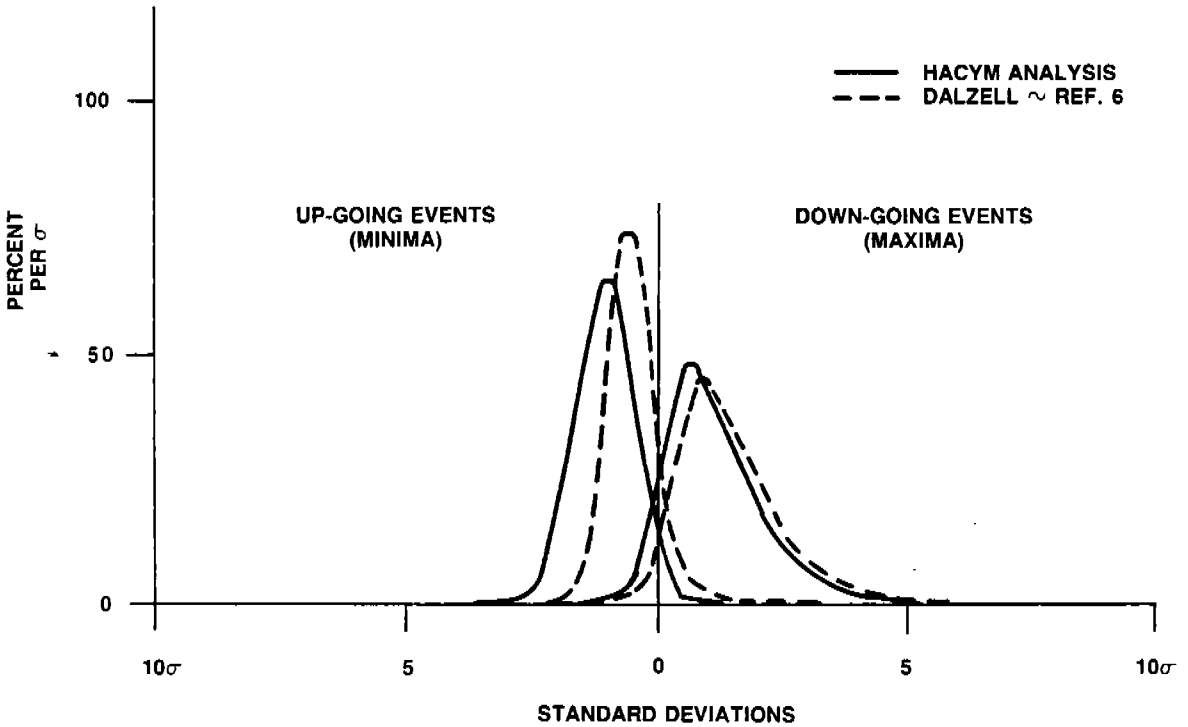

Fig. 10b. $\sigma_x = 1.0$.

Fig. 10. Comparison of Marginal Distributions of Half-Cycle Events with Maxima and Minima Distributions from Dalzell's Nonlinear Simulation (L + Q + C).

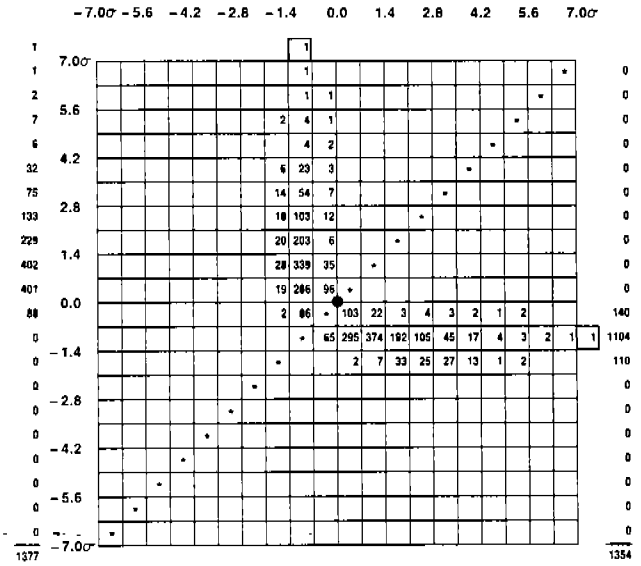

Fig. 11a. Half-cycle analysis of nonlinear output (L+Q), σ_x = 1.0 ($\pm$ 7σ, zero mean, 10 samples combined.

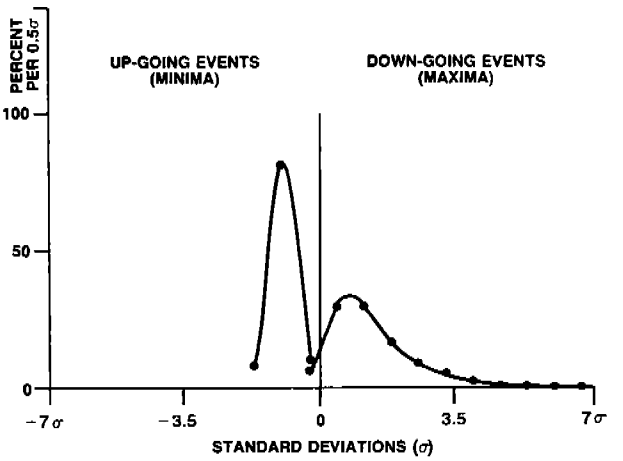

Fig. 11b. Probability density distribution of maxima and minima.

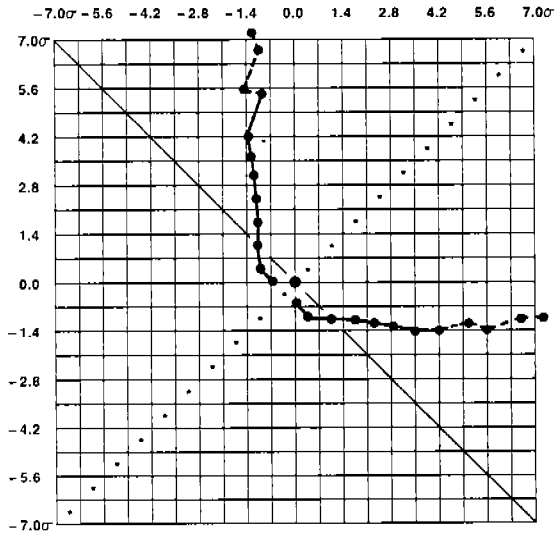

Fig. 11c. Mean value distribution of amplitude events.

[---DENOTES LESS THAN 5 EVENTS AVAILABLE TO DEFINE MEAN.]

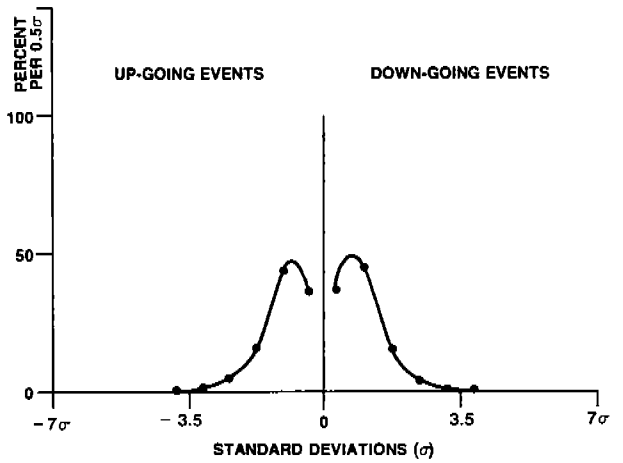

Fig. 11d. Probability density of amplitude events.

Fig. 11. HACYM Analysis of Combined Output (L+Q) of Dalzell's Nonlinear Response Simulation, σ_x = 1.0.

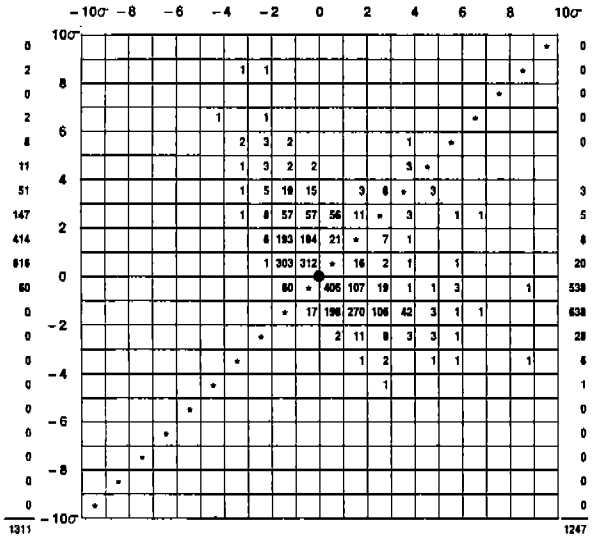

Fig. 12a. Half-cycle analysis of nonlinear output (L+Q+C), σ_x = 1.0 ($\pm 10\sigma$; zero mean, 10 samples combined).

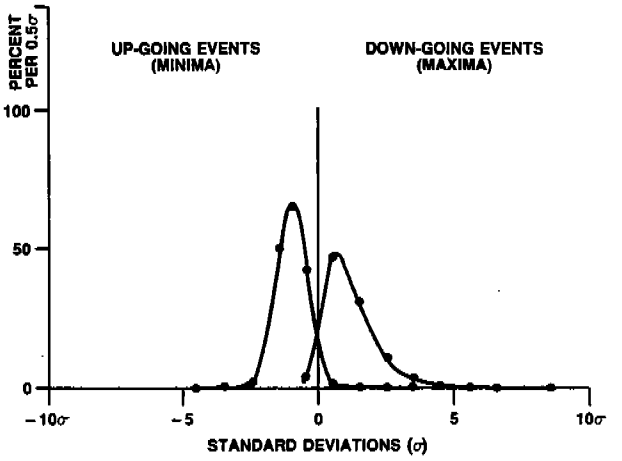

Fig. 12b. Probability density distribution of maxima and minima.

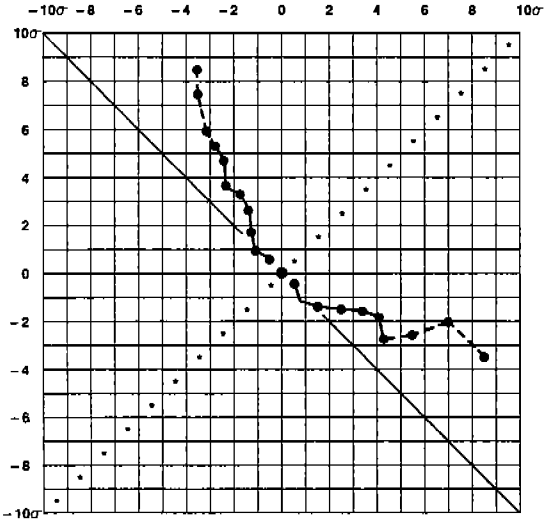

Fig. 12c. Mean value distribution of amplitude events.

[---DENOTES LESS THAN 5 EVENTS AVAILABLE TO DEFINE MEAN.]

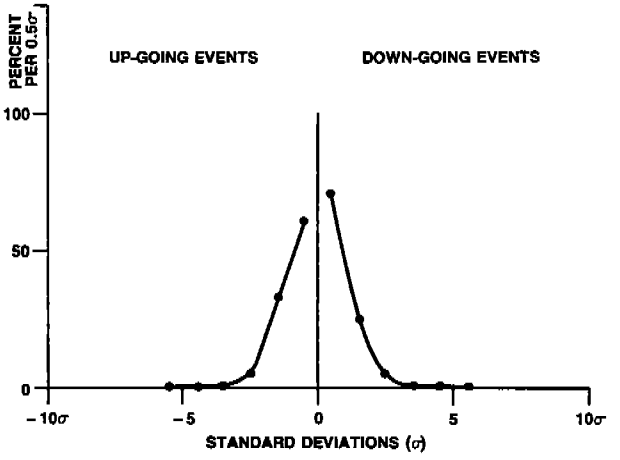

Fig. 12d. Probability density distribution of amplitude events.

Fig. 12. HACYM Analysis of Combined Output (L+Q+C) of Dalzell's Nonlinear Response Simulation, σ_x = 1.0.

The analysis of Figure 12 can be compared directly with that of Figure 9 since only a change in excitation level is involved. It will be noted first that the half-cycle event distribution of Figure 12(a) employs a matrix scale of $\pm 10\sigma$ vs $\pm 5\sigma$ for 9(a). Unlike the $\sigma_x = 0.25$ case the distribution of events in the outer portion of the matrix of Figure 12(a) is very sparse so that approximately the entire outer halves of the MVDAE curve of Figure 12(c), are developed from sample distributions involving less than 5 events. Thus, the comparatively smooth distribution curve of Figure 9(c) does not evolve. That such a result might occur at a high input excitation level is not surprising considering that the increased quadratic (x16) and cubic (x64) constituents exhibit these same characteristics, see Figures 7 and 8. The distribution curves of amplitude events in Figure 12(d) are not as symmetric as in the other cases investigated for reasons that are not self-evident. Moreover, the peak of the distributions occur at = $\pm 0.5\sigma$ or less in contrast to Figure 9(d) where they occur at $\pm 1\sigma$. (Note that the ordinate of 9(d) must be multiplied by a factor of 2 in order to be comparable to that of Figure 12(d). *

Although the foregoing results apply specifically to the generic ship motion model employed by Dalzell[3] in his original simulation there are certain trends which are noteworthy.

(a) Utility of Mean Value Distribution of Amplitude Events (MVDAE)

The MVDAE curve provides a relatively clear indication of the linearity or nonlinearity of input and output variables. Additionally, the development of comparative asymmetry in the density distributions of maxima and minima also reflects nonlinearity but not as clearly. In any case HACYM analysis of the variables provides both statistics. As regards the influence of quadratic and cubic term constituents, in this instance the quadratic term has a pronounced influence on the nonlinearity of the MVDAE curve and asymmetry of the distributions of maxima and minima. The cubic constituent on the other hand has a significant influence on the distribution of amplitude events in contrast to the MVDAE. It remains to be determined whether an orthogonal relationship exists between the two constituents as regards these distributions.

(b) Other Evidence of Nonlinear Behavior from HACYM Analysis

Nonlinearity of a response variable is generally important because it can lead to more extreme or qualitatively different responses than if it were linear. The tendency toward more extreme values is evident upon comparing the half-cycle analyses of Figures 5(a), 6(a), 9(a), 11(a) and 12(a). First, examination of the scale of the normalized matrix and the proximity of half-cycle events to the outer boundary leads to the following observations:

* A reduced size class interval (0.5σ) was used here and in other figures where sharply peaked distributions were encountered.

Variable	Matrix Scales	Proximity of Events to Outer Boundary of Matrix
Input wave spectrum	±5σ	Comfortably within boundary
Linear response (more narrow-band)	±5σ	Within boundary but closer than input
Combined output (L+Q), σ_x = 0.25	±5σ	Boundary exceeded by two events
Combined output (L+Q), σ_x = 1.0	±7σ	Boundary exceeded by two events
Combined output (L+Q+C), σ_x = 1.0	±10σ	Events approaching boundary

It is clear that the combination of nonlinearity and high input excitation resulted in more extreme values of the normalized response in this particular realization. Nonlinear response maxima were increased over the purely linear response at σ_x = 0.25. (At ±5σ two events exceeded the boundary of the matrix in the nonlinear model). The complete (L+Q+C) nonlinear model when excited at σ_x = 1.0 produced extreme events approaching ±10σ whereas the linear model produced extreme events approaching only ±5σ.

The tendency toward more extreme responses was accompanied by an evident tendency toward fewer events of an extreme nature within the normalized matrix. This behavior arose from the tendency of the nonlinear constituents in Figures 3 and 4 (i.e., Y2(t) and (Y3(t)) to primarily augment the largest events of the linear response constituent in the time-series. The thinning out of half-cycle count distributions as they approach maximum response values is also reflected in the MVDAE curve when it is coded to identify mean values derived from less than five half-cycle events; see Figures 5(c), 6(c), 9(c), 11(c), and 12(c).

(c) Comparison of HACYM and "Zero Up/Down Crossing" Analyses of Wave Data.

The Zero Up-Crossing (ZUC) Method is frequently used to analyze time series wave height data and to determine whether or not the wave height process is narrow-band Gaussian in character. In this method peak/trough excursions (and vice versa) which do not result in a crossing of mean water level are discarded. Moreover, wave heights are measured in terms of the total distance between successive troughs and peaks defined in this manner. (If statistics are accumulated as height excursions from peaks to succeeding troughs it would be identified as a "zero down-crossing" method. It is generally held that either procedure is acceptable for the intended purpose). Inasmuch as HACYM analysis is a more consistent method of analysis (all peak/trough excursions are retained regardless of whether or not they cross mean water level) it is of some interest to compare the results of each method as applied to analyzing wave height time-series data.

To this end it is clear that since the ZUC method results in wave height excursions which correspond to double amplitude values, a HACYM analysis of amplitude events when multiplied by two would give comparable statistics except

for the zero-crossing restriction. A first approximation to ZUC method results can be obtained by eliminating those events which fall in the upper right and lower left quadrants of the half-cycle matrix, i.e., those events in which the trough of the wave is above mean water level or the crest is below mean water level. Unfortunately there is no simple method for augmenting the amplitude of the half-cycle events from which these (generally small) amplitude events have been deleted so as to make the time series data continuous again. The results presented below are thus approximate. Since these unaugmented half-cycles are not in the majority and since the percentage of augmentation is generally not large, the approximation is believed adequate for purposes of illustrating certain features.

The normalized half-cycle analysis of the input wave spectrum (Figure 5(a)) has been modified in Figure 13(a) as suggested above. Figure 13(b) compares the effect of this modification on the distribution of maxima and minima for reference purposes. With the exception of overlapping portions of the distributions, the ZUC method does not result in excessive distortion of the true distribution of maxima and minima. With respect to the distribution of amplitude events, however, this is not true as shown in Figure 13c. The fact the ZUC method tends to result in a Rayleigh type distribution as illustrated in Figure 13(d) strongly suggests that it is not a suitable test of whether or not the process is narrow-band Gaussian. It might, of course, be argued that since the HACYM and ZUC distributions tend to merge at high values of σ, the latter method is adequate for approximating the distribution of maxima. The results of the HACYM analysis of Figure 11, however, illustrate that the distribution of amplitude events of Figure 13(d) gives little suggestion of any substantial nonlinearity of the process. The significance of this fact with respect to maxima is evident by comparing Figures 6(a) (linear, Gaussian output) where all events fell well within the $\pm 5\sigma$ bounds of the normalized matrix to Figure 11(a) where, for the nonlinear model and excitation level at hand, a $\pm 7\sigma$ matrix was not large enough to contain all of the events. Obviously failure to detect that nonlinear behavior is involved contributes to the possibility of the ZUC method leading to inappropriate conclusions regarding maxima as well.

4.0 FURTHER ANALYSIS OF HURRICANE CAMILLE WAVE DATA

The evident ability of the MVDAE distribution to detect nonlinear behavior in random time series data has prompted a re-examination of a normalized HACYM analyses of wave height data available from a previous investigation of hurricane Camille, Buckley, et al[2]. In this study half-hour data samples from 1000 to 1618 hours were normalized on a scale of $\pm 6\sigma$. The results of re-examination are summarized in Figure 14. An associated correlation of significant wave height, average wind velocity and the wave spectrum peakedness parameter $S(f)\max/Hm_o^2$ is provided in Figure 15 for the same time period. (The latter is proportional to the peak energy density divided by the area under the spectrum and hence is a rough measure of the peakedness of the spectrum). Wave height spectra are provided in Figure 16.

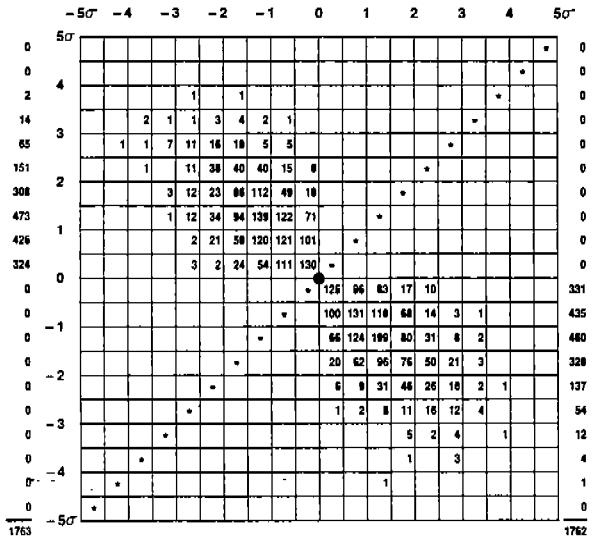

Fig. 13a. Half-cycle analysis of input wave spectrum modified to approximate application of zero up/down crossing method.

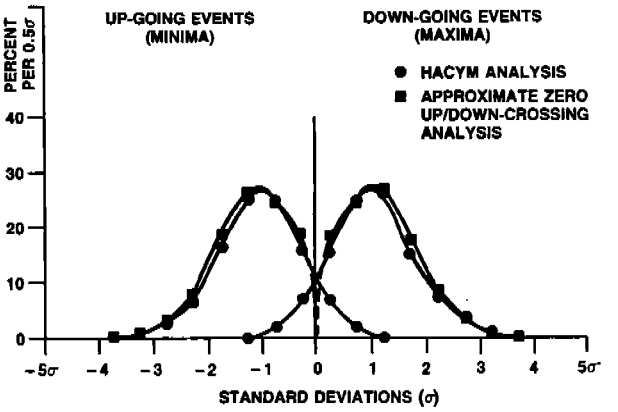

Fig. 13b. Probability density distribution of maxima and minima.

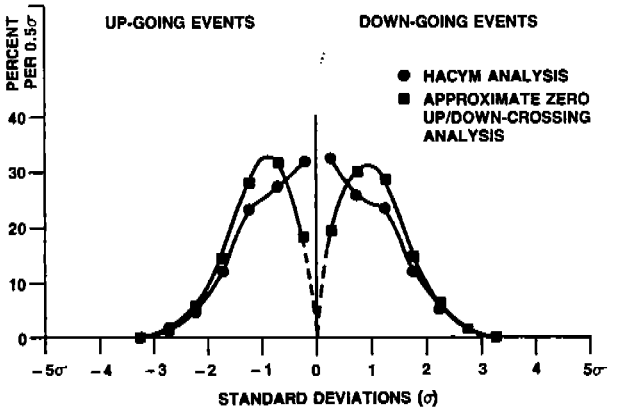

Fig. 13c. Probability density distribution of amplitude events.

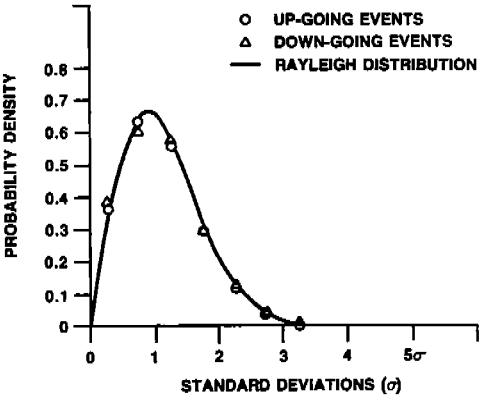

Fig. 13d. Comparison of approximate zero up/down crossing analysis results to a Rayleigh distribution.

Fig. 13. HACYM Analysis of Input Wave Spectrum Modified to Approximate Results of Zero Up/Down Crossing Analysis.

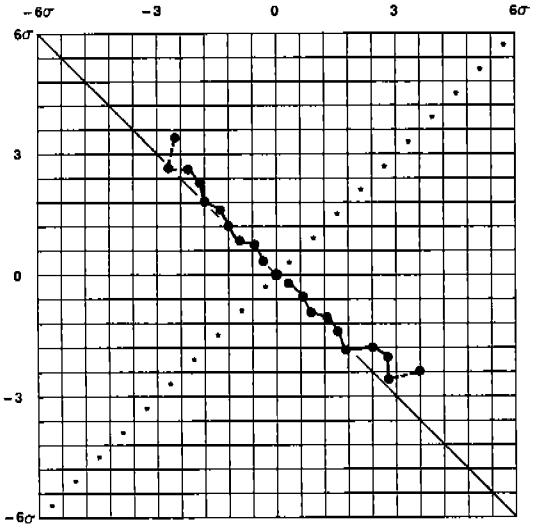

Fig. 14a. 1000–1030 hrs.

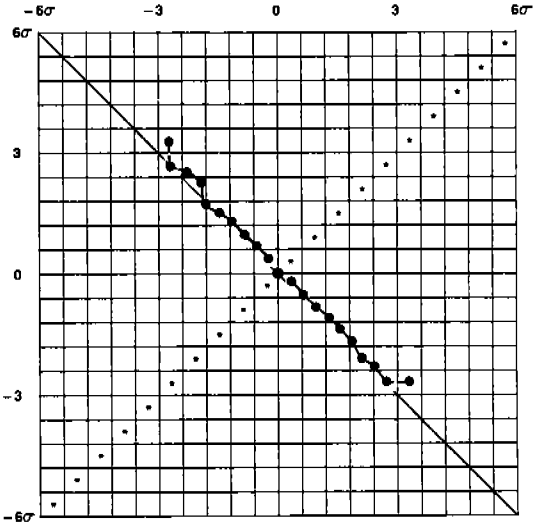

Fig. 14b. 1030–1100 hrs.

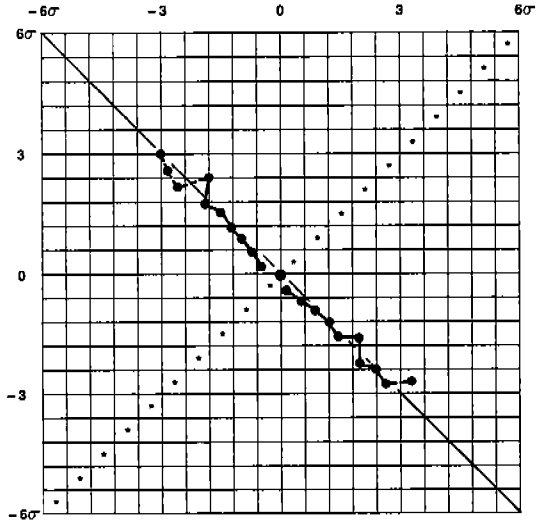

Fig. 14c. 1100–1130 hrs.

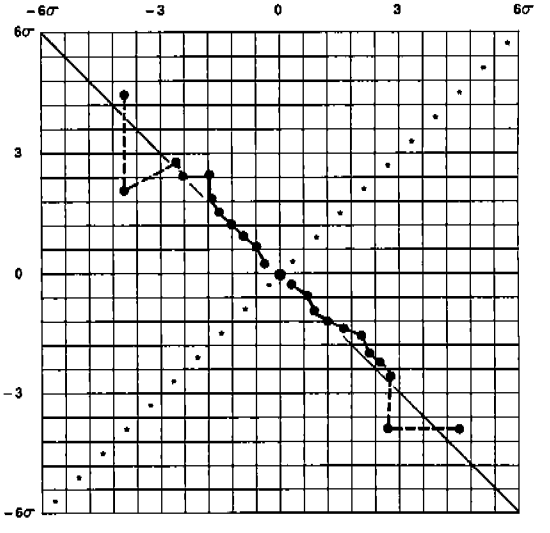

Fig. 14d. 1130–1200 hrs.

[---DENOTES LESS THAN 5 EVENTS AVAILABLE TO DEFINE MEAN.]

Fig. 14. Mean Value Distribution of Amplitude Events from HACYM Analyses of Hurricane Camille Wave Data.

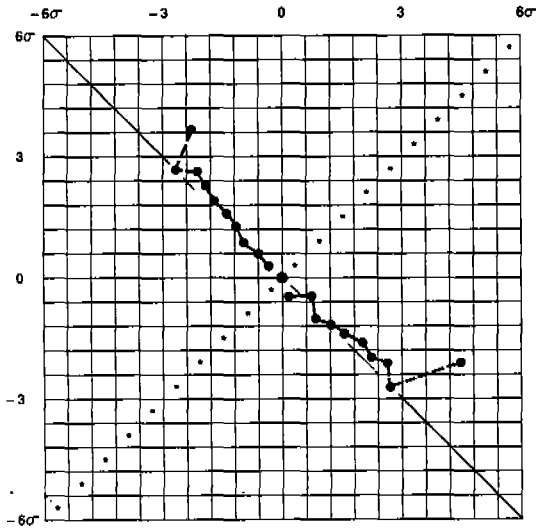

Fig. 14e. 1200–1230 hrs.

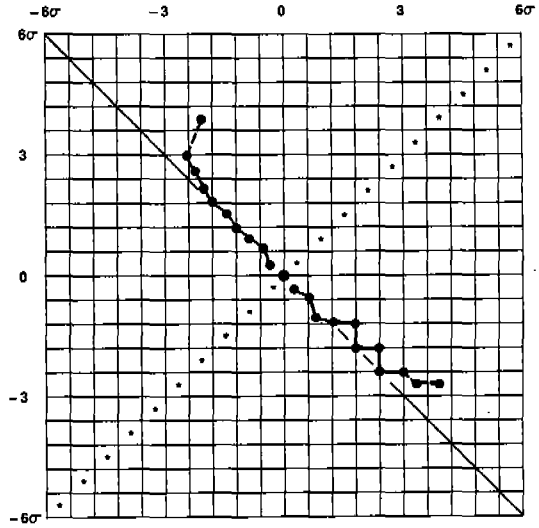

Fig. 14f. 1230–1300 hrs.

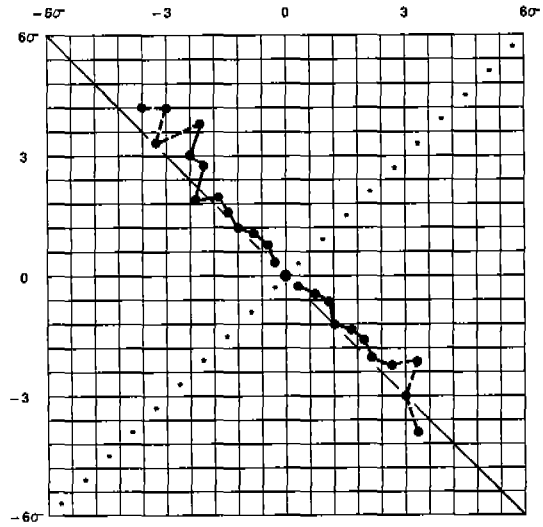

Fig. 14g. 1300–1330 hrs.

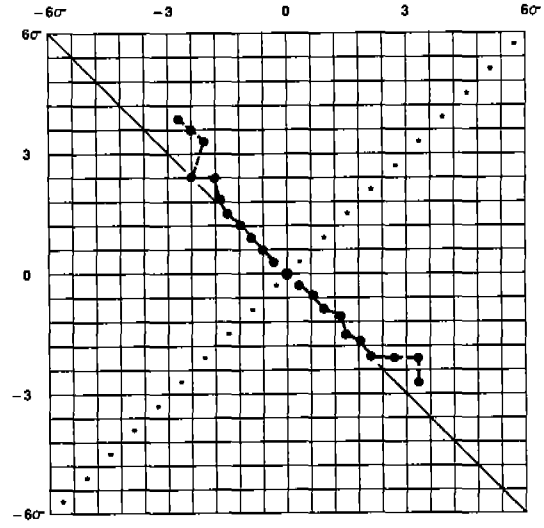

Fig. 14h. 1330–1400 hrs.

[---DENOTES LESS THAN 5 EVENTS AVAILABLE TO DEFINE MEAN.]

Fig. 14. (Continued).

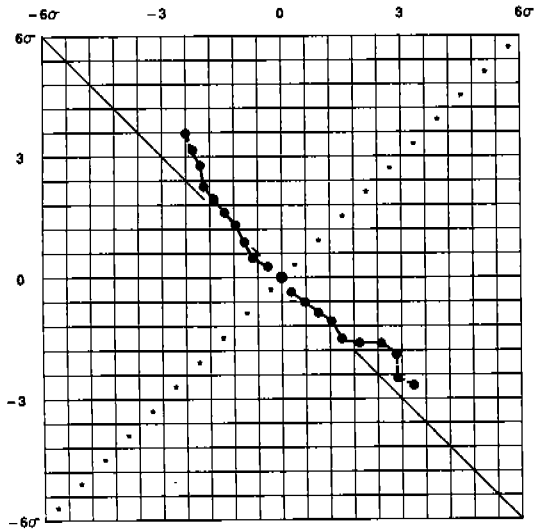

Fig. 14i. 1400–1430 hrs.

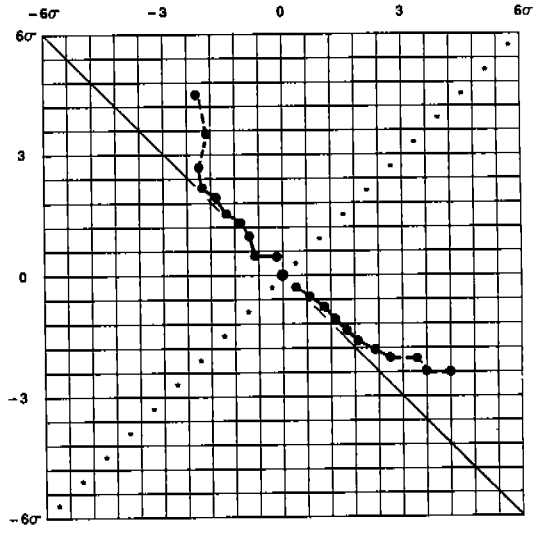

Fig. 14j. 1430–1500 hrs.

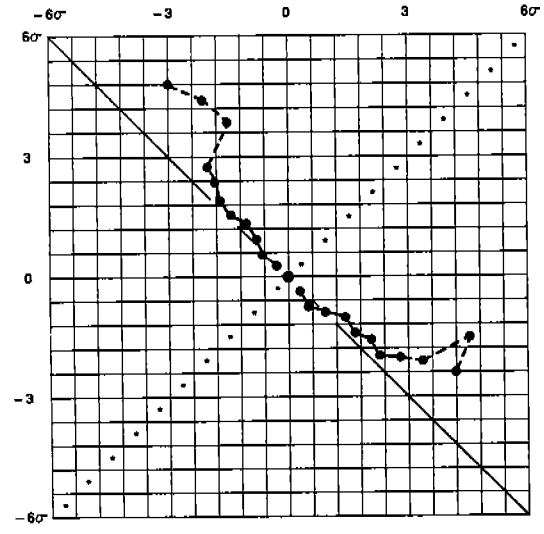

Fig. 14k. 1500–1530 hrs.

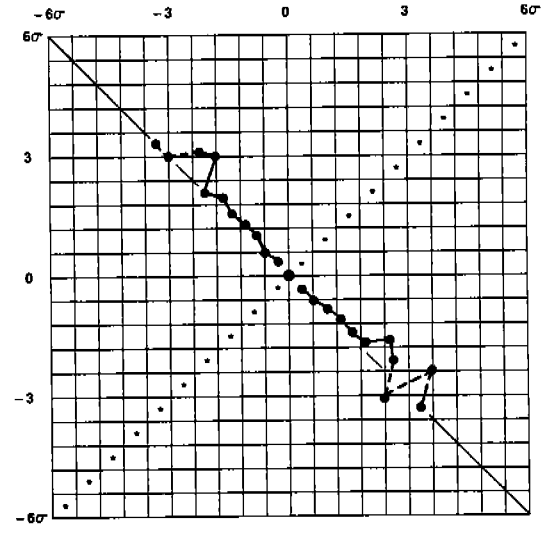

Fig. 14l. 1530–1600 hrs.

[---DENOTES LESS THAN 5 EVENTS AVAILABLE TO DEFINE MEAN.]

Fig. 14. (Continued).

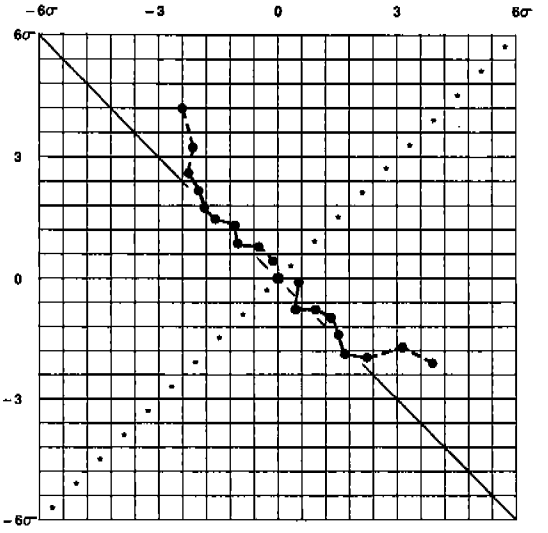

Fig. 14m. 1600–1618 hrs.

Fig. 14. (Continued).

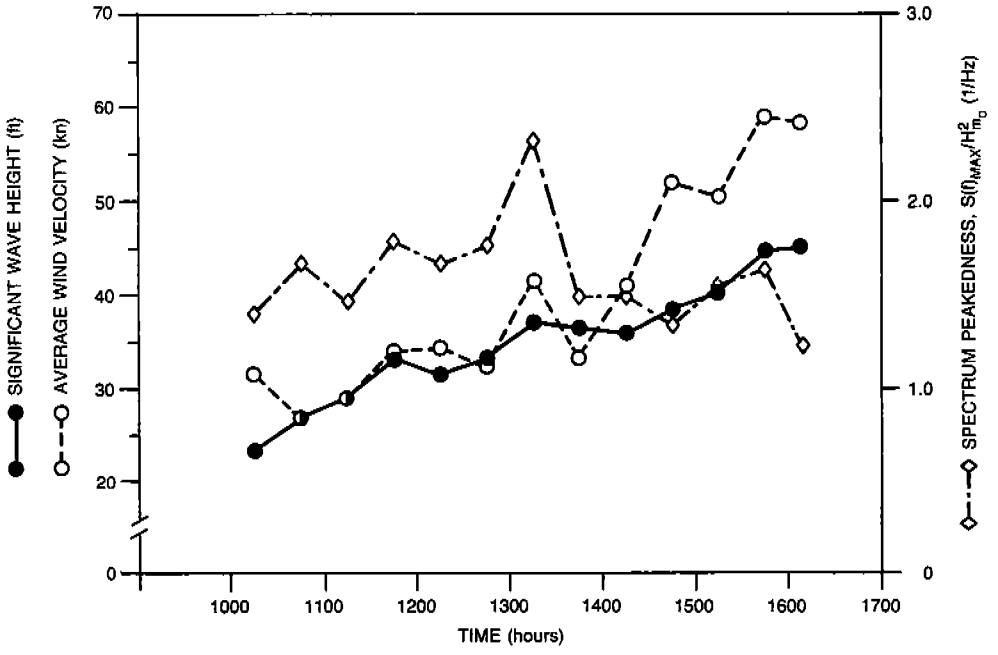

Fig. 15. Significant Wave Height, Average Wind Velocity and Spectrum Peakedness vs. Time During Hurricane Camille (1000-1618 hours).

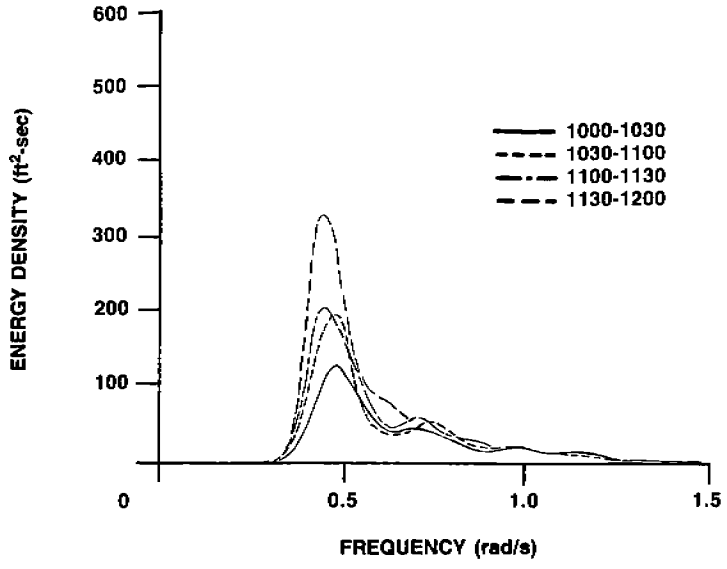

Fig. 16a. 1000-1200 hours.

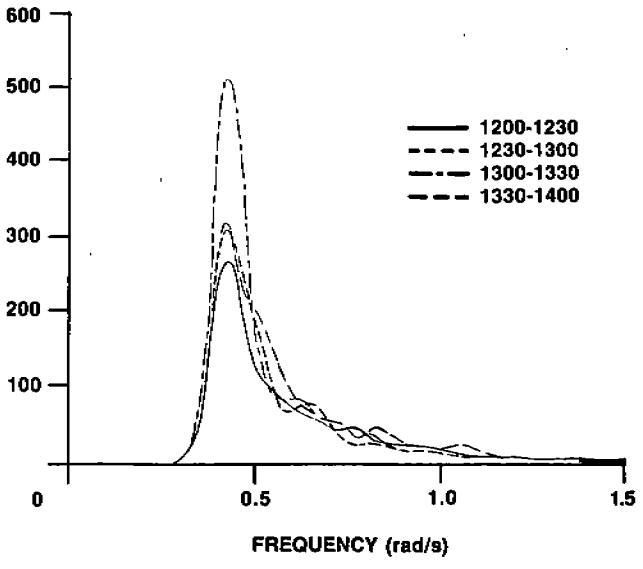

Fig. 16b. 1200-1400 hours.

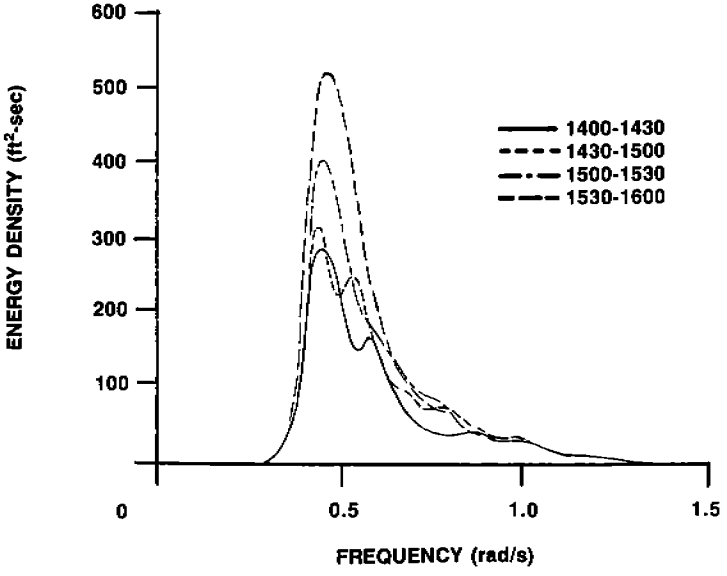

Fig. 16c. 1400-1600 hours.

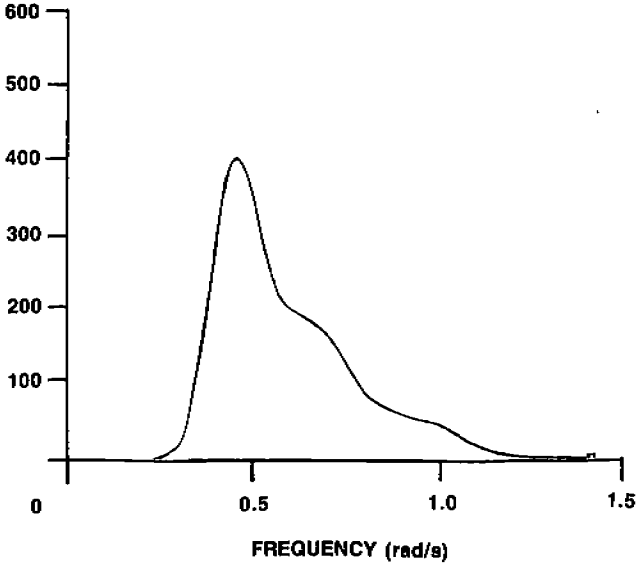

Fig. 16d. 1600-1618 hours.

Fig. 16. Wave Spectra from Hurricane Camille.

The nonlinearity of the wave height time series data as evidenced in the MVDAE distribution curves can be characterized as follows:

(a) 1000 to 1200 hours

A modest indication of nonlinear behavior exists in Figures 14(a)-(d) notably for the period 1000 - 1030 hours. In the succeeding two half-hour intervals the distribution curves are substantially linear despite the fact that significant wave height continued to build during this period. The average wind velocity on the other hand decreases abruptly from the 1000 - 1030 to the 1030 - 1100 time interval. Thereafter wind velocity increased steadily during the remainder of the two hour interval. Spectrum peakedness generally increased during the interval with significant half-hour variations which had no obvious relationship to either nonlinearity of the MVDAE curve or average wind velocity. The dominant feature of the two hour interval is an episodic wave event(H_{max}/Hm_o = 2.4) which produced four outlying, sequential half-cycle events.

(b) 1200 to 1400 hours

During this two hour interval there is a modest but clear indication of nonlinearity in the MVDAE curves of figures 14(e)-(h) with the final half-hour exhibiting the most pronounced trend in this regard. Significant wave height shows a generally consistent build-up during the period despite an abrupt increase in wind velocity during the 1300 - 1330 time interval. The wave spectrum of Figure 16(b) indicates a substantial energy constituent centered at modal frequency during this time. In the next half-hour, an abrupt decrease in average wind velocity and spectrum peakedness occur accompanied by an evident leveling off of significant wave height.

(c) 1400 to 1618 hours

During this period a substantial increase in average wind velocity occurred together with a significant increase in nonlinearity of the MVDAE curves of figures 14(i)-(m). The trend toward pronounced nonlinearity is broken during the 1530-1600 interval following a brief cessation of the build-up in average wind velocity during the previous half-hour. The wind build-up resumes in the next half-hour, however, which is followed by a return to pronounced nonlinearity in the MVDAE curve. Spectrum peakedness is seen to decrease abruptly during the 1400 to 1618 hours interval with the lowest value during the entire analysis period occurring at the end when data gathering ceased due to power loss on the platform from which the measurements were made.

Despite the obvious difficulty of drawing clear and supportable generalizations from this re-analysis of hurricane Camille wave and wind data one central finding does emerge, namely that the most linear MVDAE curves were obtained when average wind velocity was lowest, (1030 to 1130 hours) and that the most nonlinear curves were obtained during a period of a prolonged and rapid build-up in wind velocity (1400 to 1618 hours). Considering that the wind driven sea and swell waves were almost certainly bi-directional early in the data analysis period and that the observed seaway was surely influenced by wind field anomalies well upwind of the measurement site, it is interesting that such an evident trend was found despite these attendant complexities.*

* It is also of interest that parametric steepness is limited by the $\frac{Hm_o}{T_p^2} = 0.00776g$ boundary of Figure 2 does not fully identify the total extent of nonlinearity of a seaway.

In view of these findings it seems reasonable to expect that analyses of short fetch, unidirectional (small scale) seaways under the influence of strong local winds would be revealing in regard to wave breaking and transient seaway build-up characteristics. It will be noted, however, that such analyses would be seriously impeded without continuous and accurate time series measurements of wave height and related parameters such as wind velocity and direction.

5.0 TOWING TANK MODELING OF A NONLINEAR RANDOM SEAWAY

This investigation is the result of the second of the three major tasks associated with this study. Its primary purpose is to compare the nonlinearity of waves measured during a particular thirty minute interval of hurricane Camille to that of waves generated at model scale in a towing tank where the original wave spectrum was modeled. The comparison will be made on the basis of a half-cycle analysis of the prototype and model scale time series wave height data as well as on the basis of the time series characteristics of the largest wave events.

Two commercial towing tank facilities were tasked to conduct essentially duplicate experiments so that in the event the tank waves were found to be poor replications of the original waves the result could not arbitrarily be attributed to the wave making mechanics of a particular facility. Each was provided with the wave height spectrum ($Hm_o \approx$ 40 ft.) obtained from hurricane Camille during the 1500 to 1530 hrs interval when the seaway was especially nonlinear, see Figure 14(k). The selection of model scale was left to the individual facility with the stipulation that the significant wave height be as high as possible without compromising attainment of the given spectrum. A minimum of 500 wave height events were requested with multiple runs permitted as needed to minimize wave reflection effects. Time series wave height measurements were called for at a "primary" location to be selected by the facility as that most likely to satisfy the wave making requirement. In addition measurements were required at a "secondary" location approximately 100 feet from the wave maker. This requirement was subsequently amended to correspond to the location in the tank which the facility regarded as the furthest location from the wave maker at which data acquisition would normally begin during a model towing experiment. Video coverage was required at the primary location with a background scale erected so that time series wave height measurements could later be compared to the instantaneous wave profile and also so that the visual character of a breaking wave could be compared to the measured wave profile at an instant of interest.

Letter reports summarizing the test results were also required and these are presented here in Appendices C and D. The facilities selected were the Arctic Offshore Corporation (A.O.C.) in Escondido, California and the Davidson Laboratory of the Stevens Institute of Technology (D.L.) in Hoboken, New Jersey.

Procedures

Wave making at A.O.C. was conducted at a scale of approximately 1:30 using a single flap, single segment waveboard. Two data gathering runs were made, the first of which (Run 1001) was intended to closely model the hurricane Camille wave spectrum. The second run (2000) employed a wave maker control program designed to

model JONSWAP spectra but which could produce a spectrum shape similar to the Camille spectrum. Capacitance type wave probes were located 82 and 194 feet from the waveboard. (See Figure 2.1 of Appendix C). Each of the runs was continuous and produced approximately 400 wave events.

At the Davidson Laboratory, wave making was conducted at a scale of approximately 1:50 using a double flap waveboard. Seven statistically independent data gathering runs were made. Resistance type probes were located 70 and 170 feet from the waveboard.

Additional information regarding the test and data analysis procedures is contained in Appendices C and D.

Results

In the case of the A.O.C. tests, only Run 1001 has been considered as immediately applicable to the original objectives. With respect to model scale the following result was obtained (expressed as full scale values):

Run No.	Hm_o (primary) (ft)	Hm_o (secondary) (ft)	Scale Factor (primary) -
1001	39.1	37.6	29.4

A comparison of the Camille and test wave spectra is provided in Figure 17 for the primary (Wave 2) and secondary (Wave 3) probe locations. At each location the wave energy was somewhat greater than the Camille values near the mode of the spectrum and less at frequencies well above the mode especially for the secondary probe location.

The results of a half-cycle analysis of the time series wave data from each location is presented in Figures 18(a) and (b) while the mean value distribution of amplitude events are shown in Figures 18(c) and (d). In the case of the latter, the corresponding distribution from the Camille wave data is superimposed. (It was necessary here to adjust the Camille distribution for the difference in matrix scales, i.e., $\pm 6\sigma$ vs $\pm 5\sigma$). At the primary location, the trends of the distributions are quite similar out to the point where the curves are defined by fewer than 5 events (dashed portion of the curves. In this regime the trend of the hurricane wave data is more nonlinear. At the secondary location, the tank data show slightly less nonlinearity than at the primary location. Selected time series events are shown in Figure 19 for the A.O.C. data. These particular waves were selected for examination on the basis of their being the largest (forward face, peak to trough) waves in the time series. See circled half-cycle wave events in Figure 19(a). These particular waves are characterized by their elevation/amplitude ratio which corresponds to the mean value of the trough to peak data excursion divided by one half of the total excursion. Thus for a wave having a preceding trough as far below mean water level as the following crest is above e/a = 0. As an indication of front face wave steepness, the time interval from trough to crest has also been determined for the three largest waves in Figure 19.

Comparison of Figures 19(b), (c) and (d) shows that while waves corresponding to the lowest and intermediate values of e/a happen to have similar values of trough to crest height (H_d), the front face steepness of the latter was

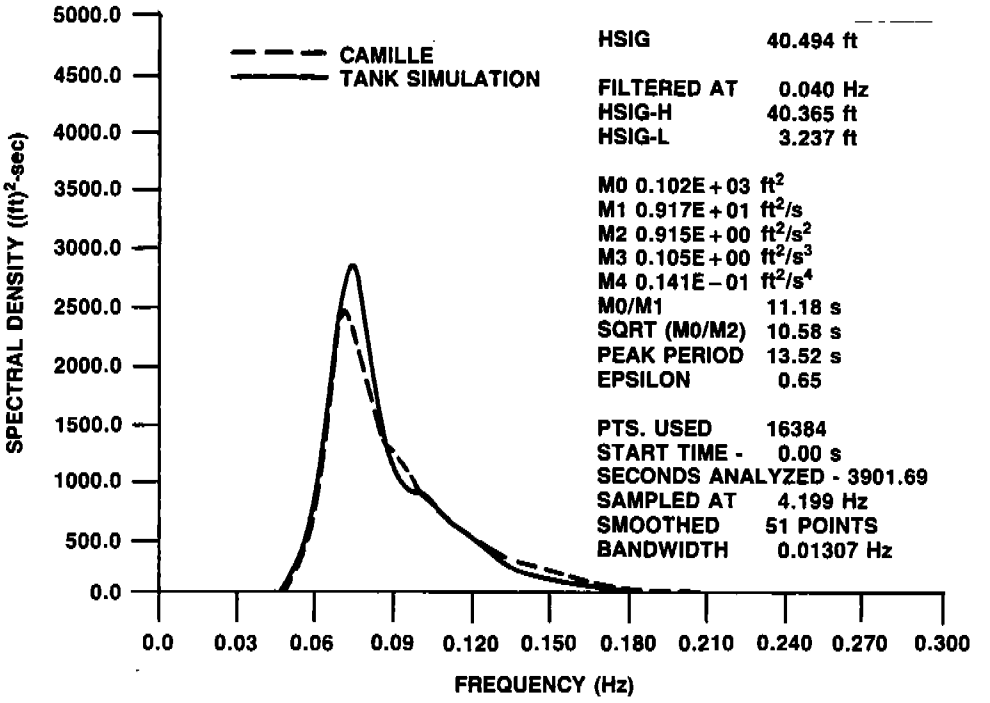

Fig. 17a. Wave-2 spectral density plot for test no. 1001.

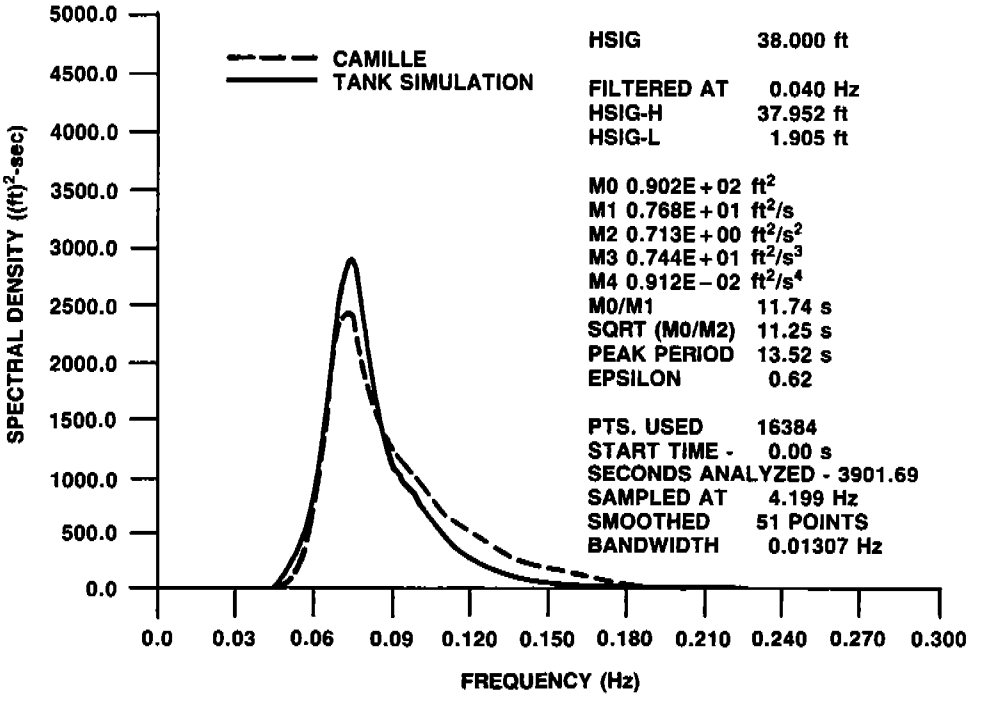

Fig. 17b. Wave-3 spectral density plot for test no. 1001.

Fig. 17. Comparison of Desired and Achieved Wave Spectra from A.O.C. Experiment (Full-Scale).

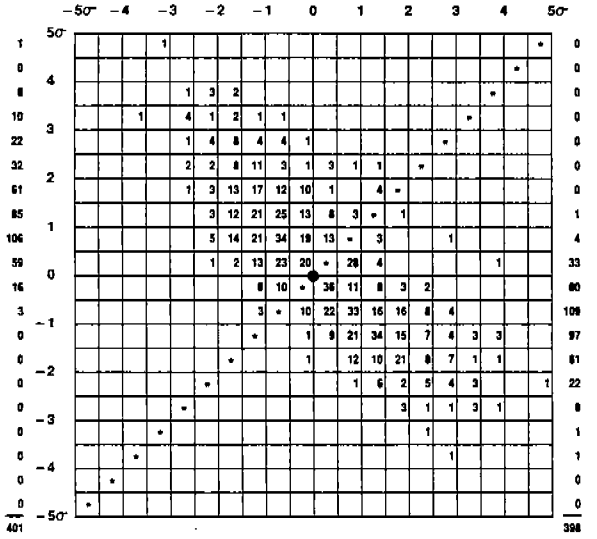

Fig. 18a. Half-cycle analysis of primary wave probe output (Run 1001).

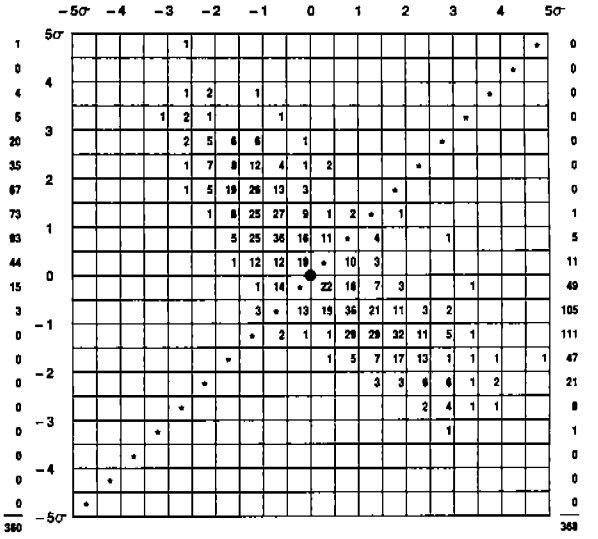

Fig. 18b. Half-cycle analysis of secondary wave probe output (Run 1001).

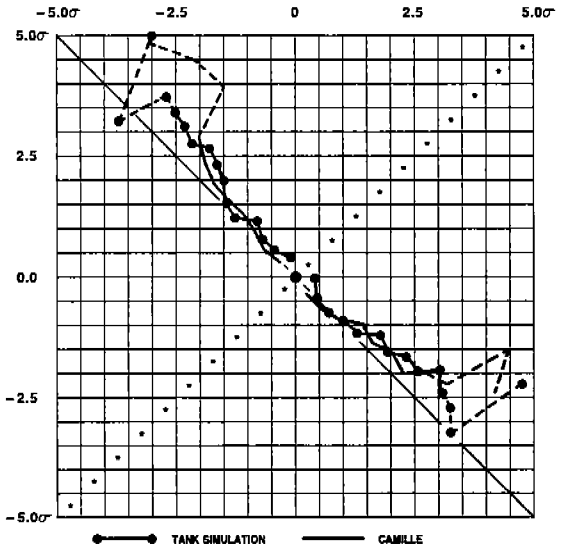

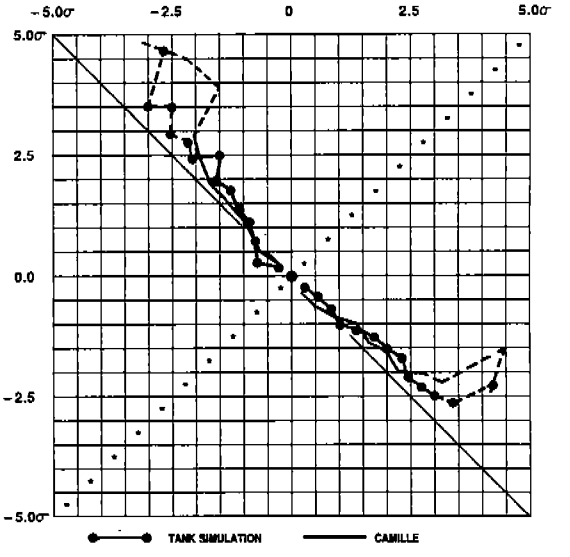

[---DENOTES LESS THAN 5 EVENTS AVAILABLE TO DEFINE MEAN.]

Fig. 18c. Mean value distribution of amplitude events — primary probe.

Fig. 18d. Mean value distribution of amplitude events — secondary probe.

Fig. 18. HACYM Analysis of Wave Probe Measurements from A.O.C. Experiment.

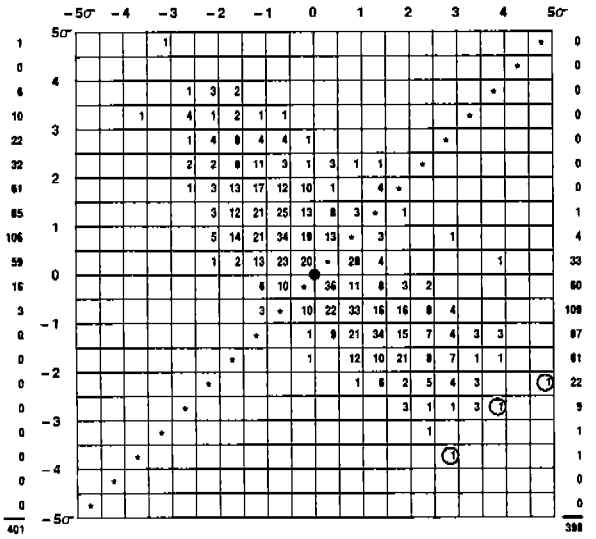

Fig. 19a. Identification of highest waves.

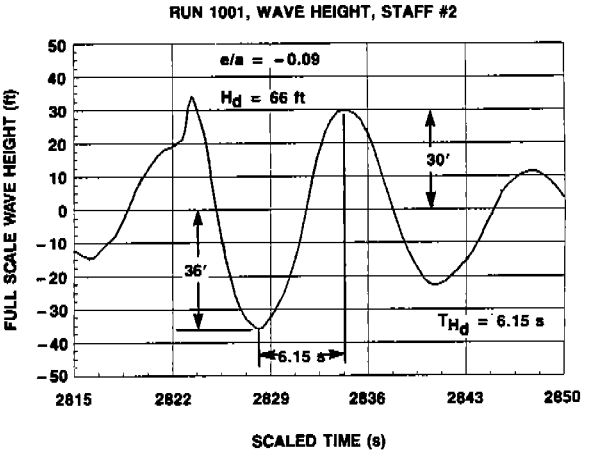

Fig. 19b. Lowest elevation/amplitude ratio.

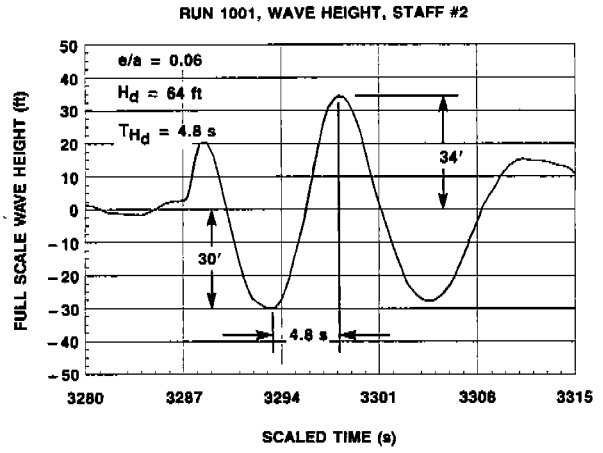

Fig. 19c. Intermediate elevation/amplitude ratio.

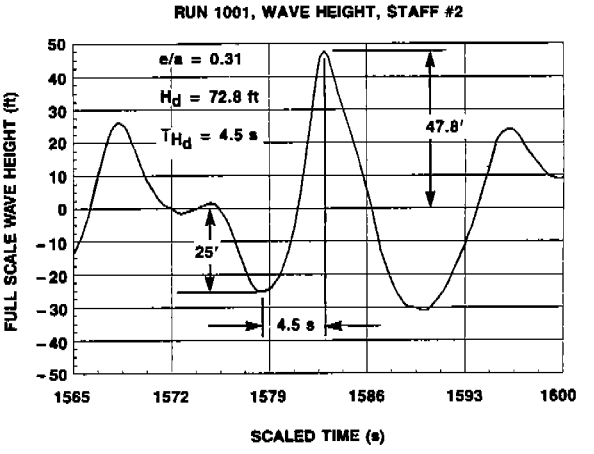

Fig. 19d. Highest elevation/amplitude ratio.

Fig. 19. Time Series Characteristics of Highest Waves at Primary Probe — A.O.C. Experiment.

appreciably greater with a rise time of 4.8 vs 6.15 seconds. The wave having the highest value of e/a was somewhat higher and steeper on the front face than either of the other two waves. Moreover, the time series character of this wave is also noticeably different from the other two.

Figure 20 contains a group of three waves from hurricane Camille (1500-1530 hours) which were selected on a similar basis, see the circled half-cycle events in Figure 20(a). In this data set the e/a values tended to be higher, although for the wave having the highest value (e/a = 0.48), the rise time was similar to that for the scaled-up tank wave which had the highest value of H_d. Using the parameter H_d/Th_d^2 as a measure of front face steepness, the tank wave was slightly steeper (3.60 vs 3.36). The time series character of the Camille wave, however, suggests that the upper half of the wave may well have been steeper. (See discussion below).

The results of the Davidson Laboratory experiment with respect to scale is as follows for each of the seven runs which constituted the total test sample. In this case the tank data are presented at model scale.

Run No.	Hm_o (primary) (inches)	Hm_o (secondary) (inches)	Scale Factor -
36	8.9815	8.5416	53.4
37	8.9446	8.5514	53.7
39	9.0866	8.5720	52.8
40	9.0504	8.5708	53.0
45	9.1497	8.5945	52.5
46	8.9967	8.5383	53.4
52	8.7950	8.6174	54.6

The scale factor on the average was just over 1:53 for this wave making experiment while the reduction in significant wave height from primary to secondary wave probe location was 5 percent which is about the same as that found for the A.O.C. facility.* Figure 21 compares the average of the measured and the scaled down Camille wave spectra at primary and secondary staff locations. The match near the mode of the spectrum is good at both staff locations whereas the energy at frequencies above the mode is somewhat lower for the tank waves especially at the secondary probe. The loss of wave energy at the higher frequencies for the secondary probe location is similar to that shown in Figure 17 for the A.O.C. wave making experiment.

Results of a half-cycle analysis of the complete set of time series data from each probe location is contained in Figures 22(a) and (b). The respective mean value distributions of amplitude events are shown in Figures 22(c) and (d) with the corresponding distribution for hurricane Camille (1500-1530 hrs) superimposed. As in the case of the A.O.C. data, the distributions of Figures 22(c) and (d) match that for Camille rather well until the dashed portion of the distribution curve is reached where the trend toward nonlinearity is greater for the hurricane driven seaway.

---

* The modal period of the test spectrum was based on a target scale factor of 1:50 rather than an achieved value of 1:53 hence the test modal period was greater than intended by $\sqrt{\frac{53}{50}} = 1.03$.

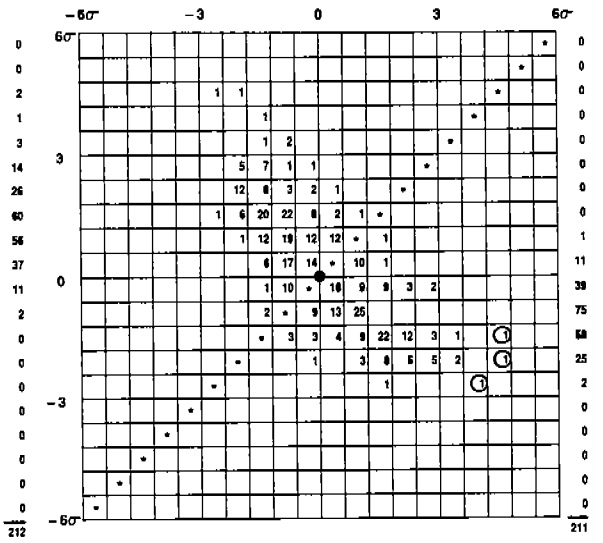

Fig. 20a. Identification of highest waves.

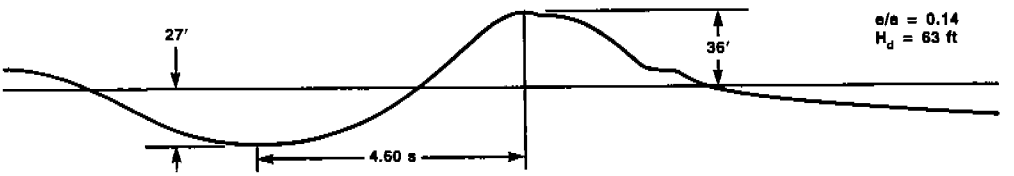

Fig. 20b. Lowest elevation/amplitude ratio.

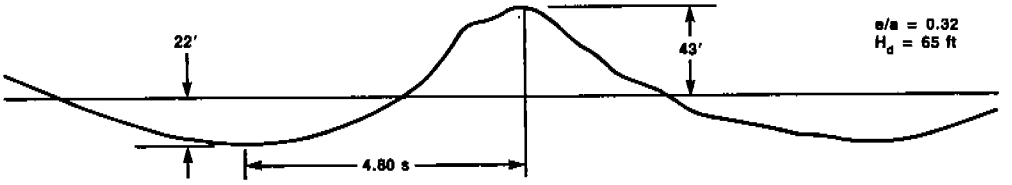

Fig. 20c. Intermediate elevation/amplitude ratio.

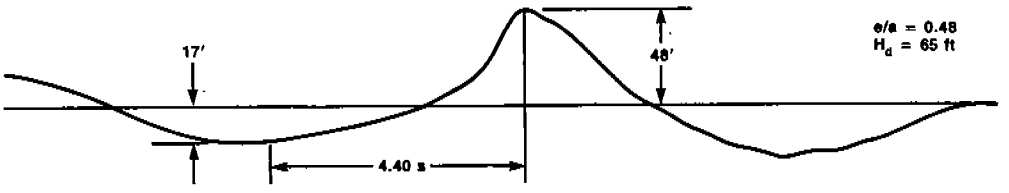

Fig. 20d. Highest elevation/amplitude ratio.

Fig. 20. Time Series Characteristics of Highest Waves — Hurricane Camille 1500-1530 Hours.

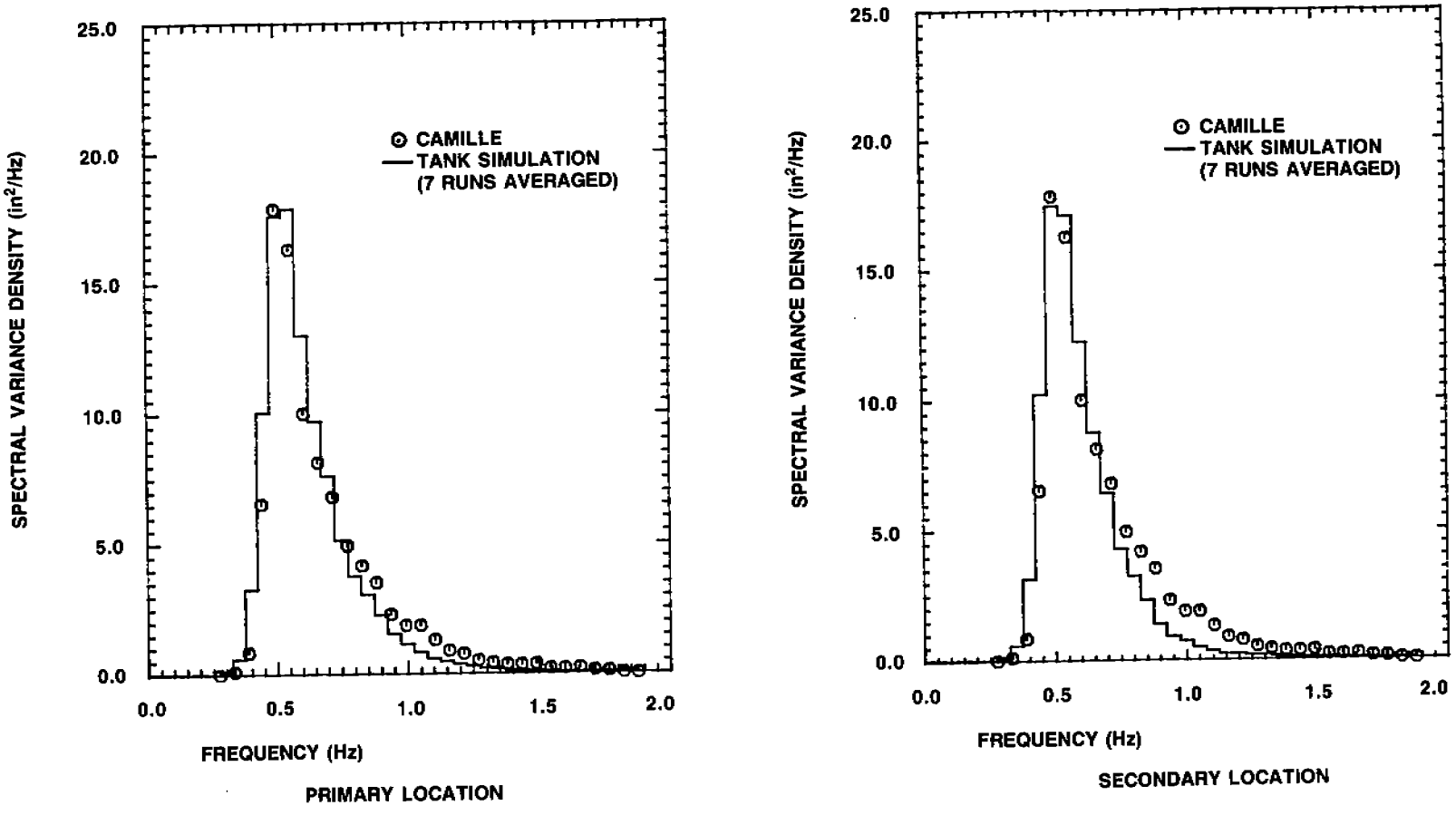

Fig. 21. Comparison of Desired and Achieved Wave Spectra from D.L. Experiment (Model Scale).

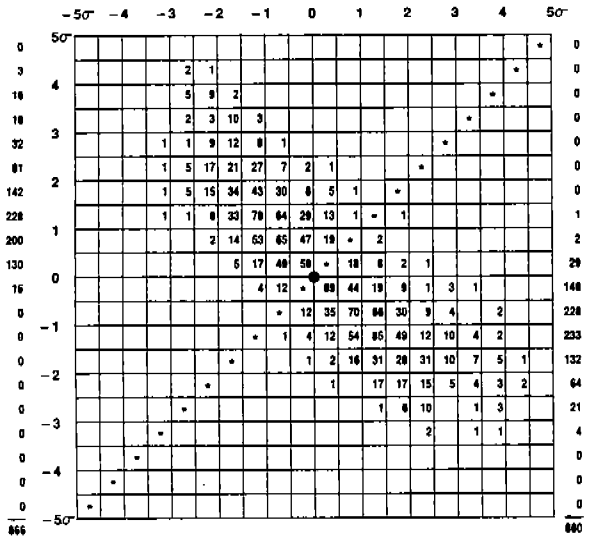

Fig. 22a. Half-cycle analysis of primary wave probe output (7 runs combined).

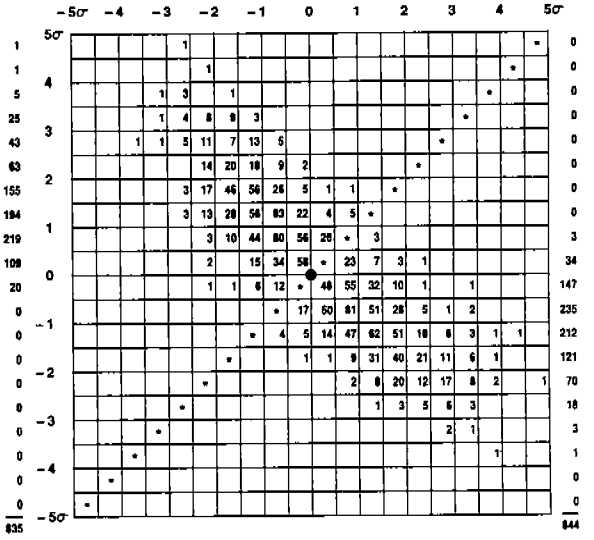

Fig. 22b. Half-cycle analysis of secondary wave probe output (7 runs combined).

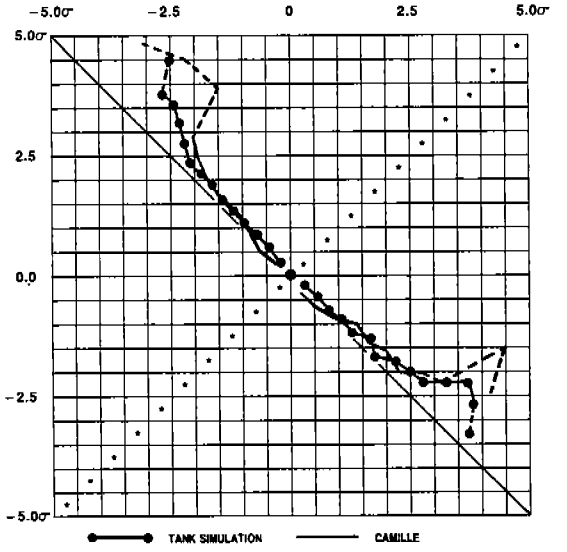

Fig. 22c. Mean value distribution of amplitude events — primary probe.

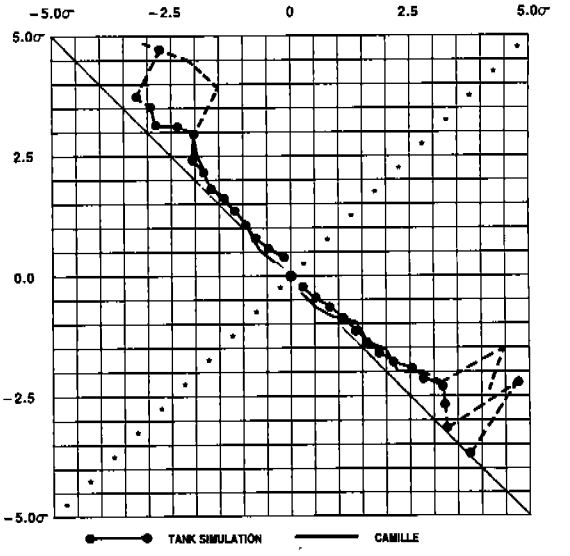

Fig. 22d. Mean value distribution of amplitude events — secondary probe.

[---DENOTES LESS THAN 5 EVENTS AVAILABLE TO DEFINE MEAN.]

Fig. 22. HACYM Analysis of Wave Probe Measurements from D.L. Experiment.

Selected time series wave events of maximum amplitude are shown at model scale in this instance with full-scale value of wave height and rise time given in the upper right hand corner of Figures 23(b), (c), and (d). Scale factors employed were taken from the individual runs in question.

Before considering the time series of these particular waves, a parametric characterization of all the waves shown in Figures 19, 20, and 23 will be undertaken. The parameters which will be considered are the forward face peak to peak wave height H_d, rise time Th_d elevation/amplitude ratio e/a, and steepness parameter H_d/Th_d^2. These are presented in Table 2 in order of increasing values of e/a.

Table 2. Characterization of Largest Waves in Test Tank Experiment.

A.O.C. Waves				D.L. Waves				Camille Waves			
H_d (ft)	T_{H_d} (s)	e/a	$H_d/T_{H_d}^2$ (ft/s²)	H_d (ft)	T_{H_d} (s)	e/a	$H_d/T_{H_d}^2$ (ft/s²)	H_d (ft)	T_{H_d} (s)	e/a	$H_d/T_{H_d}^2$ (ft/s²)
66	(6.15)	-0.09	(1.75)	62.5	4.72	-0.01	2.81	63	4.60	0.14	2.98
64	4.80	0.06	2.78	69	5.12	0.09	2.63	65	4.80	0.32	2.82
72.8	4.50	0.31	3.60	64.1	(7.61)	0.26	(1.11)	65	4.40	0.48	3.36

With the exception of the highest wave in the A.O.C. time series, all of the wave heights are in the mid to high 60's. The rise times show more variability, but with the exception of the lowest e/a wave in the A.O.C. group and the highest e/a wave in the D.L. group, the rise times lie between 4.40 and 5.12 seconds. The e/a ratios for the tank waves are similar to one another but are clearly lower than those for the Camille waves. The steepness parameters for wave fronts having similar values of e/a are themselves similar with the exception of the waves cited above as having noticeably different rise times (see circled values).

The time series characteristics of the waves shown in Figures 23(b) and (c) do not appear to be unusual. However, that on Figure 23(d) is suggestive of a wave on wave conformation where the comparatively long rise time of the front face is due to the particular interaction of the waves at the time of measurement. Whether or not such a conformation is unusual is not known.

Discussion

The primary purpose of the test tank wave making experiments was to compare the nonlinear characteristics of tank waves with those of full-scale hurricane waves where the wave height spectrum of the hurricane data sample was duplicated at model scale. The question to be answered then is: What was the basis for comparison and what did it reveal? Before attempting to answer it several matters should first be discussed.

Sample Size and Stationarity: The hurricane Camille 1500 to 1530 hours data

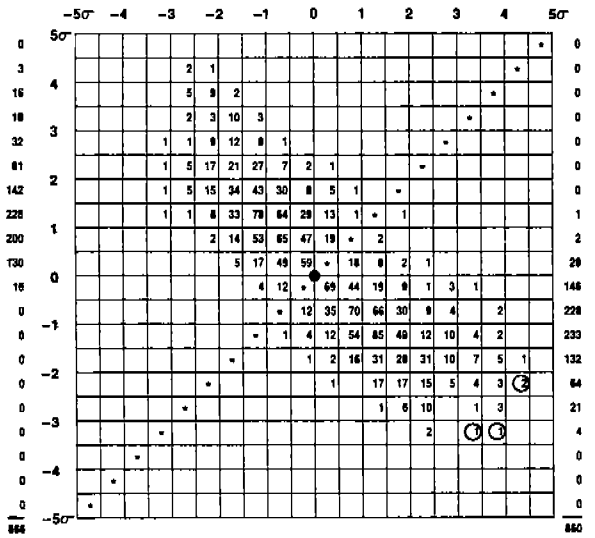

Fig. 23a. Identification of highest waves.

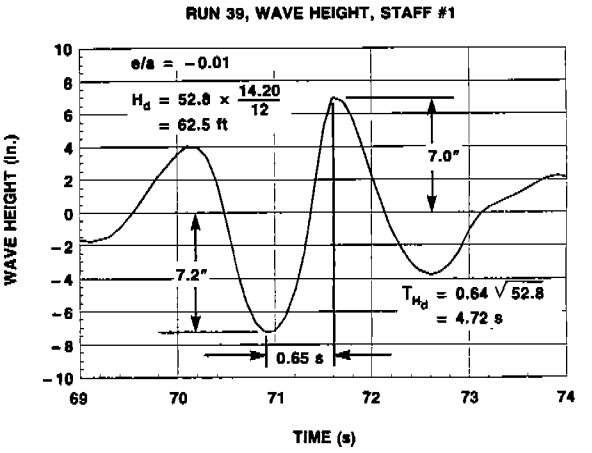

Fig. 23b. Lowest elevation/amplitude ratio.

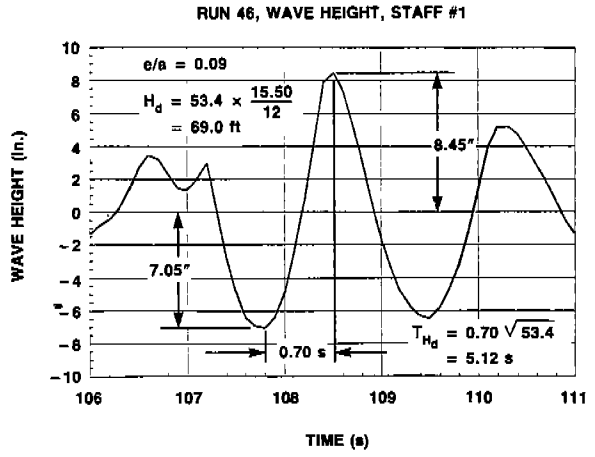

Fig. 23c. Intermediate elevation/amplitude ratio.

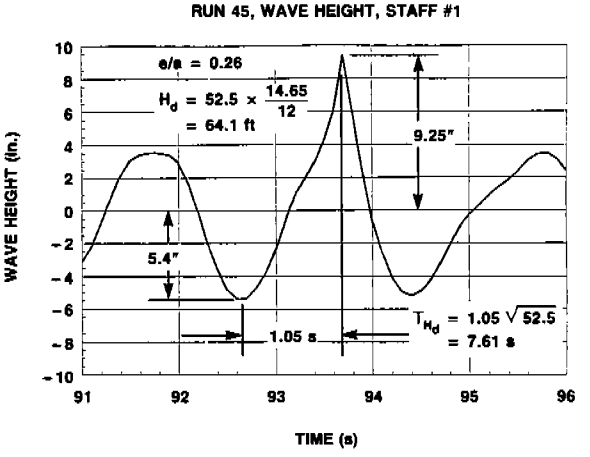

Fig. 23d. Highest elevation/amplitude ratio.

Fig. 23. Time Series Characteristics of Highest Waves at Primary Probe — D.L. Experiment.

sample produced approximately 211 half-cycle events of each type (i.e., up-going and down-going) see Figure 20(a). It is obvious from the analyses of Figures 14(a) through (m) that the normalized wave characteristic were far from stationary during the storm, particularly when the subject data sample was taken, so that while the test tank wave making experiments could be considered to represent a stationary random processes, the storm waves could not. In the case of the A.O.C. experiment approximately 400 half-cycle events were produced while in the D.L. experiment approximately 860 were produced in total. As far as the test tank data samples are concerned there seemed little merit in truncating them to 211 events since one might as well have the best available characterization of half-cycle statistics for the associate time series. Nevertheless, the statistics of maxima in particular should be examined with reservations since there is a range of up to 4 to 1 in the sample sizes involved.

When examining the parametric or time series characteristics of the largest waves in a linear, Gaussian process, one must admit the possibility of significant variations in such characteristics. A comparable examination of the largest events from a nonlinear process must admit to the same variability except when the nonlinearity has reduced the variability of the largest events in some unique way. Obviously a major dilemma exists since both randomness and uniqueness may be present. In the case of hurricane driven waves, extreme nonlinearity is associated with severely breaking waves so that the assessment of uniqueness is not especially difficult.

With these admonitions in mind, the following observations are offered. The MVDAE curve for the primary wave staff measurements is very similar to that from the Camille data out to a point where the largest wave heights occur. Beyond that point the data suggest that the Camille waves are more nonlinear. With respect to the parametric characteristics of the largest waves, Table 2 suggests that there is less variability associated with the Camille waves.

Variability in the time series characteristics of the largest of the tank waves tends to obscure any uniqueness. In the case the Camille time series events shown in Figures 20(b),(c), and (d) there is an apparent trend toward steepness in the upper half of the forward face of the waves as the e/a ratio increases. Because of the availability of time series wave height measurements from the test tank breaking wave experiments of Duncan, Wallendorf and Johnson[8], further characterization of the wave of Figure 20(d) is possible.

In these experiments breaking waves of both a spilling and plunging character were generated by deterministic means described in the reference. Figure 24 presents sequential time series wave height measurements from four adjacent wave probes positioned along the centerline of the tank[9]. The wave in question was characterized as a plunging breaker. Using a scale factor derived from the trough to crest height of the time series labeled "Plunging Breaker" and the corresponding height of the Camille wave of Figure 20(d), the former has been scaled-up and plotted over the latter in Figure 25. In this comparison, the time-scale of the tank wave was increased by the square root of the scale factor, mean water levels were made coincident as were the wave crests along the time scale. It is apparent that there is considerable similarity in the two time series wave

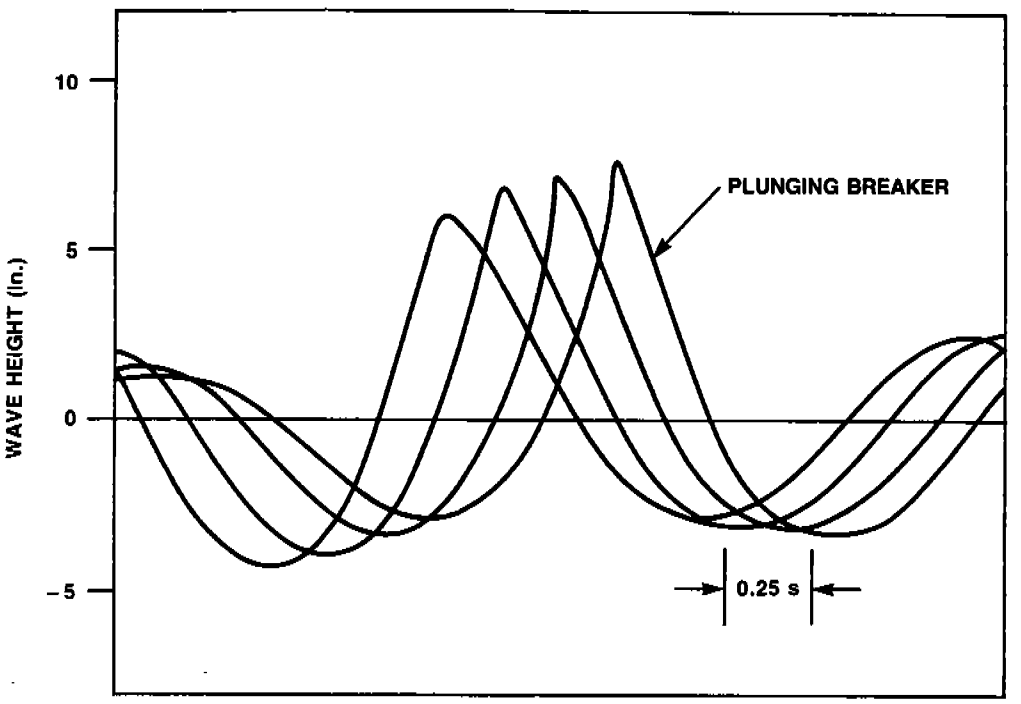

Fig. 24. Time Series Wave Heights from Staggered Wave Probes for Model Scale Plunging Breaker - Hydromechanics Laboratory, U.S.N.A.

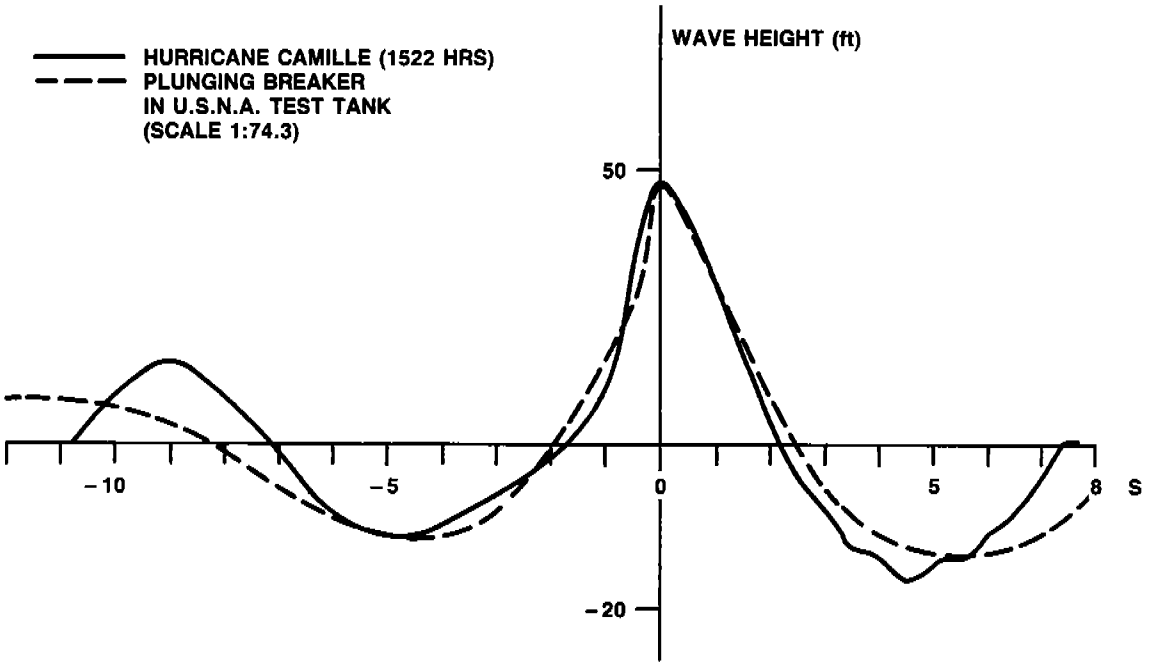

Fig. 25. Time Series Comparison of Model Scale Plunging Breaker and Wave From Hurricane Camille (1522 hours).

events so that one may infer that the Camille wave could have broken with somewhat of a plunging character. This is in contrast to the tank waves recorded on video tape at the A.O.C and D.L. where only spilling breakers were observed. While the limited data base at hand precludes drawing firm conclusions, this finding is at least consistent with the trend toward greater nonlinearity in the largest Camille's waves as compared to those from either of the two towing tank experiments, Figures 18(c) and 22(c). This should not be construed as an inherent limitation of tank wave making since long crested as opposed to short crested waves were generated.

Before moving on to other matters, several incidental observations regarding the towing tank wave making experiments should be made. The first concerns the repeatability of an extreme wave event in the time series data from the A.O.C. experiments. As previously mentioned Run 1001 which most closely approximated the Camille wave spectrum was supplemented by Run 2000 which involved a JONSWAP spectrum approximation. Figure 26 shows that the resulting spectra at the primary staff location were in fact quite similar. As shown in Figure 27, there was a major wave event in each of the time series which were very similar to one another and which occurred at about the same time after "time zero" in the wave making sequence. It was subsequently determined[10], that the respective wave making sequences were not statistically independent. This result is of particular interest in that if a time series wave height event of particular interest (i.e., one of which is potentially critical from a model motion or loads response point of view) could be embedded in a statistically acceptable realization and made to appear at a predetermined location and time in the tank, an experiment could be performed having both desirable statistical and deterministic qualities.

From the point of view of approximating the Camille wave spectrum, the dual flap wave maker at the Davidson Laboratory appeared to provide a somewhat better match at high frequencies than the single flap wave maker at Artec Offshore Corporation. Considering that the loss of energy in this regime was progressive with the distance from the wave maker and that the D.L. primary wave staff was proportionately further from the wave maker than that at A.O.C., the capability of the dual flap wave maker may be somewhat greater in this regard than is evident in a comparison of the wave spectra of Figures 17(a) and 21(a). With respect to the nonlinearity of the respective time series wave height data no substantial difference was evident so that the merits of the dual flap wave maker in this regard were not self-evident.

6. NUMERICAL MODELING OF A NONLINEAR RANDOM SEAWAY

The wave spectrum chosen for nonlinear modeling is the same as that employed in the towing tank wave making experiments, namely, hurricane Camille, 1500-1530 hours. As in the generic nonlinear ship motion response model of Section 3.0, functional polynomial modeling was employed although in this case only linear and quadratic terms were considered. The approach taken to numerical modeling is summarized in Appendix E. In contrast to the modeling of nonlinear ship motions, Appendix B, nonlinearity derives from second order wave-wave interaction theory

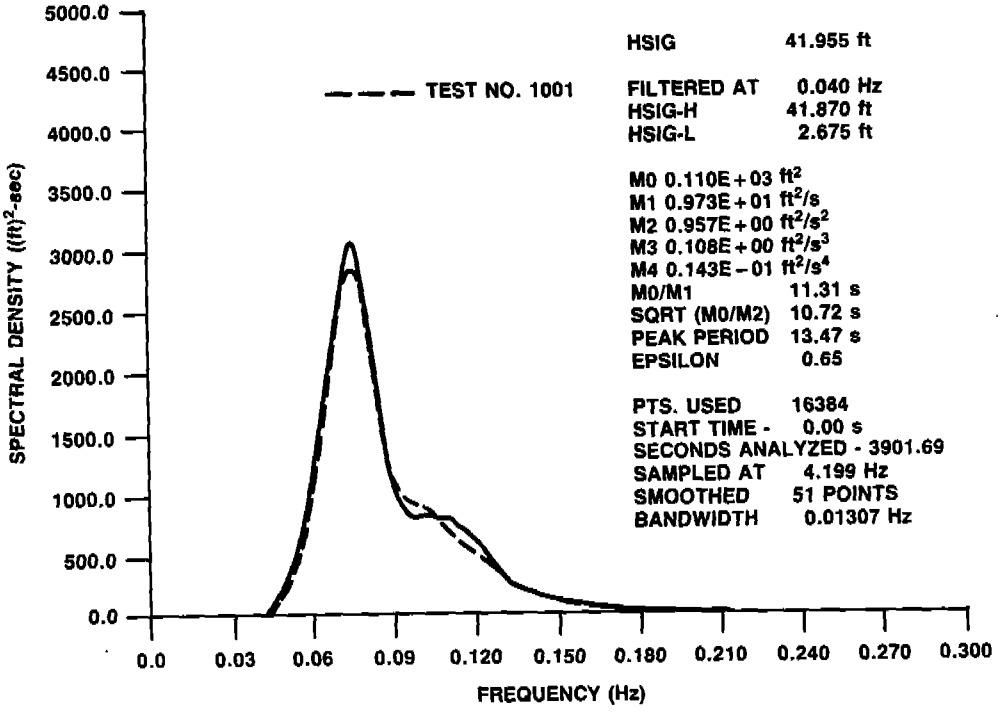

Fig. 26. Spectrum from Wave Gage 2 for 60 Minute Simulation Using JONSWAP Spectrum.

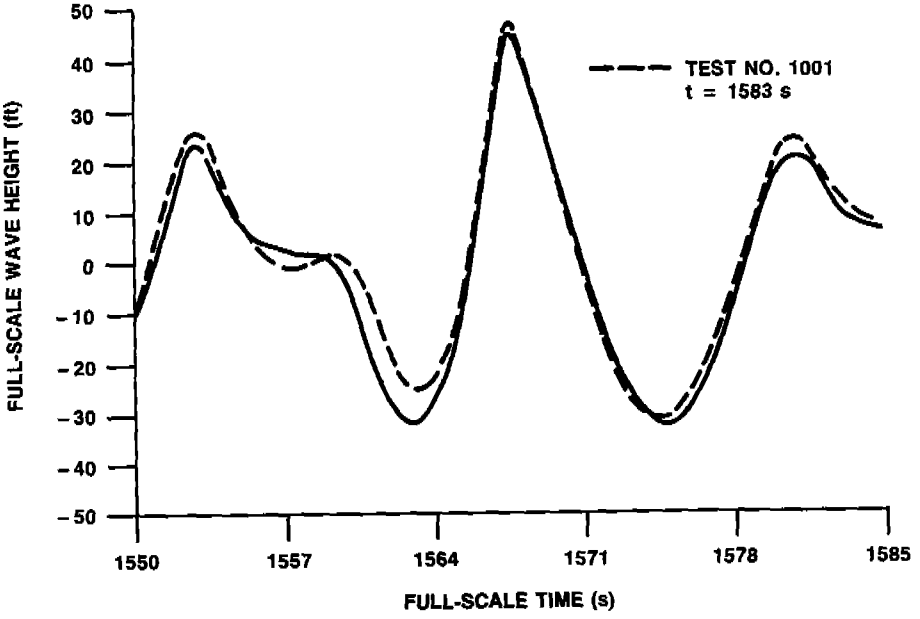

Fig. 27. Comparison of Waves of Highest Elevation/Amplitude Ratio from A.O.C. Test Runs 1001 and 2000.

rather than nonlinear equations of motion. The time series realizations generated consisted of 10 statistically independent samples which have been treated here as one large sample as in the case of the ship response simulation. The number of wave events associated with this combined output is substantially greater than that from the half-hour of hurricane wave data (approximately 1112 vs 211) which helps to define the statistical characteristics of the modeled seaway in a more complete manner than the natural seaway. It could, of course, result in the largest waves in the former being somewhat higher than the latter.

Figure 28 shows the combined linear and nonlinear times series for Sample 9 as well as a separate trace for the quadratic constituent so that its time-series character can be examined. Because the primary effect of this constituent is to raise and flatten wave troughs and raise and steepen wave peaks, it must also steepen and elevate the waves. particularly the largest ones. The influence of the quadratic constituent on the shape of the wave spectrum is relatively small as shown in Appendix E.

Results of HACYM analysis of the combined ten sample time series are shown in Figure 29. The probability density distributions of maxima and minima of Figure 29(b) reflect relatively modest nonlinear behavior. Beyond about 2σ the distribution curves show some irregularity for reasons which are not immediately apparent. The MVDAE curve of Figure 29(c) exhibits less tendency toward nonlinearity than the superimposed distribution curve from the hurricane Camille wave data while the probability density distribution curves of 29(d) are approximately as symmetric as in the HACYM analyses of Section 3.0.*

Time series wave events of maximum amplitude which are identified in Figure 30(a) are shown in Figures 30(b), (c), and (d). Of the three candidate wave events of intermediate elevation/amplitude ratio, that having the steepness wave front was selected for characterization. Because of the increased plotting scale compared to Figure 28, the influence of nonlinear wave-wave interaction is more evident. These waves are compared parametrically in Table 3 to those previously obtained from hurricane Camille, Figure 20.

Table 3. Characterization of Largest Waves in Numerical Model.

Nonlinear Numerical Waves				Camille Waves			
H_d (ft)	T_{H_d} (s)	e/a	$\frac{H_d/T_{H_d}^2}{(ft/s^2)}$	H_d (ft)	T_{H_d} (s)	e/a	$\frac{H_d/T_{H_d}^2}{(ft/s^2)}$
63	3.5	−0.03	5.14	63	4.60	0.14	2.98
67.5	4.6	0.20	3.19	65	4.80	0.32	2.82
62	3.0	0.32	6.89	65	4.40	0.48	3.36

* Differences in the respective MVDAE curves as low values of σ are due to slight differences in defining the mean values of the respective time series.

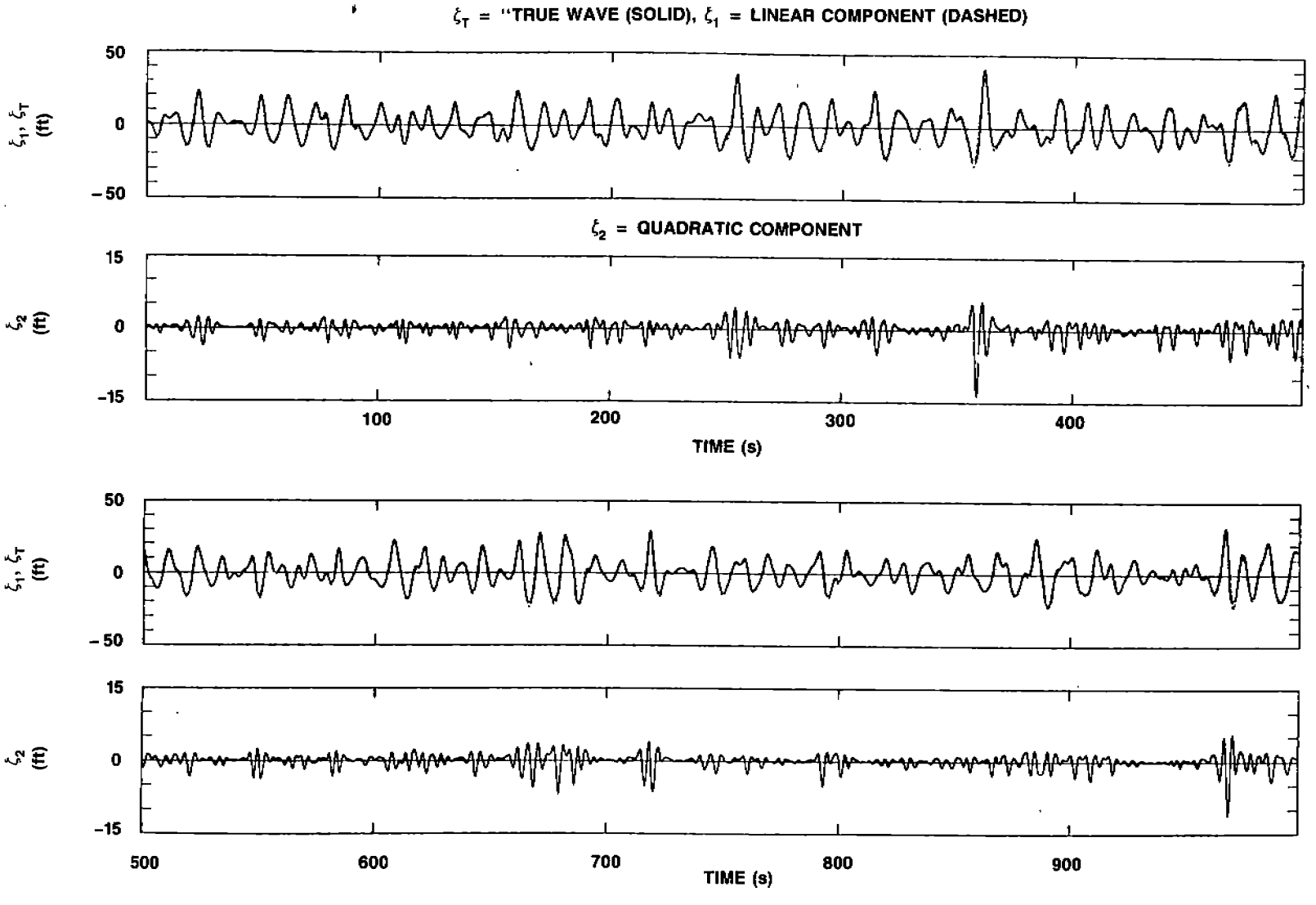

Fig. 28. Simulated Time Series of Numerical Model of Nonlinear Random Seaway - Camille 1500-1530 hrs (Sample 9).

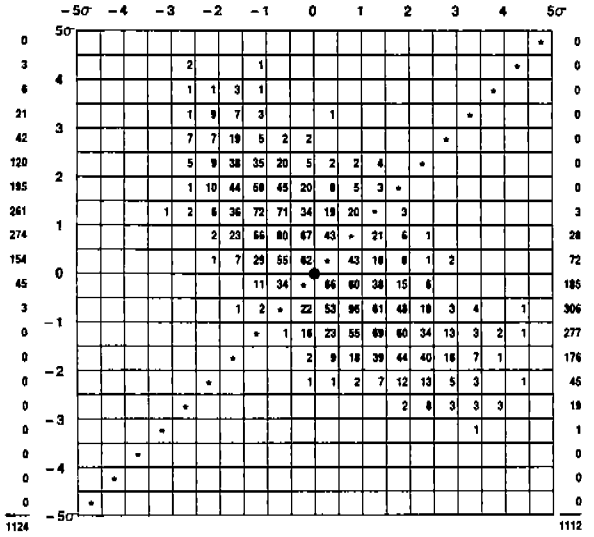

Fig. 29a. Half-cycle analysis.

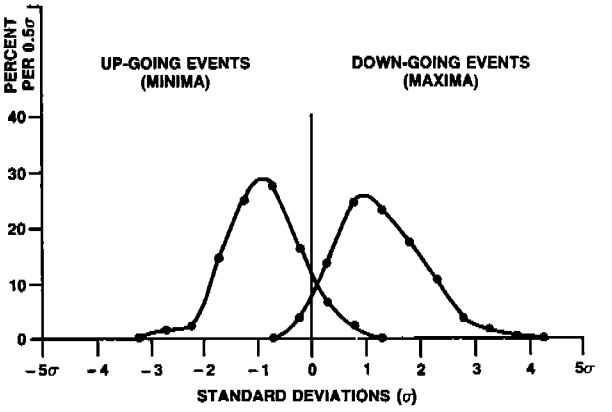

Fig. 29b. Probability density distribution of maxima and minima.

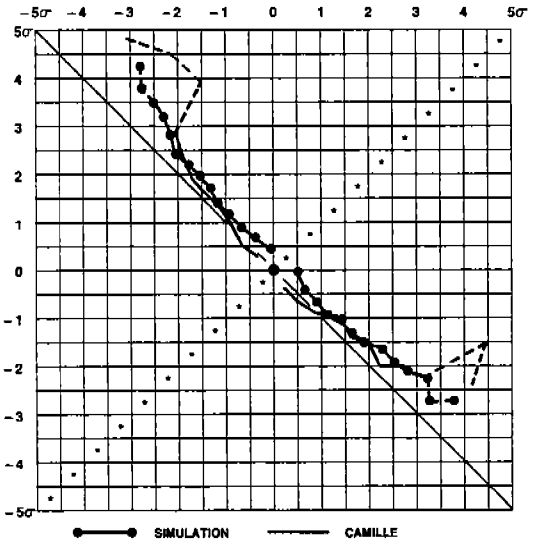

[---DENOTES LESS THAN 5 EVENTS AVAILABLE TO DEFINE MEAN.]

Fig. 29c. Mean value distribution of amplitude events.

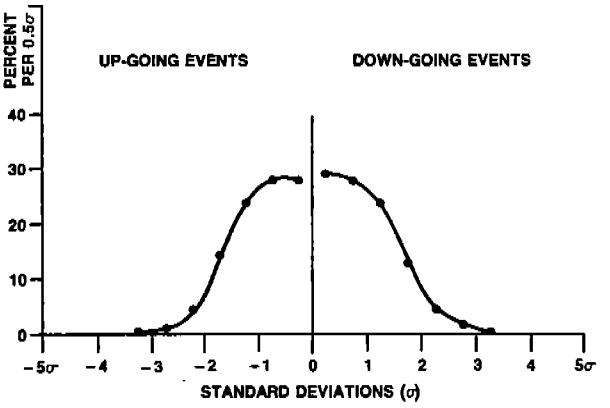

Fig. 29d. Probability density distribution of amplitude events.

Fig. 29. HACYM Analysis of Numerical Model of Nonlinear Random Seaway — Camille 1500-1530 Hours.

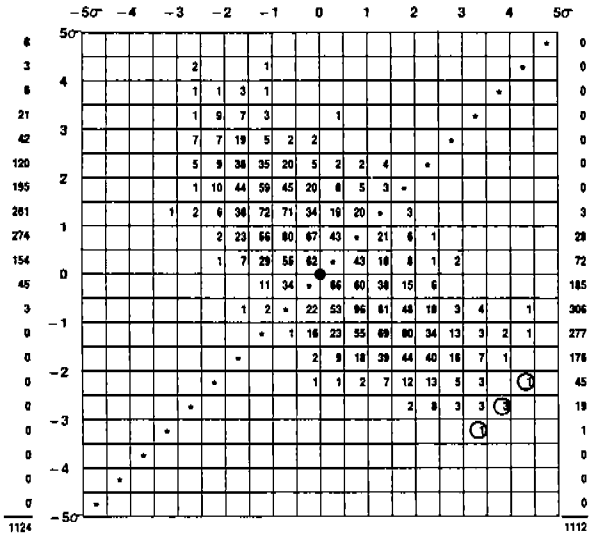

Fig. 30a. Identification of highest waves.

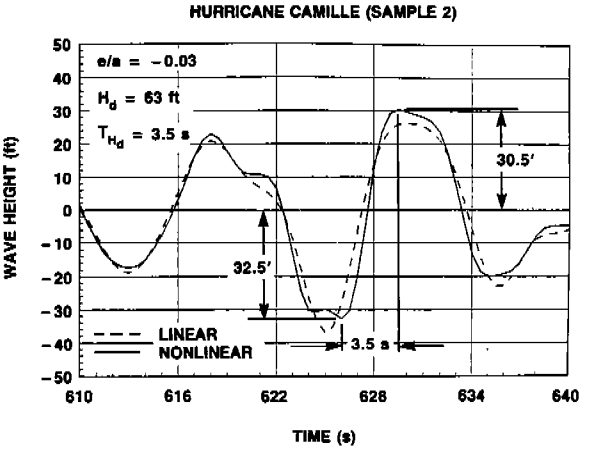

Fig. 30b. Lowest elevation/amplitude ratio.

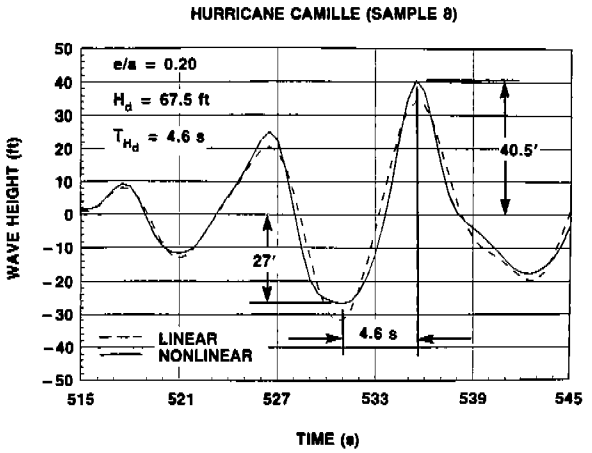

Fig. 30c. Intermediate elevation/amplitude ratio.

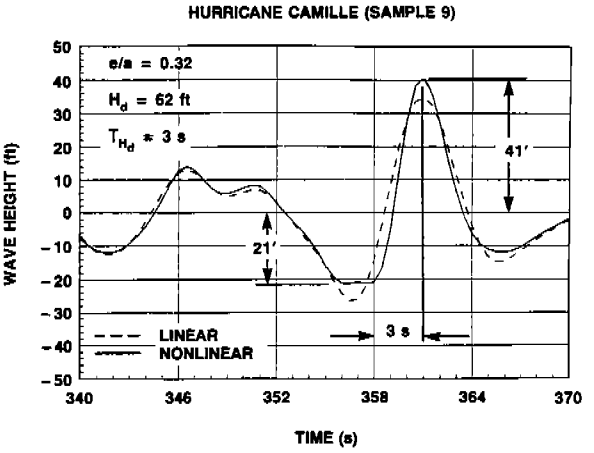

Fig. 30d. Highest elevation/amplitude ratio.

Fig. 30. Time Series Characteristics of Highest Waves in Numerical Model of Nonlinear Random Seaway — Camille 1500-1530 Hours.

Aside from the generally lower values of elevation/amplitude ratio for the numerically modeled waves (which apparently reflects the comparative trends of Figure 29(c), the most striking difference in the two sets of waves lies in the greater parametric steepness of the numerical waves. For characterization purposes, a value of the front face steepness parameter H_d/Th_d^2 can be obtained from the following expression:

$$\frac{H}{L} = \frac{1}{1.1 \times 5.12 \times 4} \left(\frac{H_d}{Th_d^2} \right)$$

Here a wave height to length ratio is postulated for a regular wave of height H_d and period $2Th_d$. The linear estimate of wave length in English units, $L = 5.12T^2$ is increased by a factor of 1.10 to account for second order wave steepness effects on wave phase velocity. A nominal value of H/L = 1/7 will be taken as an estimate of a physical upper limit of wave steepness. In the case of the numerical wave having an e/a ratio of 0.32, the H/L value=6.89/22.53=1/3.27. The comparable Camille wave has an H/L value = 3.36/22.53 = 1/6.7. For the wave having the lowest e/a ratio we find the numerical wave has an H/L ratio of 5.14/22.53 = 1/4.38 while for the corresponding Camille wave H/L = 2.98/22.5 3 = 1/7.56. It thus appears that the steepening of the linear waves evident in Figures 30(b), (c), and (d), can result in unrealistic front face steepness apparently due to a lack of wave breaking when front face steepness would call for it.

This finding should not be construed as suggesting that numerical modeling of breaking waves is incapable of modeling a steep seaway, but rather that "off the shelf" wave-wave interaction theory has important limitations as applied to a hurricane driven seaway.

7.0 OVERVIEW OF RESULTS AND RECOMMENDED DEVELOPMENT INITIATIVES

The purpose of this section is to review the objectives of the study and the results of the preceeding sections to determine the extent to which they were fulfilled. Following this, development initiatives are considered with respect to (a) additional seaway characterizations required for structural design of ships and offshore platforms in extreme seas and (b) the determination of critical loads and motions for these same structures.

The prospectus for this study which is contained in Section 1.0 calls attention to the fact that methods and analytical expertise exist for linear, Gaussian seaway modeling but that there is evidence that dangerous waves occur which may not be accounted for by such modeling and that this could warrant extensive changes in design and simulation procedures. It recommended in particular that the study pursue the analysis of wave characteristics in extreme seas:

(1) Developing further the techniques for identifying the special characteristics of extreme waves from storm records, and

(2) Developing alternative statistical or deterministic wave treatments which can be utilized expediently in testing, simulation, and analysis schemes.

Before reviewing the results of Section 3.0 thru 6.0 as they relate to these objectives, it is important to note the general limitations of the approach which was taken in satisfying them. First of all, the study has employed "off-the-shelf" methods and simulation data. Thus, the previously established HACYM method of time series data analysis which had an apparent but unproven ability to detect nonlinear random processes was investigated further with respect to this capability. The simulation used to assess its capabilities was a nonlinear mathematical ship response model previously developed by Dalzell[3]. Secondly, results of previous HACYM analyses of hurricane Camille wave height time series data were used to demonstrate for the first time the efficacy of the mean value distribution of amplitude events (MVDAE) in detecting nonlinear characteristics of such a seaway. While time series data from a seaway of extreme parametric steepness was available for analysis, comparable data for a seaway containing episodic waves (see Table 1) was not analyzed for lack of time series data from such a seaway.

The towing tank wave making experiments also employed hurricane Camille wave data for the same reason. As far as wave making capabilities were concerned these experiments employed state-of-the art random wave making procedures at two well qualified commercial facilities. No consideration was given to generating a seaway of more or less linearity.

Numerical modeling of the hurricane Camille seaway employed second order wave-wave interaction theory which contained no constraints on wave steepness so that breaking wave phenomena associated with such a seaway was not replicated. As in the case of the towing tank wave making experiments, consideration of possible improvements was set aside until short comings of the available method had been identified.

Overview of Results

The results of HACYM analysis of the output of Dalzell's nonlinear ship response model (Task 1) demonstrated the ability of the method to identify a nonlinear random process. In particular the MVDAE, which was formed here for the first time, was found to be especially useful. At the same time it was clear from the results that nonlinearity was most evident for the quadratic constituent of the associated functional polynomial model. The influence of the cubic constituent in contrast was most evident in the tendency of the HACYM event distribution to stretch at its extremities. The range of the normalized response variable, for example, nearly doubled in the simulation at hand, i.e., from about $\pm 5\sigma$ (linear) to $\pm 10\sigma$ (linear + quadratic + cubic constituents) for a fourfold increase of input excitation to the model.

Using an approximation to the Zero Up/Down Crossing method of wave data analysis it was shown that this commonly used method can lead to erroneous conclusions or inferences regarding the linearity of the wave height process. HACYM analysis on the other hand provides a comprehensive characterization of the same data especially with regard to the assessment of nonlinearity.

Although it provides a clear indication of the existence of nonlinearity in a random process, HACYM analysis does not provide an equally clear indication of its unique characteristics. In order to help overcome this limitation, time series extractions of the largest amplitude events in the data sample were used to identify the character of these events. This approach was also employed in the analysis of hurricane Camille wave data and associated towing tank and numerically modeled waves.

HACYM analysis of hurricane Camille wave height data from 1000 to 1618 hours revealed that the nonlinearity of the seaway, as evidenced in the MVDAE curves, increased as the center of the storm approached the measurement site. Comparison of this nonlinearity with average wind velocity suggested that the two were correlated in this storm with an apparent time lag of about 30 minutes. These findings suggested that HACYM analysis methods are suitable for assessing the changing nonlinearity of wave height time series data. They further suggest that it is essential that continuous as opposed to sampled data be provided and that wind or any other related parameter be continuously correlated with the wave data in order to adequately characterize the nonlinear process. Inasmuch as the majority of measured wave data today are provided as sampled wave spectra (e.g. 20 minute data samples taken anywhere from once every hour to every three hours) this requirement represents a significant departure from conventional practice. Moreover, any departures in the time series data from accurately measured values of wave height vs time could easily result in erroneous indications of linearity or nonlinearity.

It is important to note again that only characterizations of Camille wave height data have been provided for lack of similar data from severe winter storms which have been found to produce the episodic waves of Table 1.

The towing tank wave making experiments revealed that much of the nonlinearity in the original time series hurricane Camille wave data (1500-1530 hours) was recaptured when the measured wave spectrum was modeled. Each of the towing tank facilities involved appeared to have some difficulty, however, in attaining all of the desired energy density in the high frequency portion of the spectrum. At the secondary (downstream) probe this discrepancy was increased somewhat over that at the primary probe. Generally the elevation/amplitude ratios of the largest waves in the hurricane Camille time series was greater than that of the towing tank waves. Because of the small data samples necessarily involved, this observation must be regarded as subject to confirmation by additional experiments and especially by analysis of additional wave height data from severely breaking seas. The time series character of a deterministically generated plunging breaker at the U.S. Naval Academy Hydromechanics Laboratory was found to be quite similar to that for the hurricane Camille wave having the highest elevation amplitude ratio in the interval 1500-1530 hours. This suggests that if plunging breakers were not present in towing tank random seaways when full-scale seaway data indicates that they should be, discrete severely breaking waves could alternatively be formed by similar deterministic procedures in order to evaluate associated model response characteristics. In addition, wave data from one experiment (Figure 27) showed that a deterministically generated random seaway could reproduce a particular extreme wave event at a known location in a towing tank. Both of these findings suggest

that with respect to the modeling of steep breaking seaways, towing tank wave making has potential capabilities beyond those demonstrated in the subject experiments.

Computer modeling of the hurricane Camille seaway (1500-1530 hours) using existing wave-wave interaction theory produced a wave height time series which exhibited somewhat less nonlinearity in the MVDAE curve than the actual seaway. The manner in which the large linear waves in the time series were modified by wave-wave interaction appeared to be reasonable, i.e., wave troughs were raised and flattened, crests were elevated and the front face of the waves steepened. A parametric comparison of front face steepness, however, indicated that two out of three of the largest waves were much steeper than the largest waves in the Camille time series. It is believed that since the wave-wave interaction theory employed did not provide for wave breaking, wave front steepness could reach unrealistic values in this particular simulation.

This result demonstrates the need for including breaking wave characteristics when modeling a seaway as steep as that of hurricane Camille near its center. It also demonstrates that HACYM analysis of time series wave height data is insufficient for identifying all of the important nonlinear qualities of the waves. Extraction and characterization of the largest half-cycle events, helps to overcome this deficiency due in part to the fact that the influence of non linearity is most pronounced for the largest waves.

Based upon the foregoing it is concluded that: (a) HACYM analysis together with time series data extraction is an effective method for identifying important nonlinear qualities of time series wave data; (b) wave making in towing tanks which replicates the original wave spectrum tends to produce model scale time series waves of similar nonlinearity to the original waves and, (c) wave-wave interaction theory apparently requires incorporation of a wave breaking mechanism when used to model a seaway of extreme nonlinearity.

Given these findings it is believed appropriate to place primary emphasis in the near future on obtaining and analyzing time series wave height data from extreme seas. It is suggested that neither physical or numerical modeling can logically proceed in the absence of such data. Physical modeling appears to offer a generally acceptable basis for investigating nonlinear behavior of waves and model responses without major development activity.

Recommended Development Initiatives

An important aspect of identifying extreme seas to be considered in the design of dynamically responding structures is the need for identifying seaway and ship (or platform) characteristics which in combination result in critical loads or motions. In this context the phrase "extreme seas" takes on a meaning which is more complex than is often considered. From an engineering point of view is it believed to be self evident that this complexity must be accepted if reliable

structures are to be designed except in those cases where empirical design criteria have been found thru continuing experience to achieve this result.* Situations requiring a rational determination of critical loadings most often concern operations in extreme seas and/or highly nonlinear behavior in less than extreme seas. For purposes of recommending development initiatives this discussion will relate first to Extreme Seas in which load and motion problems are generally apparent and then to Critical Seaway/Operation/Response Characteristics where knowledge of seaway characteristics is insufficient for the identification of critical loadings.

Extreme Seas:

The envelope of extreme combinations of significant wave height and modal frequency shown in Figure 2 was derived from NOAA buoy and offshore platform wave spectrum measurements, Buckley[5]. This envelope and the characteristic shapes of the point spectra used to define it provide a broad, parametric definition of extreme seas. In view of the apparent correlation between the nonlinearity of hurricane Camille time series waves, (Figure 14), and the proportion of high frequency wave energy in the associated spectra, (Figure 16) it is evident that the parametric variables Hm_o and f_p associated with this envelope will not necessarily reflect the elevated and breaking character of a seaway which can develop in the presence of strong, gusty winds.

Given that parametric descriptions of extreme seas are now available, it is believed appropriate to state that emphasis should now be placed on acquiring and analyzing time series wave height data which will permit characterization of distinctive and dangerous waves in extreme seas. While the HACYM method as illustrated here in Sections 3 and 4 is believed suitable for identifying such waves in time series data, it is not widely known or used. Other problems exist as well. The majority of wave data published at this time are presented in wave height spectral density format which does not permit identification of the original time series data from which the spectrum was determined. In some cases, such as data from NOAA buoys, time series measurements were not made in the first place. Moreover, spectra are normally determined from sampled measurements, e.g., 20 minutes of data obtained anywhere from once an hour to once every three hours or more. Examination of Figure 14 reveals that the nonlinear character of the hurricane Camille seaway was sufficiently variable that only continuous data was suitable for HACYM analysis. Moreover, the companion plots of wave spectra and average wind velocity vs time suggest that there is a relationship between changing wind strength, the nonlinear character of the MVDAE curves and concurrent changes in wave spectrum shape. While the data at hand are insufficient to establish the particular nature of this relationship, it is believed evident that HACYM analysis of time series wave data should be accompanied by analysis of concurrent time

*This leads to an important secondary problem of identifying circumstances in which empirical criteria are not reliable. This matter is generally resolved on the basis of unusual overall geometry or anticipated service experience which suggest that empirical criteria will do not apply to the situation at hand.

series wind velocity (among other variables) in order to obtain a more complete understanding of the unique characteristics of storm driven waves and of the wind conditions which produce them.

From a date acquisition and analysis point of view, a number of charges are required in current practice in order to accomplish this. The first development initiative recommended in Table 4, is intended to provide documentation for utilizing the HACYM method together with a PC computer program which will enable public or private investigators to proceed with time series wave data acquisition and analysis in HACYM format with a minimum of development time and cost.

The second initiative is directly related to the first and calls for a survey of those investigators who now engage in, or can gather time series wave height data so that the documentation and programming associated with the first initiative will be as effective.

The final initiative recommended here under the Extreme Seas heading anticipates the thrust of the discussion which follows, i.e., that knowledge of seaways which are less than extreme will also be required for identifying extreme loads and motions of ships and platforms, and further that the seaway information should be assimilated into Design Wave Climates so as to permit the assessment of extreme loads which reflect operation in associated general ocean areas. Some initial steps in accomplishing this initiative have been taken as reported in Buckley[11].

Critical Seaway/Operation/Response Characteristics:

The discussion which follows applies primarily to buoyant platforms and ships rather than fixed offshore platforms. Moreover, because the inherent complexity of evaluating seaway induced loads and motions arises largely due to additional variables such as speed, heading, and loading primary consideration will be given to problems associated with ships for illustration purposes.

In dealing with seaway loadings which are critical because of a particular combination of seaway, speed, heading and displacement conditions, it is generally not obvious as to which particular combination might be critical for a particular component of ship structure so that the identification of critical circumstances of loading is a significant problem. Heavy weather damage surveys of ships reveal that wave impact loadings are a dominant cause of damage and so it is implicit that nonlinear loadings are likely to be involved. While less obvious, it is possible that nonlinear ship motions can be involved. From this it is presumed that (a) scale model testing in waves as opposed to numerical (i.e. computer modeling) should be given primary consideration at this time and (b) HACYM analysis of load and motion data might prove to be of value where nonlinear behavior is suspected.

These matters, for several reasons, can be examined on an ad hoc basis using data available from operation of SL-7 high speed container ships. First of all, because of a major research program sponsored by the Ship Structure Committee (see Stambaugh and Wood[12]) full-scale load and motion data from a variety of heavy seas operation are available for analysis. Second, several types of heavy weather damage were associated with this class of ship which it will be shown can be related to the full-scale motion data measured in high seas. The first of the heavy

Table 4. Recommended Development Initiatives.

A. Seaway Characteristics:

1. Standardized HACYM wave data analysis methods and provide a PC code for its implementation.
2. Survey potential time-series wave data sources including NOAA and offshore platform operators.
3. Establish design wave climates.

B. Seaway/Operation/Response Characteristics:

1. Survey available test tank wave making capabilities with respect to extreme seas and episodic waves.
2. Survey free-running model operations and existing/potential test sites for determining critical loading conditions.
3. Summarize full-scale SL-7 load and motion data. Identify critical loading/motion conditions.

C. Seaway Loadings

1. Plan research program to establish water impact load criteria.

weather damage problems involved hull girder lateral bending loads forward which occurred when the ship was operated at high speed (approximately 30 knots) at a bow seas heading in rough seas. An example of this type of damage is reviewed in Buckley[1] (Section 3.2, pg 16 and Appendix A, Case 28). A particular damage incident was summarized as follows:

> "In this instance the SL-7 class container ship S.S. SEA-LAND GALLOWAY experienced damage in a relatively moderate seaway of 8-12 ft seas, 13-20 ft swells, with local winds of 30 to 40 knots. Discussion of SL-7 class heavy weather damage experience with a naval architect familiar with the ship revealed that it had been proceeding at approximately 30 knots when it encountered an unusually large long-crested wave in the seaway which could be seen approaching from a distance, but which could not be avoided nor the ship slowed substantially before it was encountered. The resulting bending moment on the forward portion of the hull girder was sufficiently large as to cause paint to flake off locally due to plastic tensile strains on one side of the hull while on the opposite side local "crinkling" of the plating occurred. In addition to this information, an unpublished list of extreme scratch gage readings by ship and date furnished by Teledyne Engineering Services revealed that the incident in question produced the 4th highest hull girder scratch gage strain reading recorded on this class of ship out of a total of 36,011 individual readings."

The reason that the ship could be operated at high speed in rough seas was its freedom from deck wetness under these conditions as evidenced in an investigation later conducted by O'Dea[13] using a towed 1:60 scale model. During the course of this investigation it was observed that:

> "The design of the bow flare on this hull proved to be very effective in preventing green water from boarding over the stem or sides. Even at thirty knots in Sea State 7 bow seas, where spray-type wetness occurred frequently, shipping of water to a measurable depth on deck was a rare event. This was true despite the fact that relative motion commonly exceeded the freeboard, as indicated by clipping of the relative motion signals. In fact, visual observation of this condition often indicated the simultaneous occurrence of a spray sheet coming directly over the bow and a wave elevation near stations 2 or 3 clearly above the level of the deck but being pushed away from the deck by the flared bow sections. Two photographs of this effect are shown in Figure 15. An extended series of experiments was run in the condition mentioned above (Sea State 7, 30 knots, Bow seas), corresponding to one and one-half hours full scale, and in this time period only one occurrence of measurable depth of water on deck occurred."

The relative freedom from deck wetness later necessitated reballasting the model "to a trimmed water line which reduced the freeboard forward by about 40 percent" in order to cause deck wetness which was an objective of the test program.

The second of the heavy weather damage problems was somewhat anomalous in view of the tendency toward dryness in rough seas since this one involved deck wetness and damage forward while hove-to in very high seas. An instance of this type of damage is summarized in the Deck Log abstract of Figure 31, with the incident in question occurring during the 12-16 hours watch, Buckley[1] (pg 25). An incident which occurred under somewhat similar circumstances but which did not result in reportable damage is described by Buckley[1] (pg 32) as follows:

> "On 19 December 1973, the SEA-LAND McLEAN proceeded down the English Channel in gusty winds of 30 to 35 mph. As it moved westbound into the North Atlantic the wind veered from south to west and finally northwest. The wind velocity dropped early-on as did the barometer so that at 0840 hrs (GMT) the wind was blowing 10 mph from the west with 5-foot waves at a barometric pressure of 28.68 inches of mercury. Two hours later at 1050 hrs the barometer had dropped slightly to 28.66 inches of mercury, but the wind had risen to 50 mph with an observed wave height of 25 ft. In successive two-hour intervals the wind rose to 70, 80, 90, and 100 mph (87 knots). At 1510 hrs with the wind at 80 mph, the ship was hove-to and remained that way for approximately 6 hours at which time a violent slam occurred (the peak stressing case), which prompted the captain to turn the ship around and run before the storm."

This stressing case produced a peak to peak midship bending stress of approximately 54 ksi which is clearly of an extreme nature. Insight into the apparent paradox of freedom from deck wetness at high speed in high seas and a pronounced deck wetness problem when hove-to in extreme seas is available from HACYM analyses of full-scale SL-7 data performed originally by Band, Lavis and Associates (BLA)[14]. In this investigation pitch, roll and midship bending stress data were analyzed for portions of two voyages. One interval (Voyage 59W, Interval No. 20) corresponded to bow seas operation at 29.7 knots in rough seas. The other (Voyage 29W, Interval 41) contained the extreme bending stress event described above. Figures 32, 33 and 34 contain MVDAE curves determined from the results of HACYM analyses by BLA of pitch angle, midship bending stress and roll angle respectively with data from the two intervals placed side by side in each figure for ease of comparison. It is apparent in Figure 32 that pitch response was nonlinear in each interval but of opposite sign with the larger pitch angle response occurring in the interval of hove-to operation. The nonlinear bow-up motion of Figure 32(a) combined with the protective action of the bow flare described above resulted in substantial freedom from deck wetness. The nonlinear bow-down pitch motion of Figure 32(b) on the other hand was conducive to deck wetness as suggested in the Deck Log entries for 1200-1600 and 1600-2000 hours of Figure 31 (for a different SL-7 ship and voyage). The first finds the vessel "---pitching deeply in a very

1/16/74

00-24 0033 Texel L/V abeam 130°, 8.2.0′ cast. Vessel pitching mod. to easily in a rough to mod. SW'ly sea and mod. avg. swell. Weather moderating after 0230. Shipping seas over fore dk and hatches. Routine inspections.
Bar. 30.08 Wind SW×W 5 (19-29 kn)

04-08 0800 Moderate to rough SSW'ly sea. Vessel taking light seas over bow and main deck. Heavily o'cast. Routine inspections.
Bar. 29.84 Wind SSW 5-6 (19-31 kn)

08-12 0759 Greenwich buoy to port 5.7 mi. 0842 Owers L/V to st'bd 9.6 mi. 0927 St. Katherines Pt. to st'bd 11.7 mi. off c/c to 269° g&t 1021 Anvil Pt. to st'bd 11.8 mi. 1058 Bill of Portland to st'bd 6.9 mi. off 1100 engine room given 90 min. notice to slowdown. Partly cloudy with rain, passing squalls. Vessel pitching mod. in a rough SW'ly sea, taking heavy spray across decks. Routine inspections.
Bar. 29.46 Wind SW 7-8 (32-46 kn)

12-16 1222 r/s 60 rpm. Approaching Berry Head, maneuvering to let Pilot off vessel. 1255 Pilot Roggen away in launch p/s. 1308 increase to 80 rpm. 1323 increase to 90 rpm. 1327 gyro 200°, 1342 reduce to 80 rpm. to ease vessel in heavy seas and increasing wind. 1405 r/s 75 rpm. 1425 r/s 60 rpm. 1449 r/s 55 rpm. 1451* r/s 45 rpm. O'cast vessel rolling mod. and pitching deeply in a very high rough WSW sea and very high and steep swells. Shipping seas over decks and hatches. Routine inspections.
Bar. 29.42 Wind WSW 11 (64-73 kn)

16-20 1648 c/c 240° gyro. 1838 r/s to 30 rpm. 1851 r/s to 25 rpm. 1900 i/s to 30 rpm. on port engine. Heavy wind gusts, short, deep and heavy swells. Vessel pitching deeply at times, taking seas over bows, hatches, and main deck. Routine inspections.
Bar. 29.75 Wind W×N 11 (64-73 kn)

20-24 Vessel hove to in storm conditions, mountainous seas. Master conning. Partly cloudy good vis. Vessel proceeding on 30 rpm. port eng, 25 rpm. stbd engine to maintain steerage way. Pitching and rolling heavily at times in a very rough NNW'ly sea. Taking heavy spray across weather decks.
Bar. 30.21 Wind 8-9 (39-54 kn)

*Entries this date Jan. 16, 1974
1450 Vessel encountered mountainous swell, shipped heavy sea over foc'sle head from a direction of approx. 15° on the port bow. Tension winch control stations torn off foc'sle head, other damage to be ascertained when access to foc'sle head is possible. In ships office, port bent out, office flooded. Rooms #31, #32 on 01 level, windows broken, rooms flooded. Room #33 window bent at hinges, some salt water damage. Room #13 at 02 level two windows bent at hinges some salt water damage. Rms. #31, #32, Section of overhead, paneling approx. 5′×5′ broken off in each room. 1500-1630 Lower mooring station fwd pumped dry with ships educter, water entered through holes in foc'sle head where bases on tension winch controls had been anchored. 1630 Open windows Rms. #31, #32 and ships office temporarily plugged with mattresses etc. to prevent further entry of sea water.

Fig. 31. Abstract of Deck Log from S.S. *SEA-LAND MARKET* in Southwest Wind Field of Winter Storm.

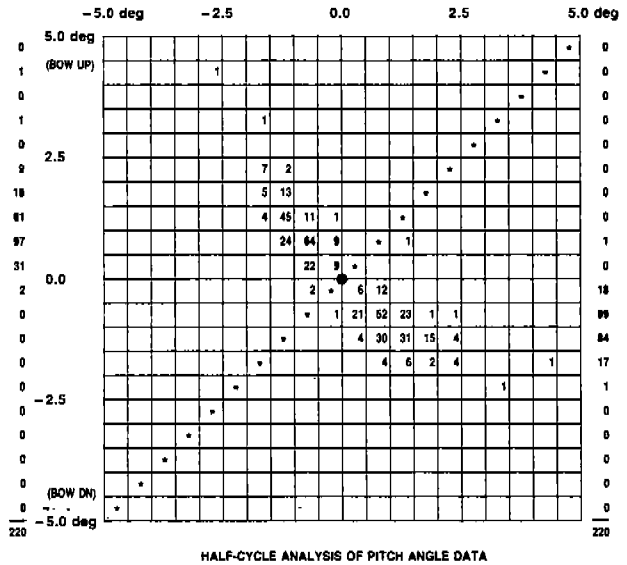

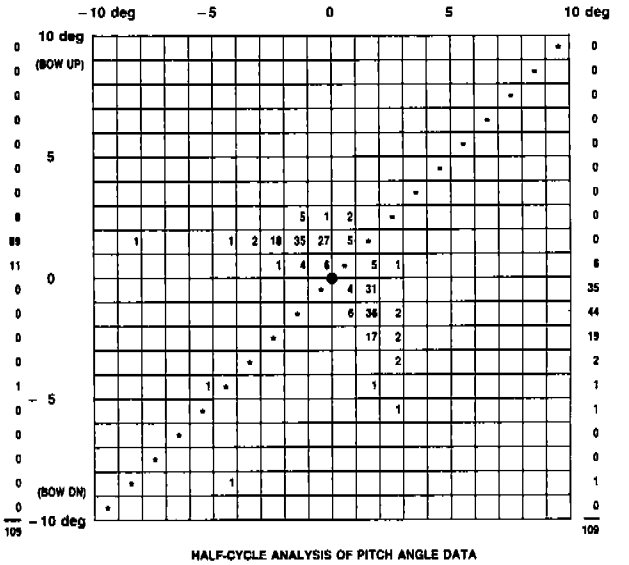

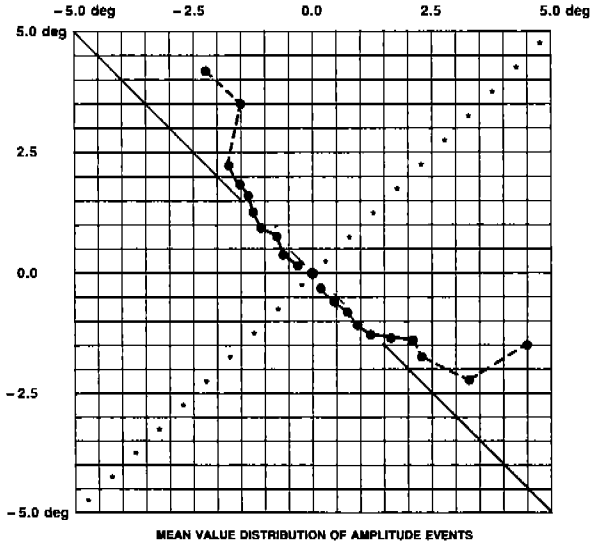

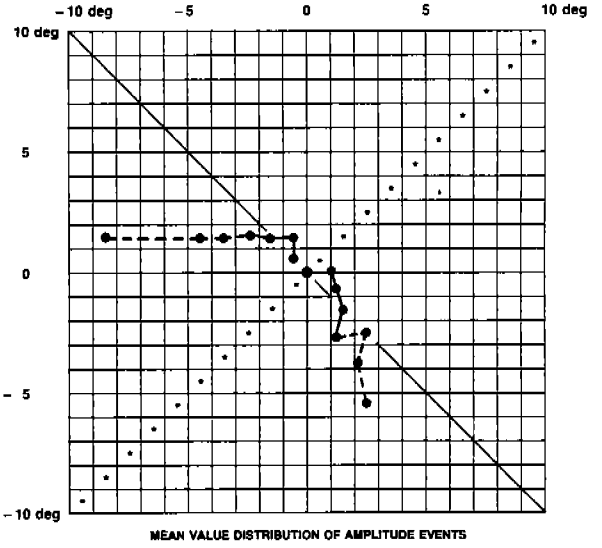

[---DENOTES LESS THAN 5 EVENTS AVAILABLE TO DEFINE MEAN.]

Fig. 32a. Voyage 59W; Interval No. 20; Speed = 29.7 kn; V_W = 45 mph; Beaufort No. 9; Seas 24° Off Port Bow.

Fig. 32b. Voyage 29W; Interval No. 41; Speed = Hove to; V_W = 100 mph; Beaufort No. 12; Head Seas.

Fig. 32. Half-Cycle Analysis of SL-7 Pitch Angle Data for Two Severe Operating Conditions.

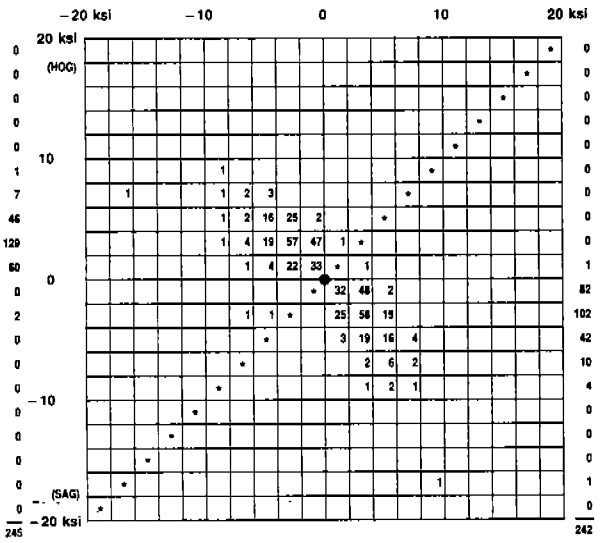

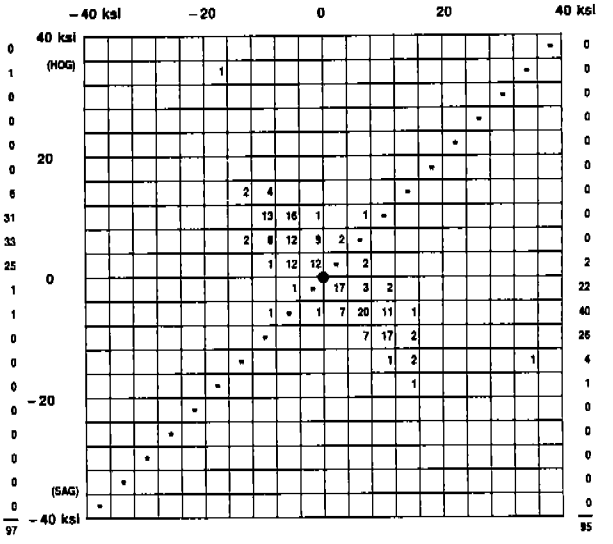

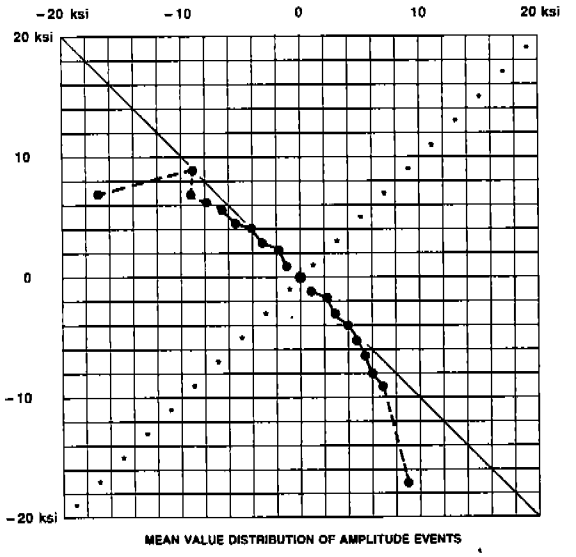

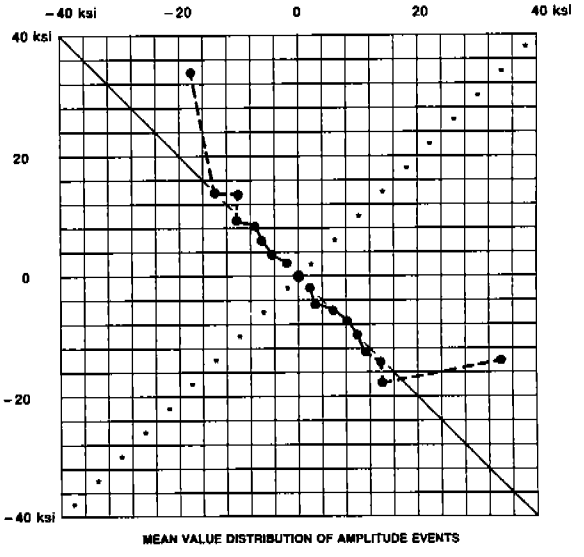

[---DENOTES LESS THAN 5 EVENTS AVAILABLE TO DEFINE MEAN.]

Fig. 33a. Voyage 59W; Interval No. 20; Speed = 29.7 kn; V_W = 45 mph; Beaufort No. 9; Seas 24° Off Port Bow.

Fig. 33b. Voyage 29W; Interval No. 41; Speed = Hove to; V_W = 100 mph; Beaufort No. 12; Head Seas.

Fig. 33. Half-Cycle Analysis of SL-7 Midship Bending Stress Data for Two Severe Operating Conditions.

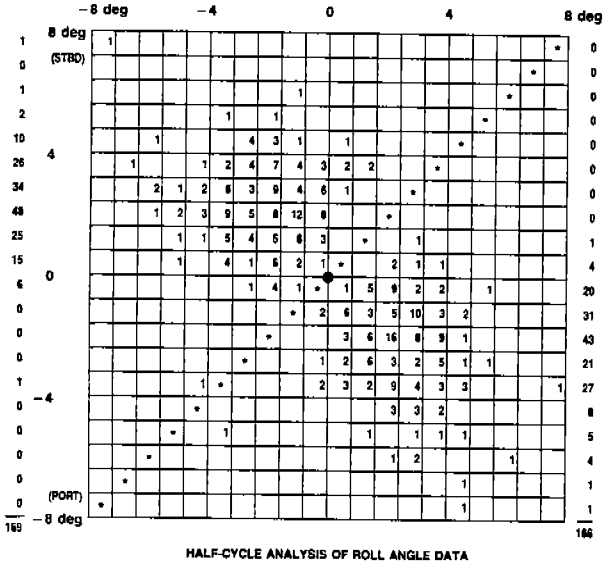

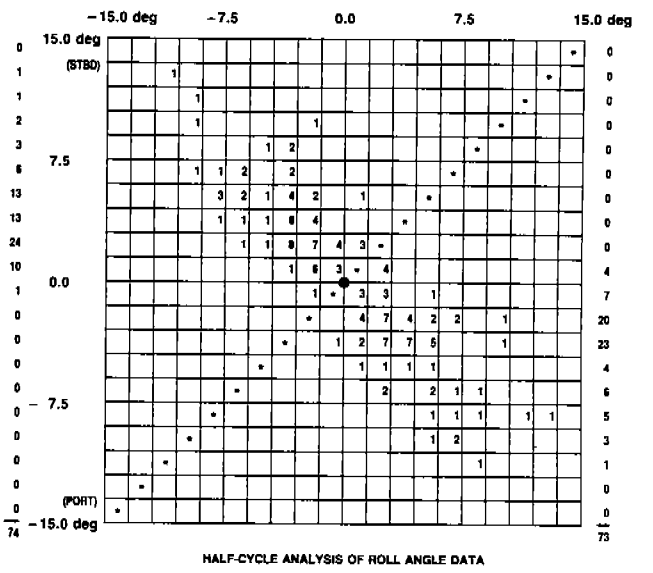

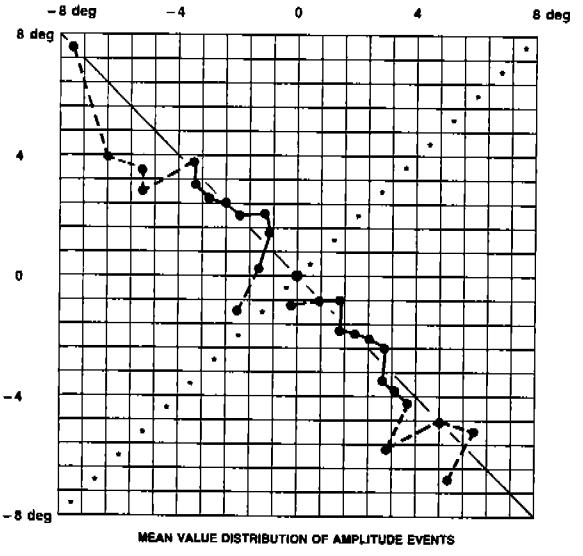

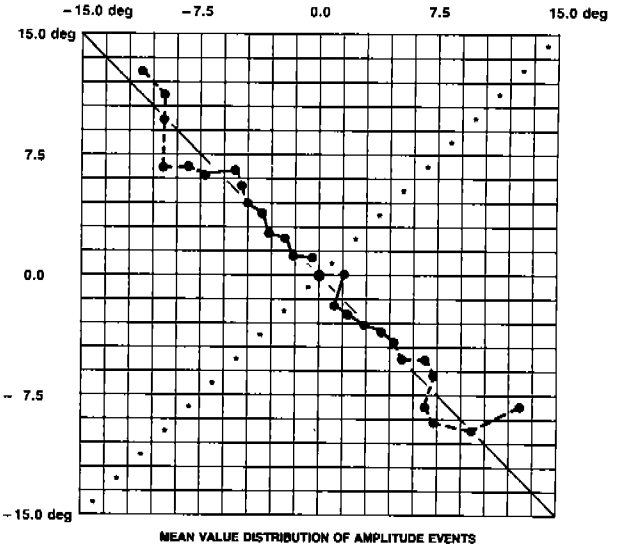

[- - - DENOTES LESS THAN 5 EVENTS AVAILABLE TO DEFINE MEAN.]

Fig. 34a. Voyage 59W; Interval No. 20; Speed = 29.7 kn; V_W = 45 mph; Beaufort No. 9; Seas 24° Off Port Bow.

Fig. 34b. Voyage 29W; Interval No. 41; Speed = Hove to; V_W = 100 mph; Beaufort No. 12; Head Seas.

Fig. 34. Half-Cycle Analysis of SL-7 Roll Angle Data for Two Severe Operating Conditions.

high rough WSW sea---- and the second finds the "Vessel pitching deeply at times, taking seas over bows, hatches, and main deck." The foredeck and deckhouse damage of the 1200-1600 hours entry is suggestive of the serious nature of the deck immersion problem under these conditions as well as the probable cause of the slam loading of Interval No. 41 which was involved in the extreme midship bending stress incident of this interval.

Results of tank tests of an SL-7 model in the early stages of design of this ship suggested that the favorable pitch and foredeck dryness characteristics of Figure 32(a) were due to hull form forward and that ship masters might later operate the ship at high speed in high seas. This proved to be the case with severe hull girder lateral bending stresses forward resulting during bow seas operation as previously noted. The bow-down motion of Figure 32(b) was also detected during these model tests and was attributed to the Vee hull form aft associated with the twin screw propulsion system and after hull displacement requirements.

The MVDAE curves of Figure 33 show significant nonlinearity for maximum midship bending stress events. In the case of Figure 33(a) the origin of the slam load input resulting in the peak bending stress event is not known for certain but is believed to be due to an asymmetric bow flare slam. The nonlinear (sagging) trend of the MVDAE curve over much of the stress range (±20 ksi) is believed due to the inherent nonlinearity of bow flare dynamic loadings with wave height. The MVDAE curve of Figure 33(b) is nearly linear over much of the stress range (±40 ksi) until a major hogging stress event occurred. In this case the deck wetness (i.e., immersion) loading is significant only for a major wave encounter with the extreme stress event reflecting a dominant hogging stress peak.

The roll motion MVDAE curves of Figure 34 exhibit less consistency in their trends than either pitch angle or midship bending stress especially in the case of Interval 20 which is associated with high speed operation at a bow seas heading. This suggests that several independent causes of roll motion are involved, e.g., bow flare, midship hull form, and rudder loads. When hove-to, roll motions are larger (±15 degrees full scale vs ±8 degrees) but less complex. In each case the distribution of the largest roll motion events is "thin" which suggests that based upon the results of Task I., if functional polynomial modeling were considered, a substantial cubic constituent would be present.

The nonlinear pitch behavior of the SL-7 evident in Figure 32 is believed to be related to the apparent paradox of relative freedom from deck wetness in one extreme operating condition and quite the opposite in an other. It further illustrates the potential difficulty of identifying and quantifying operating conditions which can result in extreme loadings. Tank tests with an SL-7 model hove-to using an extreme, model scale wave spectrum taken from the measured data of Changery et al[15] as generalized by Buckley[5] should apply provided dynamic deck immersion loads can be properly scaled-up to the full-sized ship (see below). High speed, rough seas operation, however, presents more of a problem in identifying critical loads because of the need for obtaining an adequate data sample and the possible need for generating either short crested seas or a seaway containing an outlying wave conformation of uncertain time series character.

In general, a search for all operating conditions which might result in critical loadings on the structure of a ship such as the SL-7 could be very expensive and time consuming if conducted in a towing tank. For this and other reasons such a search is seldom conducted in the design of even highly unconventional ships despite the fact that heavy weather damage is more often than not related to a combination of high seas, particular operating circumstances, and unique features of the ship in question as opposed to simply a storm driven seaway of an extreme nature such as those involved in constructing the extreme boundary of Figure 2.

One possibility for conducting a comprehensive search is free-running model tests in a fetch limited wind driven seaway, Crago[16]. The prospects of a seaway of particular interest occurring at a desired scale on a particular day when the model and test crew are available to run are remote so that free-running model tests for purposes of gathering design data are regarded here as impractical. With respect to the identification of potentially critical circumstances of loading which might later be investigated in a test tank under "design conditions," free-running model tests should be considered, however. In order to provide an illustration of certain important features of free-running model tests recourse will be made to the results of capsizing tests conducted in San Francisco Bay using a 1/55 scale model of the SL-7, Oakley et al[17]. Capsizing phenomena have certain important features in common with damaging seaway induced loadings: they occur in severe seas, involve significant nonlinear effects, are subject to particular ship operating circumstances and are often strongly influenced by the unique features of the ship. Of primary importance in this instance is the fact that Oakley, et al[17] proceeded to identify three distinctive circumstances or modes which were found to lead to capsizing, see Figure 35.

Before examining their findings it is of interest to first characterize two measured wave spectra which were of particular interest in the investigation. The spectrum of Sequence [4] in their Figure 5 was integrated and found to correspond to a significant wave height of 1.165 ft or 64.1 ft full-scale (f_p = 0.057 hz) while that of their Figure 15, Sequence [3], was found to correspond to 1.50 ft or 82.5 ft full-scale (f_p 0.045 hz). Since both of these full-scale values of significant wave height lie well outside of the extreme boundary of Figure 2, the capsizings of the SL-7 model were not an immediate indication of full-scale stability deficiencies. From the point of view of identifying capsize modes on the other hand, these test conditions are of considerable interest.

Figure 35 identifies the three capsize modes which were observed. From the point of view of combined seaway/operation/response variables the modes were characterized as follows:

> "Mode 1: Low Cycle Resonance-----" The model, while operating in following or quartering seas, encounters a group of especially steep and regular waves."
>
> "Mode 2: Pure Loss of Stability-----" This usually occurs in a following sea at high speed. The model is observed to encounter one or more very steep and high waves and, with little or no preliminary rolling motion, simply loses all stability when a crest moves into the a midships position and

"By observing the capsizes and the motion picture records of them, it became clear that the attenuation of stability by the waves played a very important role in nearly all capsizes. Further, it was possible to distinguish three distinct modes of capsizing which may be described as follows.

Mode 1: Low Cycle Resonance. This refers to an oscillatory rolling motion which builds up rapidly, i.e., in two to five cycles, to a very large amplitude, culminating in a capsize.

The phenomenon appears to occur in approximately the following sequence. The model, while operating in following or quartering seas, encounters a group of especially steep and regular waves. When the crest of a wave is about amidships, the stability of the model is greatly reduced and it takes a large roll. This wave moves on past the model and a trough comes into the amidships position while the model is heeled over, resulting in sharply increased stability. This causes the model to "snap" back upright, acquiring a high roll angular velocity by the time it reaches the upright position. Another wave crest, meanwhile, is moving into the amidships position, resulting in diminished stability once again as the ship starts rolling past upright and to the other side. The ship then rolls far over to the side against a diminished restoring moment. If now another trough moves into the amidships position with the correct timing, the roll will be stopped and the model snaps upright again. This process continues until either the model capsizes or it moves out of the wave group and the motion dies down. This mode of capsize is seen to be related to the Mathieu motion instability. It results directly from the periodic stability variations experienced by the ship moving through waves and in its most pronounced form takes place at one-half the encounter frequency, thus at the first Mathieu unstable frequency.

Mode 2: Pure loss of Stability. This usually occurs in a following sea at high speed. The model is observed to encounter one or more very steep and high waves and, with little or no preliminary rolling motion, simply loses all stability when a crest moves into the amidships position and "flops" over. The essential prerequisite for this to occur is a model speed nearly equal to the wave phase velocity so that the model remains almost stationary relative to the crest for a sufficient length of time to capsize. The necessary wave would be of about the same length as the model and the height would be sufficient to immerse the deck in the crest with the model upright. This, of course, implies a high model speed since a Froude number of 0.4 is required for the model speed to be exactly equal to wave speed in waves of length equal to model length. From motion picture records of several capsizes of this nature, it appeared that a model speed lying between the group velocity (one-half the phase velocity) and the phase velocity could result in this mode of capsize.

Mode 3: Broaching. This is the most dynamic mode, in appearance, and has received the most attention in the previous literature. In this mode of capsize, the model is struck from astern by three or four steep breaking seas in succession. As each wave strikes it, the model is forced to yaw off course to such an extent that the steering system is unable to correct the heading in the time interval between waves. The breaking seas striking the model and the dynamic heeling moment resulting from the turn combine to cause capsizing, again with the crest of a wave amidships. The essential features of broaching are the breaking waves striking the model in series, and the large heading deviation and associated angular velocity.

On several occasions, broaching was observed to occur without capsizing but with such total loss of directional control that the model swung through ninety degrees from a following sea course to beam seas. This was observed to occur most frequently in the light displacement condition where the rudder was less deeply immersed and therefore less effective."

Note: Underlines added for emphasis.

Fig. 35. Extract from "Motions and Capsizing in Astern Seas" (ref. 16)

'flops' over."

"Mode 3: Broaching-----" In this mode of capsize, the model is struck from astern by three or four steep breaking seas in succession."

These results are of interest with respect to the subject matter of this report:

(1) First of all it is a simple matter to determine whether or not a given test seaway is realistic in a full-scale context using Figure 2. This helps to avoid unrealistic interpretations of the results.

(2) The above deterministic characterizations of destabilizing wave patterns are compatible with HACYM analysis of time series wave height measurements in the model test seaway, e.g., see Figures 19 and 23. The same may be said of similar analyses of time series wave height data from full-scale storms, see Figure 20.

(3) The conduct of free-running model capsize tests in seaways which are beyond realistic levels of severity are nevertheless useful since they can assure that capsizings (and related "mode" characterizations) can be attained without the hazards of full-scale operation. In view of the fact that nonlinear motions are apt to be involved as in the case of critical loadings (see Figure 32), HACYM analysis of response data for severe and lesser seaway conditions is of value even though those seaway conditions corresponding to design criteria are not attained, or alternatively are exceeded.

(4) The acquisition and analysis of time series wave height data from a variety of storm conditions which produce large, steep, grouped or ungrouped waves is as important to rational analyses of ship capsizing tendencies (astern, stern quartering headings) as it is to rational load assessments (head, bow quartering headings) in the same seas. The initiatives of Table 4 (Item A) can therefore be equally important to the resolution of seakeeping problems as to structural problems.

(5) An ability to recreate critical wave/operating conditions (as to type and magnitude) under controlled test conditions in a seakeeping facility so as to attain design data is of considerable importance.

(6) An ability to identify and characterize seaway/operation/response conditions which are likely to result in critical loads or motions is a fundamental prerequisite. Free-running model tests may provide the most realistic approach to achieving this capability at the present time.

The development initiatives of Table 4 are intended to investigate the feasibility of pursuing these matters in regard to seaway induced loadings. Initiative B.1. seeks to determine if commercially available test facilities can replicate wave spectra corresponding to the extreme boundary of Figure 2 and if so at what scale. In the case of that portion of the boundary corresponding to hurricane Camille we effectively have answers to this question from two facilities as summarized here in Section 5.0. Ultimately, the question of modeling critical wave conditions in a test tank must involve wave conformations, model speeds, and headings analogous to those of Modes 1 thru 3 of Figure 35 but related to critical structural loadings rather than capsize behavior. For the time being this matter must be set aside for lack of knowledge of critical circumstances of loadings.

The apparent ability to reproduce a specific wave conformation in an otherwise random realization of a storm driven seaway, Figure 27, in encouraging.

Initiative B.2. is intended to assess experience to date with the design, construction and operation of free running models so as to obtain a clear summary of what can or cannot be done within the existing state-of-the-art. In addition, existing and potential test sites should be surveyed in order to determine which sites are most suitable for free-running model tests. Section III of Oakley et al[16] identifies some of the factors involved in selecting a viable test site. In this instance one additional criterion should be imposed, namely, that the scale of the seaways expected to occur in the test area should be generally compatible with those which can be generated in test tanks so that testing of a free running model under controlled wave conditions is also possible.

Initiative B.3 calls for analysis of existing full-scale SL-7 loads and motions data so as to identify those critical load or motion conditions which free-running model tests should be expected to identify and which towing tank tests might then be expected to quantify. The availability of full-scale data from a variety of severe seaway conditions affords a unique opportunity to conduct such an assessment.

The final initiative of Table 4 (C.1) does not follow directly from the wave research reported here, but stems rather from a realization that the majority of critical structural loadings occurring in storm driven seaways involve wave/water impact loadings, e.g., Buckley[1], Section 3.0, and further that the present state-of-the-art is deficient for dealing with such loading problems because impacts on and by roughly contoured water surfaces have a profound influence on the temporal and spatial characteristics of the dynamic loadings which result. The present state-of-the-art of load prediction generally fails to recognize these effects in a realistic manner and to provide appropriate scaling laws for model test data. Thus an initial research planning effort is recommended in Table 4.

8.0 CONCLUSIONS

Task I. Half-cycle matrix (HACYM) analysis of input and output realizations from Dalzell's nonlinear simulation model showed that this analysis method provides a clear indication of the nonlinearity of a time series random variable. The mean value distribution of amplitude events (MVDAE) is the most suitable statistic obtained from the matrix for this purpose. Analysis of time series wave height data using conventional zero-up (down) crossing procedures fails to provide an accurate assessment of the linear, Gaussian quality of the data.* HACYM analysis combined with the recovery of time series data for major events overcomes the failings of this method.

Correlation of MVDAE curves derived from a previous HACYM analysis of hurricane Camille wave data with 30 minute average wind velocities showed that nonlinearity of the wave height time series correlated with rapid increases in wind velocity. Correlations with wave spectra determined from the same data suggested that the nonlinearity was also related to the amount of energy present at the higher frequencies of the spectrum.**

---

* See discussion of Section 3.0, Pg. 24.

** Other wave making experiments have shown that short crestedness and nonlinearity are related. (See reference 25, pg. 73.)

Task 2. The nonlinearity of waves generated in two different towing tanks approached that of the original hurricane Camille seaway when the wave spectrum was approximated by mechanically generated waves. Differences in nonlinearity appeared to be related to difficulties involved in attaining the same high frequency energy levels as the full-scale seaway. High frequency energy was also noted to decrease with distance down the tank from the primary wave probe. Time series data for a plunging breaker generated at a third facility was found to closely match the steepest and most elevated wave in the original hurricane time series data.

Task 3. While numerically modeled hurricane Camille time series waves showed somewhat less nonlinearity than the original time series data, the flattening of the wave troughs and elevation of crests due to nonlinear wave-wave interaction was realistic. At the same time, however, the forward face wave steepness was greater than that of the largest hurricane waves apparently due to failure of the numerical waves to become unstable and break.

9.0 RECOMMENDATIONS

Recommended development initiatives are summarized in Table 4 and discussed in Section 7.0. These initiatives are intended first of all to provide time series wave height data from storm driven and other seaways with emphasis on data which contain the unique and dangerous waves of Table 1. This first initiative is unusual in that it is directed toward the community which acquires wave data as opposed to an ad hoc initiative which could be accomplished entirely by a particular researcher or group. It is hoped that the findings of Section 4.0 will help to stimulate interest in acquiring the needed time series wave height and wind data. The remaining initiatives are directed toward the assessment of nonlinear responses (i.e., loads and motions) of marine craft and structures. These would appear to be a digression in a study concerned primarily with extreme wave characteristics. They are not. Rather they recognize that our primary interest after all is in loadings to be used in structural design and that such loadings can arise from operation in other than extreme seas. Moreover, what needs to be known about waves to permit a rational assessment of design loads is dictated by a combination of factors: the seaway itself, variables associated with the configuration of the craft or structure, the way it is operated in the seaway, and finally variables associated with response to the seaway.

Of these factors, the first of course is the subject of this report; the second is largely prescribed and therefore involves no basic research initiatives; the fourth, like the first, is complicated by nonlinear behavior only more so. The brief examples involving this last subject which are presented in Section 7.0 are intended to suggest that the methods employed here in dealing with nonlinear behavior of the seaway have potential application to this important area as well.

ACKNOWLEDGEMENTS

The author wishes to thank Mr. John F. Dalzell for making available the time series input and output files of his nonlinear response model which were analyzed in Task 1, for the preparation of Appendix B and for performance of Task 3 and the preparation of Appendix E. This study could not have been performed without his assistance. The author also wishes to thank Messrs. James A. Kuny and David P. Kihl for their programming and data processing support during all phases of the study.

Finally, he wishes to thank Ms. Louise A. Wallendorf and Prof. Bruce H. Johnson of the U.S. Naval Academy Hydromechanics Laboratory for making available time series spilling and plunging wave data.

REFERENCES

1. Buckley, W. H. "A Study of Extreme Waves and Their Effects on Ship Structure," Ship Structure Committee Report SSC-320, 1983.
2. Buckley, W.H., R.D. Pierce, J.B. Peters and M.J. Davis. "Use of the Half-Cycle Analysis Method to Compare Measured Wave Height and Simulated Gaussian Data Having the same Variance Spectrum," Ocean Engineering, Vol II, No. 4, pp 423-445, 1984.
3. Dalzell, J.F., "An Investigation of the Applicability of the Third Degree Functional Polynomial Model to Nonlinear Ship Motion Problems," Davidson Laboratory, SIT-DL-82-9-2275, December 1982.
4. Marmarelis, P.Z. and V.Z. Marmarelis, Analysis of Physiological Systems-The White Noise Approach, Plenum Press, New York, 1978.
5. Buckley, W.H., "Climatic Wave Spectra for Use in Design of Ships and Offshore Platforms," DTNSRDC -SD-87-173-33, January 1987.
6. Dalzell, J.F., "Approximations to the Probability Density of Maxima and Minima of the Response of a Nonlinear System," U.S. Naval Academy Report EW-22-84, October 1984.
7. Cartwright, D.E. and M.S. Lonquet-Higgins," The Statistical Distribution of the Maxima of a Random Function," Proceedings of the Royal Society of London, Vol. A237, pp 212-232, 1956.
8. Duncan, J. H., L. A. Wallendorf, B. H. Johnson, "An Experimental Investigation of the Kinematics of Breaking Waves," Proceedings of IAWR Seminar (Maritime Hydraulics Section) on Wave Analysis in Laboratory Basins," 1-4 Sept 1987, pp 411-422.
9. Courtesy of Ms. Louise Wallendorf, U.S. Naval Academy Hydromechanics Laboratory.
10. Telephone conversation, Dr. J. Ian Collins, Arctic Offshore Corporation.
11. Buckley, W.H. "Extreme and Climatic Wave Spectra for Use in Structural Design of Ships," (to be published in Naval Engineers Journal, A.S.N.E.).
12. Stambaugh, K.A. and W.A. Wood, "SL-7 Research Program Summary, Conclusions and Recommendations," Ship Structure Committee Report SSC-313 (SL-7-28), August 1981.
13. O'Dea, J.F., "Relative Motion and Deck Wetness Investigation of the SL-7 Containership," DTNSRDC/SPD-1081-01, April 1983.
14. Anon, "Application of the Half-Cycle Matrix Method of Random Data Analysis to the Study of Ship Loads and Motions," Band, Lavis and Associates Report No. 197-2 Revision A, June 1984.
15. Changery, M., C. Williams, and W. Buckley, "Climatic Wave Spectra and Wind Data from Selected NOAA Buoys through 1985," DTNSRDC-SD-87/173, July 1987.
16. Oakley, Jr. O.H., J.R. Pauling and P.D. Wood, "Ship Motions and Capsizing in Astern Seas," Tenth Symposium Naval Hydrodynamics, June 24-28, 1974.
17. Crago, W.A. "The Use of Free-Running Models at Sea in the Assessment of Seakeeping and Other Aspects of Performance," Proceedings of the Nineteenth General Meeting of the American Towing Tank Conference, Vol. 1, pp 227-253, 1981.

18. Buckley, W.H., "The Application of Half-Cycle Counting Techniques to the Analysis of Ocean Wave Data," Proceedings of the Nineteenth General Meeting of the American Towing Tank Conference, Vol. 1, pp 429-466, 1981.
19. Yang, J.N., "Statistics of Random Loading Relevant to Fatigue," Journal of Engineering Mechanics, American Society of Civil Engineers, pp 469-475, 1974.
20. Bedrosian, E. and S.O. Rice, "The Output Properties of Volterra Systems (Nonlinear Systems with Memory) Driven by Harmonic and Gaussian Inputs," Proceedings IEEE, Vol. 59, No. 12, December 1971.
21. Hasselmann, K., "On Nonlinear Ship Motions in Irregular Waves," Journal of Ship Research, Vol 10, No. 1, 1966.
22. Hineno, M. "The Calculation of the Statistical Distribution of Maxima of Nonlinear Responses in Irregular Waves," Trans. Society of Naval Architects of Japan, Vol 156, December 1984.
23. Dalzell, J.F., "Statistics of Nonlinear Response to Short Crested Nonlinear Seas: The Quadratic Case," DTNSRDC-87/007, April 1987.
24. Longuet-Higgins, M.S., "Resonant Interactions Between Two Trains of Gravity Waves," Journal of Fluid Mechanics, Vol. 12, pp 481-500, 1962.
25. Stansberg, C.T. and S. P. Kjeldsen, "MARINTEK Ocean Basin Wave Catalogue 1988," Report No. 511031.00, January 19, 1988.

APPENDIX A

THE HACYM METHOD OF RANDOM DATA ANALYSIS[2]

Figures 1 and 2 illustrate the basic procedure for half-cycle counting time series data and for entering individual counts into an associated data matrix, or HACYM*. The signal is first level banded into uniform intervals on either side of the reference data level. Each data interval has been given a designator ($+J$ through $-J$) for identification. Whenever a data peak (maximum or minimum) occurs, it is identified with a particular data interval designator. In Fig. 1, the half-cycle ① has a first peak of $-B$ and second peak $+E$. (Note: in Fig. 1 the half-cycle identifiers ① through ⑥ have been entered to illustrate the procedure. Normally the data bin would contain a number which corresponds to the number of times the data sample in question had half-cycle excursions corresponding to that particular data bin.) This procedure is repeated for other half-cycle excursions such as ② – ⑥ until all of the data have been processed.

The signal employed here illustrates certain basic features of the dispersion pattern of half-cycle counts within the HACYM. First, matching half-cycles will fall into data bins symmetrically disposed on either side of the null diagonal, i.e. about the diagonal formed by the darkened squares. Thus, if the HACYM were folded along the null diagonal, the data bins containing matching half-cycles would fall one upon the other. Second, a half-cycle count located on the reference level diagonal, such as ⑤, is symmetrical about the reference data level. Third, the up-going half-cycles ①, ③ and ⑤ all appear on the right-hand side of the null diagonal, while the down-going half-cycles ②, ④ and ⑥ all appear to the left of the null diagonal.

Figure 2 illustrates the significance of the location of a half-cycle count within the HACYM. In this figure, the half-cycle excursion previously designated ① has been characterized in terms of its mean value and amplitude which, in this case, are 1 1/2 and 3 data intervals, respectively. It will be seen in the HACYM of Fig. 2 that the location of a half-cycle count with respect to the null diagonal is a direct measure of the amplitude of the half-cycle excursion, while the location with respect to the reference level diagonal is a direct measure of its mean value. Half-cycle counts having positive means fall to the right of the reference level diagonal and vice versa.

If, following the processing of a large amount of random data, a three-dimensional figure were to be constructed such that the ordinate at each data bin corresponded to the number of half-cycle counts in the data bin and if the figure were normalized to contain unit volume, the individual ordinates would then correspond to the joint probability of a particular mean value occurring in combination with a particular amplitude

Using an analytical approach developed by Yang (1974), Andrews* recently analysed an idealized narrow-band Gaussian process in HACYM format. One of the band-limited white noise spectra employed in the analysis is shown in Fig. 3 and the resulting distribution of half-cycle counts for a particular number of half-cycle events in Fig. 4. (Note: in this case the half-cycle count distribution corresponds to the expectation of

*An unpublished analysis of the statistics of peak/trough events by J.N. Andrews, DTNSRDC.

half-cycle events rather than that for a sample realization.) The principal characteristics of the dispersion pattern are: (a) symmetry about the diagonals of the HACYM and (b) a Rayleigh distribution of peak counts,

$$p(x' = 0) = \frac{x}{c^2} \exp\left(-\frac{x^2}{2c^2}\right), \text{ where } C^2 = \frac{1}{2m} \sum_{i=1}^{m} X_i^2,$$

for the associated histograms of Peak Counts and Amplitude Occurrences. The characteristic of symmetry suggests that in a Gaussian process, half-cycle data events having the same absolute values of mean and amplitude can be expected to have an equal probability of occurrence.

Figures 5 and 6 illustrates the interrelationship of the statistics of peak and peak/trough events for Gaussian narrow-band and broad-band time series data. For illustration purposes the time-series variable is considered to be generated by the projection on the real axis of a vector rotating in the complex plane. In the narrow-band case of Fig. 5, the length of the vector is a random variable while the rotational frequency is a constant. If the random variable is Gaussian, then the probability density distribution $p(x)$ of the real, random variable $x(t)$ will be Gaussian, i.e. the probability of finding $x(t)$ between any two given values of x, (i.e. x_n and x_{n+1}), is given by the Gaussian distribution function shown schematically in Fig. 5. The probability distribution $p(x' = 0)$ for peak events will, on the other hand, have a Rayleigh distribution as is well known. Since peak events have both positive and negative values, separate asymmetric distribution functions apply as shown in Fig. 5. This is also true of the joint probability distribution of the mean and amplitude values of successive peak/trough events as shown in the half-cycle matrix. In this case the three dimensional distribution function has only small variations in mean values as compared to amplitude values. An important property of the HACYM is that the marginal distribution of peak/trough events provides the distribution of peak events, both positive and negative as discussed in Buckley (1980).

The more general case of a broad-band random variable (Fig. 6) is represented here as being generated by a vector in the complex plane which is subject to variations in both length and angular velocity. In this representation the angular velocity is not an independent random variable since it must be constrained to result in the variance spectrum associated with $x(t)$. For purposes of this schematic representation, however, this constraint is not of immediate consequence. Again, if $x(t)$ is Gaussian the probability density distribution $p(x)$ will be Gaussian. The probability distribution function peaks events, however, will not follow a Rayleigh distribution. This can be seen qualitatively by examining the schematic distribution of peak/trough events in the HACYM of Fig. 6 and recalling that the marginal distribution of events by rows provides distribution of peak events. The overlap in the respective distributions of peak events results from positive peaks occurring below the mean value of $x(t)$, i.e. below mean water level in the case of ocean waves, and vice versa. For a Gaussian process of arbitrary bandwidth, the probability distribution function for peak events was derived some years ago by Cartwright and Longuet-Higgins (1956). Having defined a bandwidth parameter ϵ which is derived from the mean value of $x(t)$ and the second and fourth moments of the variance spectrum about its mean, they derived the probability distribution of peak events for a range of the parameter from the idealized narrow band case ($\epsilon = 0$) to the limiting broad-band case ($\epsilon = 1.0$). Their result is shown in Fig. 7 for the one-sided distribution of peak events. It can be seen that for the broad-band Gaussian case ($\epsilon = 1$) the three dimensional distribution of peak/trough events in the HACYM will result in a unimodal Gaussian distribution. It is suggested here that the half-cycle matrix provides an improved basis for examining the distribution of the maxima of a stochastic variable having a variance spectrum of finite bandwidth. This assertion stems from the fact that both the random variable and the HACYM distribution are bivariate.

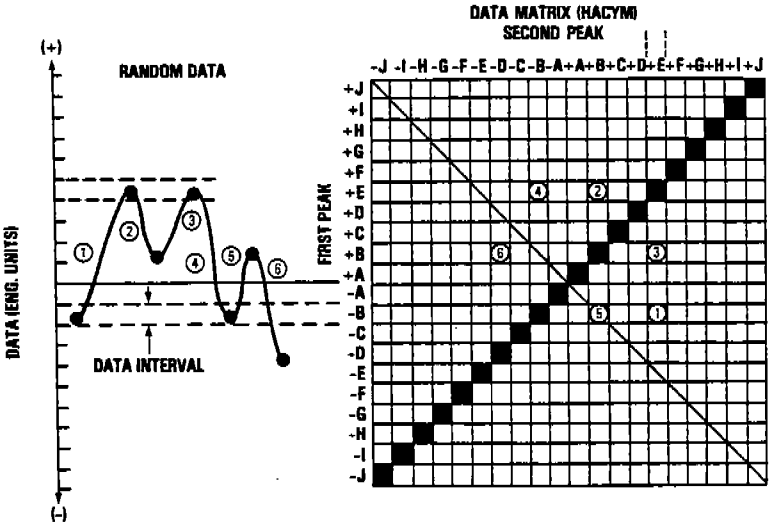

FIG. 1. Half-cycle counting of random data.

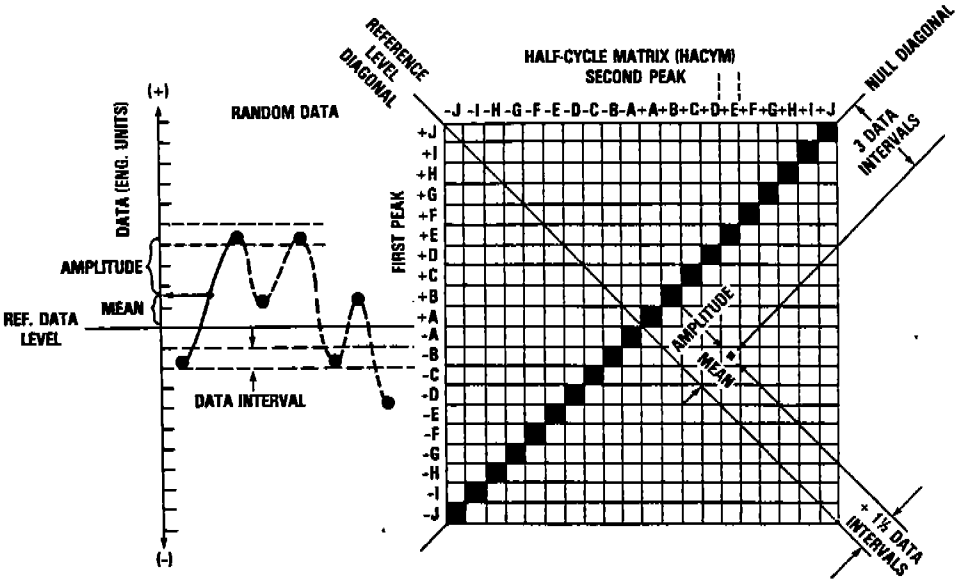

FIG. 2. Characterization of half-cycle data excursions within the HACYM.

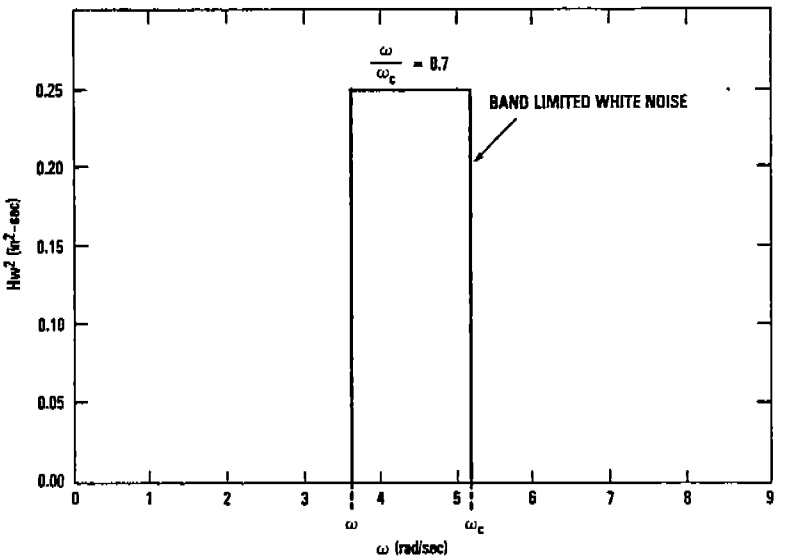

FIG. 3. Narrow-band variance spectrum.

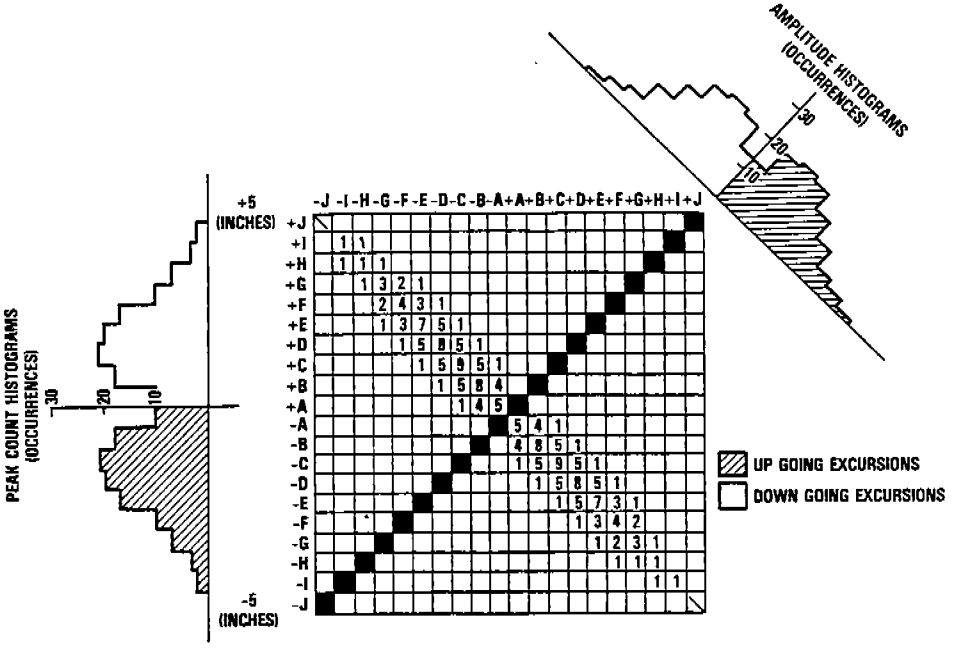

FIG. 4. HACYM analysis of narrow-band variance spectrum $\left(\frac{\omega}{\omega_c} = 0.7\right)$.

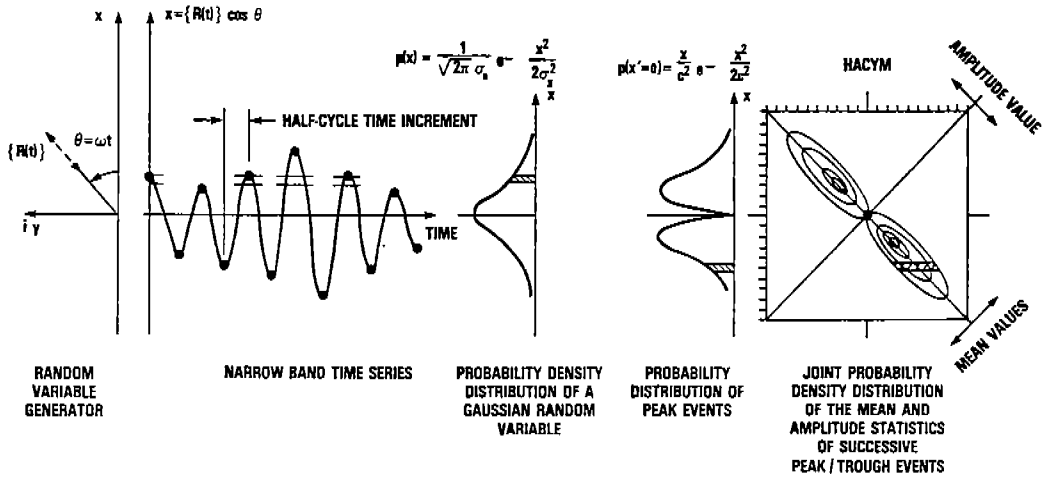

FIG. 5. Narrow-band Gaussian random variable.

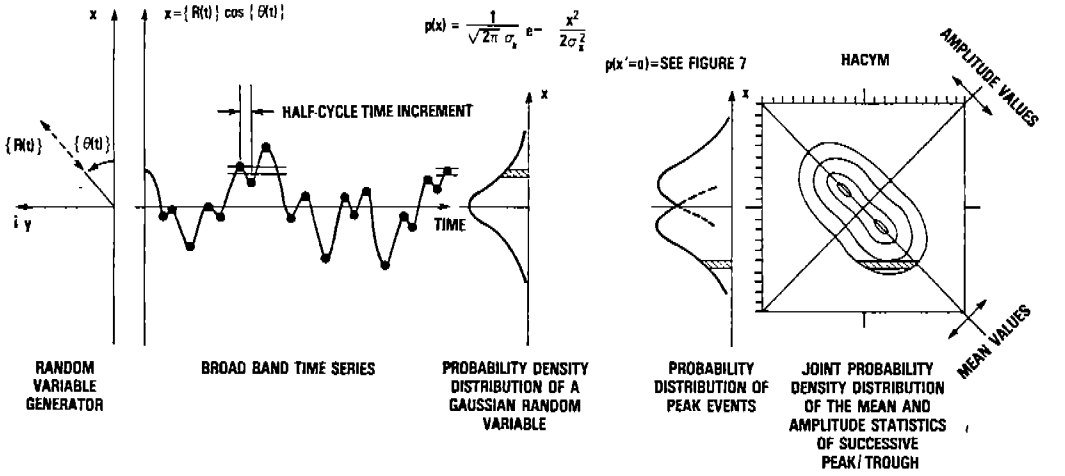

FIG. 6. Broad-band Gaussian random variable.

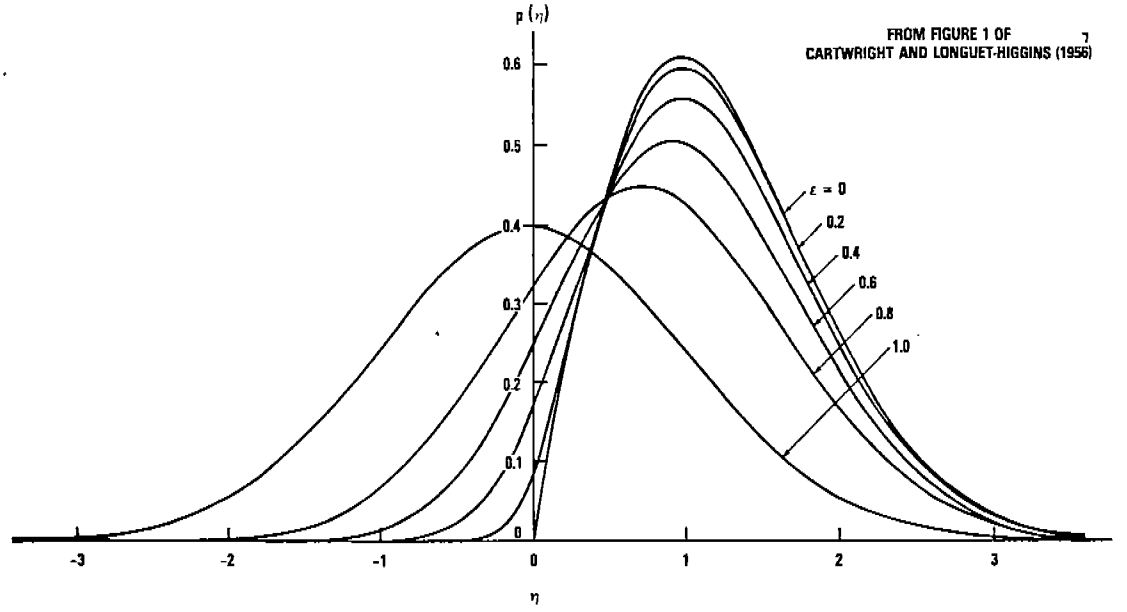

FIG. 7. Probability distribution of the heights of maxima for different values of the width ϵ of the energy spectrum.

APPENDIX B
SYNOPSIS OF REFERENCE (3)
by
John F. Dalzell

Introduction

The objective of the work reported in Dalzell[3]* was to explore the applicability of the third degree functional polynomial model to nonlinear seakeeping problems, and to attempt the development of an approach by which third degree nonlinearities in observed responses of ships to waves might be interpreted. As a necessary part of that investigation, long time histories were simulated of the response to random Gaussian waves of a nonlinear system defined by a relatively arbitrary nonlinear differential equation. Subsequently, and for similar reasons, statistically identical time histories were simulated in the work reported in Dalzell[6] The only difference between the simulations of Dalzell[3] and Dalzell[6] was the pseudo-random noise generator of the computer used in the two investigations.

Though there was an interest in maxima in both investigations, the time histories were not analyzed by the half-cycle count approach. When the need arose in the present project to do so, it was convenient to use the time histories produced in Dalzell[6] because they had been stored on tape. The objective of this Appendix is to briefly summarize the mathematical background to the simulations referenced in Section 3 of the report. (A complete summary will be found in Dalzell[3].)

The General Mathematical Model of the Third Degree

The mathematical model underlying the simulation is the Volterra functional series expansion. This is a time-domain formulation relating the response of a nonlinear system to an excitation, and is analogous to a Taylor Series with memory. The complexity of the Volterra series increases geometrically with the degree of the nonlinearity, so that in attempts at practical use the series has to be truncated to form a "functional polynomial". In the investigations cited the interest was in nonlinearities up to the third degree, and the resulting functional polynomial may be written,

$$\begin{aligned} Y(t) = & \int g_1(\tau_1)\, X(t-\tau_1)\, d\tau_1 \\ & + \int\int g_2(\tau_1,\tau_2)\, X(t-\tau_1)\, X(t-\tau_2)\, d\tau_1\, d\tau_2 \\ & + \int\int\int g_3(\tau_1,\tau_2,\tau_3)\, X(t-\tau_1)\, X(t-\tau_2)\, X(t-\tau_3)\, d\tau_1\, d\tau_2\, d\tau_3 \,. \end{aligned} \qquad (B.1)$$

In Equation B.1, and subsequently, the omission of limits on integrals signifies limits of $-\infty$ to ∞. $Y(t)$ is the response as a function of time, t. $X(t)$ is the excitation, also a function of time which is assumed to be zero-mean. The τ_j are time differences. The first term, a single convolution, is the linear term, and its kernel, $g_1(\tau_1)$, is a linear impulse response. The second term is the quadratic, (degree two) nonlinearity. Its kernel, $g_2(\tau_1,\tau_2)$ is a quadratic impulse response. Similarly, the third term is the cubic (degree three) nonlinearity with cubic impulse response function $g_3(\tau_1,\tau_2,\tau_3)$.

In the context of weakly nonlinear systems it is natural to call the linear term "first order", the second (quadratic) term "second order" and the third (cubic) term "third order".

The model is mathematically unique if all the kernels are symmetric in their arguments, and this is assumed. There are some very general additional restrictions on the kernels, essentially that

* References appear on page

the integrals of the absolute value of each kernel must exist. Additionally, if the excitation, $X(t)$, is stochastic it must be strictly stationary. This too is assumed since it is the same assumption which has been tacitly been accepted for some time in the seakeeping field.

Simulation of the response time series is carried out by converting Equation B.1 into summation form — essentially by doing the integrals numerically for each time step. The "raw materials" for this operation will be discussed subsequently. Briefly, there must be available numerical renditions of the excitation, $X(t)$, in time series form, as well as a compatable numerical rendition of the various impulse responses, $g_n(\tau_1, \ldots \tau_n)$. A general property of the mathematical model was used to make it less time consuming to study the behavior of each or all of the three components as a function of the magnitude of excitation. This is a homogeneity property, which is that if the excitation, $X(t)$ is replaced by $C\,X(t)$, where C is a constant, then the term of degree n is multliplied by C^n. Thus, a time series corresponding to each of the three terms of the model was simulated and stored separately for a nominal level of excitation. If $Y_1(t)$ denotes the time series from the linear term of Equation B.1, $Y_2(t)$ denotes that from the quadratic term, and $Y_3(t)$ denotes that from the cubic term, the total response, $Y(t)$, to an excitation C times the nominal is defined by:

$$Y(t) = C\,Y_1(t) + C^2\,Y_2(t) + C^3\,Y_3(t)\,,$$

where simple time step by time step addition is implied.

Simulation of Excitation Time Series

For purposes of the investigation what was required was samples in time series form of a zero-mean, random Gaussian "excitation" process whose variance spectrum approximated a water wave point spectrum. The numerical approach to the simulation of the excitation time series corresponding to $X(t)$ was quite conventional and totally based in linear system theory. The first stage in the simulation was to produce samples in time series form of band limited white Gaussian noise starting from the computer pseudo-random number generator. The algorithm used approximates the Gaussian property to about five standard deviations. Any linear transformation of a Gaussian process is another Gaussian process, so that the next and last step in the excitation simulation was to apply a linear passive digital filter to the noise records to produce the Gaussian wave-like process desired. The digital filter was configured so that the resulting time series has the nominal variance spectral form:

$$S_{XX}(\omega) = 5\sigma_X^2\omega_0^4 \exp[-1.25(\omega_0/\omega)^4]/\omega^5\,, \qquad (B.2)$$

where S_{XX} = the variance spectrum,
σ_X^2 = the variance,
ω = frequency, circular,
ω_0 = the "modal" frequency.

The values of the variance and the modal frequency are parameters to the simulation. The spectral form of Equation B.2 is the same as the ITTC two parameter, Pierson-Moskowitz, and Bretschneider wave point spectra. The values of the excitation variance and modal frequency were chosen arbitrarily to produce excitation time series with a time behavior similar to that of small scale long-crested laboratory waves. This was accomplished by setting the modal frequency, $\omega_0 = 2\pi$ to make typical wave component periods of the order of one second. A time step, $\Delta t = 0.0625$ seconds yielded adequate time resolution for the processes studied. The nominal variance of the simulations was set at $\sigma_X^2 = 0.0625$, so that the nominal rms excitation was $\sigma_X = 0.25$, and accordingly the "significant height" of the nominal excitation level was unity.

For the purposes of the present and the previous work, a data base was required which corresponded to a very long time domain sample of the excitation and response. Practical computational matters dictated that the overall data base be composed of a number of "handy sized" samples. In the simulations each sample was made long enough to contain about 150 "waves" so that each corresponded to what is often achieved in zero forward speed towing tank experiments. Ten such statistically independent samples of excitation were generated to produce the time series data base of Dalzell[6]. Thus the data base used in the present work corresponds to about an order of magnitude more sample duration than is usually obtained in laboratory experiments, or for that matter, full scale ship trials.

Simulation of the Impulse Responses

The impulse response functions, $g_n(\tau_1 \ldots \tau_n)$, required by the mathematical model, Equation B.1, contain the dynamics of the nonlinear system which is being excited by $X(t)$. As matters turn out we do not know how to compute the impulse responses directly from the characteristics of the system, and so must proceed indirectly. If it is presumed that each impulse response function is sufficiently smooth and integrable, there is no mathematical trouble about existence of an n-fold Fourier transform. In particular it is assumed as part of the basic mathematical model that to each n^{th} degree impulse response function there corresponds an n^{th} degree *frequency response function*, $G_n(\omega_1 \ldots \omega_n)$, where the ω_j are circular frequencies. The multi-dimensional Fourier transform pairs relating impulse and frequency response functions may be defined as follows:

$$g_n(\tau_1, \ldots \tau_n) = \frac{1}{(2\pi)^n} \int\int \ldots \int G_n(\omega_1, \ldots \omega_n) \exp\left[i \sum_{j=1}^{n} \omega_j \tau_j \right] d\omega_1 \ldots d\omega_n$$

$$G_n(\omega_1, \ldots \omega_n) = \int\int \ldots \int g_n(\tau_1, \ldots \tau_n) \exp\left[-i \sum_{j=1}^{n} \omega_j \tau_j \right] d\tau_1 \ldots d\tau_n \,. \qquad (B.3)$$

Thus, if the frequency response functions can be derived from the system characteristics, the first of Equations B.3 may in principle be used to compute the impulse response functions. This is the strategy which was used in the simulations. The origin of the frequency response functions used will be outlined in the next section. Once the required frequency response functions were available in numerical form, an FFT based numerical version of the first of Equations B.3 was used to compute the impulse response functions used in the time domain simulation.

It should perhaps be remarked before passing on that there are some practical restrictions on the procedure which are essentially imposed by the infinite time difference limits on the integrals in Equation B.1, and the infinite frequency limits on those of Equations B.3. To accomplish straight-forward numerical integrations of Equation B.1, $g_n(\tau_1 \ldots \tau_n)$ must approach zero outside of a finite space in the domain of the time differences $(\tau_1 \ldots \tau_n)$. Similarly, a straight-forward multi-dimensional finite Fourier transform corresponding to the first of Equations B.3 requires that $G_n(\omega_1 \ldots \omega_n)$ must approach zero outside of a finite space in the domain of the frequencies $(\omega_1 \ldots \omega_n)$. These are sometimes nearly mutually exclusive requirements. Thus, there is some judgement and compromise involved in actually arriving at a practical impulse response simulation from a given set of frequency response functions. In the present type of simulation the excitation is band limited. There thus can be no nonlinear interactions of significance which involve frequencies well outside the excitation band. Under these circumstances the frequency response functions may be essentially truncated at frequencies well outside the excitation band, and this strategy was employed in the simulations under discussion. Fortunately, it is possible to check the adequacy of the respresentation of the computed impulse response functions with deterministic excitation, and this was carried out for the simulations under discussion with reasonably positive results, Dalzell[3].

Definition of a Set of Frequency Response Functions

In the work of Dalzell[3] it was necessary to simulate some sort of nonlinear system to third order. However, it made little difference to that exploratory investigation which one of an enormous number of possibilities was actually used — other than that the qualitative nature of the system not be pathologically different than that of a ship motions system. The strategy adopted was to postulate a not too complicated nonlinear differential equation with constant coefficients, expand the equation in a functional series, derive the corresponding frequency response functions up to third order according to the methods of Bedrosian[20], and then play with the coefficients of the equation so as to produce a plausable weakly nonlinear third order system.

The general differential equation postulated was as follows:

$$\sum_{j=1}^{3} \left\{ A_j[\ddot{Y}(t)]^j + B_j[\dot{Y}(t)]^j + C_j[Y(t)]^j \right\} = X(t)\,, \tag{B.4}$$

where $X(t)$ and $Y(t)$ are the excitation and response respectively, and the A_j, B_j, and C_j coefficients are constants. The expansion method requires that the linear coefficients (A_1, B_1, C_1) not all vanish. The first three frequency response functions resulting from the expansion may be written as follows:

$$\begin{aligned}
G_1(\omega) &= 1/D_1(i\omega)\,, \\
G_2(\omega_1,\omega_2) &= -D_2(-\omega_1\omega_2)\,G_1(\omega_1)\,G_1(\omega_2)\,G_1(\omega_1+\omega_2)\,, \\
G_3(\omega_1,\omega_2,\omega_3) &= -G_1(\omega_1+\omega_2+\omega_3)\Big\{ D_3(-i\,\omega_1\omega_2\omega_3)\; G_1(\omega_1)\,G_1(\omega_2)\,G_1(\omega_3) \\
&\quad + \frac{2}{3} D_2(-\omega_1\{\omega_2+\omega_3\})\,G_2(\omega_2,\omega_3)\,G_1(\omega_1) \\
&\quad + \frac{2}{3} D_2(-\omega_2\{\omega_1+\omega_3\})\,G_2(\omega_1,\omega_3)\,G_1(\omega_2) \\
&\quad + \frac{2}{3} D_2(-\omega_3\{\omega_1+\omega_2\})\,G_2(\omega_1,\omega_2)\,G_1(\omega_3) \Big\}\,,
\end{aligned} \tag{B.5}$$

where the auxilliary function is defined as:

$$D_n(\alpha) = A_n\alpha^2 + B_n\alpha + C_n\,, \tag{B.6}$$

and thus a selection of specific values for the nine constants in Equation B.4 allows numerical values to be obtained for the frequency response functions defined in Equations B.5 for any arbitrary combination of frequencies.

Some remarks are in order before proceeding further. It may be noted in Equations B.5 that the expressions for the quadratic and cubic frequency response functions involve all the response and auxilliary functions of lesser degree. Unfortunately this continues on for frequency response functions of higher degree, so that, despite the fact that the exponent, j, of Equation B.4 was limited to three in an attempt to produce a third order system, frequency response functions of all higher orders may be derived for Equation B.4. In effect, the functions, Equations B.5 and B.6, do not define a complete solution to the equation — the most that can be claimed if only these functions are used to define the system is that any simulations resulting should be correct simulations of the equation to third order. In the context of the work of Dalzell[3] truncation of the series of frequency response functions after the third was not at all bothersome — all that was wanted was a trial third order system with the correct mathematical properties. The distinction

between simulating Equation B.4 and simulating Equation B.4 to third order should be kept in mind in the event that an attempt is made to attach more significance to the equation than was originally intended.

The strategy adopted in the selection of coefficients was partially dictated by the above considerations. In order to try to avoid the situation where the neglected nonlinearities of order higher than the third might in reality be significant, the specification of a weakly nonlinear system was attempted. The first step was to select the linear coefficients so as to produce a stable linear sub-system. The numbers chosen were:

$$A_1 = \frac{1}{(2\pi)^2}, \qquad B_1 = \frac{1}{4\pi}, \quad \text{and} \quad C_1 = 1.$$

These numbers define a linear single degree of freedom system in which the response amplitude is unity at zero frequency, 2.0 at resonance, and decays to zero relatively rapidly. The resonant frequency is 2π radians per second so as to locate the resonance at the peak of the excitation spectrum. Qualitatively this system resembles a lightly damped ship heave response to wave elevation, or a relatively heavily damped roll response to wave slope excitation. It may be noted from Equations B.5 and B.6 that the linear coefficients define $G_1(\omega)$. It is clear also that if $G_1(\omega)$ is zero for any frequency in the arguments of the quadratic and cubic frequency response functions, these functions will also be zero. To aid the numerical Fourier transform work described earlier a high frequency window was applied to the numerical value of $G_1(\omega)$ to insure a known finite space of non-zero values for all the functions. The effect was to use the theoretical value of $G_1(\omega)$ for $(\omega < 7\pi)$, zero $G_1(\omega)$ for $(\omega > 8\pi)$, and apply an attenuator in between.

In selecting the quadratic coefficients, (A_2, B_2, C_2), of Equation B.4 the intention (largely for lack of better information) was to produce a quadratic frequency response function resembling that known for added ship resistance in waves. Trials and errors established that A_2 and C_2 needed to be zero , and B_2 needed to be much smaller than B_1 to produce the qualitative behavior desired.

With linear and quadratic coefficients selected, the cubic coefficients, (A_3, B_3, C_3), remained. In this case there was no previous qualitative guidance. Arbitrarily, it was decided to select these so as to produce a moderate change in the amplitude response per unit excitation at linear resonance as excitation amplitude increases. It was found that A_3 had to be zero to accomplish this, and B_3 and C_3 had to be much smaller than the corresponding linear coefficients. A more extensive discussion of the theoretical response of the final system to monochromatic excitation is to be found in Dalzell[3].

When the final coefficients selected are substituted into Equation B.4 and some simplifications made, the actual equation which was simulated to third order becomes:

$$A_1\ddot{Y}(t) + B_1\left\{\dot{Y}(t) - 0.0844[\dot{Y}(t)]^2 + 0.0032[\dot{Y}(t)]^3\right\} + C_1\left\{Y(t) + 0.0075[Y(t)]^3\right\} = X(t). \tag{B.7}$$

As is suggested by the form of the equation, the result was a system with both quadratic and cubic damping, and a hardening spring constant characteristic.

APPENDIX C

LETTER REPORT AOC-87-432

December 1987

SIMULATION OF CAMILLE WAVE SPECTRUM IN THE TEST BASIN AT ARCTEC OFFSHORE CORPORATION.

Prepared for: David Taylor Research Center
Bethesda
Maryland 20084-5000

Contract No.: N0O1678M2461

Prepared By: J. Ian Collins

Table of Contents

1. INTRODUCTION AND OBJECTIVES

Hurricane Camille which struck the US Gulf Coast in August 1969 produced some of the most severe sea-states that have been recorded by wave staffs. Examination of the wave records has been made by several specialists and the characteristics of the statistical properties have been documented.

Of considerable interest is the expectation of the degree of agreement in the equivalent wave behavior which could be simulated in a model test basin using "standard technology". It is possible to take an existing time history taken during a storm at a specific location and reproduce it exactly at a specific point in the test basin. In this case, the request by DTRC under a Task Order NOO16787M2461, was to reproduce a representative sea having a closely matched spectrum to that recorded in the Gulf of Mexico on August 17 1969 at 1500-1530 CST using AOC's standard software. The tests were made on October 27, 1987 in a test basin measuring 298 feet long by 48 feet wide in a water depth of 13.5 feet located in Escondido, California, at a scale of 1:30.

2. TEST SET-UP

The test basin was the deep water basin located at Arctec Offshore Corporation's offices in Escondido, California. The basin is illustrated in Figure 2.1 which shows the location of the wave sensors. The basin was operated at a depth of 13.5 feet which corresponds to water depth of 405 feet at ascale of 1:30.

The wave sensors were capacitance type wave probes which were calibrated over a range of 60 feet (prototype) corresponding to a digital range of 2048. Figures 2.2, 2.3, and 2.4 illustrate the calibrations achieved. The calibrations are seen to be quite linear although it is noted that there is a slight curvature apparent in the calibrations. For purposes of these tests the calibrations were treated as being linear with the constants

shown in the Figures. Further detailed analysis which may be contemplated for this data may warrant consideration of a non-linear calibration fit.

3. WAVE SIMULATION PROCEDURE

The particular wave model assumed in these tests was assumed to be of the form:

$$\zeta(t) = \Sigma\, a_n \cos (2\pi\, t\, f_n + \varepsilon_n)$$

where,

ζ is the instantaneous sea surface elevation above the mean,
a_n is the amplitude of the n^{th} wave component,
f_n is the frequency of the n^{th} component.

This would actually be simulated by generating a voltage time series, V(t), which takes into account the transfer function between the waveboard motions and the waves and the control system response.

In the test basin the particular time series was generated by selecting 2048 values of an according to the desired spectral shape S(f) as:

$$1/2\, a_n^2 = \int_{\Delta f} S(f)\, df$$

and selecting 2048 random phases, ε_n, which were generated from a uniform distribution between 0 and 2π. The two arrays of 2048 data points in the frequency domain yield a time series of 4096 points in the frequency domain by use of the classical Inverse Fast Fourier Transform (IFFT). The frequency steps Δf were selected to generate a time step of 20 hertz in the model basin. Hence with this scheme, if applied exactly as stated, would yield a repeating time series having a period of 204.8 seconds at model scale coresponding to 1122 seconds at a scale of 1:30. In

order to avoid this undesirable characteristic, at each cycle of 204.8 seconds a new series of 2048 random phases were generated and a different 4096 time series results. The two series were merged using a faded overlap routine and the process repeated for more cycles to generate a time series of 120 minutes (prototype scale) which should have all of the desired statistical properties and contain no repeat sequences.

Other equivalent numerical simulations can be used to generate the basic time series. In this scheme it is noted that only the phases are randomized. Other investigators have chosen to also randomize the amplitudes, a_n, but as discussed in Rice (1951) this should produce equivalent statistics as has been well demonstrated by Elgar et al (1984). In the case of free surface water waves the dispersion relationship causes different components to propagate at different speeds thereby adding additional natural "randomness and incoherence" in the wave basin.

A worthwhile improvement in the modeling of large, non-linear, sea states should probably consider the fact that for large waves there would undoubtably occur certain fixed phase relationships such that the phases may not be independent between frequencies. This is the subject of ongoing research and was not attempted to be implemented in this brief demonstration test program.

Once the time series had been generated according to the above procedure it was used as the control signal to the servo-controlled hydraulic actuator which drives the waveboard. The resulting waves were recorded and their spectrum computed. The standard data reduction was to record the first 4096 data points at 20 hertz (model time scale), use an FFT routine to compute the spectrum and then apply a running rectangular smoothing window in the frequency domain. The choice of frequency domain smoothing width is arbitrary. A too narrow window will give unstable (in the statistical sense) estimates whereas a too broad window will sacrifice resolution.

The choice of smoothing filter was made to be consistent with the field

data supplied. It would have been best to work to the identical resolution as the spectrum recorded during Camille but the details of the field data analysis were not readily available. The spectral plot provided indicates a record time of 1804.75 seconds. Buckley (1987) presents examples of archived data which indicate a sample rate of 0.67 seconds which would indicate that the records consist of about 2700 points. If a sample size of 2048 points is assumed which have been processed to yield 40 spectral values between zero and 0.3 hertz then the equivalent degrees of freedom in the spectral estimates would be 2048/40 ≈ 51 thereby supporting the use of a 51 point running mean as a reasonable choice of smoothing filter for a simulated 30 minute record.

During the calibration the first step was to read off the desired spectral ordinates from the spectrum supplied and transform these according to the frequency domain characteristics of the waveboard and its associated control system response to determine the "input" spectrum. The time series was generated by IFFT for 4096 time steps using random phases. The resulting waves were recorded in the test basin and their spectra compared with the desired. If a good match was not achieved the input voltage spectrum was corrected and the process repeated until a "good" match was achieved. At this point a longer time series was made and the voltage time history recorded on a magnetic cassette tape for test use.

The target spectrum is illustrated in Figure 3.1. AOC has built in to the wavemaking software procedure described in this section the capability to automatically iterate on several standard spectral forms. For these tests an option called "Custom" was used to model the spectrum as closely as practical but in addition a "standard" JONSWAP form was also tried for comparison purposes. The JONSWAP functional form was more amenable to an automatic computer controlled iteration scheme whereas the "custom" option requires a more hands-on iteration where the operator defines the input values for each iterative cycle. Figure 3.1 shows the given spectrum and two selected "Standard" spectral forms corresponding to the best fit ISSC and JONSWAP forms. Following the iterative calibration procedures discussed in the preceeding paragraphs test tapes

were made for the JONSWAP and Custom (i.e. actual) spectral shapes. (The ISSC approximation was considered to be too far removed and was not tested.)

4.TEST RESULTS

4.1 Spectra

Figures 4.1 through 4.3 present the results for the simulated spectra for a duration of 30 minutes (prototype time of 1950 seconds) using the "custom" spectrum fit and Figures 4.4 through 4.6 present similar results using the "canned" JONSWAP approximation with $\gamma = 1.5$. The general match between the simulated and the observed is not notably better between these two approaches. Two general features are noted: a) The simulated sea-state spectra lie above the desired at frequencies below 0.6 hertz. b) The simulated sea-state spectra are always lower than the desired for the high frequency tail of the spectra. This is as might be expected since the high frequency waves tend to be damped by the lower wave frequency components as the wave energy is propagated. This behavior is particularly marked for the wave gage 3 which was located further from the wave generator. In the real sea, such spectra would be generated in conditions of strong local winds which continually feed energy into the higher frequencies. This phenomenon was not simulated in these scaled tests.

The original intent was to simulate the sea-state defined by Figure 3.1 which was obtained from a 30 minute record. The test tapes were made for a longer (scaled) period and tests were made for a simulated duration of 60 minutes. Examples of the results are given in Figures 4.7 through 4.10 for the two spectra approximations. It is seen that for the longer duration tests, the wave heights increase for the same control attenuator settings and the tendency for the higher frequencies to damp out with travel distance is clearly seen by comparison of the spectra between gages 2 and 3.

4.2 Time Histories and Statistical Distributions of Wave Heights

A total time duration of almost 4000 seconds was measured for the sea-states corresponding to the two spectral distributions. Figures 4.11 and 4.12 show the complete tme series for gage location 2. In both simulations there is a notable large wave near the 1600 second time period. These events have been plotted on an expanded time scale on Figures 4.13 and 4.14. It is seen that an wave height of about 77 feet occurs in a sea-state having a significant wave height value of about 40 feet.

Figures 4.15 and 4.16 present statistical summaries for all wave heights recorded during the tests. These plots are derived from a standard "mean down crossing" analysis (i.e. trough to crest heights) and show that such large waves are a little higher than would be predicted by the the traditional Rayleigh distribution function but not excessively so.

5. COMMENTS AND CONCLUSIONS

An attempt was made to create a simulation of time domain waves having a spectrum which closely matched that recorded during Hurricane Camille of August 17 1969. Arctec Offshore Corporation's standard spectral simulation process was used to perform this simulation at a scale of 1:30 in a basin measuring 298 feet long by 48 feet wide in a water depth of 13.5 feet.

Waves were measured at three locations in the test basin: in the center of the basin and 12 feet from the side, at a distance of 82 feet from the wave generator, and 8 feet from the side at distance of 195 feet from the wave maker. The wave time histories were simulated for one hour (prototype scale) although the original measurements were for a 30 minute period only.

The wave records were analysed for their spectral content and wave height probability distribution was also derived from the recorded waves

in the basin. Wave spectra were examined from the first 30 minutes (approximately) and from the entire record length. The wave spectra for the entire duration generally showed higher energy levels than those from the first 30 minutes. This was thought to be the result of build up of energy due to imperfect absorption of wave energy by the beach. The beach is known to have reflection coefficients in the range of about 5% which would correspond quite well with the observed wave height increase of about 5% between the first 30 minutes and the full hour.

The wave height probability distributions in general coincide quite well with the Rayleigh distribution but the largest waves in the record were a little higher than such a distribution would indicate. This observation from the tests does not agree with many cases of wave height distributions measured during storms in the ocean which tend to show that the deviation from the Rayleigh distribution is towards the low side. If this observation is supported by further data from field and test basins then it would indicate that results from structural tests in wave basins may be on the conservative side.

It was noted from the test data that the wave heights would decay with travel distance, largely due to loss of energy at the higher frequencies. This would be expected for such a stormy sea-state as was measured during Camille. The presence of white caps indicates energy dissipation which would be replaced in the real sea by wind-wave energy transfer. This phenomenon is not simulated in the test basin. For severe seas the wave maker has to be overdriven in the higher frequency range, thereby allowing for the decay process, to match the desired spectrum at one place in the test basin.

6. REFERENCES

Rice, S. O. (1951) "Mathematical Analysis of Random Noise", Bell System Technical Journal, Vols. 23 and 24. Also available in "Selected Papers on Noise and Stochastic Processes", Dover Publications, 1954.

Elgar, S., Guza, R. T., and Seymour, R. J. (1984). "Prediction of Wave Group Statistics ", Proceedings, 19th International Conference on Coastal Engineering, Houston Texas, September.

Buckley, W. H. (1987). "Climatic Wave Spectra for Use in Design of Ships and Offshore Platforms", DTNSRDC Report SD-87-173-33, January.

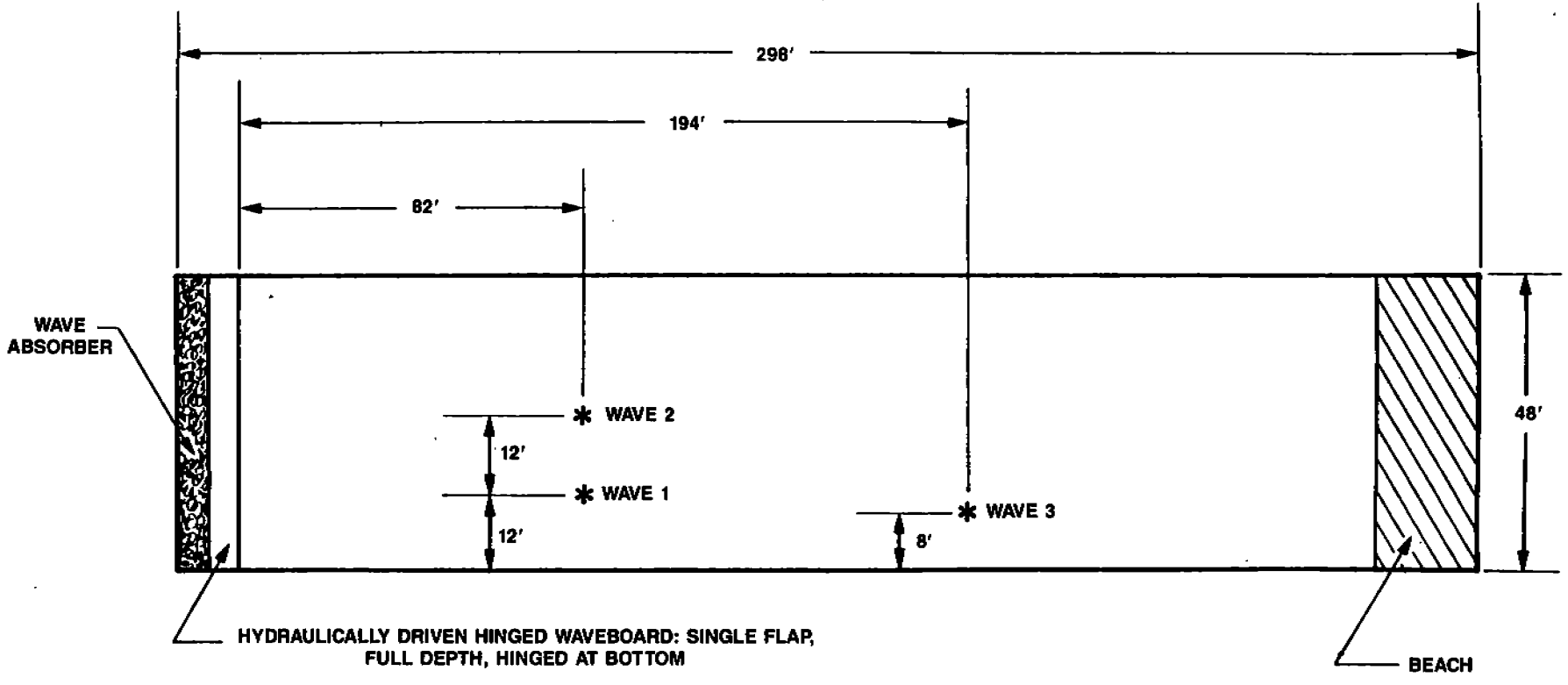

WAVE BASIN and TEST SET-UP

Figure 2.1

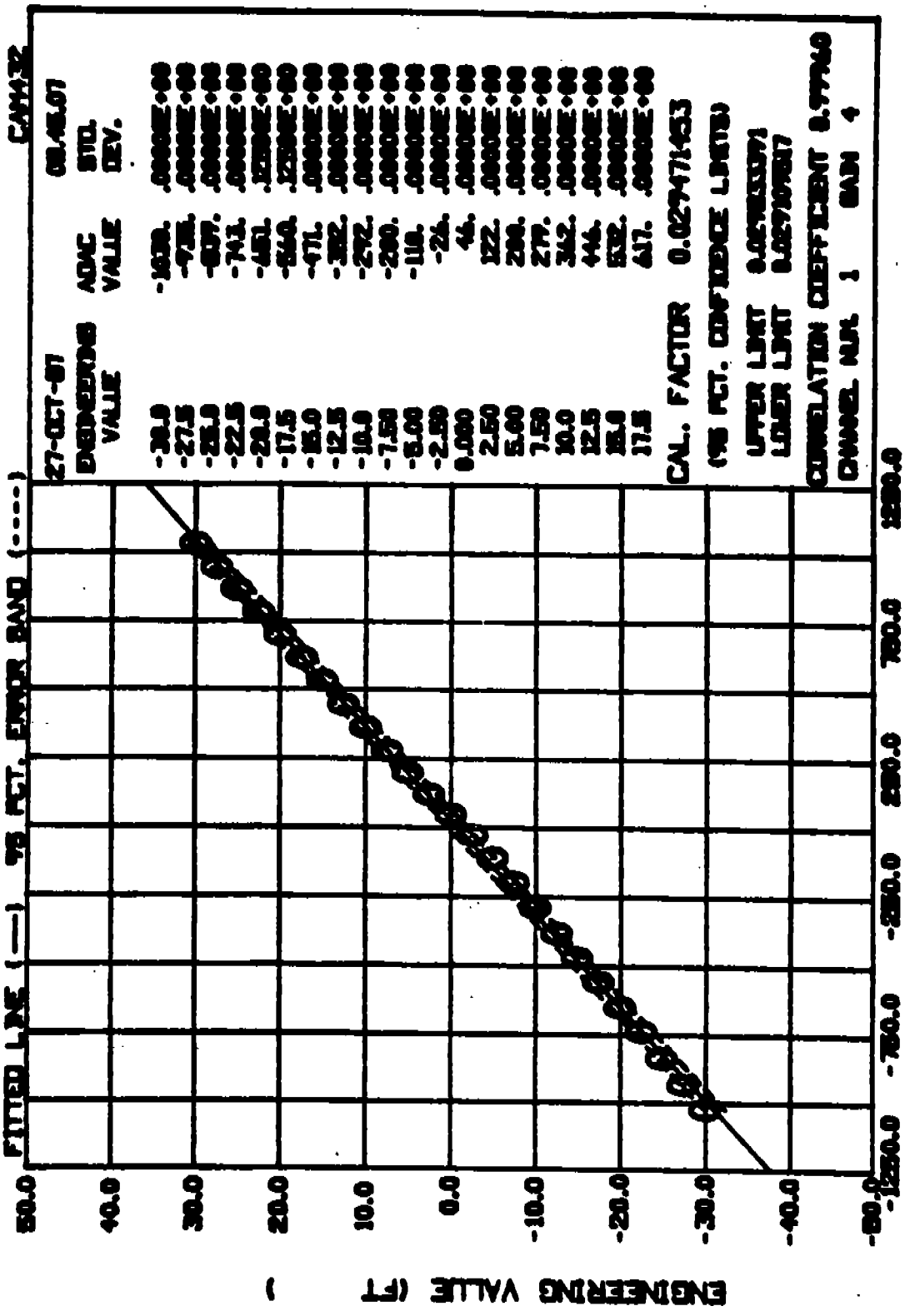

Figure 2.2(a) Calibration for Wave Probe 1

Project: CAM432 Ch. name: WAVE1 Page 2

Engineering Value	ADAC Value	STD. DEV.
-30.0	-1030.	.00000E+00
-27.5	-935.	.00000E+00
-25.0	-839.	.00000E+00
-22.5	-743.	.00000E+00
-20.0	-651.	.12500E+00
-17.5	-560.	.12500E+00
-15.0	-471.	.00000E+00
-12.5	-382.	.00000E+00
-10.0	-292.	.00000E+00
-7.50	-200.	.00000E+00
-5.00	-110.	.00000E+00
-2.50	-26.	.00000E+00
0.000	46.	.00000E+00
2.50	122.	.00000E+00
5.00	200.	.00000E+00
7.50	279.	.00000E+00
10.0	362.	.00000E+00
12.5	446.	.00000E+00
15.0	532.	.00000E+00
17.5	617.	.00000E+00
20.0	699.	.12500E+00
22.5	781.	.00000E+00
25.0	864.	.00000E+00
27.5	946.	.00000E+00
30.0	1031.	.25000E+00

Figure 2.2(b) Calibration for Wave Probe 1

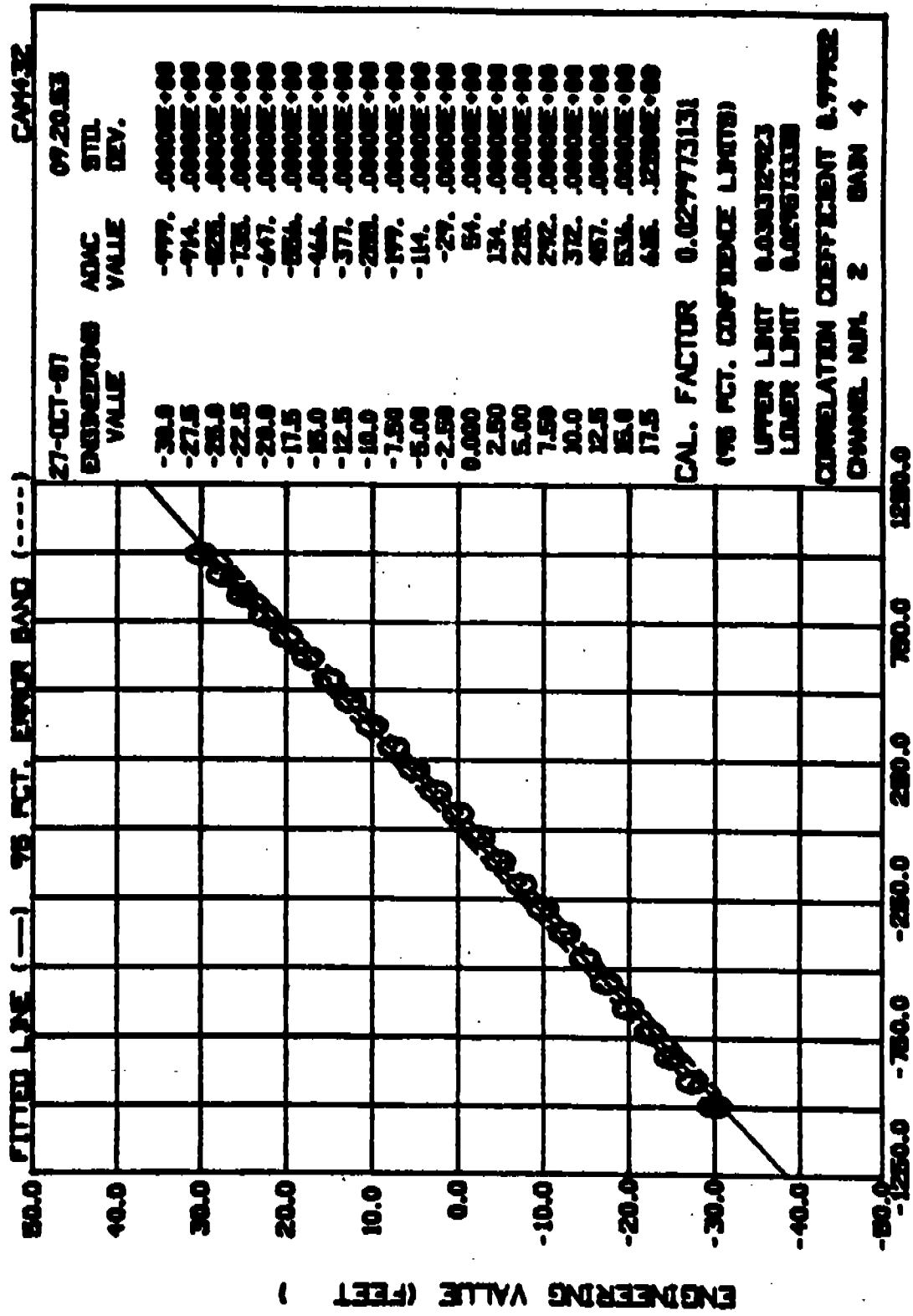

Figure 2.3(a) Calibration for Wave Probe 2

Project: CAM432 Ch. name: WAVE-2 Page 2

Engineering Value	ADAC Value	STD. DEV.
-30.0	-999.	.00000E+00
-27.5	-914.	.00000E+00
-25.0	-825.	.00000E+00
-22.5	-735.	.00000E+00
-20.0	-647.	.00000E+00
-17.5	-556.	.00000E+00
-15.0	-466.	.00000E+00
-12.5	-377.	.00000E+00
-10.0	-288.	.00000E+00
-7.50	-199.	.00000E+00
-5.00	-114.	.00000E+00
-2.50	-29.	.00000E+00
0.000	54.	.00000E+00
2.50	134.	.00000E+00
5.00	215.	.00000E+00
7.50	292.	.00000E+00
10.0	372.	.00000E+00
12.5	457.	.00000E+00
15.0	536.	.00000E+00
17.5	615.	.12500E+00
20.0	694.	.00000E+00
22.5	768.	.00000E+00
25.0	844.	.00000E+00
27.5	917.	.00000E+00
30.0	995.	.00000E+00

Figure 2.3(b) Calibration for Wave Probe 2

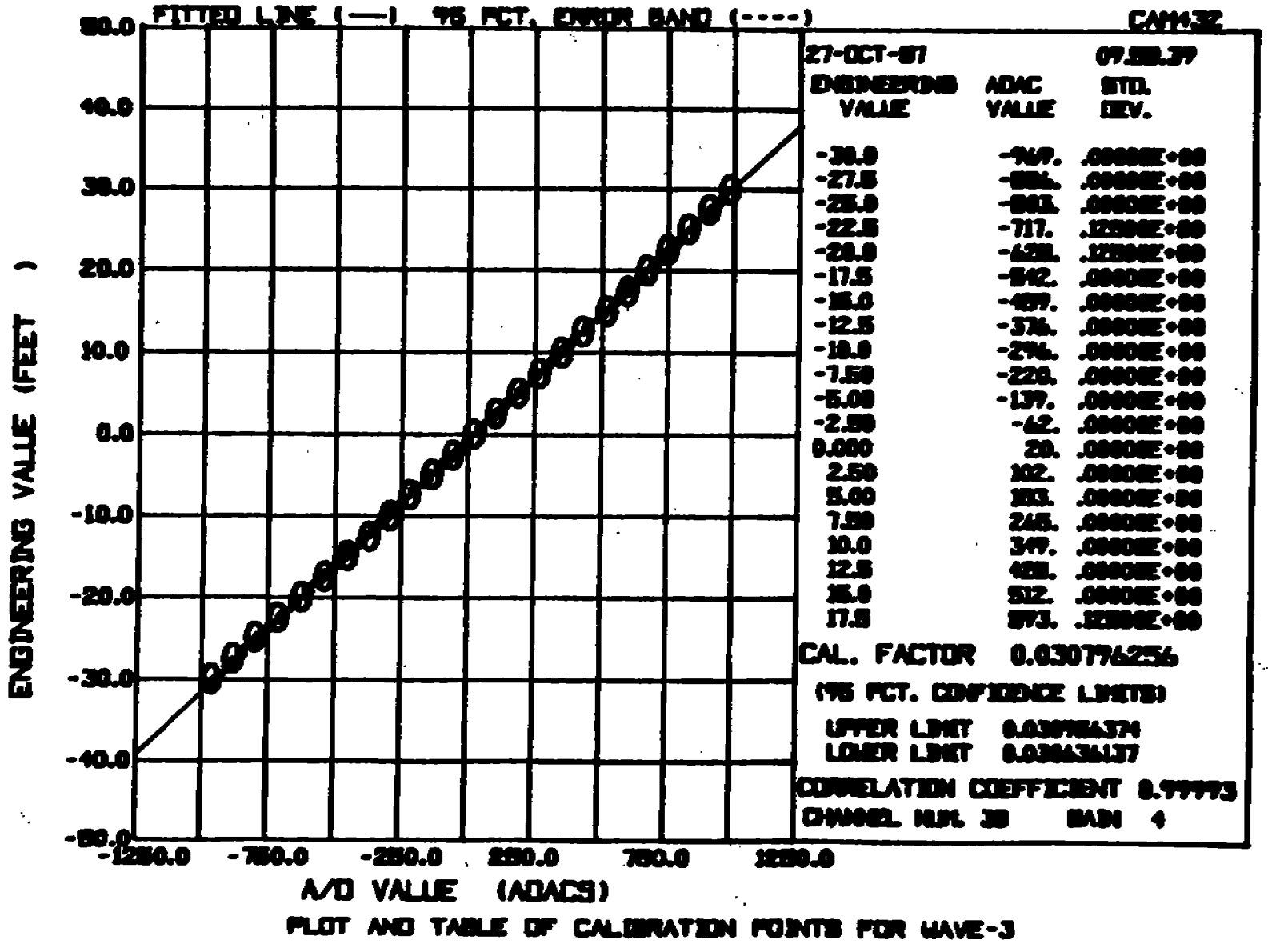

Figure 2.4(a) Calibration for Wave Probe 3

Project: CAM432 Ch. name: WAVE-3 Page 2

Engineering Value	ADAC Value	STD. DEV.
-30.0	-969.	.00000E+00
-27.5	-886.	.00000E+00
-25.0	-803.	.00000E+00
-22.5	-717.	.12500E+00
-20.0	-628.	.12500E+00
-17.5	-542.	.00000E+00
-15.0	-459.	.00000E+00
-12.5	-376.	.00000E+00
-10.0	-296.	.00000E+00
-7.50	-220.	.00000E+00
-5.00	-139.	.00000E+00
-2.50	-62.	.00000E+00
0.000	20.	.00000E+00
2.50	102.	.00000E+00
5.00	183.	.00000E+00
7.50	265.	.00000E+00
10.0	349.	.00000E+00
12.5	428.	.00000E+00
15.0	512.	.00000E+00
17.5	593.	.12500E+00
20.0	667.	.12500E+00
22.5	744.	.00000E+00
25.0	823.	.00000E+00
27.5	904.	.00000E+00
30.0	983.	.00000E+00

Figure 2.4(b) Calibration for Wave Probe 3

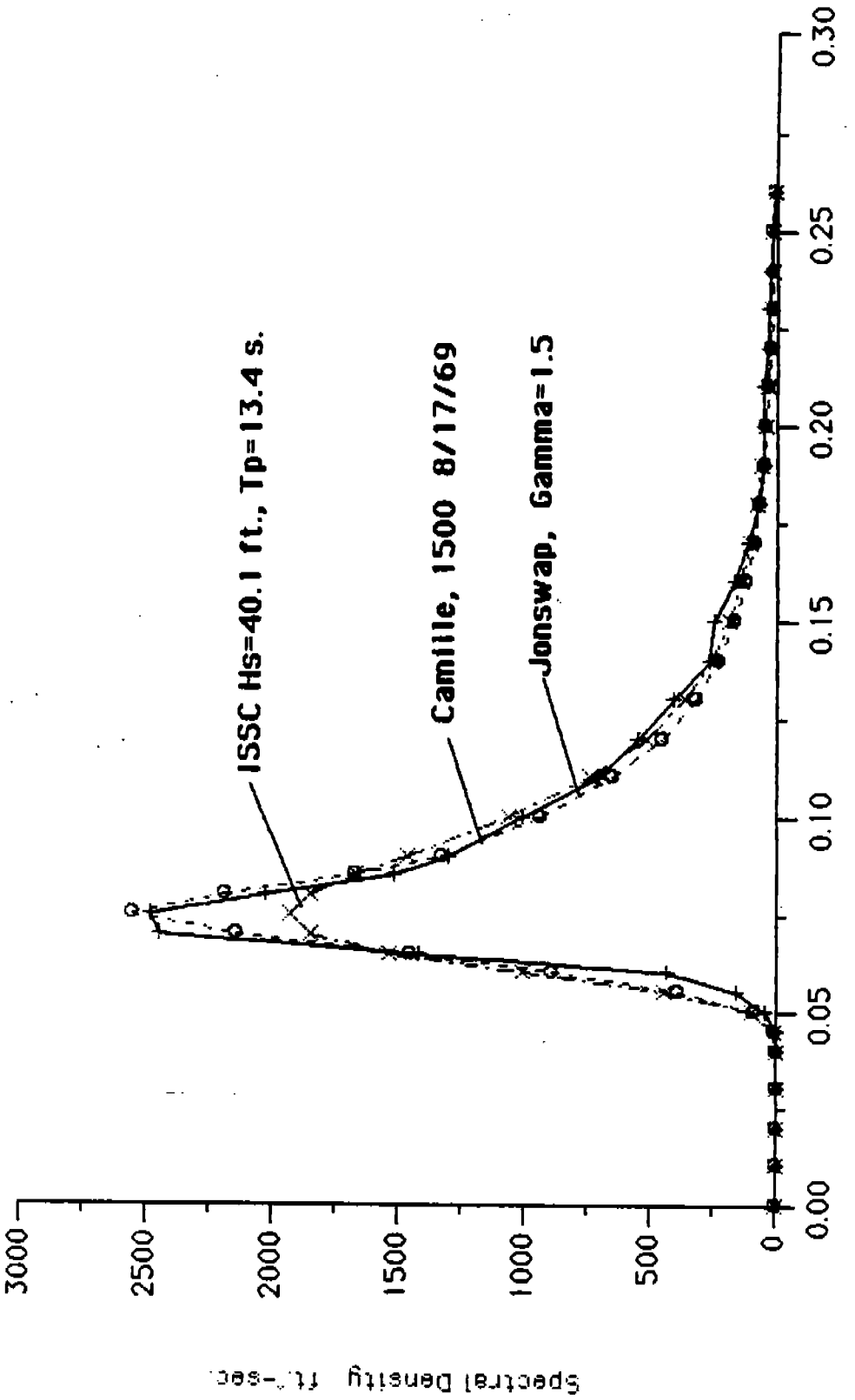

Figure 3.1 Measured Camille Spectra with JONSWAP and ISSC Models

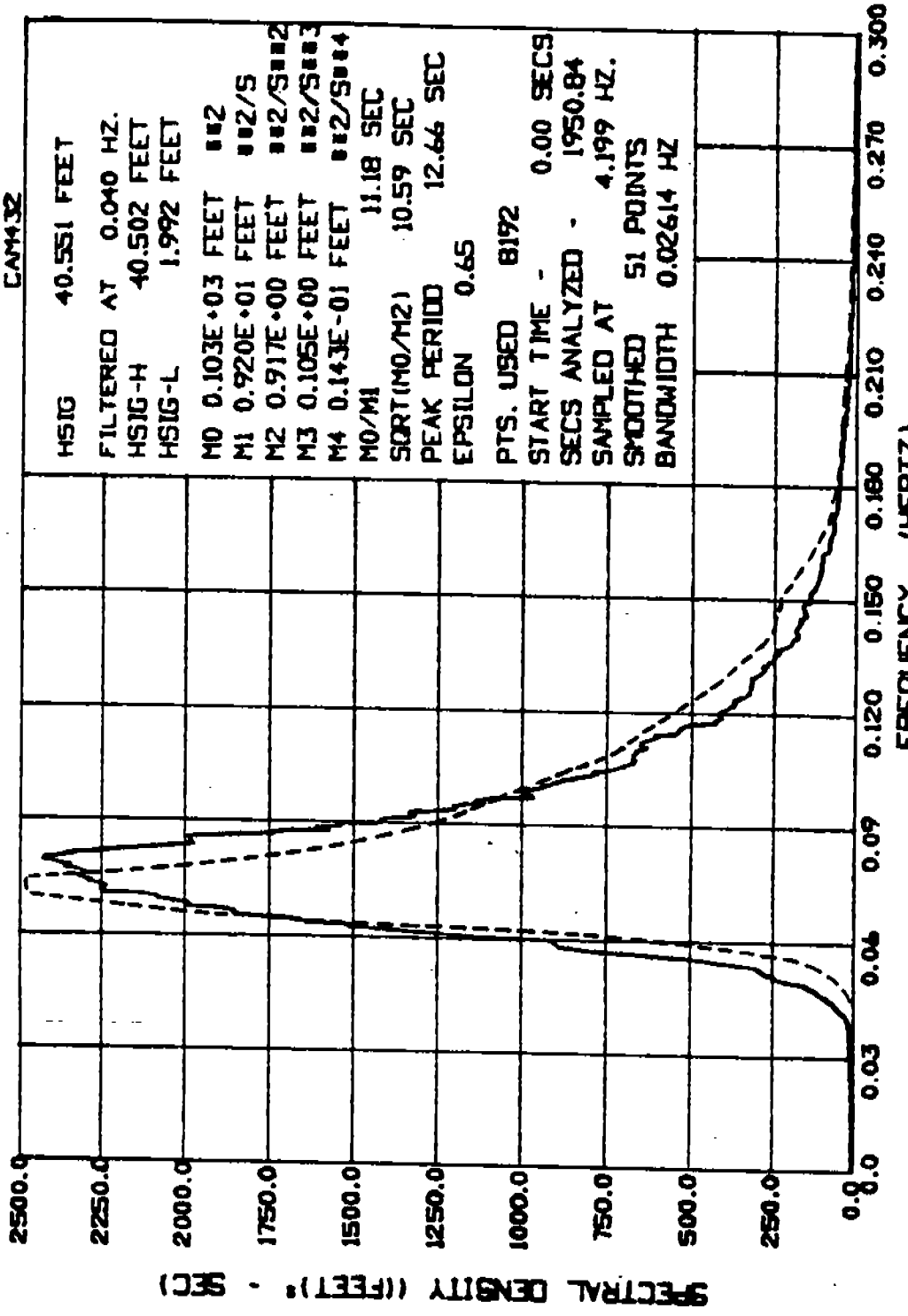

Figure 4.1 Spectrum from Wave Gage 1 for 30 Minute Simulation Using Custom Spectrum

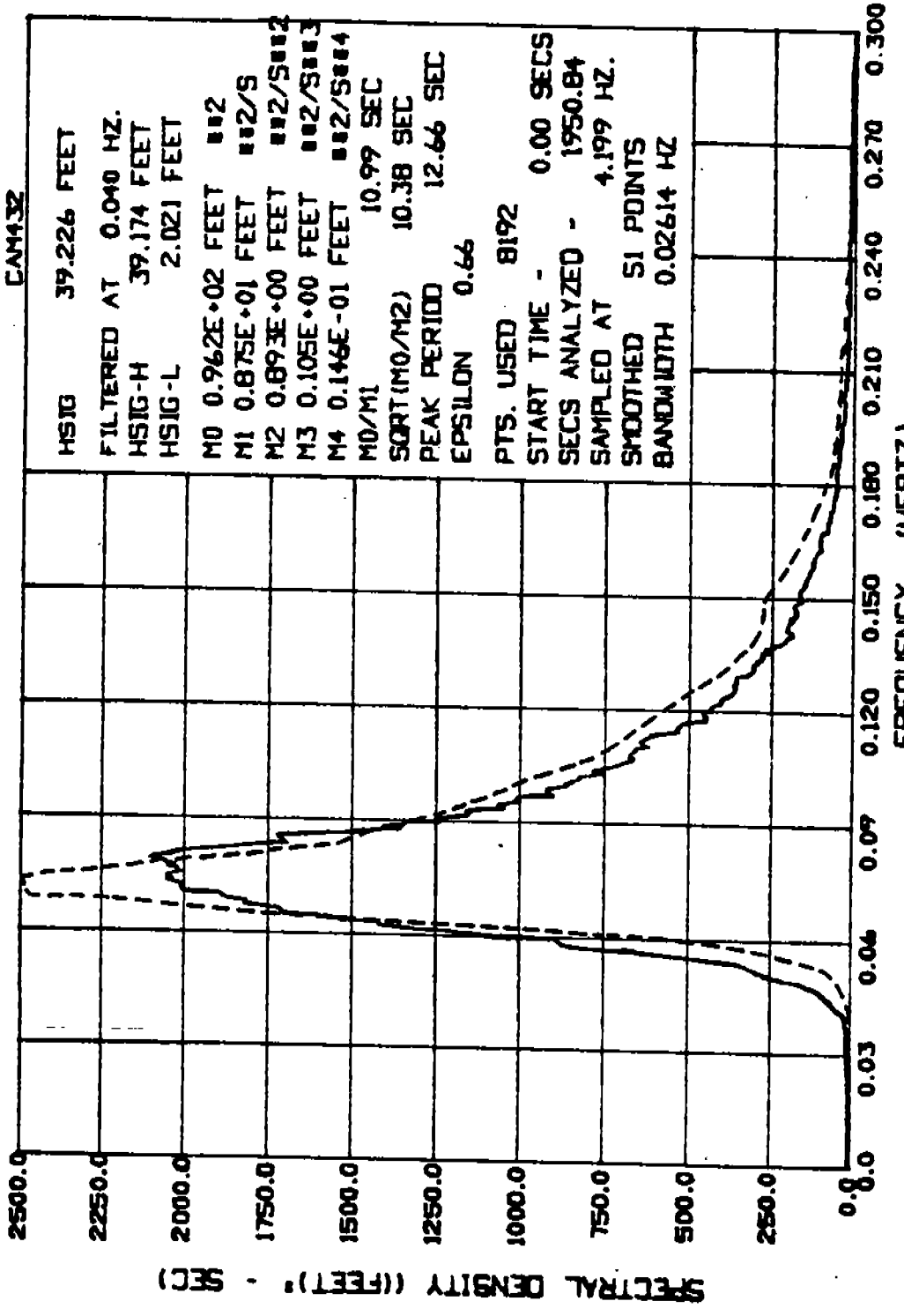

Figure 4.2 Spectrum from Wave Gage 2 for 30 Minute Simulation Using Custom Spectrum

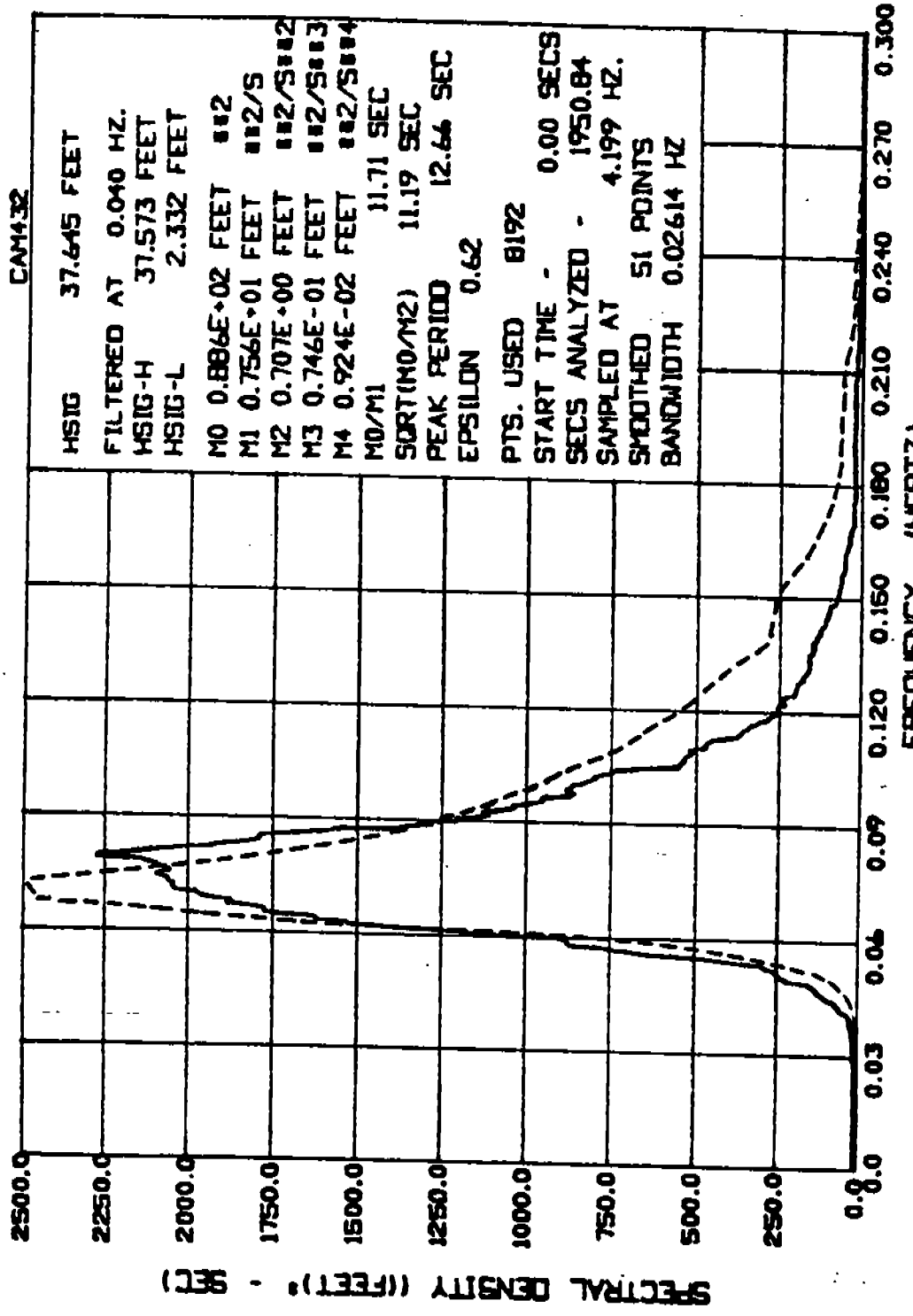

Figure 4.3 Spectrum from Wave Gage 3 for 30 Minute Simulation Using Custom Spectrum

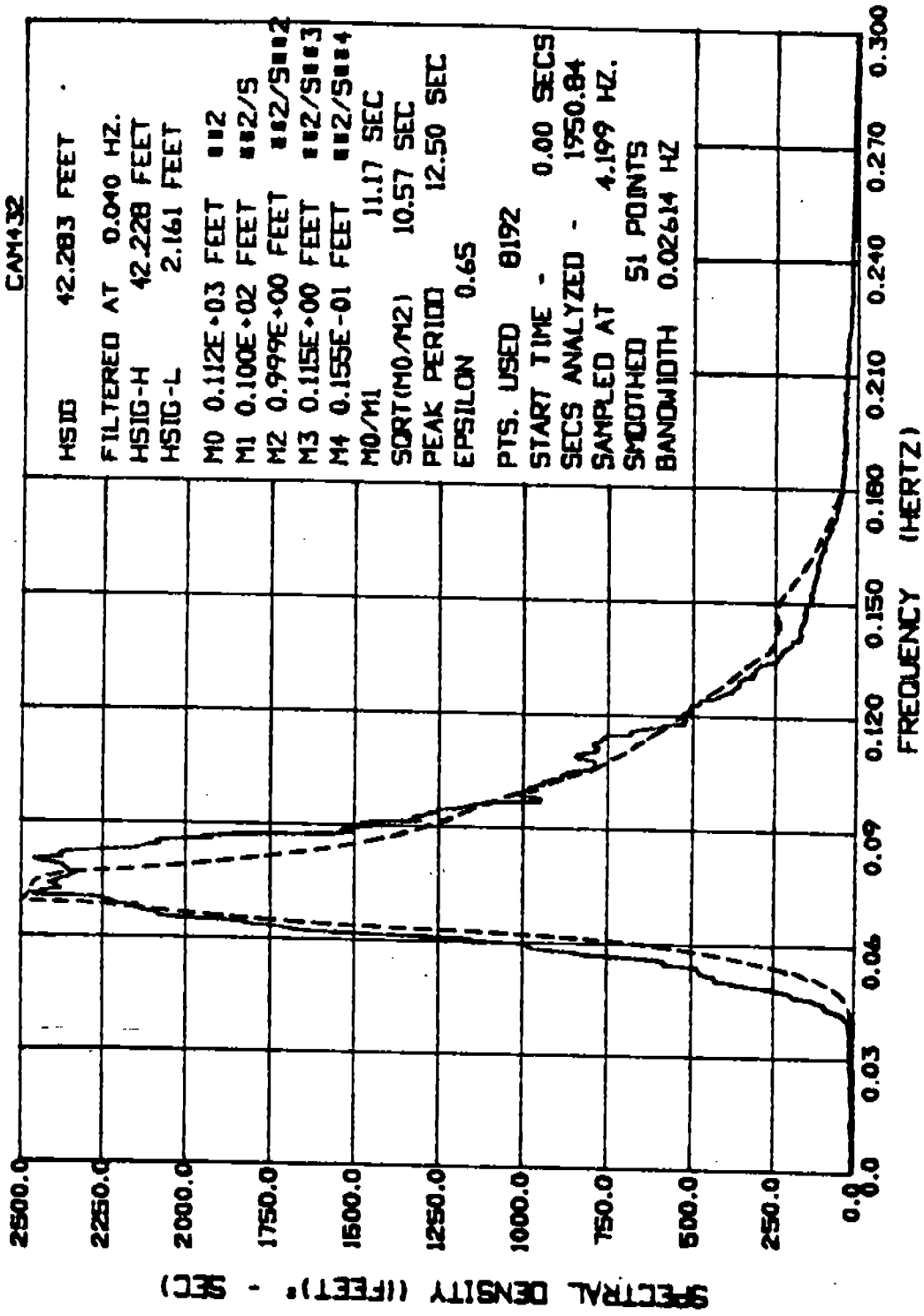

Figure 4.4 Spectrum from Wave Gage 1 for 30 Minute Simulation Using JONSWAP Spectrum

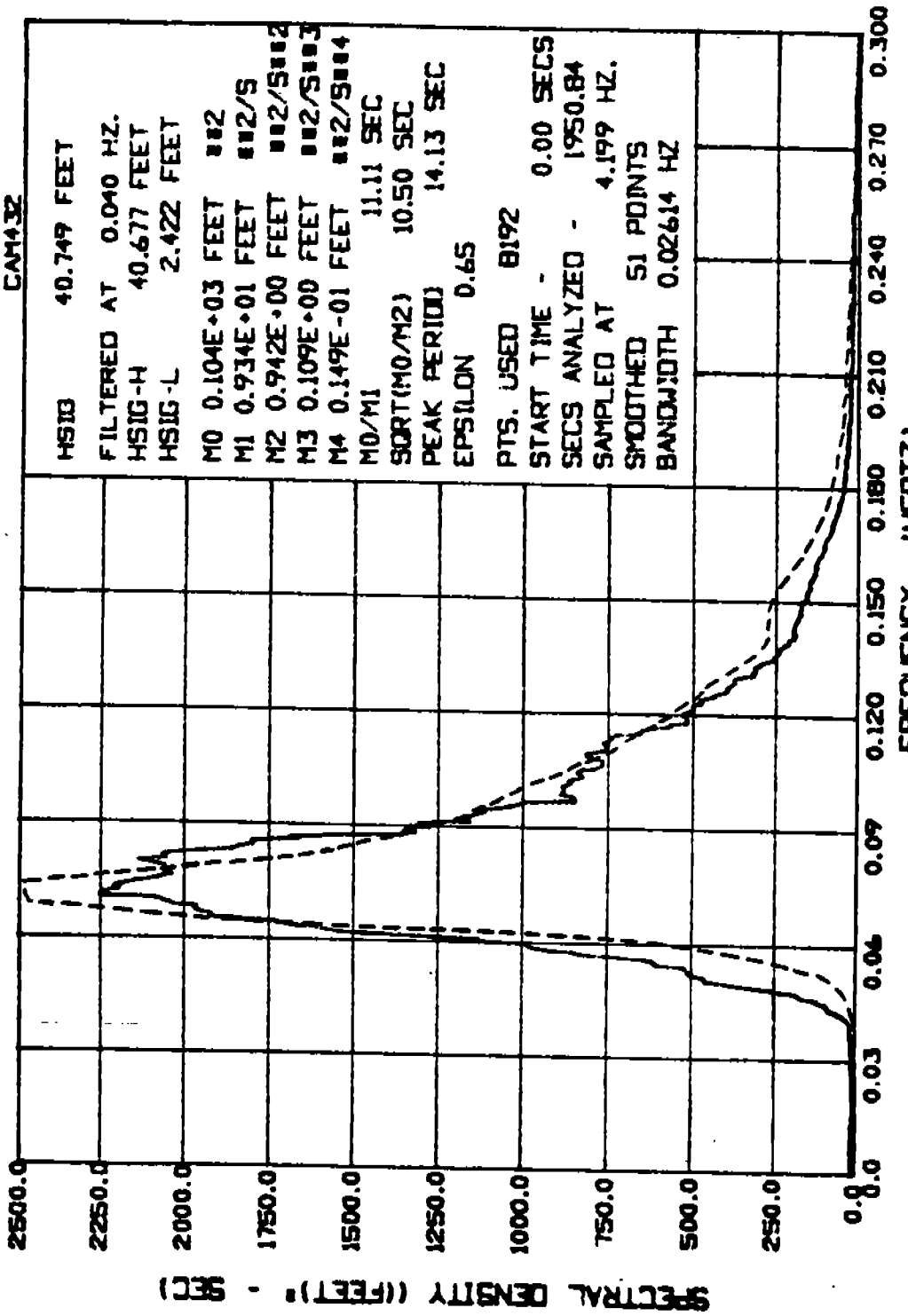

Figure 4.5 Spectrum from Wave Gage 2 for 30 Minute Simulation Using JONSWAP Spectrum

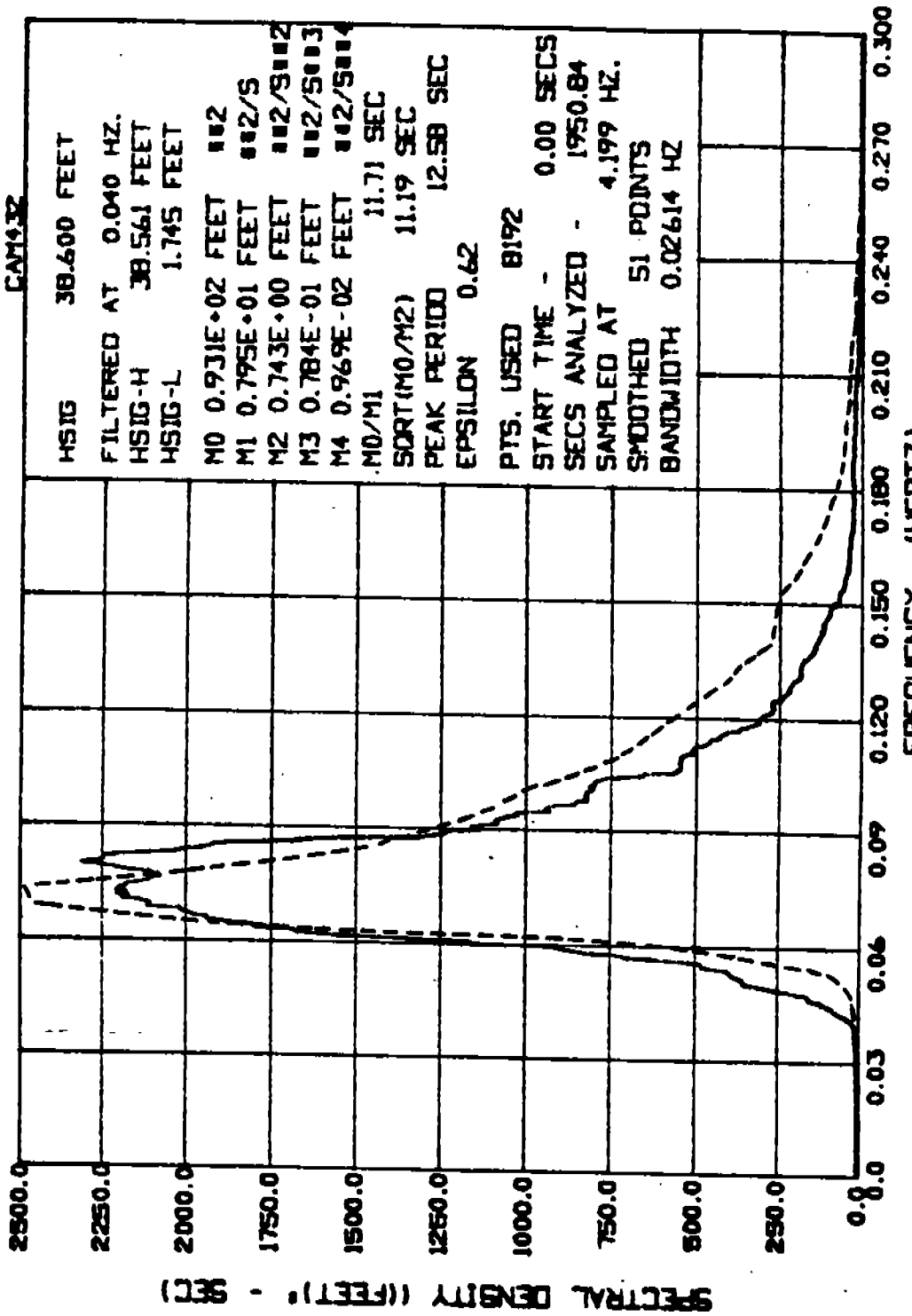

Figure 4.6 Spectrum from Wave Gage 3 for 30 Minute Simulation Using JONSWAP Spectrum

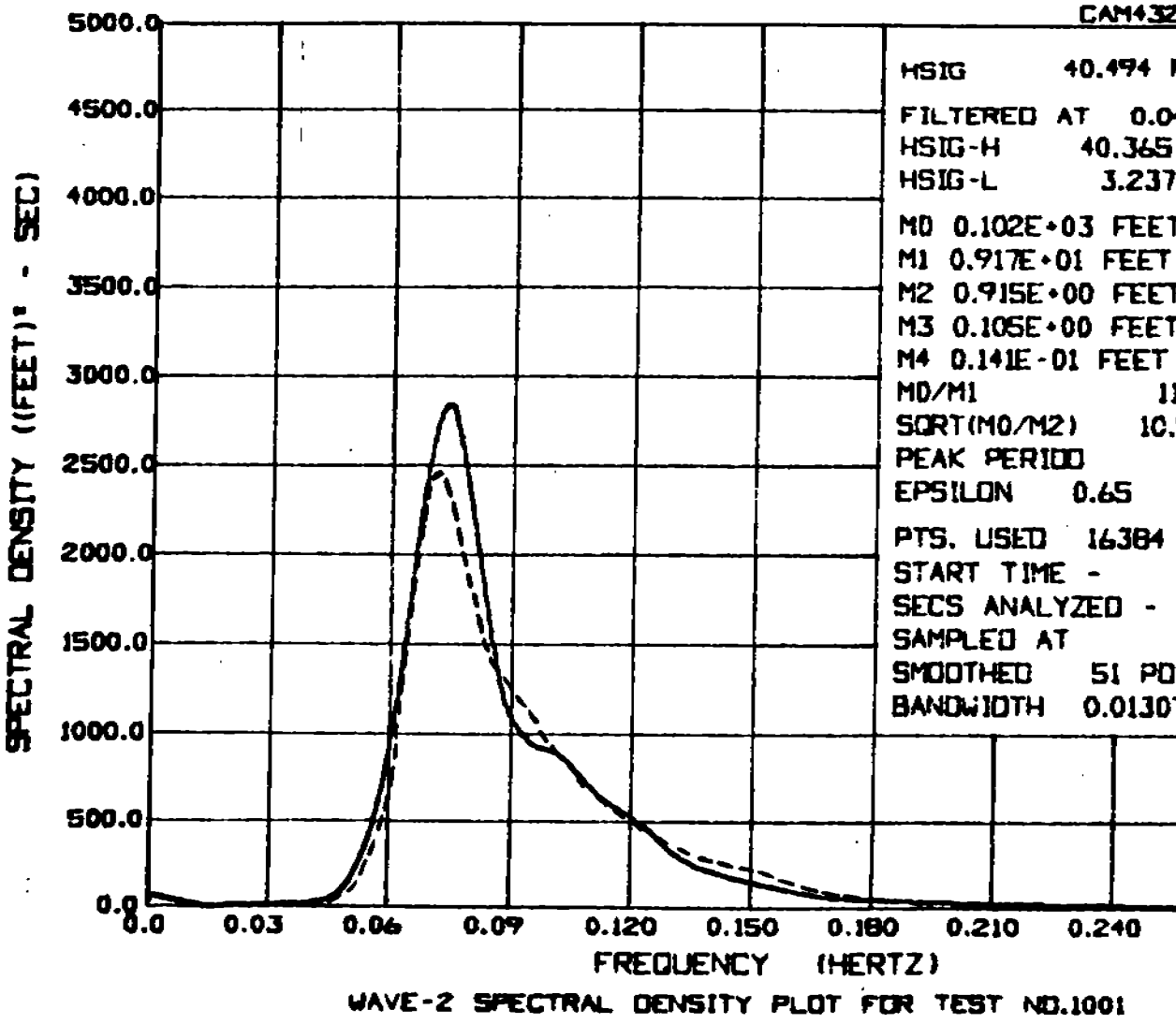

Figure 4.7 Spectrum from Wave Gage 2 for 60 Minute Simulation Using Custom

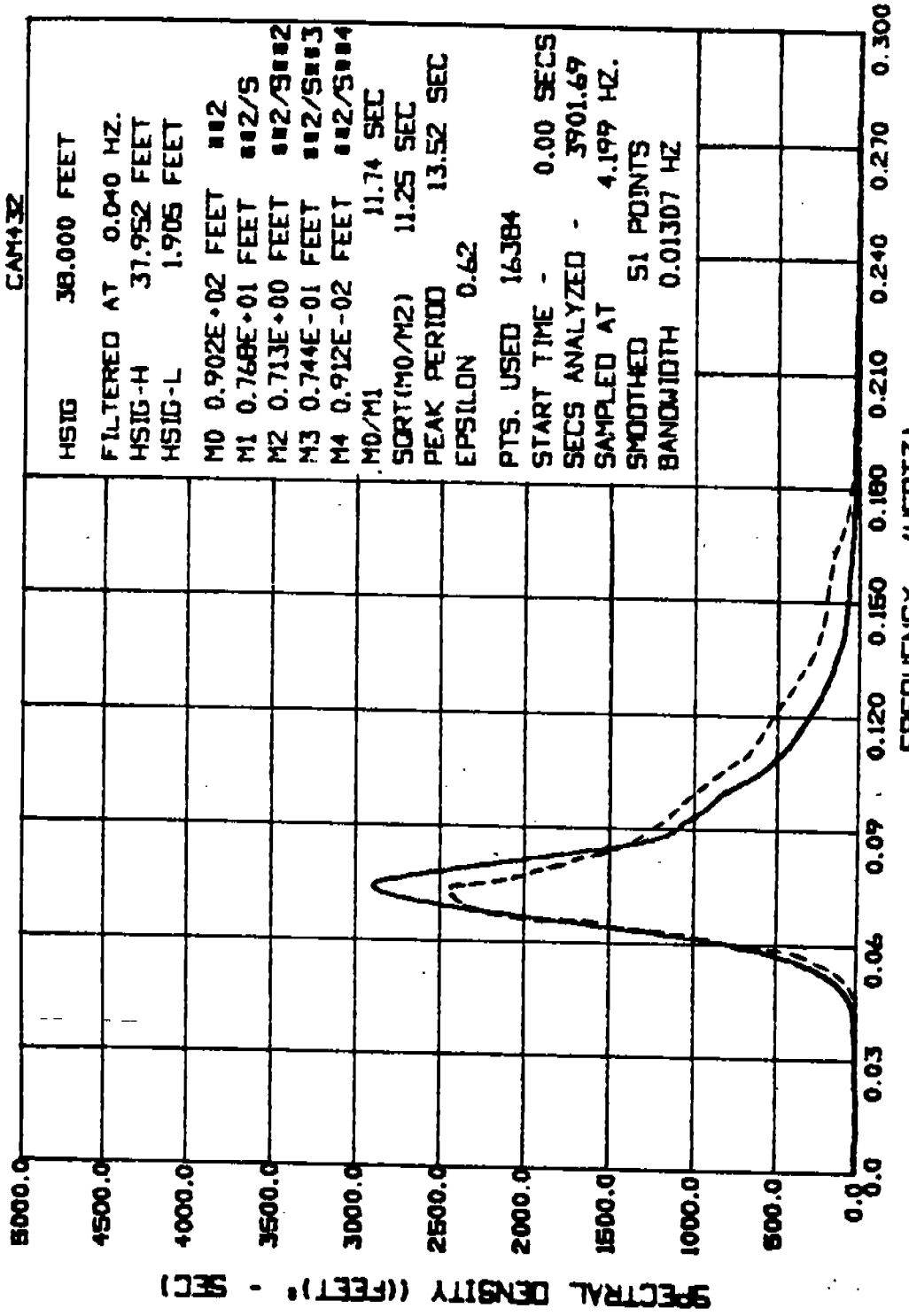

Figure 4.8 Spectrum from Wave Gage 3 for 60 Minute Simulation Using JONSWAP Spectrum

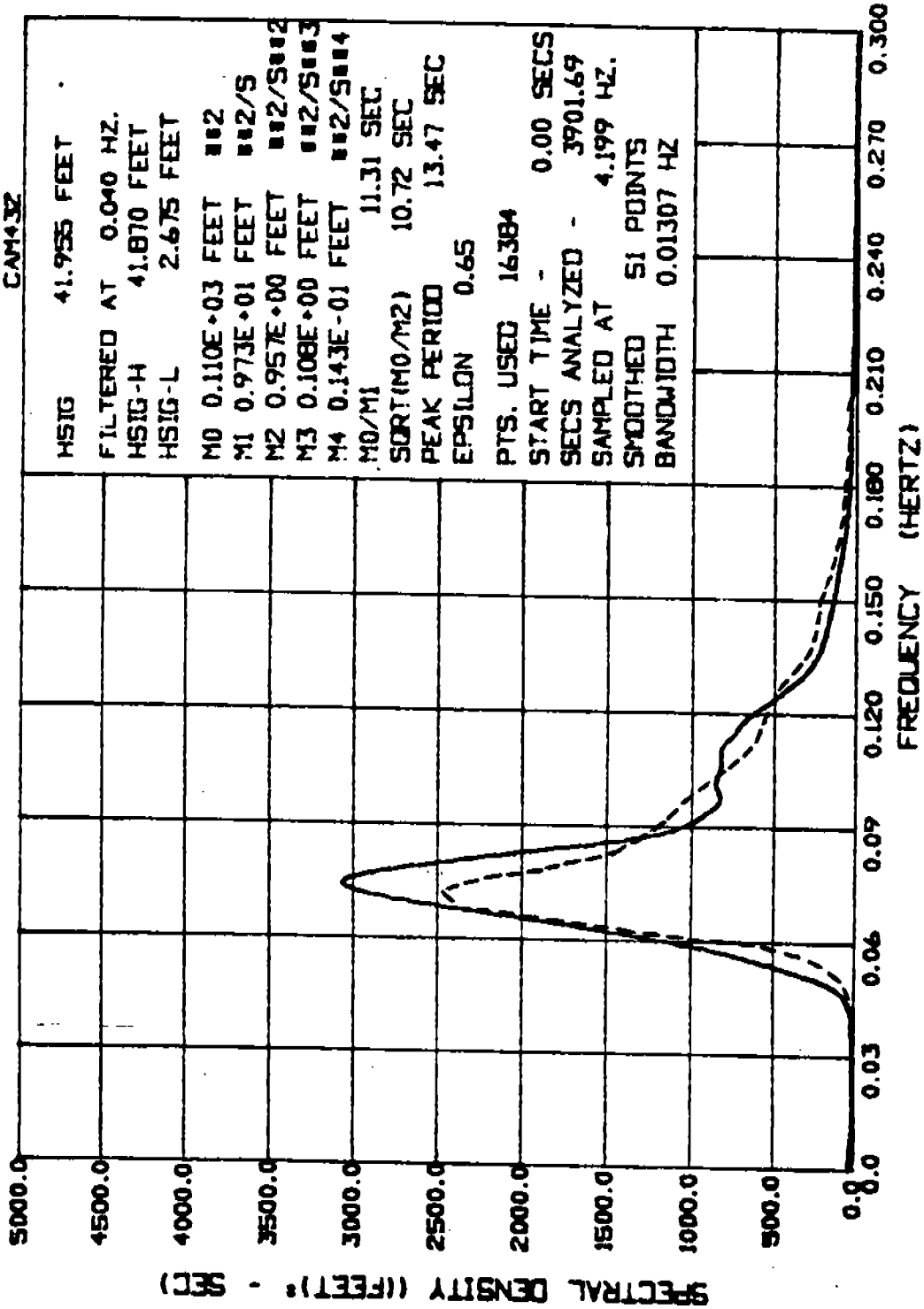

Figure 4.9 Spectrum from Wave Gage 2 for 60 Minute Simulation Using JONSWAP Spectrum

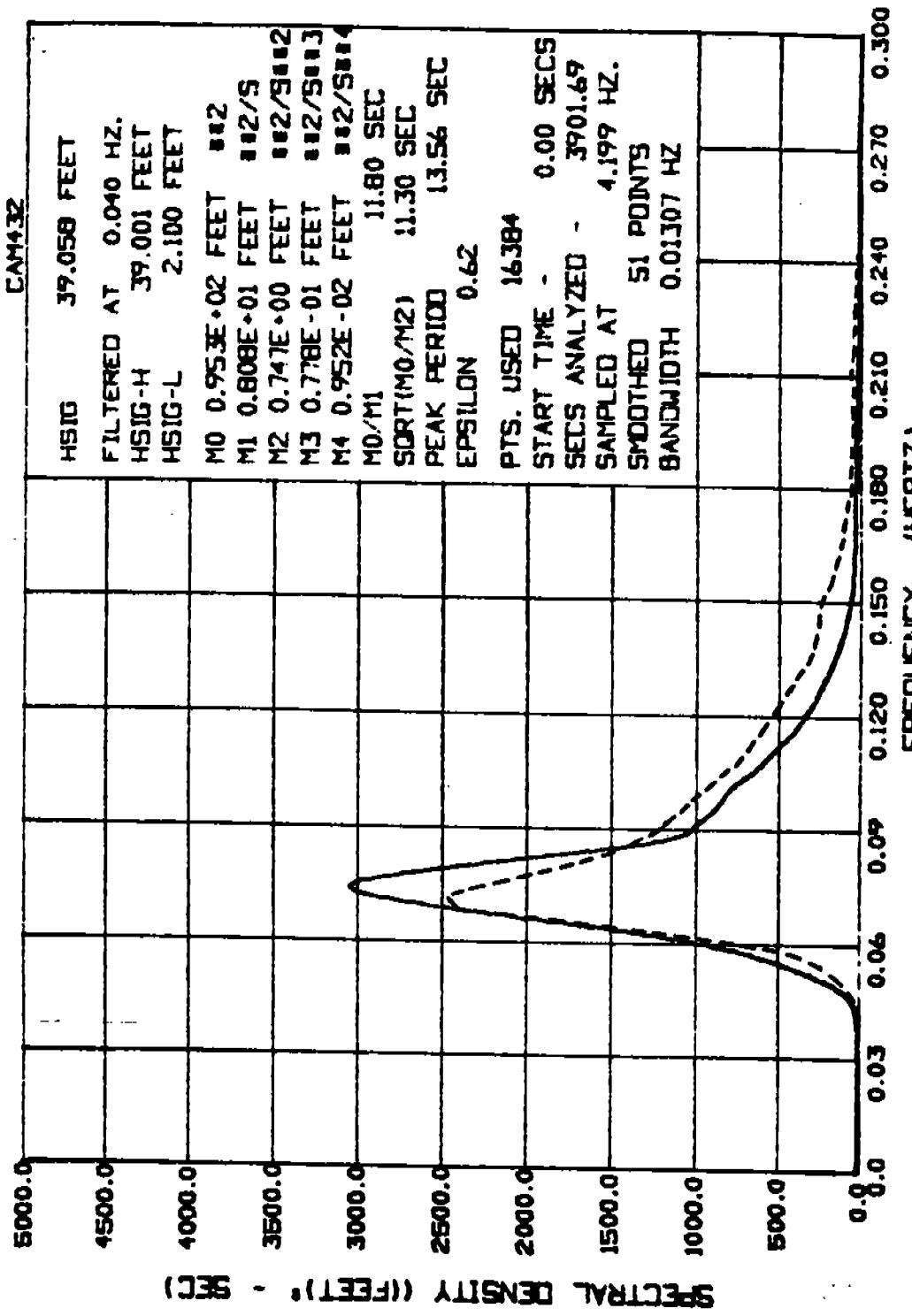

Figure 4.10 Spectrum from Wave Gage 3 for 60 Minute Simulation Using JONSWAP Spectrum

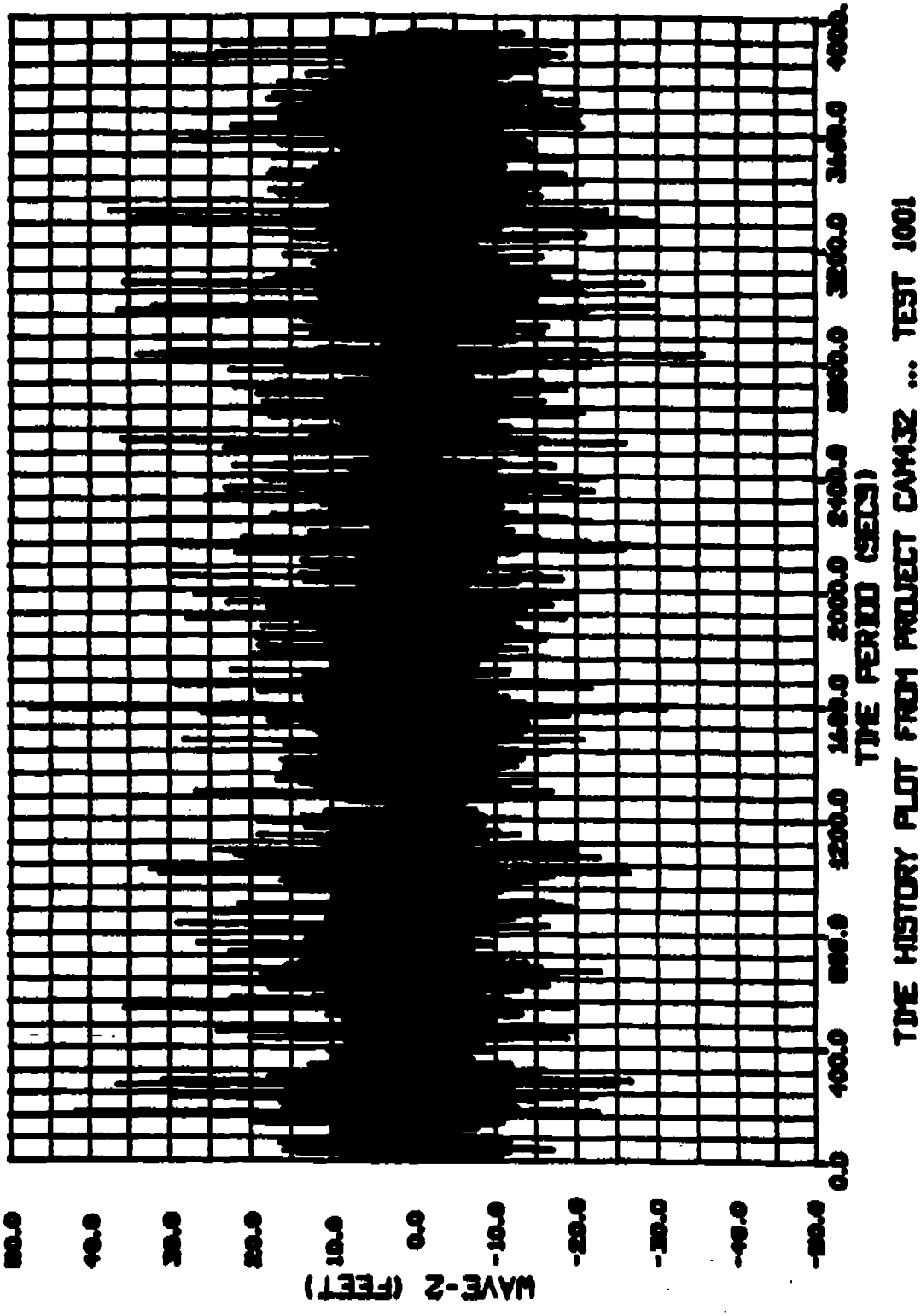

Figure 4.11 Time Series at Gage 2 for "Custom" Spectrum

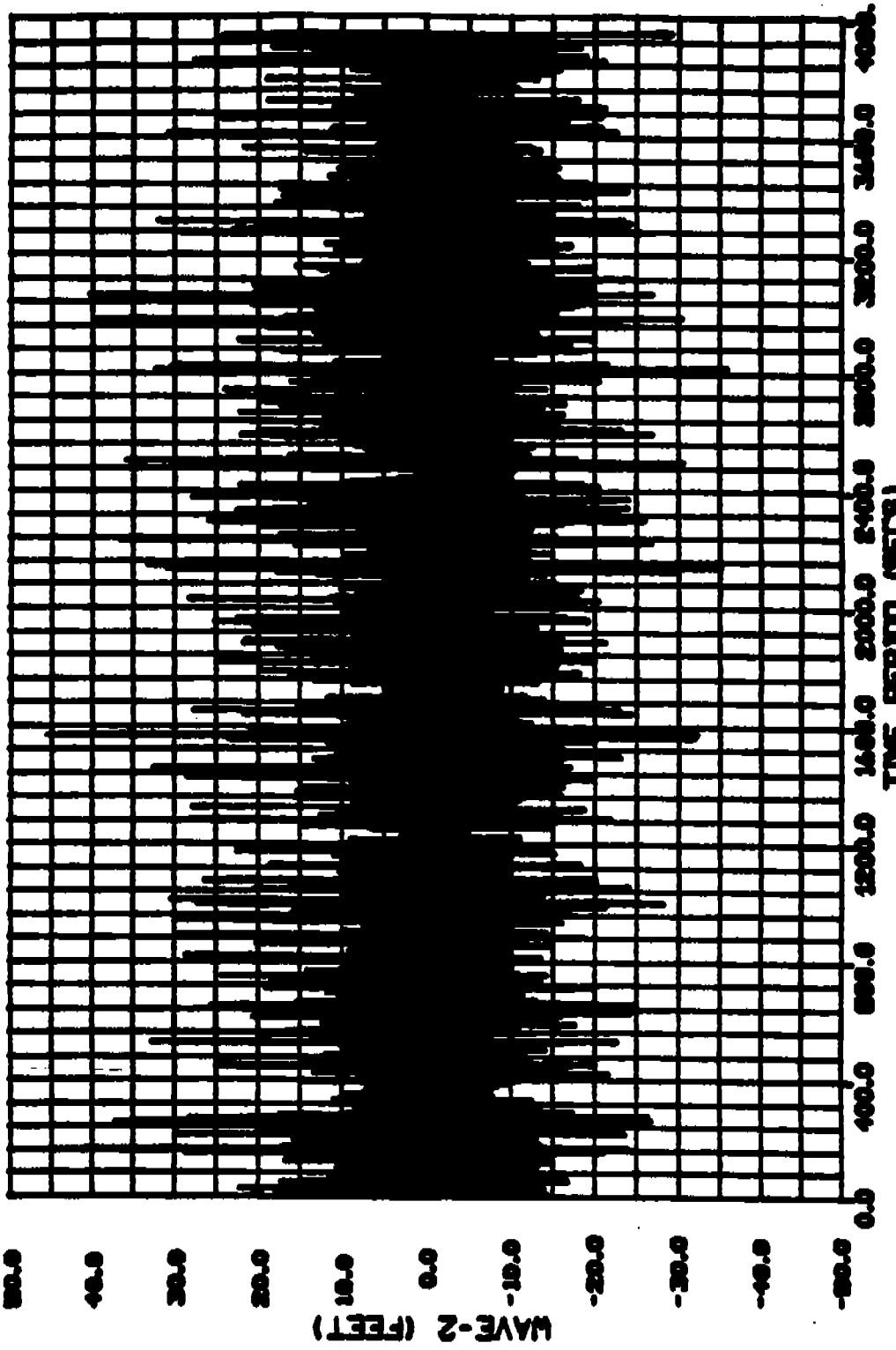

Figure 4.12 Time Series at Gage 2 for JONSWAP Spectrum

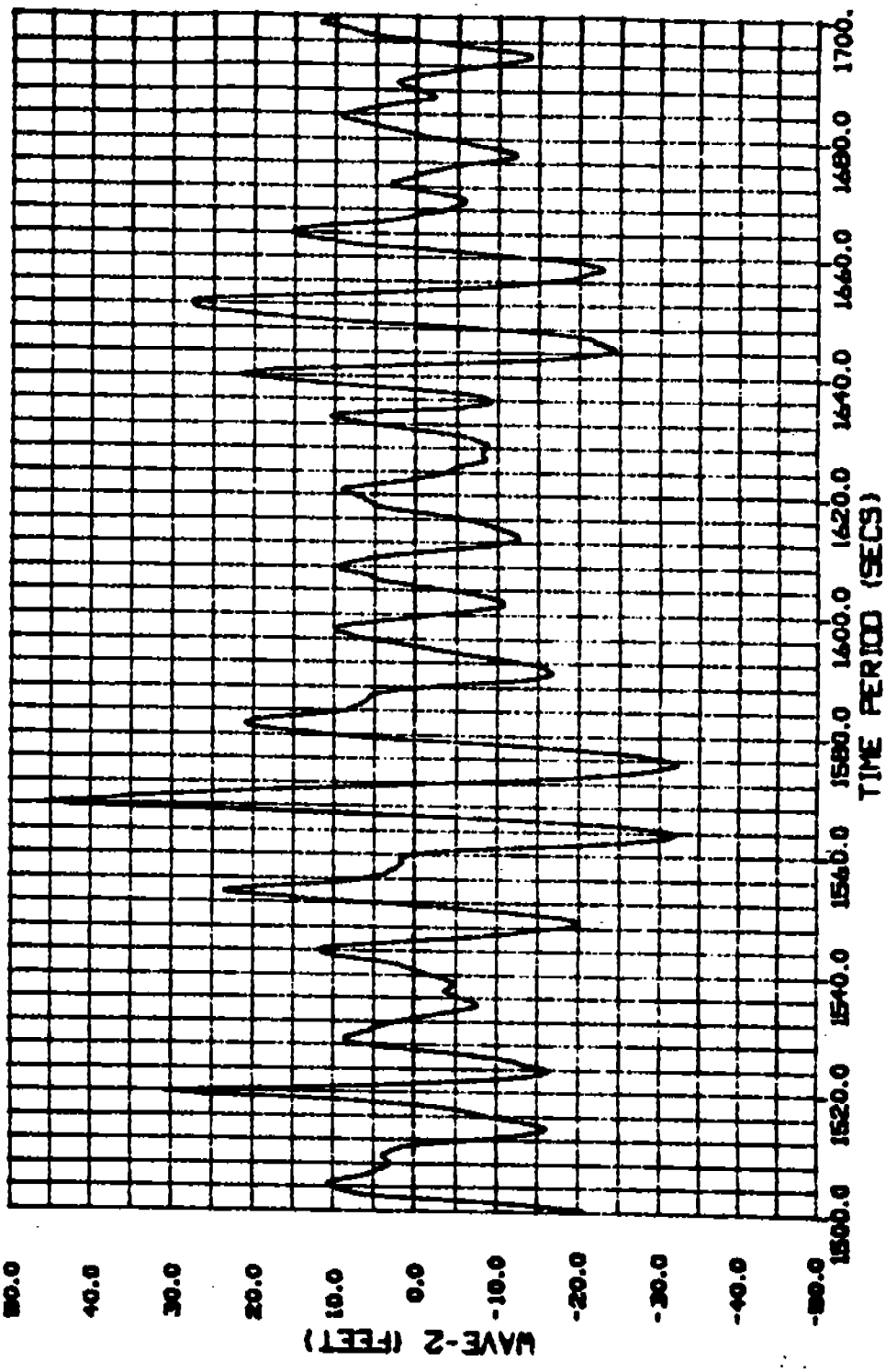

Figure 4.13 Expanded Time Scale of "Episodic" Wave from Test 1001

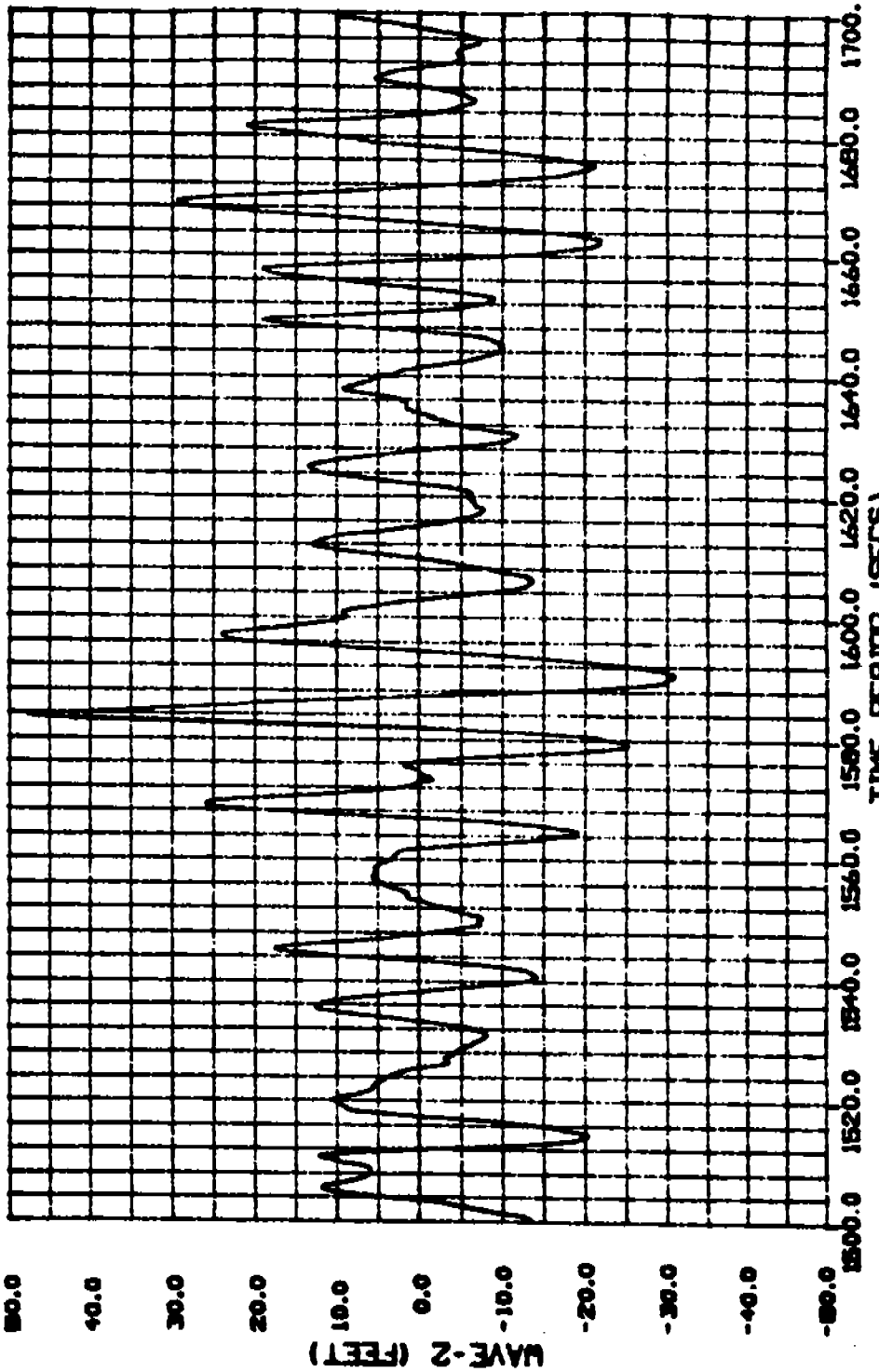

Figure 4.14 Expanded Time Scale of "Episodic" Wave for Test 2000

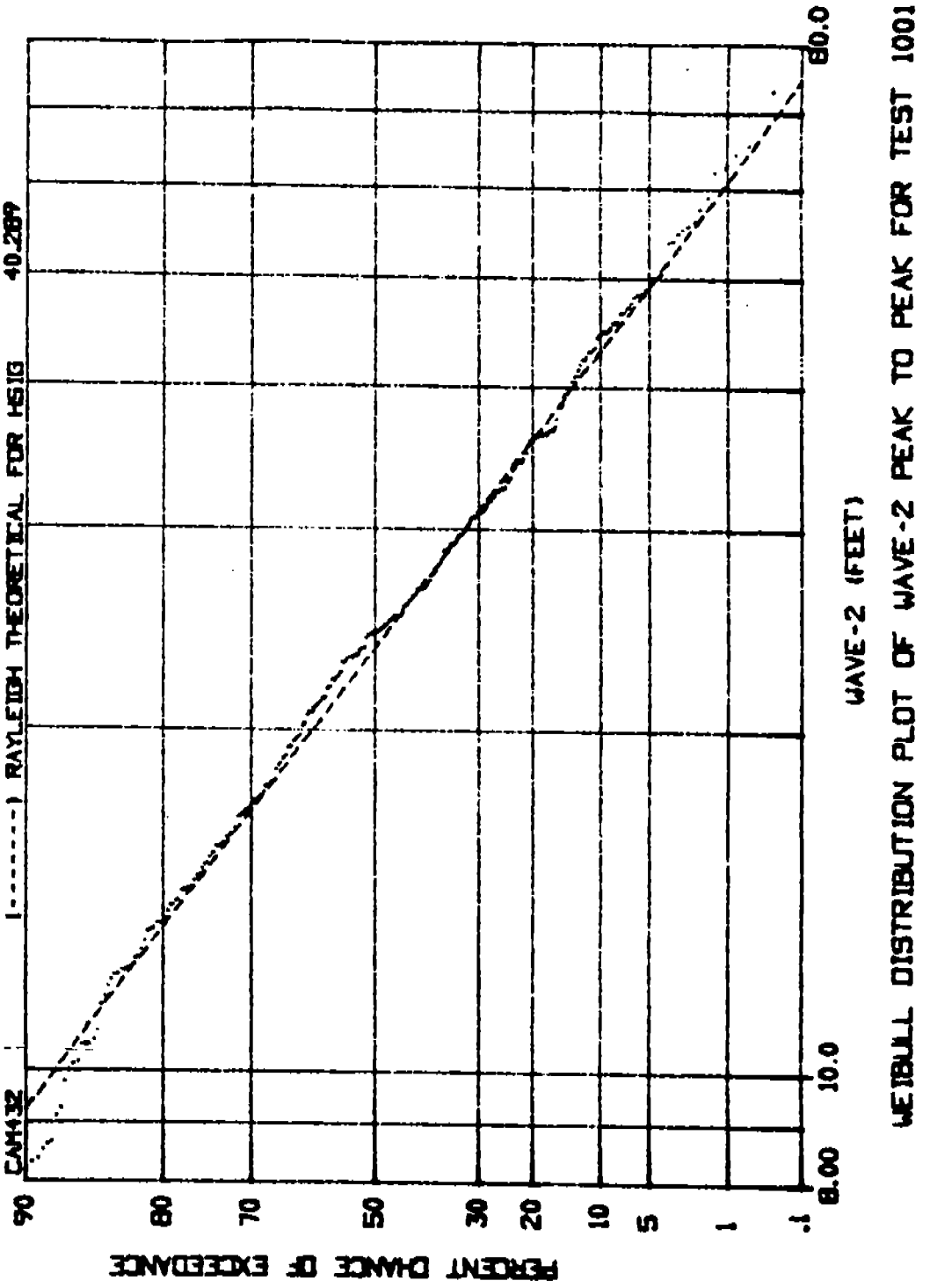

Figure 4.15 Wave Height Probability Distribution for Test 1001

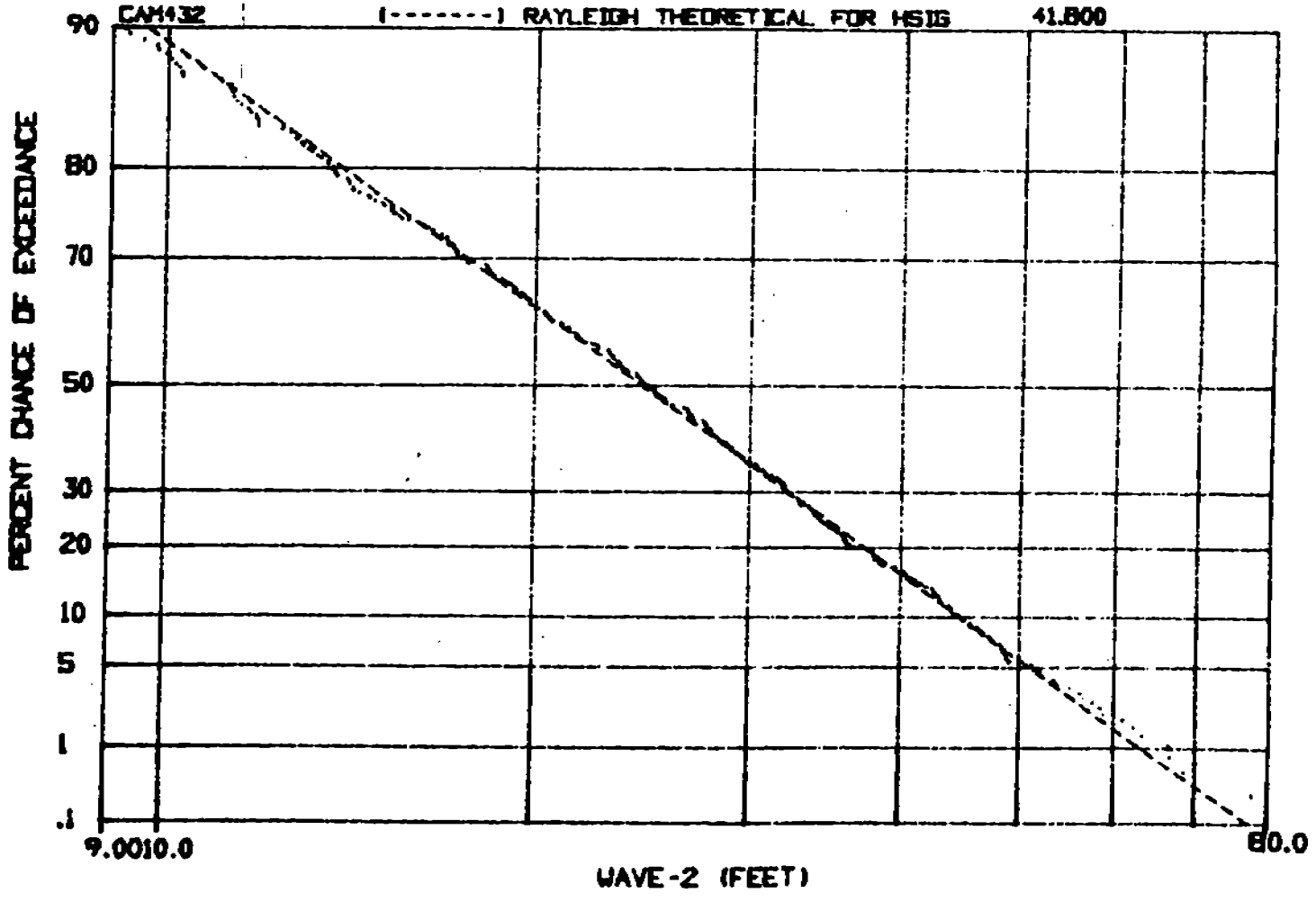

WEIBULL DISTRIBUTION PLOT OF WAVE-2 PEAK TO PEAK FOR TEST 2000

Figure 4.16 Wave Height Probability Distribution of Test 2000

STEVENS INSTITUTE OF TECHNOLOGY
DAVIDSON LABORATORY
Castle Point Station, Hoboken, New Jersey 07030

APPENDIX D

TECHNICAL REPORT SIT-DL-87-9-2595

NOVEMBER 1987

GENERATION OF HURRICANE CAMILLE WAVES IN A TOWING TANK

by
Han C. Yu

Prepared for
David Taylor Naval Ship R&D Center
under
Contract N00167-87-M-2444
(Davidson Laboratory Project 5314/200)

Approved: Glenn McKee
Glenn McKee, Chief
Mathematical Services Division

TABLE OF CONTENTS

INTRODUCTION

The wave spectrum has been one of the principal measures for describing the characteristics of the seaway. A study of hurricane Camille time series wave data using a new method of analyzing time series, known as the half-cycle matrix (HACYM), revealed that large, steep, elevated waves are found near the height of the storm [1]. A more recent study of measured wave data concluded that "The wave spectrum alone is not sufficient to characterize the roughness of an irregular sea. Some time histories have been found that contain steep asymmetric waves while others do not contain such waves, but they have in some cases identical wave spectra" [2].

Therefore it is of interest to compare the characteristics of tank generated waves with the recorded storm waves. The purpose of this work is to generate and record a series of steep irregular waves using a model scale hurricane Camille spectrum and to produce measured wave spectra, time histories, and videotapes of wave profiles through Davidson Laboratory standard procedures.

TEST PROGRAM

Scale Factor

A plot of hurricane Camille wave spectrum was provided by Mr. William Buckley of the NSRDC. Since the plot did not include a table of spectral ordinates nor significant wave height, the ordinates were read and integrated to yield a 40.04 feet significant wave height with a modal frequency of 0.46 Rad/sec in full scale.

In order to determine an appropriate model scale factor, the significant wave heights vs. modal periods at three scale ratios were plotted against the Davidson Laboratory Tank-3 irregular wave capacity line [3] in Figure 1. It turned out that the required wave spectrum is slightly out of the capacity limit of the wave maker. An absolute limit on the scale wave height was 11 inches freeboard; so based on experimental practice, the modal frequency was to scale, but the significant wave height was reduced to bring the point under the wave capacity line. This lead to a scale ratio of 1/50.

At 1/50 scale, the Camille spectrum requires 9.61 inches of significant wave height, while the maximum capacity significant wave height is 9.0 inches. The desired wave spectrum in model scale was thus prepared by multiplying a scale factor of $\sqrt{50}$ on its frequency, and by multiplying a factor of $(1/50)^{2.5}$ $(9.0/9.61)^2$ on the spectral ordinates. Both full scale and resulting model wave spectral ordinates are given in Table 1.

Irregular Wave Generation Procedure

A description of the Davidson Laboratory wave maker in Tank 3 is given in (Appendix A) [3], and the standard irregular wave generation procedure is given in (Appendix B) [4]. In brief, it is a three step procedure:

1. Define the desired wave spectral shape.
2. Generate a particular realization of a Gaussian random process having the desired wave spectral shape and having a one inch significant wave height.
3. Scale up the generated time series from one inch significant height to desired significant height, and drive the wave machine accordingly.

Using the desired model wave spectral shape file, a total of 21 particular wave data files were prepared. Each wave data file can produce 128 seconds of statistically independent irregular waves.

Test Set Up

Two 4-foot long resistance type wave wires were used to measure the wave elevation at two tank locations, namely "primary" and "secondary" locations. The primary tank location was 70 ft away, and the secondary location was 170 feet away from the wave maker. At the primary tank location, an 8 feet wide by 22 inches high grid plate was placed on the side wall of the tank to visualize the wave profile. The horizontal grid lines were drawn at two inch intervals from the mean water level, and the vertical grid lines were drawn at every 6 inches centered at the wave wire location. A video camera was used at the primary tank location to record the instantaneous wave profile. The top portion of the screen was split to show the run number and the time elapsed since starting the data collection.

During the tests two wave wire signals were digitized at a rate of 250 scans per second, and the time histories were recorded on the Davidson Laboratory data acquisition computer hard disk. A total of seven complete runs were made. An oscillograph record of the wave elevation was also made.

RESULTS

The recorded time histories were analyzed by the Davidson Laboratory standard spectrum analysis program using the Blackman-Tukey algorithm. The resulting wave spectra at both tank locations for each run are tabulated in Tables 2 - 15 with appropriate parameters, such as sampling interval, and degrees of freedom, etc. Tables 16 and 17 show the average wave spectrum at each tank location using all data from seven runs.

Comparison of the obtained and desired wave spectra is made, in Figures 2 - 17, by plotting the obtained wave spectrum in histograph form and over-plotting the desired wave spectral ordinates using symbols.

Since further analysis of the data was to be performed at the NSRDC, time histories of the wave elevation at every 0.1 second were prepared in ASCII files. The file contains two columns of numbers, in FORTRAN FORMAT(2F8.3), representing the wave elevation in inches at primary and secondary tank location respectively. The file also contains run number, wave wire locations, sample interval, and desired significant wave height as a five-line header. Table 18 shows the first 40 lines of an ASCII file as a sample. The ASCII time history files were electronically transferred to the NSRDC via the telephone line on November 4, 1987.

DISCUSSION

In the course of the present work, two difficulties were experienced. The first one was that the required wave spectrum was out of the wave maker capacity. As explained above, the decision was to keep the period to scale and generate smaller waves.

The wave maker is equipped with a safety feature which shuts off the hydraulic system if the acceleration of the flap is greater than a threshold value. Due to the choice of modal period and wave height, the maximum acceleration threshold was exceeded for 14 of the 21 wave realizations,

stopping the run prematurely. The seven complete runs make up the time history data.

REFERENCES

1. Buckley, W.H., R.D. Pierce, J. B. Peters and M.J. Davis, "Use of the Half-cycle Analysis Method to Compare Measured Wave Height and Simulated Gaussian Data Having the Same Variance Spectrum", Ocean Engineering, Vol. 110, No. 4, pp 423-445, 1984.

2. Myrhaug, D. and Soren P. Kjeldsen, "Steepness and Asymmetry of Extreme Waves and the Highest Waves in Deep Water", Ocean Engineering, Vol. 13, No. 6 pp 549-560, 1986.

3. "Proceedings of the 20th American Towing Tank Conference," August 2, 3, 4, 1983, pp 1297-1304.

4. Dalzell, J.F., "PDP-11/23 Operating Notes," unpublished Davidson Laboratory Operating Manual.

Table 1. Spectral Shape File Ordinates

Full Scale		Model Scale		Model Scale	
Freq rad/s	Ordinates ft**2-sec	Freq rad/s	Ordinates in**2-sec	Freq hz	Ordinates in**2/hz
0.25	0.00	1.74	0.00	0.28	0.00
0.29	3.16	2.08	0.02	0.33	0.14
0.34	18.97	2.43	0.14	0.39	0.85
0.39	146.24	2.78	1.04	0.44	6.56
0.44	397.62	3.12	2.84	0.50	17.85
0.49	363.63	3.47	2.60	0.55	16.32
0.54	223.71	3.82	1.60	0.61	10.04
0.59	181.81	4.17	1.30	0.66	8.16
0.64	152.57	4.51	1.09	0.72	6.85
0.69	110.67	4.86	0.79	0.77	4.97
0.74	93.28	5.21	0.67	0.83	4.19
0.79	79.05	5.56	0.56	0.88	3.55
0.83	51.38	5.90	0.37	0.94	2.31
0.88	41.90	6.25	0.30	0.99	1.88
0.93	41.90	6.60	0.30	1.05	1.88
0.98	30.04	6.94	0.21	1.11	1.35
1.03	20.55	7.29	0.15	1.16	0.92
1.08	17.39	7.64	0.12	1.22	0.78
1.13	11.86	7.99	0.08	1.27	0.53
1.18	9.49	8.33	0.07	1.33	0.43
1.23	7.91	8.68	0.06	1.38	0.35
1.28	7.91	9.03	0.06	1.44	0.35
1.33	8.70	9.37	0.06	1.49	0.39
1.37	4.74	9.72	0.03	1.55	0.21
1.42	4.74	10.07	0.03	1.60	0.21
1.47	5.53	10.42	0.04	1.66	0.25
1.52	3.16	10.76	0.02	1.71	0.14
1.57	2.37	11.11	0.02	1.77	0.11
1.62	0.79	11.46	0.01	1.82	0.04
1.67	0.00	11.80	0.00	1.88	0.00

Note 1. Full scale significant wave height 40.04 feet.
Desired model scale significant wave height 9.0 inches.

2. Spectral ordinates are assumed as zero at frequencies out side of this range.

Table 2. Wave Spectrum at the Primary Tank Location, Run 36

HURRICANE CAMILLE WAVES GENERATION

Scalar Spectrum Analysis Page 1 of 1 Channel 1
W.W. 70FT

Run= 36,

640 Points 50 Lags Delta-T= 0.200000 Sec
Scale constant= 0.100000E+01 Delta-Freq.= 0.050 Hertz

Sample Variance= 0.504168E+01 *90% Conf Intv.= 0.460943E+01 (Low)
Spectrum Area = 0.504168E+01 * = 0.554162E+01 (High)

25 Deg. Freedom: for 90% Conf. Bounds Multiply
Spectral Estimates by 0.66 and 1.71
Sig Wave Height = 8.9815 Inches

Lag	Frequency Hz	Spectral Estimates in**2-sec	Lag	Frequency Hz	Spectral Estimates in**2-sec
0	0.00	0.7063E-01			
1	0.05	0.5990E-01	26	1.30	0.1755E+00
2	0.10	0.6796E-01	27	1.35	0.1726E+00
3	0.15	0.3554E-01	28	1.40	0.1209E+00
4	0.20	0.4641E-01	29	1.45	0.9532E-01
5	0.25	0.4202E-01	30	1.50	0.6936E-01
6	0.30	0.1453E+00	31	1.55	0.7282E-01
7	0.35	0.6997E+00	32	1.60	0.6593E-01
8	0.40	0.3610E+01	33	1.65	0.6162E-01
9	0.45	0.1090E+02	34	1.70	0.5732E-01
10	0.50	0.1746E+02	35	1.75	0.6231E-01
11	0.55	0.1675E+02	36	1.80	0.5094E-01
12	0.60	0.1357E+02	37	1.85	0.3977E-01
13	0.65	0.1081E+02	38	1.90	0.2361E-01
14	0.70	0.8042E+01	39	1.95	0.3088E-01
15	0.75	0.4235E+01	40	2.00	0.2488E-01
16	0.80	0.2807E+01	41	2.05	0.2905E-01
17	0.85	0.2878E+01	42	2.10	0.2009E-01
18	0.90	0.2426E+01	43	2.15	0.2084E-01
19	0.95	0.1663E+01	44	2.20	0.1790E-01
20	1.00	0.9889E+00	45	2.25	0.1710E-01
21	1.05	0.6720E+00	46	2.30	0.1140E-01
22	1.10	0.5483E+00	47	2.35	0.1871E-01
23	1.15	0.4548E+00	48	2.40	0.1279E-01
24	1.20	0.3422E+00	49	2.45	0.1245E-01
25	1.25	0.2550E+00	50	2.50	0.5431E-02

Table 3. Wave Spectrum at the Secondary Tank Location, Run 36

HURRICANE CAMILLE WAVES GENERATION

Scalar Spectrum Analysis Page 1 of 1 Channel 2
W.W. 170FT

Run= 36,

640 Points 50 Lags Delta-T= 0.200000 Sec
Scale constant= 0.100000E+01 Delta-Freq.= 0.050 Hertz

Sample Variance= 0.455993E+01 *90% Conf Intv.= 0.416899E+01 (Low)
Spectrum Area = 0.455993E+01 * = 0.501210E+01 (High)

25 Deg. Freedom: for 90% Conf. Bounds Multiply
Spectral Estimates by 0.66 and 1.71
Sig Wave Height = 8.5416 Inches

Lag	Frequency Hz	Spectral Estimates in**2-sec	Lag	Frequency Hz	Spectral Estimates in**2-sec
0	0.00	-0.1772E-01			
1	0.05	0.4021E-01	26	1.30	0.1551E+00
2	0.10	-0.3569E-02	27	1.35	0.1319E+00
3	0.15	0.5079E-01	28	1.40	0.1018E+00
4	0.20	0.5674E-02	29	1.45	0.5892E-01
5	0.25	0.5137E-01	30	1.50	0.6498E-01
6	0.30	0.1571E-01	31	1.55	0.4418E-01
7	0.35	0.4900E+00	32	1.60	0.4741E-01
8	0.40	0.3141E+01	33	1.65	0.3692E-01
9	0.45	0.1050E+02	34	1.70	0.4686E-01
10	0.50	0.1701E+02	35	1.75	0.2098E-01
11	0.55	0.1722E+02	36	1.80	0.2572E-01
12	0.60	0.1303E+02	37	1.85	0.1652E-01
13	0.65	0.8360E+01	38	1.90	0.2464E-01
14	0.70	0.6111E+01	39	1.95	0.1215E-01
15	0.75	0.4095E+01	40	2.00	0.2160E-01
16	0.80	0.3277E+01	41	2.05	0.6259E-02
17	0.85	0.2589E+01	42	2.10	0.1416E-01
18	0.90	0.1443E+01	43	2.15	0.4586E-02
19	0.95	0.9442E+00	44	2.20	0.9558E-02
20	1.00	0.7889E+00	45	2.25	0.1448E-02
21	1.05	0.3901E+00	46	2.30	0.9504E-02
22	1.10	0.3364E+00	47	2.35	0.2920E-03
23	1.15	0.1741E+00	48	2.40	0.7862E-02
24	1.20	0.1426E+00	49	2.45	-0.1537E-03
25	1.25	0.1334E+00	50	2.50	0.8824E-02

Table 4. Wave Spectrum at the Primary Tank Location, Run 37

HURRICANE CAMILLE WAVES GENERATION

Scalar Spectrum Analysis Page 1 of 1 Channel 1
W.W. 70FT

Run= 37,

640 Points 50 Lags Delta-T= 0.200000 Sec
Scale constant= 0.100000E+01 Delta-Freq.= 0.050 Hertz

Sample Variance= 0.500041E+01 *90% Conf Intv.= 0.457170E+01 (Low)
Spectrum Area = 0.500041E+01 * = 0.549626E+01 (High)

25 Deg. Freedom: for 90% Conf. Bounds Multiply
Spectral Estimates by 0.66 and 1.71
Sig Wave Height = 8.9446 Inches

Lag	Frequency Hz	Spectral Estimates in**2-sec	Lag	Frequency Hz	Spectral Estimates in**2-sec
0	0.00	0.4283E-01			
1	0.05	0.2575E-01	26	1.30	0.2080E+00
2	0.10	0.4576E-01	27	1.35	0.2290E+00
3	0.15	0.1970E-01	28	1.40	0.1680E+00
4	0.20	0.4825E-01	29	1.45	0.9956E-01
5	0.25	0.3243E-01	30	1.50	0.7594E-01
6	0.30	0.1045E+00	31	1.55	0.6224E-01
7	0.35	0.6522E+00	32	1.60	0.4001E-01
8	0.40	0.3355E+01	33	1.65	0.4350E-01
9	0.45	0.9508E+01	34	1.70	0.5268E-01
10	0.50	0.1657E+02	35	1.75	0.6060E-01
11	0.55	0.1695E+02	36	1.80	0.4675E-01
12	0.60	0.1174E+02	37	1.85	0.5379E-01
13	0.65	0.1017E+02	38	1.90	0.3998E-01
14	0.70	0.9465E+01	39	1.95	0.2919E-01
15	0.75	0.6050E+01	40	2.00	0.1774E-01
16	0.80	0.3855E+01	41	2.05	0.2006E-01
17	0.85	0.2726E+01	42	2.10	0.1765E-01
18	0.90	0.2403E+01	43	2.15	0.1677E-01
19	0.95	0.1634E+01	44	2.20	0.9179E-02
20	1.00	0.7846E+00	45	2.25	0.1675E-01
21	1.05	0.5794E+00	46	2.30	0.1097E-01
22	1.10	0.6624E+00	47	2.35	0.9995E-02
23	1.15	0.6734E+00	48	2.40	0.4085E-02
24	1.20	0.3513E+00	49	2.45	0.1028E-01
25	1.25	0.2254E+00	50	2.50	0.9983E-02

Table 5. Wave Spectrum at the Secondary Tank Location, Run 37

HURRICANE CAMILLE WAVES GENERATION

Scalar Spectrum Analysis Page 1 of 1 Channel 2
W.W. 170FT

Run= 37,

640 Points 50 Lags Delta-T= 0.200000 Sec
Scale constant= 0.100000E+01 Delta-Freq.= 0.050 Hertz

Sample Variance= 0.457039E+01 *90% Conf Intv.= 0.417855E+01 (Low)
Spectrum Area = 0.457039E+01 * = 0.502359E+01 (High)

25 Deg. Freedom: for 90% Conf. Bounds Multiply
Spectral Estimates by 0.66 and 1.71
Sig Wave Height = 8.5514 Inches

Lag	Frequency Hz	Spectral Estimates in**2-sec	Lag	Frequency Hz	Spectral Estimates in**2-sec
0	0.00	0.1184E-01			
1	0.05	0.4208E-01	26	1.30	0.2405E+00
2	0.10	0.1845E-01	27	1.35	0.1669E+00
3	0.15	0.3207E-01	28	1.40	0.1254E+00
4	0.20	0.1139E-01	29	1.45	0.1019E+00
5	0.25	0.4392E-01	30	1.50	0.6704E-01
6	0.30	0.5620E-01	31	1.55	0.5020E-01
7	0.35	0.5964E+00	32	1.60	0.5534E-01
8	0.40	0.3436E+01	33	1.65	0.3689E-01
9	0.45	0.1033E+02	34	1.70	0.2942E-01
10	0.50	0.1671E+02	35	1.75	0.2925E-01
11	0.55	0.1654E+02	36	1.80	0.3554E-01
12	0.60	0.1147E+02	37	1.85	0.3370E-01
13	0.65	0.9279E+01	38	1.90	0.3289E-01
14	0.70	0.7686E+01	39	1.95	0.2051E-01
15	0.75	0.4484E+01	40	2.00	0.2451E-01
16	0.80	0.2870E+01	41	2.05	0.2021E-01
17	0.85	0.2300E+01	42	2.10	0.2272E-01
18	0.90	0.1320E+01	43	2.15	0.2119E-01
19	0.95	0.8052E+00	44	2.20	0.1887E-01
20	1.00	0.6150E+00	45	2.25	0.1287E-01
21	1.05	0.4392E+00	46	2.30	0.1660E-01
22	1.10	0.2952E+00	47	2.35	0.1208E-01
23	1.15	0.2231E+00	48	2.40	0.1288E-01
24	1.20	0.2995E+00	49	2.45	0.1003E-01
25	1.25	0.2834E+00	50	2.50	0.1253E-01

Table 6. Wave Spectrum at the Primary Tank Location, Run 39

HURRICANE CAMILLE WAVES GENERATION

Scalar Spectrum Analysis Page 1 of 1 Channel 1
W.W. 70FT

Run= 39,

640 Points 50 Lags Delta-T= 0.200000 Sec
Scale constant= 0.100000E+01 Delta-Freq.= 0.050 Hertz

Sample Variance= 0.516035E+01 *90% Conf Intv.= 0.471793E+01 (Low)
Spectrum Area = 0.516035E+01 * = 0.567206E+01 (High)

25 Deg. Freedom: for 90% Conf. Bounds Multiply
Spectral Estimates by 0.66 and 1.71
Sig Wave Height = 9.0866 Inches

Lag	Frequency Hz	Spectral Estimates in**2-sec	Lag	Frequency Hz	Spectral Estimates in**2-sec
0	0.00	0.8005E-01			
1	0.05	0.1026E-01	26	1.30	0.2170E+00
2	0.10	0.5891E-01	27	1.35	0.2249E+00
3	0.15	0.6170E-02	28	1.40	0.1454E+00
4	0.20	0.6444E-01	29	1.45	0.1180E+00
5	0.25	-0.8521E-02	30	1.50	0.9277E-01
6	0.30	0.9944E-01	31	1.55	0.7927E-01
7	0.35	0.7012E+00	32	1.60	0.6604E-01
8	0.40	0.3526E+01	33	1.65	0.7791E-01
9	0.45	0.9194E+01	34	1.70	0.4654E-01
10	0.50	0.1731E+02	35	1.75	0.4385E-01
11	0.55	0.1962E+02	36	1.80	0.3555E-01
12	0.60	0.1406E+02	37	1.85	0.5111E-01
13	0.65	0.8977E+01	38	1.90	0.2584E-01
14	0.70	0.6194E+01	39	1.95	0.2891E-01
15	0.75	0.4218E+01	40	2.00	0.1941E-01
16	0.80	0.5381E+01	41	2.05	0.3359E-01
17	0.85	0.4795E+01	42	2.10	0.2052E-01
18	0.90	0.2089E+01	43	2.15	0.2798E-01
19	0.95	0.1515E+01	44	2.20	0.1853E-01
20	1.00	0.1347E+01	45	2.25	0.2760E-01
21	1.05	0.9619E+00	46	2.30	0.1025E-01
22	1.10	0.4768E+00	47	2.35	0.1787E-01
23	1.15	0.3578E+00	48	2.40	0.6868E-02
24	1.20	0.3964E+00	49	2.45	0.1441E-01
25	1.25	0.3695E+00	50	2.50	0.7784E-02

Table 7. Wave Spectrum at the Secondary Tank Location, Run 39

HURRICANE CAMILLE WAVES GENERATION

Scalar Spectrum Analysis Page 1 of 1 Channel 2
W.W. 170FT

Run= 39,

640 Points 50 Lags Delta-T= 0.200000 Sec
Scale constant= 0.100000E+01 Delta-Freq.= 0.050 Hertz

Sample Variance= 0.459250E+01 *90% Conf Intv.= 0.419876E+01 (Low)
Spectrum Area = 0.459249E+01 * = 0.504790E+01 (High)

25 Deg. Freedom: for 90% Conf. Bounds Multiply
Spectral Estimates by 0.66 and 1.71
Sig Wave Height = 8.5720 Inches

Lag	Frequency Hz	Spectral Estimates in**2-sec	Lag	Frequency Hz	Spectral Estimates in**2-sec
0	0.00	0.2647E-01			
1	0.05	0.1202E-01	26	1.30	0.2069E+00
2	0.10	0.3350E-01	27	1.35	0.1980E+00
3	0.15	0.1216E-01	28	1.40	0.1149E+00
4	0.20	0.2515E-01	29	1.45	0.8166E-01
5	0.25	-0.5426E-02	30	1.50	0.7521E-01
6	0.30	0.5595E-01	31	1.55	0.6438E-01
7	0.35	0.4630E+00	32	1.60	0.6155E-01
8	0.40	0.2983E+01	33	1.65	0.4454E-01
9	0.45	0.9910E+01	34	1.70	0.3621E-01
10	0.50	0.1732E+02	35	1.75	0.3316E-01
11	0.55	0.1749E+02	36	1.80	0.3307E-01
12	0.60	0.1369E+02	37	1.85	0.4461E-01
13	0.65	0.9346E+01	38	1.90	0.2995E-01
14	0.70	0.6156E+01	39	1.95	0.2083E-01
15	0.75	0.3402E+01	40	2.00	0.1591E-01
16	0.80	0.2484E+01	41	2.05	0.1237E-01
17	0.85	0.2152E+01	42	2.10	0.1264E-01
18	0.90	0.1464E+01	43	2.15	0.1553E-01
19	0.95	0.1142E+01	44	2.20	0.1592E-01
20	1.00	0.8498E+00	45	2.25	0.1487E-01
21	1.05	0.5898E+00	46	2.30	0.1378E-01
22	1.10	0.4016E+00	47	2.35	0.1147E-01
23	1.15	0.2711E+00	48	2.40	0.8748E-02
24	1.20	0.2151E+00	49	2.45	0.7773E-02
25	1.25	0.1928E+00	50	2.50	0.5096E-02

Table 8. Wave Spectrum at the Primary Tank Location, Run 40

HURRICANE CAMILLE WAVES GENERATION

Scalar Spectrum Analysis Page 1 of 1 Channel 1
W.W. 70FT

Run= 40,

640 Points 50 Lags Delta-T= 0.200000 Sec
Scale constant= 0.100000E+01 Delta-Freq.= 0.050 Hertz

Sample Variance= 0.511935E+01 *90% Conf Intv.= 0.468044E+01 (Low)
Spectrum Area = 0.511935E+01 * = 0.562699E+01 (High)

25 Deg. Freedom: for 90% Conf. Bounds Multiply
Spectral Estimates by 0.66 and 1.71
Sig Wave Height = 9.0504 Inches

Lag	Frequency Hz	Spectral Estimates in**2-sec	Lag	Frequency Hz	Spectral Estimates in**2-sec
0	0.00	0.2351E-01			
1	0.05	0.4552E-03	26	1.30	0.2328E+00
2	0.10	0.3120E-01	27	1.35	0.1302E+00
3	0.15	0.5264E-02	28	1.40	0.9942E-01
4	0.20	0.2918E-01	29	1.45	0.1194E+00
5	0.25	-0.1977E-01	30	1.50	0.1161E+00
6	0.30	0.7737E-01	31	1.55	0.8183E-01
7	0.35	0.5599E+00	32	1.60	0.6165E-01
8	0.40	0.3122E+01	33	1.65	0.5036E-01
9	0.45	0.1008E+02	34	1.70	0.3280E-01
10	0.50	0.1834E+02	35	1.75	0.3783E-01
11	0.55	0.1845E+02	36	1.80	0.4074E-01
12	0.60	0.1293E+02	37	1.85	0.5738E-01
13	0.65	0.1031E+02	38	1.90	0.3446E-01
14	0.70	0.8601E+01	39	1.95	0.2021E-01
15	0.75	0.5372E+01	40	2.00	0.1664E-01
16	0.80	0.3158E+01	41	2.05	0.2569E-01
17	0.85	0.2706E+01	42	2.10	0.1782E-01
18	0.90	0.2069E+01	43	2.15	0.1380E-01
19	0.95	0.1519E+01	44	2.20	0.1115E-01
20	1.00	0.1217E+01	45	2.25	0.1248E-01
21	1.05	0.8882E+00	46	2.30	0.1013E-01
22	1.10	0.6283E+00	47	2.35	0.1297E-01
23	1.15	0.4202E+00	48	2.40	0.1008E-01
24	1.20	0.3038E+00	49	2.45	0.1594E-01
25	1.25	0.3111E+00	50	2.50	0.1330E-01

Table 9. Wave Spectrum at the Secondary Tank Location, Run 40

HURRICANE CAMILLE WAVES GENERATION

Scalar Spectrum Analysis Page 1 of 1 Channel 2
W.W. 170FT

Run= 40,

640 Points 50 Lags Delta-T= 0.200000 Sec
Scale constant= 0.100000E+01 Delta-Freq.= 0.050 Hertz

Sample Variance= 0.459111E+01 *90% Conf Intv.= 0.419749E+01 (Low)
Spectrum Area = 0.459111E+01 * = 0.504637E+01 (High)

25 Deg. Freedom: for 90% Conf. Bounds Multiply
Spectral Estimates by 0.66 and 1.71
Sig Wave Height = 8.5708 Inches

Lag	Frequency Hz	Spectral Estimates in**2-sec	Lag	Frequency Hz	Spectral Estimates in**2-sec
0	0.00	0.3335E-01			
1	0.05	0.3481E-02	26	1.30	0.1473E+00
2	0.10	0.3162E-01	27	1.35	0.1643E+00
3	0.15	-0.1757E-02	28	1.40	0.1449E+00
4	0.20	0.2635E-01	29	1.45	0.1181E+00
5	0.25	-0.8343E-02	30	1.50	0.1179E+00
6	0.30	0.6601E-01	31	1.55	0.1144E+00
7	0.35	0.5440E+00	32	1.60	0.8414E-01
8	0.40	0.3260E+01	33	1.65	0.5166E-01
9	0.45	0.9630E+01	34	1.70	0.5049E-01
10	0.50	0.1728E+02	35	1.75	0.5681E-01
11	0.55	0.1748E+02	36	1.80	0.5463E-01
12	0.60	0.1205E+02	37	1.85	0.4555E-01
13	0.65	0.9622E+01	38	1.90	0.3138E-01
14	0.70	0.6706E+01	39	1.95	0.2624E-01
15	0.75	0.4682E+01	40	2.00	0.2729E-01
16	0.80	0.3267E+01	41	2.05	0.2063E-01
17	0.85	0.1928E+01	42	2.10	0.1861E-01
18	0.90	0.9538E+00	43	2.15	0.2233E-01
19	0.95	0.8119E+00	44	2.20	0.1877E-01
20	1.00	0.5989E+00	45	2.25	0.1574E-01
21	1.05	0.3691E+00	46	2.30	0.1217E-01
22	1.10	0.3719E+00	47	2.35	0.1429E-01
23	1.15	0.3191E+00	48	2.40	0.1668E-01
24	1.20	0.2347E+00	49	2.45	0.1460E-01
25	1.25	0.1900E+00	50	2.50	0.1339E-01

Table 10. Wave Spectrum at the Primary Tank Location, Run 45

HURRICANE CAMILLE WAVES GENERATION

Scalar Spectrum Analysis Page 1 of 1 Channel 1
W.W. 70FT

Run= 45,

640 Points 50 Lags Delta-T= 0.200000 Sec
Scale constant= 0.100000E+01 Delta-Freq.= 0.050 Hertz

Sample Variance= 0.523229E+01 *90% Conf Intv.= 0.478370E+01 (Low)
Spectrum Area = 0.523229E+01 * = 0.575113E+01 (High)

25 Deg. Freedom: for 90% Conf. Bounds Multiply
Spectral Estimates by 0.66 and 1.71
Sig Wave Height = 9.1497 Inches

Lag	Frequency Hz	Spectral Estimates in**2-sec	Lag	Frequency Hz	Spectral Estimates in**2-sec
0	0.00	0.2526E-02			
1	0.05	0.7012E-01	26	1.30	0.2098E+00
2	0.10	0.9685E-02	27	1.35	0.1621E+00
3	0.15	0.5764E-01	28	1.40	0.1645E+00
4	0.20	-0.1458E-01	29	1.45	0.1036E+00
5	0.25	0.5033E-01	30	1.50	0.8604E-01
6	0.30	0.2782E-01	31	1.55	0.5632E-01
7	0.35	0.6117E+00	32	1.60	0.8783E-01
8	0.40	0.3187E+01	33	1.65	0.6979E-01
9	0.45	0.1069E+02	34	1.70	0.8521E-01
10	0.50	0.1822E+02	35	1.75	0.6276E-01
11	0.55	0.1847E+02	36	1.80	0.6944E-01
12	0.60	0.1328E+02	37	1.85	0.5578E-01
13	0.65	0.1012E+02	38	1.90	0.5924E-01
14	0.70	0.9112E+01	39	1.95	0.3687E-01
15	0.75	0.6424E+01	40	2.00	0.3245E-01
16	0.80	0.3250E+01	41	2.05	0.2127E-01
17	0.85	0.2290E+01	42	2.10	0.2972E-01
18	0.90	0.2327E+01	43	2.15	0.1786E-01
19	0.95	0.1495E+01	44	2.20	0.2859E-01
20	1.00	0.1096E+01	45	2.25	0.1346E-01
21	1.05	0.8078E+00	46	2.30	0.2390E-01
22	1.10	0.5088E+00	47	2.35	0.1453E-01
23	1.15	0.3703E+00	48	2.40	0.2423E-01
24	1.20	0.3619E+00	49	2.45	0.2175E-01
25	1.25	0.2656E+00	50	2.50	0.4088E-01

Table 11. Wave Spectrum at the Secondary Tank Location, Run 45

HURRICANE CAMILLE WAVES GENERATION

Scalar Spectrum Analysis Page 1 of 1 Channel 2
W.W. 170FT

Run= 45,

640 Points 50 Lags Delta-T= 0.200000 Sec
Scale constant= 0.100000E+01 Delta-Freq.= 0.050 Hertz

Sample Variance= 0.461661E+01 *90% Conf Intv.= 0.422081E+01 (Low)
Spectrum Area = 0.461661E+01 * = 0.507440E+01 (High)

25 Deg. Freedom: for 90% Conf. Bounds Multiply
Spectral Estimates by 0.66 and 1.71
Sig Wave Height = 8.5945 Inches

Lag	Frequency Hz	Spectral Estimates in**2-sec	Lag	Frequency Hz	Spectral Estimates in**2-sec
0	0.00	-0.3931E-01			
1	0.05	0.8273E-01	26	1.30	0.1994E+00
2	0.10	-0.1344E-01	27	1.35	0.1195E+00
3	0.15	0.7989E-01	28	1.40	0.1361E+00
4	0.20	-0.4987E-01	29	1.45	0.6288E-01
5	0.25	0.6390E-01	30	1.50	0.7537E-01
6	0.30	0.8436E-02	31	1.55	0.6124E-01
7	0.35	0.6303E+00	32	1.60	0.7202E-01
8	0.40	0.3024E+01	33	1.65	0.3358E-01
9	0.45	0.1099E+02	34	1.70	0.5770E-01
10	0.50	0.1830E+02	35	1.75	0.2469E-01
11	0.55	0.1718E+02	36	1.80	0.4323E-01
12	0.60	0.1169E+02	37	1.85	0.1989E-01
13	0.65	0.8552E+01	38	1.90	0.2845E-01
14	0.70	0.7124E+01	39	1.95	0.1111E-02
15	0.75	0.4062E+01	40	2.00	0.2993E-01
16	0.80	0.2791E+01	41	2.05	0.1241E-01
17	0.85	0.2048E+01	42	2.10	0.2346E-01
18	0.90	0.1458E+01	43	2.15	0.4167E-03
19	0.95	0.9137E+00	44	2.20	0.2029E-01
20	1.00	0.8721E+00	45	2.25	0.1687E-02
21	1.05	0.5230E+00	46	2.30	0.1877E-01
22	1.10	0.3823E+00	47	2.35	-0.8549E-04
23	1.15	0.2123E+00	48	2.40	0.1746E-01
24	1.20	0.1848E+00	49	2.45	0.1176E-02
25	1.25	0.1660E+00	50	2.50	0.2049E-01

Table 12. Wave Spectrum at the Primary Tank Location, Run 46

HURRICANE CAMILLE WAVES GENERATION

Scalar Spectrum Analysis Page 1 of 1 Channel 1
W.W. 70FT

Run= 46,

640 Points 50 Lags Delta-T= 0.200000 Sec
Scale constant= 0.100000E+01 Delta-Freq.= 0.050 Hertz

Sample Variance= 0.505881E+01 *90% Conf Intv.= 0.462509E+01 (Low)
Spectrum Area = 0.505881E+01 * = 0.556045E+01 (High)

25 Deg. Freedom: for 90% Conf. Bounds Multiply
Spectral Estimates by 0.66 and 1.71
Sig Wave Height = 8.9967 Inches

Lag	Frequency Hz	Spectral Estimates in**2-sec	Lag	Frequency Hz	Spectral Estimates in**2-sec
0	0.00	0.4171E-01			
1	0.05	0.7426E-01	26	1.30	0.2913E+00
2	0.10	0.4790E-01	27	1.35	0.1868E+00
3	0.15	0.2765E-01	28	1.40	0.1897E+00
4	0.20	0.1823E-02	29	1.45	0.1761E+00
5	0.25	0.1424E-01	30	1.50	0.1775E+00
6	0.30	0.6147E-01	31	1.55	0.1505E+00
7	0.35	0.5405E+00	32	1.60	0.1219E+00
8	0.40	0.3017E+01	33	1.65	0.7781E-01
9	0.45	0.1005E+02	34	1.70	0.8556E-01
10	0.50	0.1738E+02	35	1.75	0.9421E-01
11	0.55	0.1696E+02	36	1.80	0.7859E-01
12	0.60	0.1239E+02	37	1.85	0.5360E-01
13	0.65	0.9902E+01	38	1.90	0.4086E-01
14	0.70	0.6631E+01	39	1.95	0.2752E-01
15	0.75	0.4931E+01	40	2.00	0.4281E-01
16	0.80	0.4978E+01	41	2.05	0.3905E-01
17	0.85	0.3462E+01	42	2.10	0.4269E-01
18	0.90	0.2392E+01	43	2.15	0.3057E-01
19	0.95	0.1568E+01	44	2.20	0.2972E-01
20	1.00	0.1438E+01	45	2.25	0.2758E-01
21	1.05	0.1161E+01	46	2.30	0.4239E-01
22	1.10	0.6786E+00	47	2.35	0.3735E-01
23	1.15	0.5149E+00	48	2.40	0.3829E-01
24	1.20	0.4440E+00	49	2.45	0.3123E-01
25	1.25	0.3611E+00	50	2.50	0.3017E-01

Table 13. Wave Spectrum at the Secondary Tank Location, Run 46

HURRICANE CAMILLE WAVES GENERATION

Scalar Spectrum Analysis Page 1 of 1 Channel 2
W.W. 170FT

Run= 46,

640 Points 50 Lags Delta-T= 0.200000 Sec
Scale constant= 0.100000E+01 Delta-Freq.= 0.050 Hertz

Sample Variance= 0.455638E+01 *90% Conf Intv.= 0.416574E+01 (Low)
Spectrum Area = 0.455638E+01 * = 0.500820E+01 (High)

25 Deg. Freedom: for 90% Conf. Bounds Multiply
Spectral Estimates by 0.66 and 1.71
Sig Wave Height = 8.5383 Inches

Lag	Frequency Hz	Spectral Estimates in**2-sec	Lag	Frequency Hz	Spectral Estimates in**2-sec
0	0.00	0.4884E-02			
1	0.05	0.5228E-01	26	1.30	0.2510E+00
2	0.10	0.1239E-01	27	1.35	0.1656E+00
3	0.15	0.3925E-01	28	1.40	0.1005E+00
4	0.20	-0.9445E-02	29	1.45	0.4465E-01
5	0.25	0.3116E-01	30	1.50	0.7792E-01
6	0.30	0.1128E+00	31	1.55	0.6826E-01
7	0.35	0.7624E+00	32	1.60	0.6162E-01
8	0.40	0.3132E+01	33	1.65	0.3620E-01
9	0.45	0.1036E+02	34	1.70	0.5694E-01
10	0.50	0.1745E+02	35	1.75	0.4176E-01
11	0.55	0.1589E+02	36	1.80	0.3581E-01
12	0.60	0.1038E+02	37	1.85	0.1427E-01
13	0.65	0.7543E+01	38	1.90	0.2786E-01
14	0.70	0.6502E+01	39	1.95	0.2766E-01
15	0.75	0.5774E+01	40	2.00	0.3990E-01
16	0.80	0.5003E+01	41	2.05	0.1634E-01
17	0.85	0.2534E+01	42	2.10	0.2110E-01
18	0.90	0.1276E+01	43	2.15	0.1191E-01
19	0.95	0.8525E+00	44	2.20	0.2346E-01
20	1.00	0.7140E+00	45	2.25	0.1538E-01
21	1.05	0.5290E+00	46	2.30	0.2455E-01
22	1.10	0.3503E+00	47	2.35	0.1198E-01
23	1.15	0.2015E+00	48	2.40	0.1829E-01
24	1.20	0.2122E+00	49	2.45	0.1037E-01
25	1.25	0.2129E+00	50	2.50	0.1938E-01

Table 14. Wave Spectrum at the Primary Tank Location, Run 52

HURRICANE CAMILLE WAVES GENERATION

Scalar Spectrum Analysis Page 1 of 1 Channel 1
W.W. 70FT

Run= 52,

640 Points 50 Lags Delta-T= 0.200000 Sec
Scale constant= 0.100000E+01 Delta-Freq.= 0.050 Hertz

Sample Variance= 0.483448E+01 *90% Conf Intv.= 0.442000E+01 (Low)
Spectrum Area = 0.483448E+01 * = 0.531387E+01 (High)

25 Deg. Freedom: for 90% Conf. Bounds Multiply
Spectral Estimates by 0.66 and 1.71
Sig Wave Height = 8.7950 Inches

Lag	Frequency Hz	Spectral Estimates in**2-sec	Lag	Frequency Hz	Spectral Estimates in**2-sec
0	0.00	0.6058E-01			
1	0.05	0.4700E-01	26	1.30	0.2112E+00
2	0.10	0.7630E-01	27	1.35	0.1781E+00
3	0.15	0.1311E-03	28	1.40	0.1557E+00
4	0.20	0.3843E-01	29	1.45	0.1553E+00
5	0.25	-0.1166E-01	30	1.50	0.1061E+00
6	0.30	0.9439E-01	31	1.55	0.9095E-01
7	0.35	0.5772E+00	32	1.60	0.7018E-01
8	0.40	0.3116E+01	33	1.65	0.9548E-01
9	0.45	0.9918E+01	34	1.70	0.8196E-01
10	0.50	0.1781E+02	35	1.75	0.7218E-01
11	0.55	0.1803E+02	36	1.80	0.3426E-01
12	0.60	0.1314E+02	37	1.85	0.4247E-01
13	0.65	0.7918E+01	38	1.90	0.4575E-01
14	0.70	0.5502E+01	39	1.95	0.4418E-01
15	0.75	0.4963E+01	40	2.00	0.2642E-01
16	0.80	0.3099E+01	41	2.05	0.4248E-01
17	0.85	0.2682E+01	42	2.10	0.3062E-01
18	0.90	0.2234E+01	43	2.15	0.2833E-01
19	0.95	0.1537E+01	44	2.20	0.1712E-01
20	1.00	0.1237E+01	45	2.25	0.2433E-01
21	1.05	0.8761E+00	46	2.30	0.1019E-01
22	1.10	0.6104E+00	47	2.35	0.2327E-01
23	1.15	0.6227E+00	48	2.40	0.2661E-01
24	1.20	0.5402E+00	49	2.45	0.3031E-01
25	1.25	0.3480E+00	50	2.50	0.1640E-01

Table 15. Wave Spectrum at the Secondary Tank Location, Run 52

HURRICANE CAMILLE WAVES GENERATION

Scalar Spectrum Analysis Page 1 of 1 Channel 2
W.W. 170FT

Run= 52,

640 Points 50 Lags Delta-T= 0.200000 Sec
Scale constant= 0.100000E+01 Delta-Freq.= 0.050 Hertz

Sample Variance= 0.464128E+01 *90% Conf Intv.= 0.424336E+01 (Low)
Spectrum Area = 0.464128E+01 * = 0.510152E+01 (High)

25 Deg. Freedom: for 90% Conf. Bounds Multiply
Spectral Estimates by 0.66 and 1.71
Sig Wave Height = 8.6174 Inches

Lag	Frequency Hz	Spectral Estimates in**2-sec	Lag	Frequency Hz	Spectral Estimates in**2-sec
0	0.00	0.5231E-01			
1	0.05	0.1227E-01	26	1.30	0.1111E+00
2	0.10	0.6570E-01	27	1.35	0.1023E+00
3	0.15	0.1477E-01	28	1.40	0.8392E-01
4	0.20	0.5008E-01	29	1.45	0.1044E+00
5	0.25	-0.1634E-01	30	1.50	0.1159E+00
6	0.30	0.1019E+00	31	1.55	0.7688E-01
7	0.35	0.5494E+00	32	1.60	0.3248E-01
8	0.40	0.2942E+01	33	1.65	0.3116E-01
9	0.45	0.9885E+01	34	1.70	0.2427E-01
10	0.50	0.1838E+02	35	1.75	0.3785E-01
11	0.55	0.1820E+02	36	1.80	0.2979E-01
12	0.60	0.1356E+02	37	1.85	0.2883E-01
13	0.65	0.8779E+01	38	1.90	0.1838E-01
14	0.70	0.5011E+01	39	1.95	0.1763E-01
15	0.75	0.3544E+01	40	2.00	0.1241E-01
16	0.80	0.2932E+01	41	2.05	0.2328E-01
17	0.85	0.2577E+01	42	2.10	0.1160E-01
18	0.90	0.1779E+01	43	2.15	0.1659E-01
19	0.95	0.9775E+00	44	2.20	0.1338E-01
20	1.00	0.7946E+00	45	2.25	0.1662E-01
21	1.05	0.6288E+00	46	2.30	0.5956E-02
22	1.10	0.3190E+00	47	2.35	0.1073E-01
23	1.15	0.2859E+00	48	2.40	0.5566E-02
24	1.20	0.2903E+00	49	2.45	0.1145E-01
25	1.25	0.1938E+00	50	2.50	0.5395E-02

Table 16. Averaged Wave Spectrum at the Primary Tank Location

HURRICANE CAMILLE WAVES GENERATION

Scalar Spectrum Analysis Page 1 of 1 Channel 1
W.W. 70FT

Run= 36, 37, 39, 40, 45, 46, 52,

4480 Points 50 Lags Delta-T= 0.200000 Sec
Scale constant= 0.100000E+01 Delta-Freq.= 0.050 Hertz

Sample Variance= 0.506391E+01 *90% Conf Intv.= 0.489260E+01 (Low)
Spectrum Area = 0.506391E+01 * = 0.524488E+01 (High)

179 Deg. Freedom: for 90% Conf. Bounds Multiply
Spectral Estimates by 0.85 and 1.20
Sig Wave Height = 9.0013 Inches

Lag	Frequency Hz	Spectral Estimates in**2-sec	Lag	Frequency Hz	Spectral Estimates in**2-sec
0	0.00	0.4598E-01			
1	0.05	0.4111E-01	26	1.30	0.2208E+00
2	0.10	0.4825E-01	27	1.35	0.1834E+00
3	0.15	0.2173E-01	28	1.40	0.1491E+00
4	0.20	0.3057E-01	29	1.45	0.1239E+00
5	0.25	0.1415E-01	30	1.50	0.1034E+00
6	0.30	0.8718E-01	31	1.55	0.8484E-01
7	0.35	0.6203E+00	32	1.60	0.7337E-01
8	0.40	0.3276E+01	33	1.65	0.6807E-01
9	0.45	0.1005E+02	34	1.70	0.6315E-01
10	0.50	0.1758E+02	35	1.75	0.6197E-01
11	0.55	0.1789E+02	36	1.80	0.5090E-01
12	0.60	0.1302E+02	37	1.85	0.5056E-01
13	0.65	0.9743E+01	38	1.90	0.3853E-01
14	0.70	0.7649E+01	39	1.95	0.3111E-01
15	0.75	0.5171E+01	40	2.00	0.2577E-01
16	0.80	0.3790E+01	41	2.05	0.3017E-01
17	0.85	0.3077E+01	42	2.10	0.2559E-01
18	0.90	0.2277E+01	43	2.15	0.2231E-01
19	0.95	0.1562E+01	44	2.20	0.1888E-01
20	1.00	0.1158E+01	45	2.25	0.1990E-01
21	1.05	0.8495E+00	46	2.30	0.1703E-01
22	1.10	0.5876E+00	47	2.35	0.1924E-01
23	1.15	0.4877E+00	48	2.40	0.1757E-01
24	1.20	0.3914E+00	49	2.45	0.1948E-01
25	1.25	0.3051E+00	50	2.50	0.1771E-01

Table 17. Averaged Wave Spectrum at the Secondary Tank Location

HURRICANE CAMILLE WAVES GENERATION

Scalar Spectrum Analysis Page 1 of 1 Channel 2
W.W. 170FT

Run= 36, 37, 39, 40, 45, 46, 52,

4480 Points 50 Lags Delta-T= 0.200000 Sec
Scale constant= 0.100000E+01 Delta-Freq.= 0.050 Hertz

Sample Variance= 0.458974E+01 *90% Conf Intv.= 0.443448E+01 (Low)
Spectrum Area = 0.458974E+01 * = 0.475377E+01 (High)

179 Deg. Freedom: for 90% Conf. Bounds Multiply
Spectral Estimates by 0.85 and 1.20
Sig Wave Height = 8.5695 Inches

Lag	Frequency Hz	Spectral Estimates in**2-sec	Lag	Frequency Hz	Spectral Estimates in**2-sec
0	0.00	0.1026E-01			
1	0.05	0.3501E-01	26	1.30	0.1873E+00
2	0.10	0.2066E-01	27	1.35	0.1498E+00
3	0.15	0.3245E-01	28	1.40	0.1154E+00
4	0.20	0.8476E-02	29	1.45	0.8180E-01
5	0.25	0.2289E-01	30	1.50	0.8490E-01
6	0.30	0.5957E-01	31	1.55	0.6850E-01
7	0.35	0.5765E+00	32	1.60	0.5922E-01
8	0.40	0.3131E+01	33	1.65	0.3871E-01
9	0.45	0.1023E+02	34	1.70	0.4313E-01
10	0.50	0.1749E+02	35	1.75	0.3493E-01
11	0.55	0.1714E+02	36	1.80	0.3683E-01
12	0.60	0.1227E+02	37	1.85	0.2905E-01
13	0.65	0.8783E+01	38	1.90	0.2765E-01
14	0.70	0.6471E+01	39	1.95	0.1802E-01
15	0.75	0.4292E+01	40	2.00	0.2451E-01
16	0.80	0.3232E+01	41	2.05	0.1593E-01
17	0.85	0.2304E+01	42	2.10	0.1775E-01
18	0.90	0.1385E+01	43	2.15	0.1322E-01
19	0.95	0.9210E+00	44	2.20	0.1718E-01
20	1.00	0.7476E+00	45	2.25	0.1123E-01
21	1.05	0.4956E+00	46	2.30	0.1448E-01
22	1.10	0.3510E+00	47	2.35	0.8680E-02
23	1.15	0.2410E+00	48	2.40	0.1250E-01
24	1.20	0.2256E+00	49	2.45	0.7891E-02
25	1.25	0.1961E+00			

Table 18. A Sample ASCII Time History File, Run 36

```
RUN 36   CAMILLE WAVES IN DAVIDSON LABORATORY TANK-3  NOV-87
SAMPLING INTERVAL : 0.1 SECOND, READ FORMAT (F8.3,F8.3)
1ST COLUMN : WAVE ELEVATN,INCHES, AT PRIMARY LOCATN, 70 FT FROM WAVE MAKER
2ND COLUMN : WAVE ELEVATN,INCHES, AT SECONDARY LOCATN, 170 FT FROM WAVE MAKER
DESIRED SIGNIFICANT WAVE HEIGHT 9.0 INCHES
   1.389   0.965
   2.428   0.912
   2.712   0.481
   2.483   0.003
   2.187  -0.586
   1.806  -1.105
   1.480  -1.300
   1.232  -1.217
   0.876  -0.893
   0.066  -0.209
  -0.889   0.735
  -1.584   1.483
  -1.958   1.890
  -2.218   1.884
  -2.194   1.271
  -1.952   0.157
  -1.686  -0.663
  -1.124  -1.217
  -0.236  -1.600
   0.725  -1.471
   1.619  -0.922
   2.193  -0.386
   2.187   0.062
   1.377   0.564
   0.821   0.858
   0.646   0.864
   0.586   0.811
   0.586   0.628
   0.580   0.292
   0.422   0.039
   0.169  -0.268
  -0.158  -0.374
  -0.448  -0.439
  -0.738  -0.374
  -1.016  -0.439
```

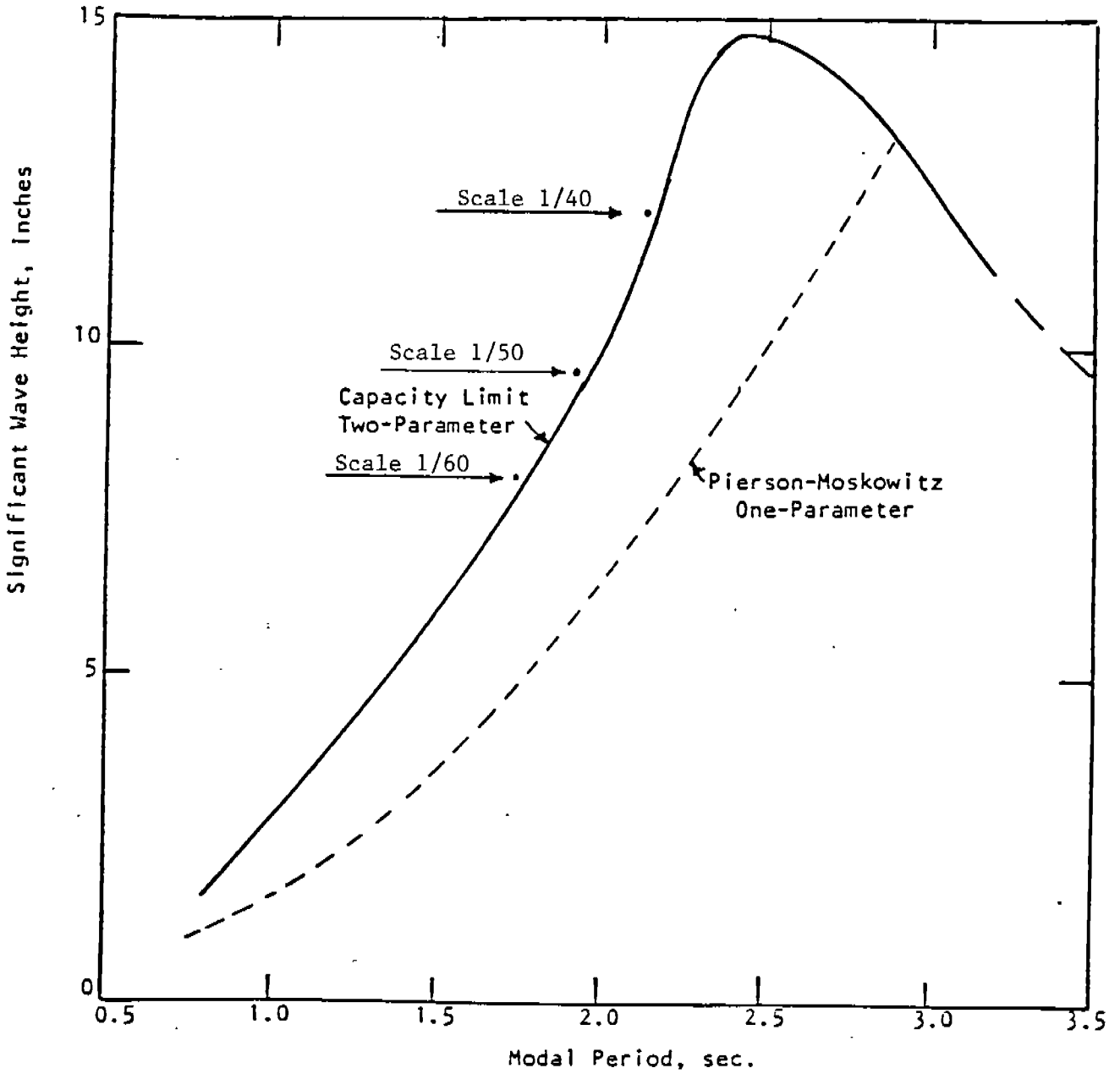

FIGURE 1 IRREGULAR WAVE CAPACITY,
ITTC TWO PARAMETER SPECTRUM,
NORMAL OPERATING DEPTH,
PRIMARILY MEAN SLOPE APPORTIONMENT. [3]

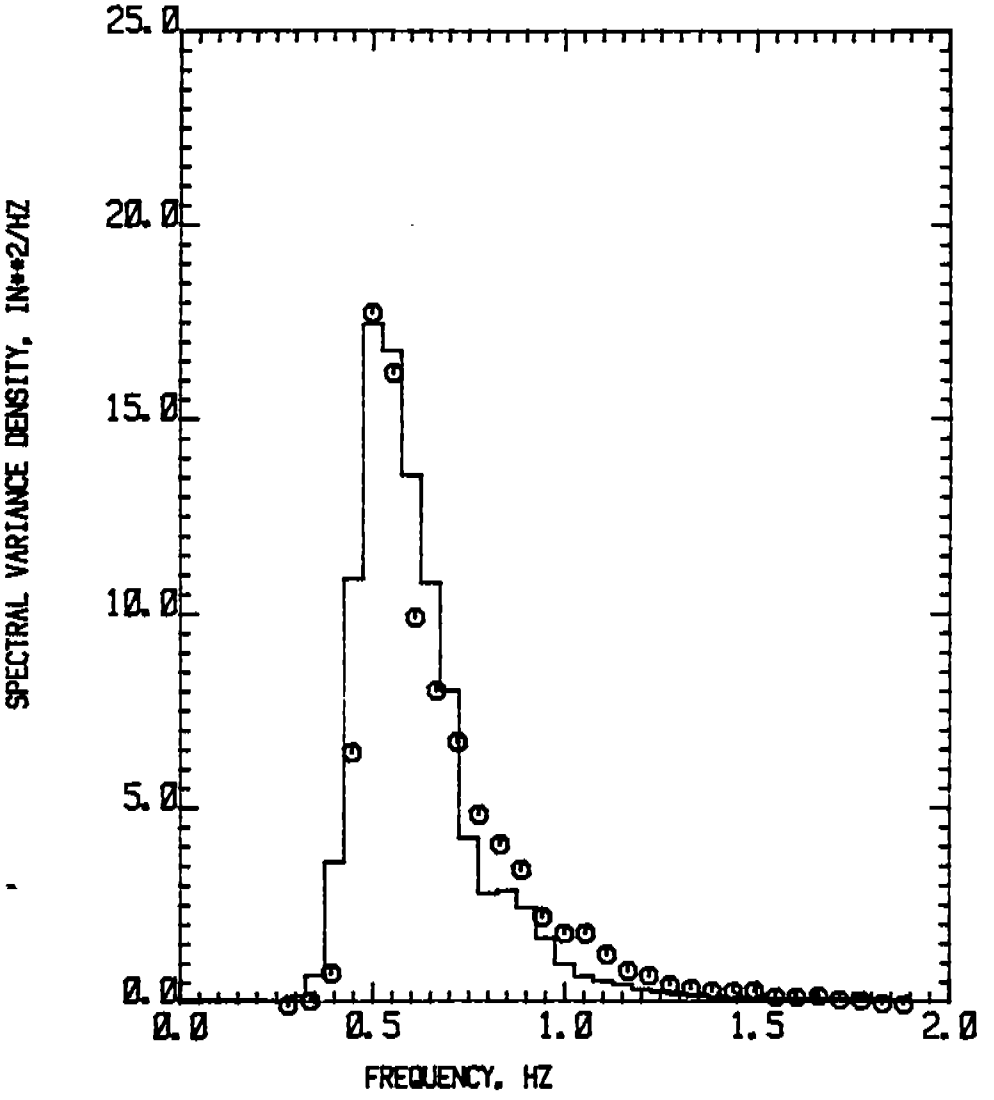

FIGURE 2 WAVE SPECTRUM AT PRIMARY LOCATION, RUN 36

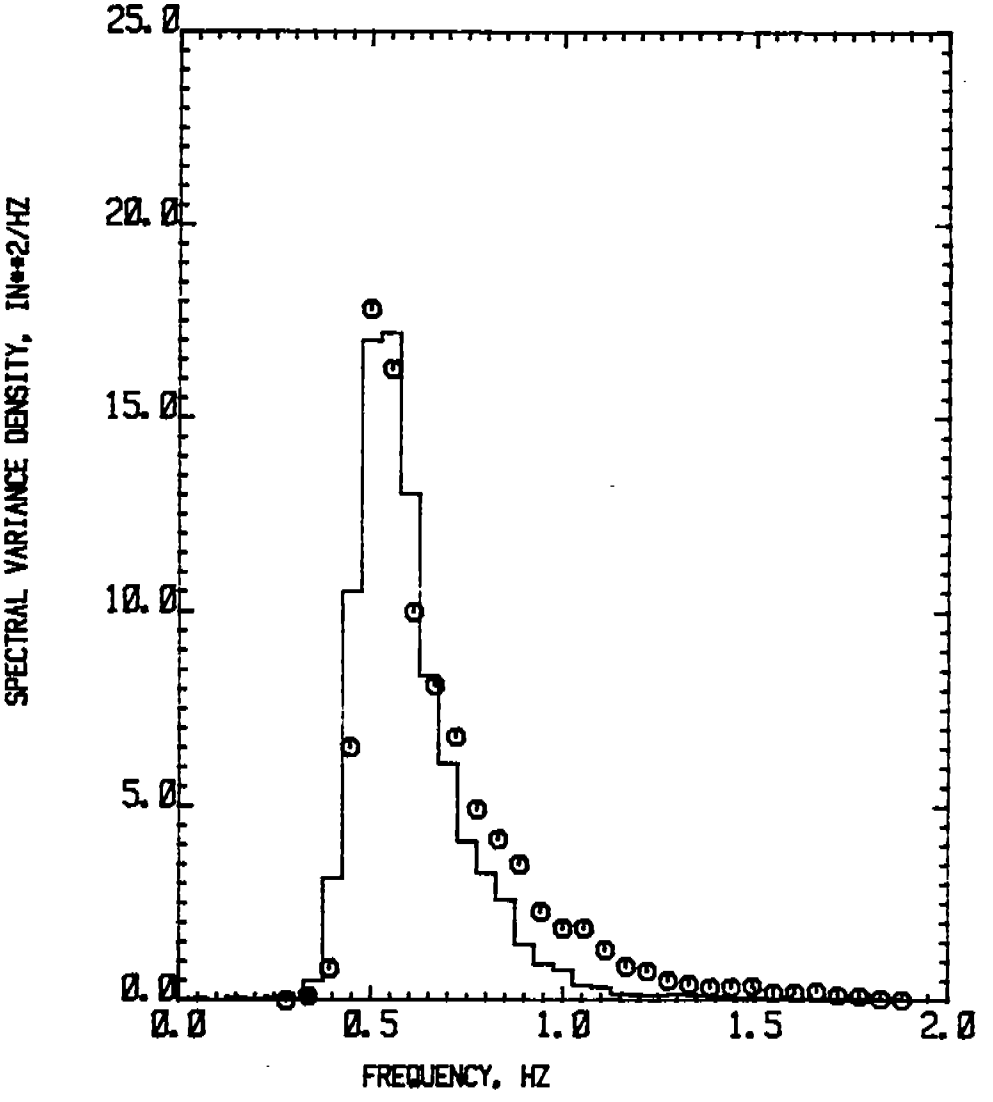

FIGURE 3 WAVE SPECTRUM AT SECONDARY LOCATION, RUN 36

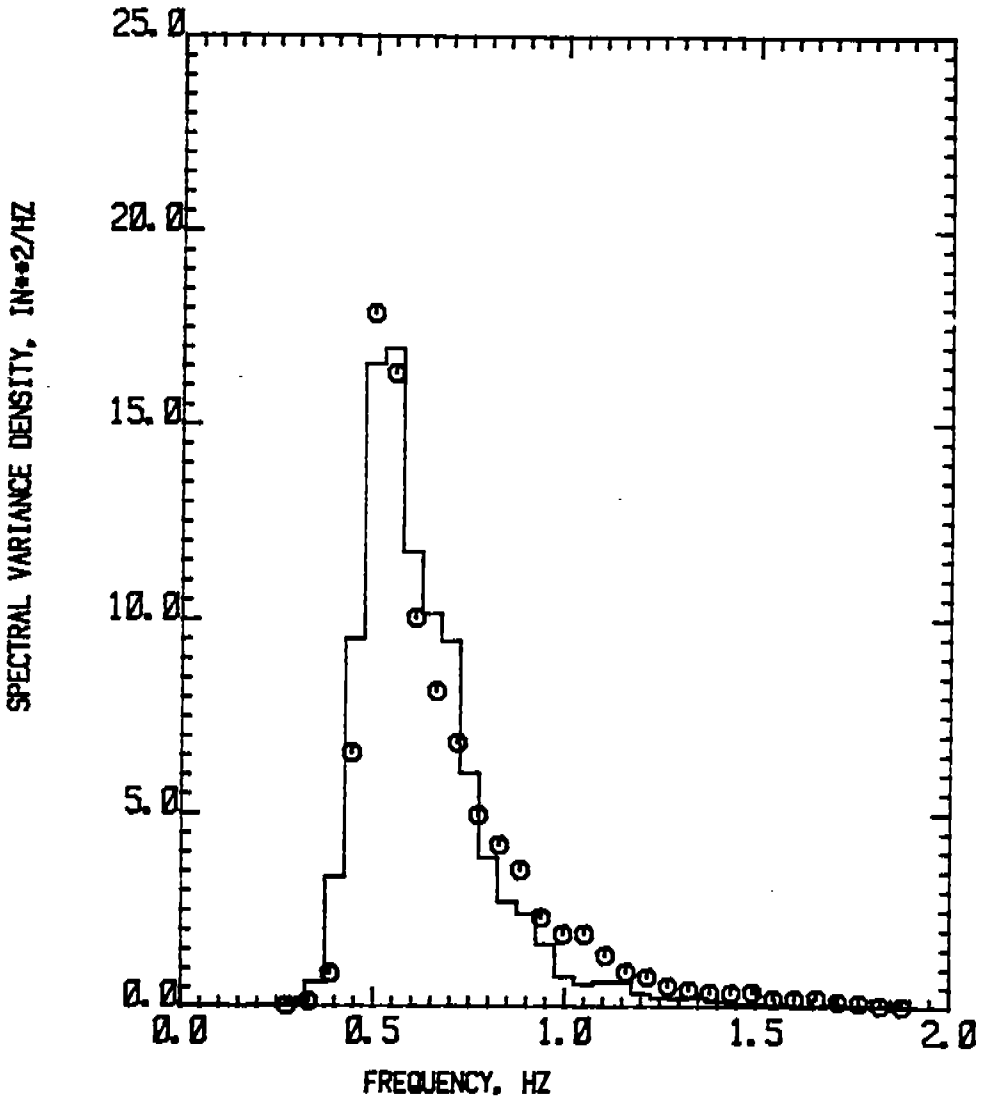

FIGURE 4 WAVE SPECTRUM AT PRIMARY LOCATION, RUN 37

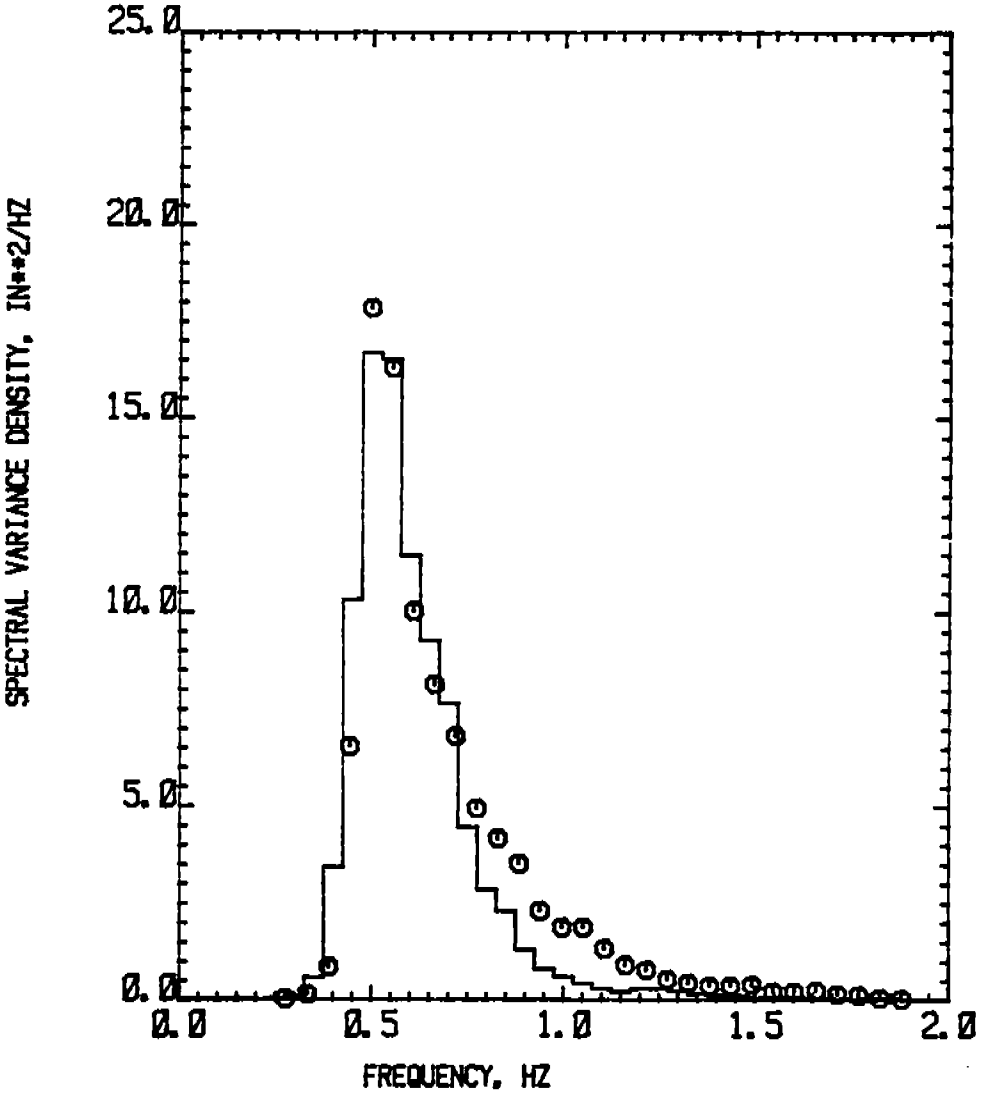

Run 37, Secondary Location

FIGURE 5 WAVE SPECTRUM AT SECONDARY LOCATION, RUN 37

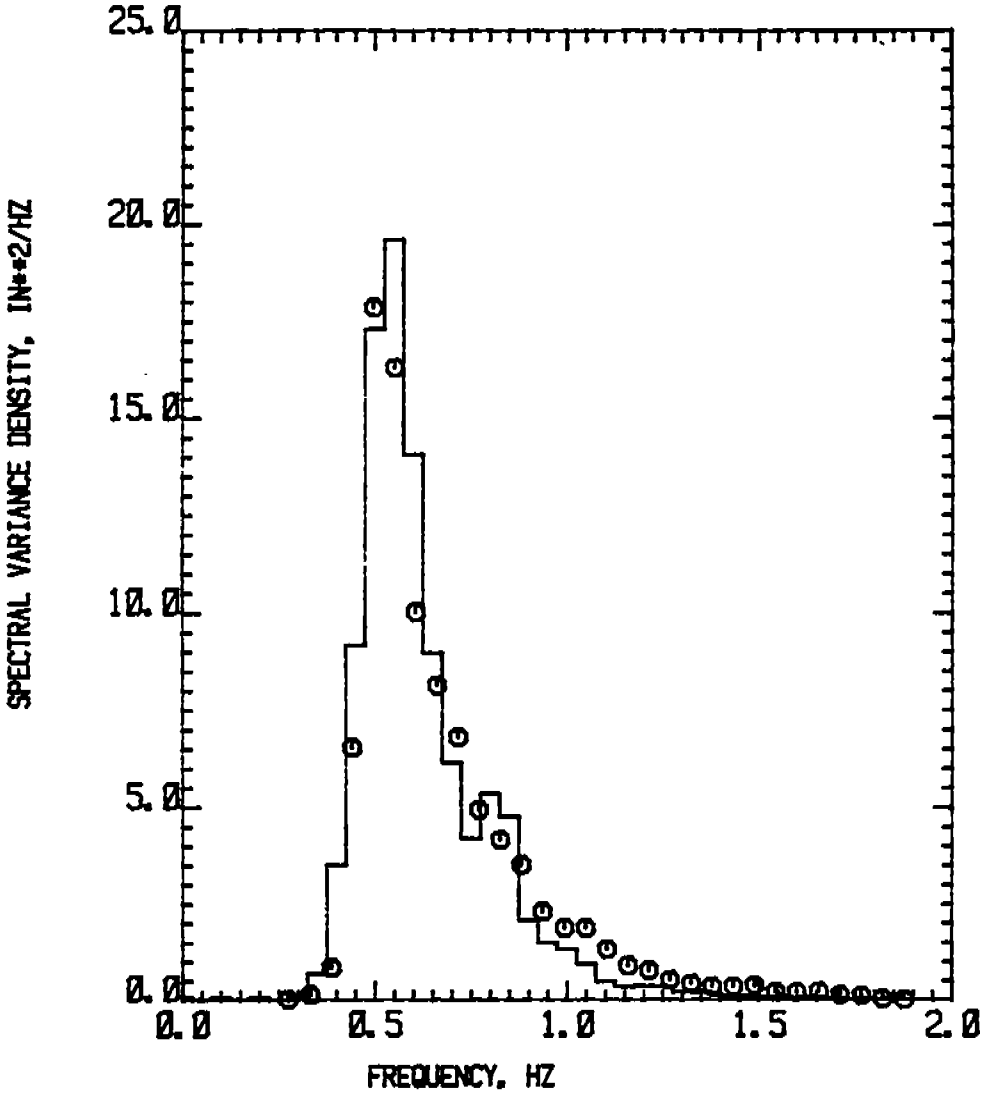

Run 39, Primary Location

FIGURE 6 WAVE SPECTRUM AT PRIMARY LOCATION, RUN 39

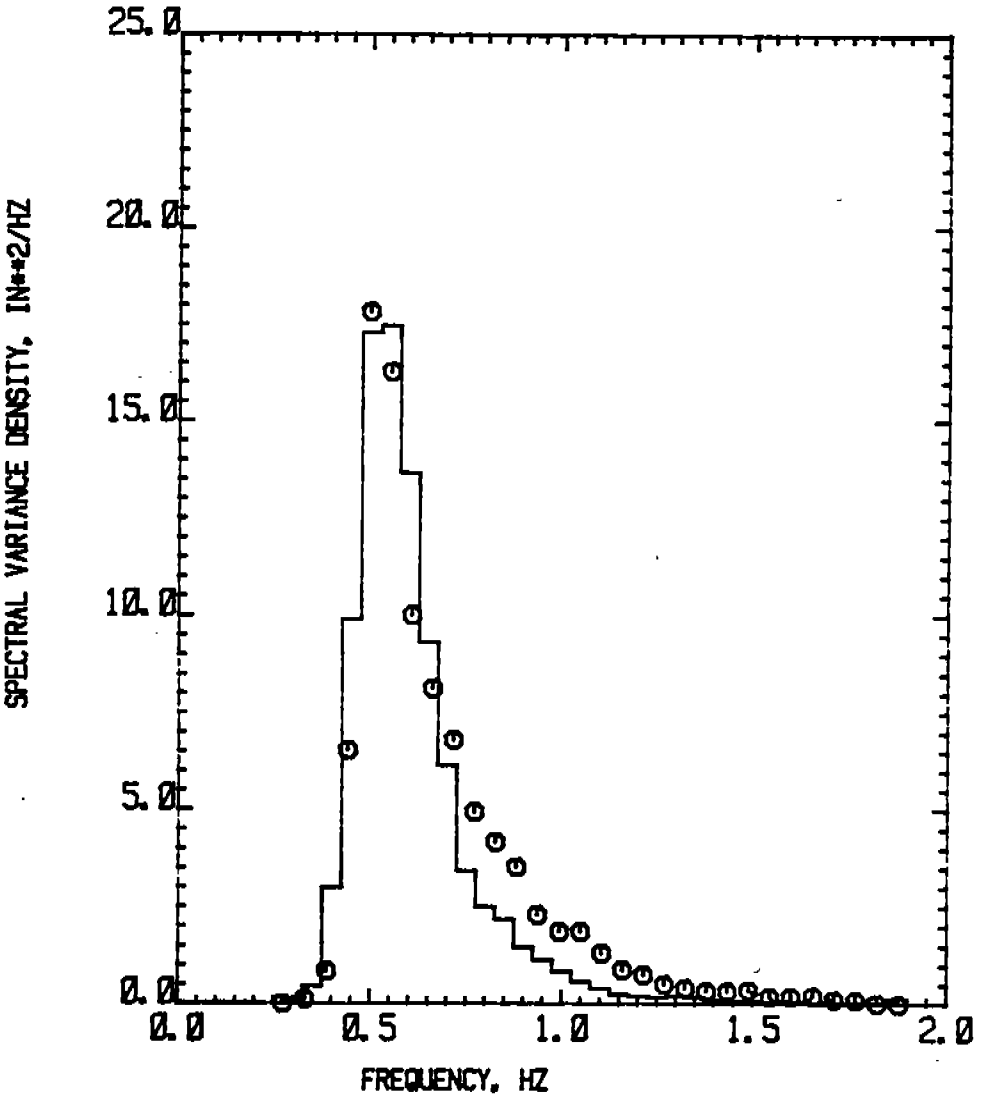

FIGURE 7 WAVE SPECTRUM AT SECONDARY LOCATION, RUN 39

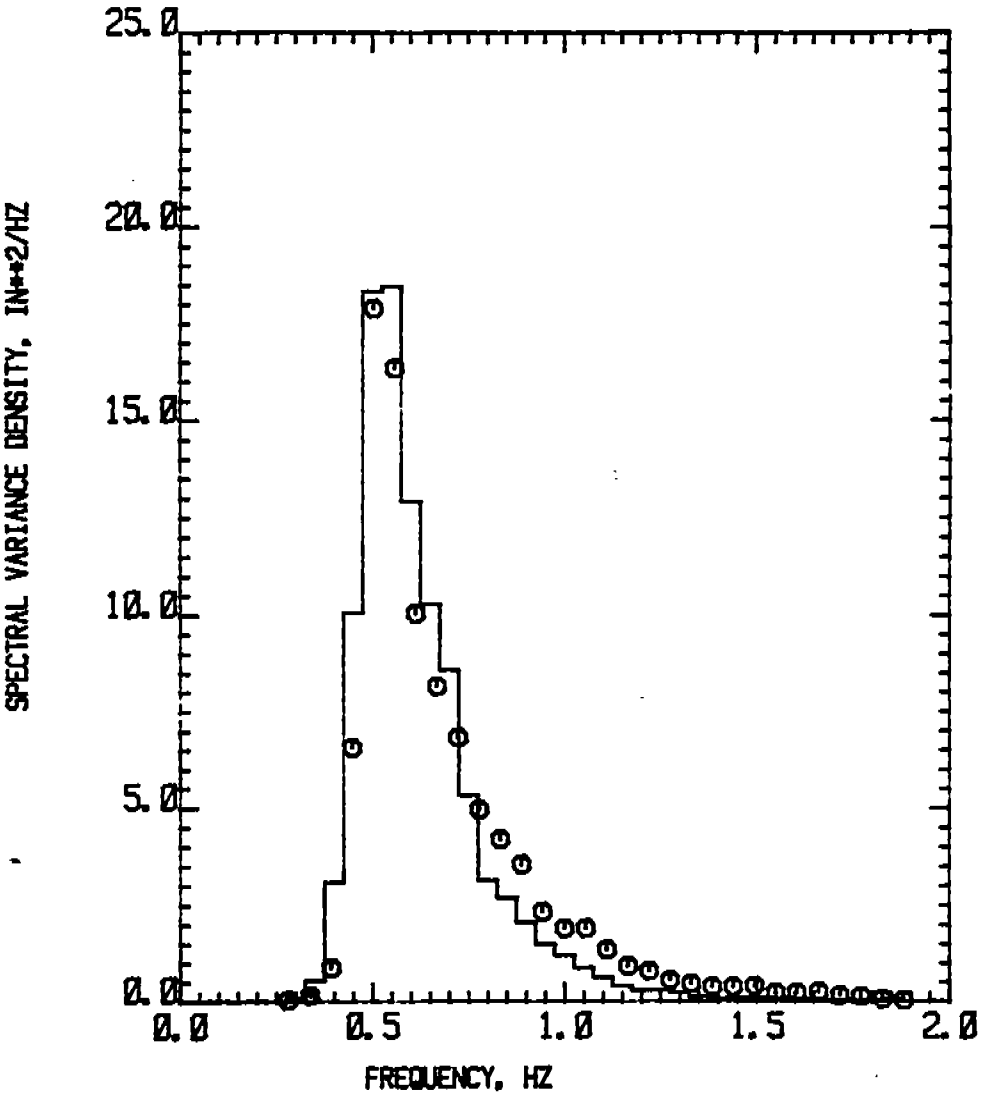

Run 40, Primary Location

FIGURE 8 WAVE SPECTRUM AT PRIMARY LOCATION, RUN 40

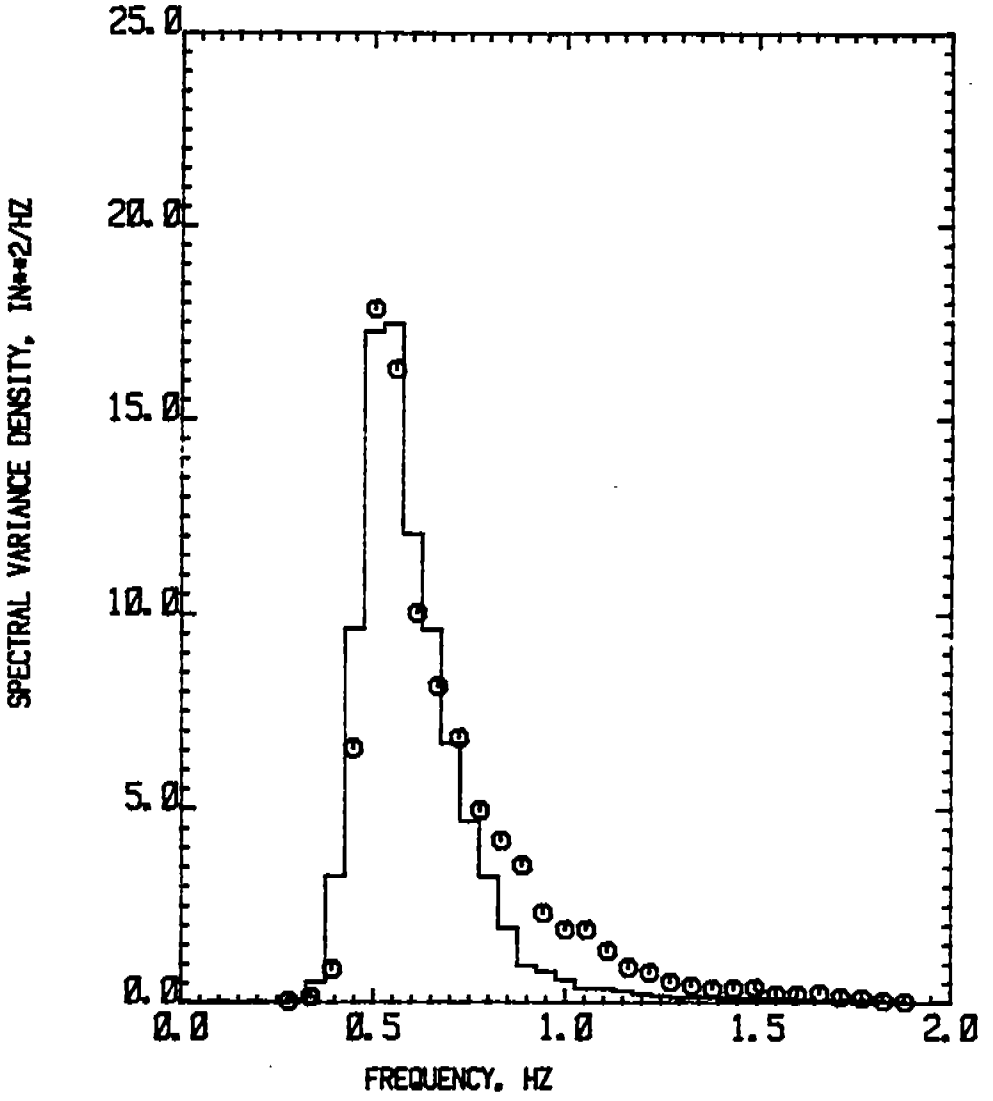

Run 40, Secondary Location

FIGURE 9 WAVE SPECTRUM AT SECONDARY LOCATION, RUN 40

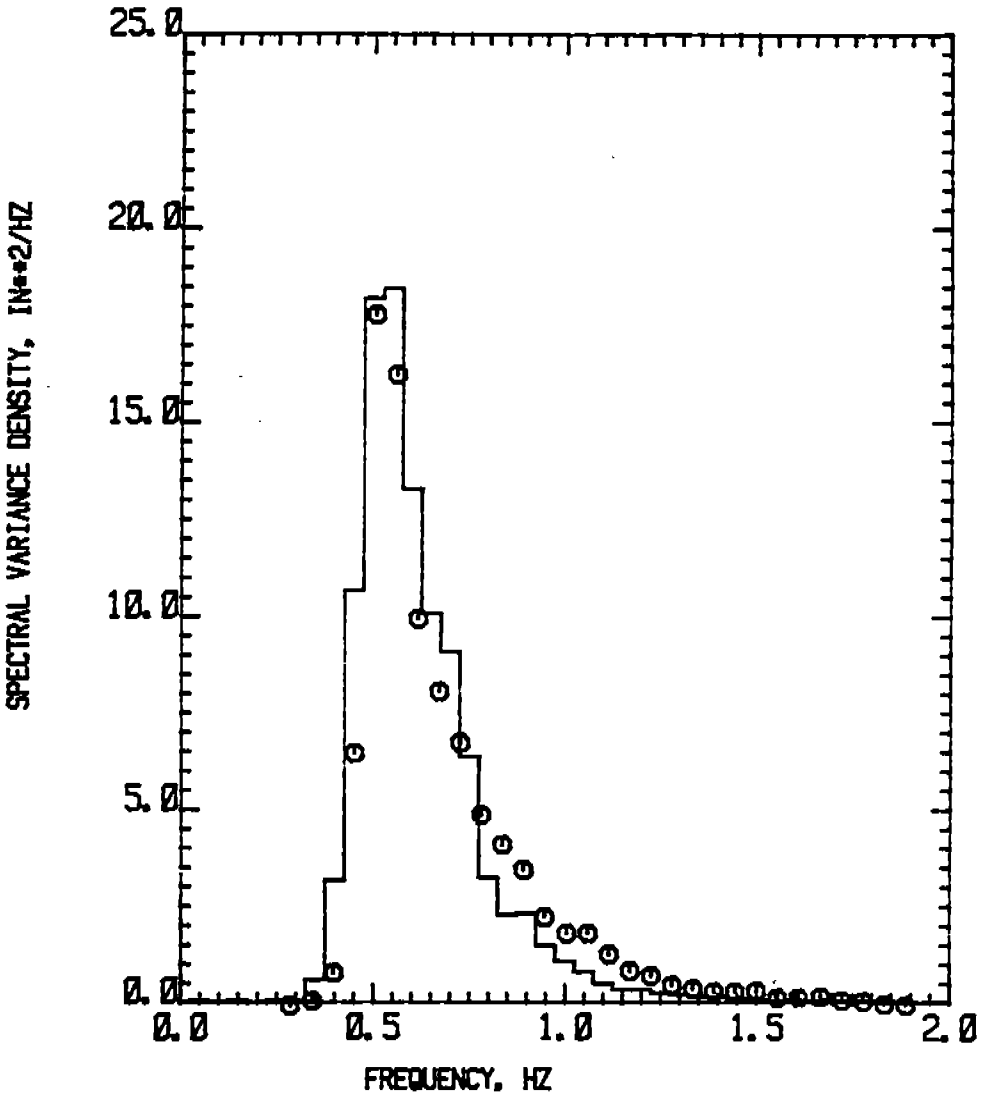

Run 45, Primary Location

FIGURE 10 WAVE SPECTRUM AT PRIMARY LOCATION, RUN 45

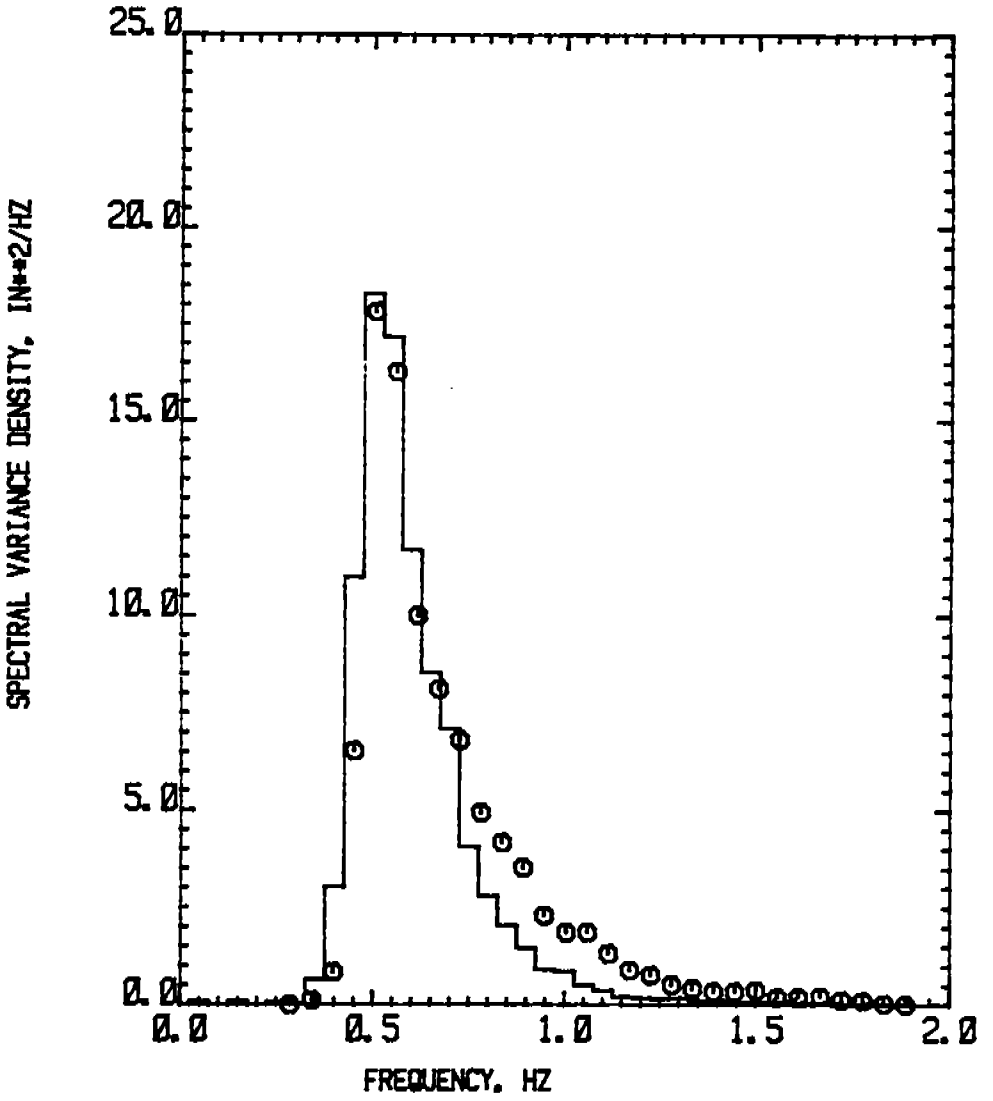

Run 45, Secondary Location

FIGURE 11 WAVE SPECTRUM AT SECONDARY LOCATION, RUN 45

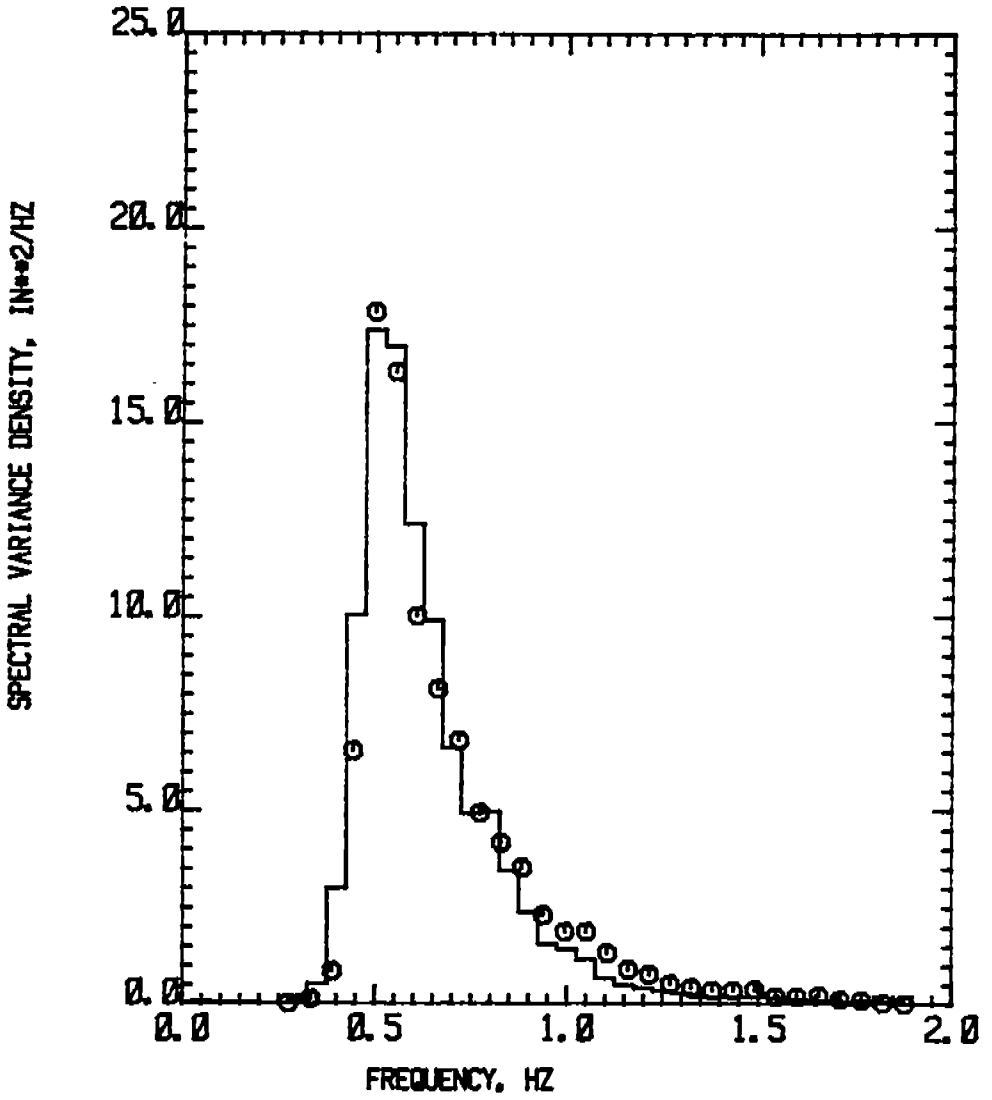

FIGURE 12 WAVE SPECTRUM AT PRIMARY LOCATION, RUN 46

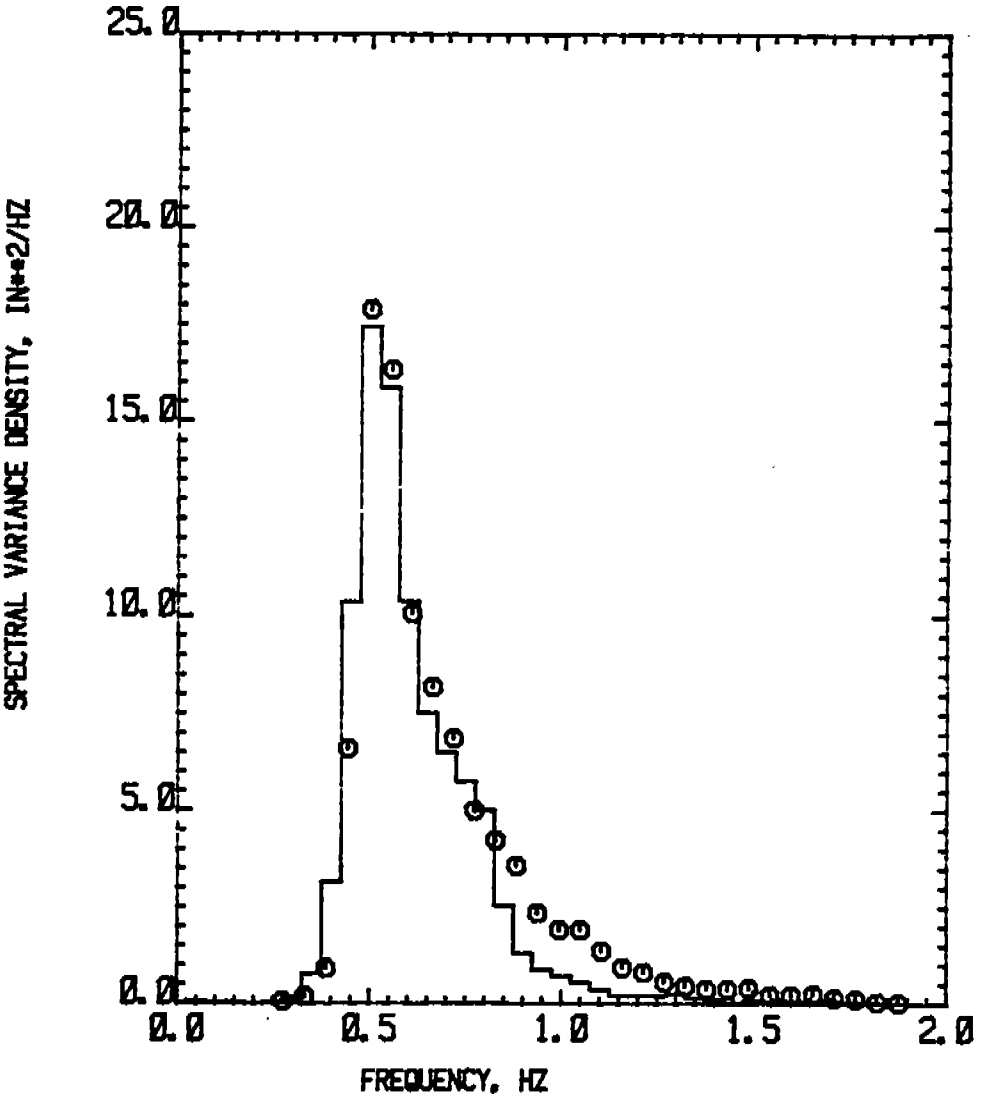

FIGURE 13 WAVE SPECTRUM AT SECONDARY LOCATION, RUN 46

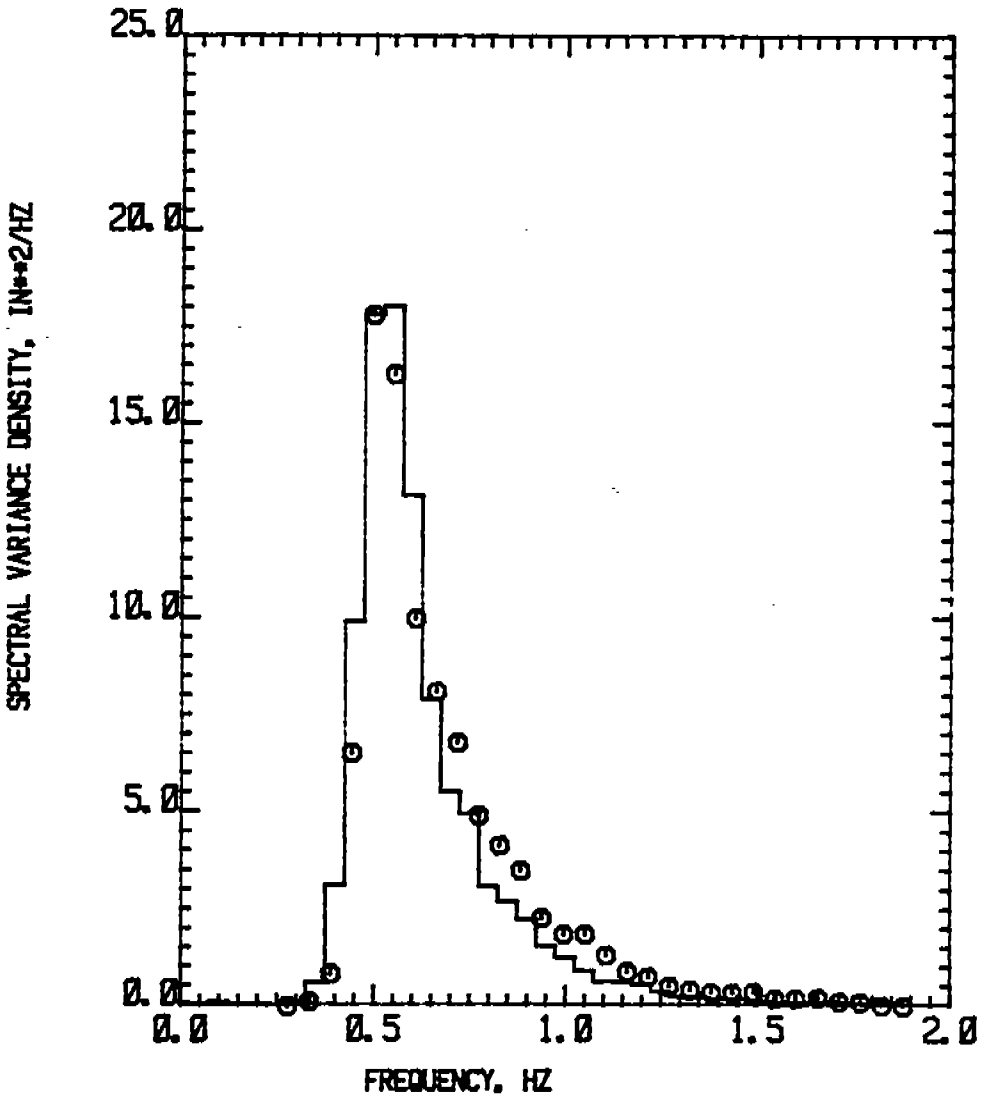

FIGURE 14 WAVE SPECTRUM AT PRIMARY LOCATION, RUN 52

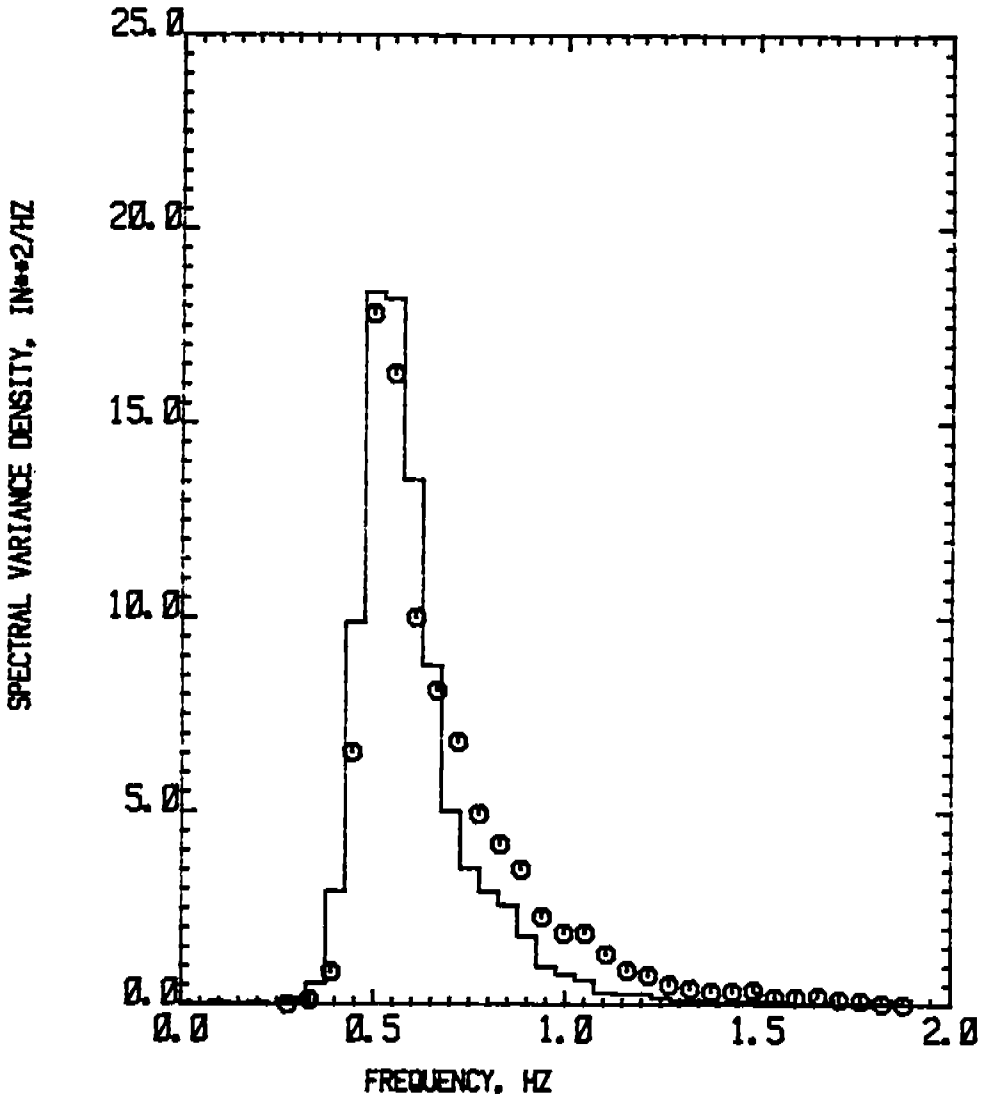

FIGURE 15 WAVE SPECTRUM AT SECONDARY LOCATION, RUN 52

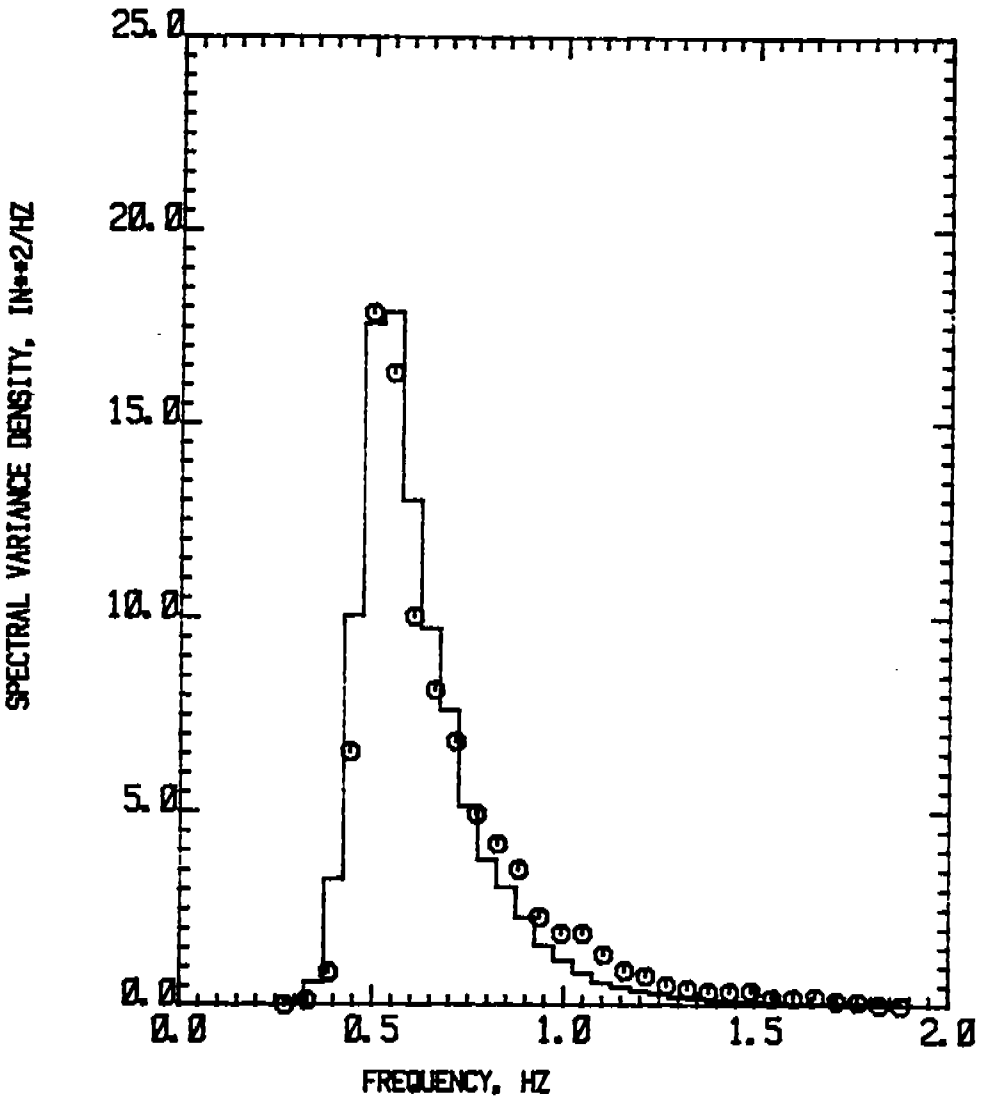

FIGURE 16 AVERAGED WAVE SPECTRUM, PRIMARY LOCATION
RUNS 36, 37, 39, 40, 45, 46, 52

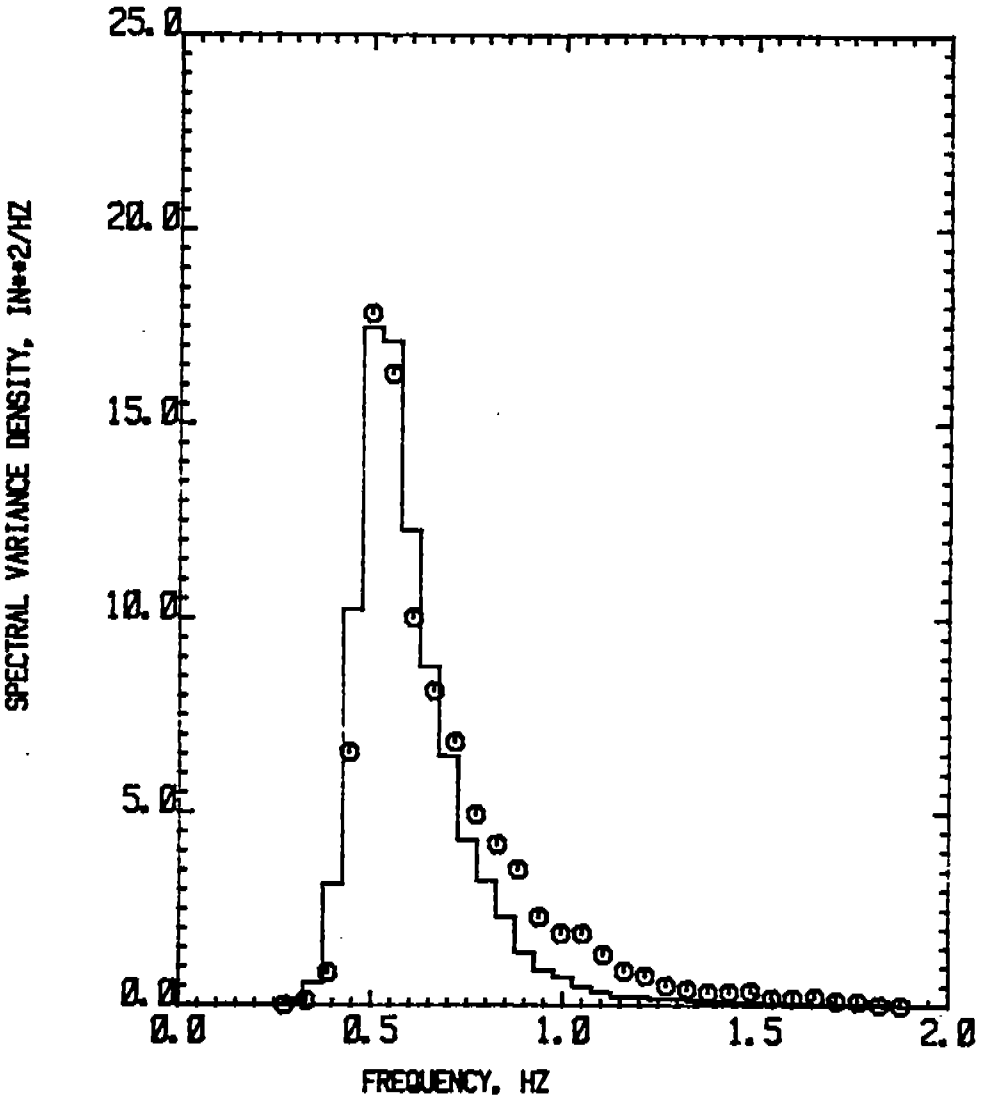

FIGURE 17 AVERAGED WAVE SPECTRUM, SECONDARY LOCATION
RUNS 36, 37, 39, 40, 45, 46, 52

(APPENDIX A)

20TH AMERICAN TOWING TANK CONFERENCE

DAVIDSON LABORATORY
STEVENS INSTITUTE OF TECHNOLOGY

AUGUST 2, 3, 4, 1983

PARTICULARS

DAVIDSON LABORATORY TANK 3 WAVE MACHINE

TYPE: Double Flap/Wetback

COMMISSIONED: 1 September 1982

SYSTEMS RESPONSIBILITY:

MTS Systems Corporation, Minneapolis, MN:

- Waveboards, Linkages and Foundation
- Actuators, Servo Valves, Service Manifold, Power Supply
- Master Control, Feedback Controllers

Davidson Laboratory

- Backbeach and Incidental Mechanical Equipment
- Computer Interface
- Computer and Software

TANK DIMENSIONS:

Length:	295 feet exclusive of dock
Width:	12 feet
Normal Operating Depth:	5.36 feet

WAVEBOARD GEOMETRY:

- Waveboards located 10.5 feet from tank end
- Hinge locations:
  - Lower 0.22 feet from tank bottom
  - Upper 3.95 feet from tank bottom
- At normal operating depth:
  - Lower Waveboard height 3.73 feet
  - Upper Waveboard height 1.40 feet
- Maximum Waveboard angles (mechanical):
  - Lower $\pm 15^{\circ}$
  - Upper $\pm 13.75^{\circ}$ (relative to lower)
- Angle limits set by software, $\pm 13.4^{\circ}$, both waveboards
- Angular velocity limits set by software:
  - Lower ±45 deg/sec
  - Upper ±60 deg/sec

MECHANICAL LINKAGE:

- Stick figure linkage schematic appended as Figure I. There are three fixed hinge points in the system, the lower waveboard hinge, the lower waveboard actuator trunnion, and a third hinge at the top of the vertical link. Extension of the lower flap actuator is magnified three times by the vertical link, which moves the triangular yoke, and ultimately the lower flap through horns at each side. The upper flap actuator is carried by the yoke and is attached directly to the upper flap.
- The nonlinear relationships between actuator extensions and waveboard angles are compensated for in the computer generated actuator extension command signals.

SEALS:

- There are no rubbing seals between the waveboards, or between waveboards and the tank. Various baffle plates are arranged so as to minimize the flow-through area. Width of the resulting cracks is typically 1/8 to 1/4 inches.

SUBMERGED BEARINGS:

- Four submerged journal bearings, two in each hinge line, self lubricating.

BACKBEACH:

- Section, Figure II
- Six layers of wooden grids at about 12° angle are attached to a pile of standard concrete blocks arranged so as to permit flow-through. The various parts are strapped together with stainless steel rods and hooks. Horizontal flow area through concrete blocks is about 35% of frontal area. Slanted grid over the foundation inspection pit required to control splashing.
- Tank sides built up locally about 16 inches
- Design was developed by cut and try with 1/8 scale model.

HYDRAULIC EQUIPMENT:

- Power supply; Variable volume
  40 gpm @ 3000 psi
  Main pump motor, 55KW
- Servo Valves:
  Lower, 2 valves, 15 gpm
  Upper, 2 valves, 5 gpm
- Actuators:
  Lower, 16 inch stroke, 15000 lb force rating
  Upper, 21 inch stroke, 5500 lb force rating

SERVO CONTROLLERS:

- Displacement, velocity, acceleration and delta pressure feedback.
- Limit detectors for all quantities capable of shutting down power supply.
- Offset and span adjustment.

MASTER CONTROL:

- Hydraulics on/off, high/low pressure, run/stop, panic button, interlocks.
- Controls duplicated at dock end of tank.

INTERFACE:

- Isolation amplifiers between computer and rest of system.
- Slow start/stop circuits which ramp signal gain up and down to provide smooth start up and stop, and to prevent computer signals from reaching servo controllers except when in run mode.
- Low pass filters (5 Hz, 6-pole Butterworth) at input to servo controllers.
- Pulse generator to communicate with computer when run/stop mode changed.
- Inclinometers mounted on waveboards, dual digital displays. (To aid in checking net static gains through the system.)

COMPUTER:

- PDP 11/23 System includes:
  LSI 11/23 CPU, memory management
  96 Kb MOS memory
  2 I/O ports
  Boot Strap Prom
  Programmable clock
  4 Channels D/A
  Dual Drive, Double Density
  Floppy System (1mb)
  Hardcopy Terminal

SOFTWARE:

- RT-11 single user operating system and FORTRAN.
- Locally developed calibration and diagnostic utilities.
- Run time Regular Wave generator.
- Irregular Wave Program generator.
  - Modified white noise/fast convolution method
  - 17 hours worth of statistically independent 2 minute samples available
  - Open loop
  - Five spectral forms, ITTC, Neumann, JONSWAP, Voznesenski-Netsvetayev, and "Swell". "Sea plus Swell" simulations possible by combination of above forms.
- Run Time Irregular Wave generator
  - Scales previously stored digital wave programs and runs the machine.
- Software corrections for:
  - Nonlinearity of LVDT actuator displacement transducers
  - Linkage nonlinearity
  - Closed loop servo frequency response
  - Filter frequency response
  - Theoretical wave machine calibration
  - Net deviations between theoretical and experimental calibrations
- Four apportionment schemes:
  - Upper flap only
  - Lower flap only
  - Limited linear regression (USNA method with upper flap only for high frequencies, and in opposed phase operation, upper flap angle limited to value equal to that of lower flap).
  - Main slope (no opposed phase operation, yields a marginally higher wave with slightly less good long wave shape than linear regression).
  - Linear regression apportionment is the standard for normal water depth.

REGULAR WAVE CAPACITY:

- Limiting regular wave capacity indicated in Figure III.

IRREGULAR WAVE CAPACITY:

- Limiting irregular wave (ITTC two parameter) capacity shown in Figure IV

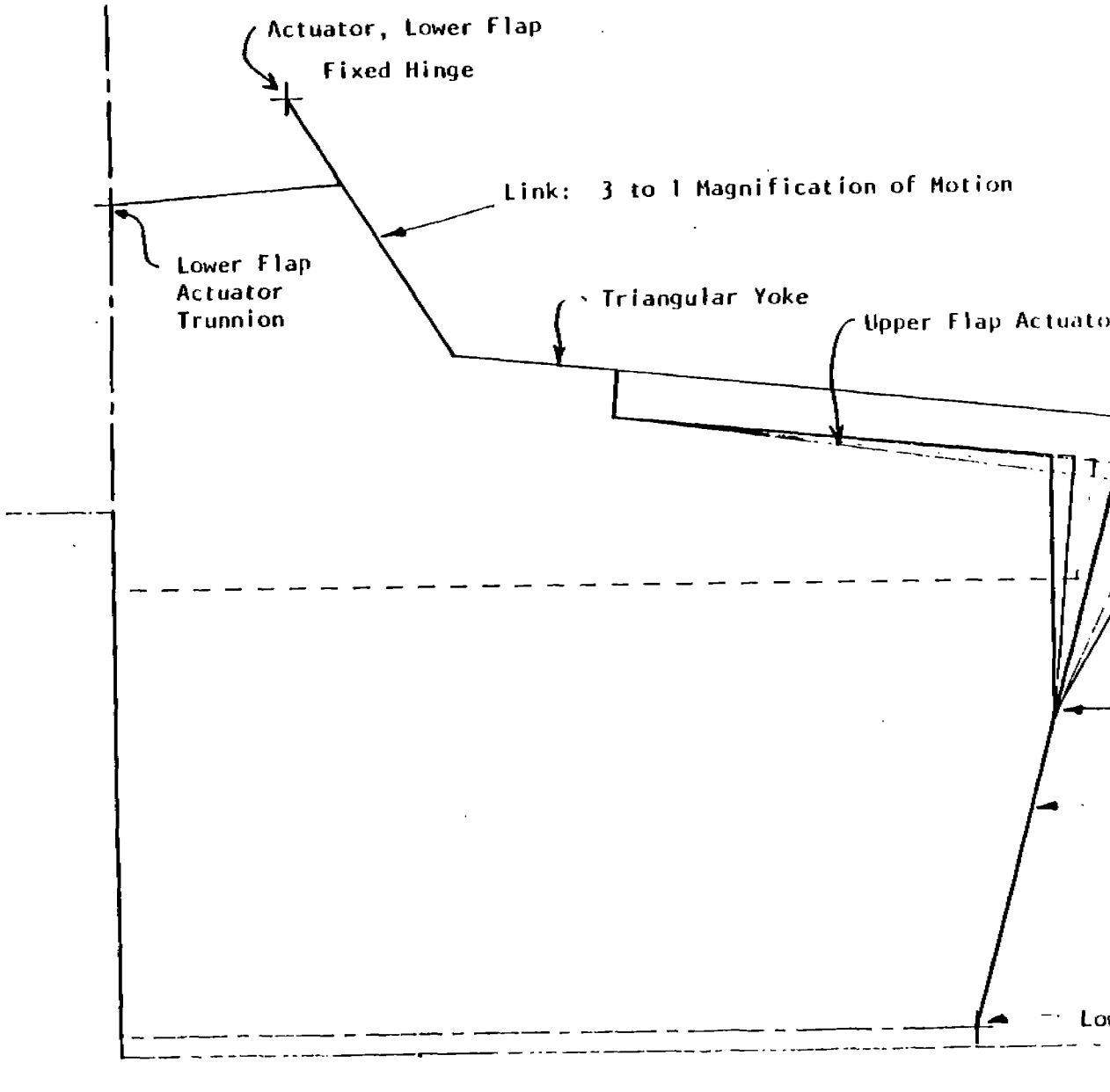

FIGURE 1 LINKAGE SCHEMATIC

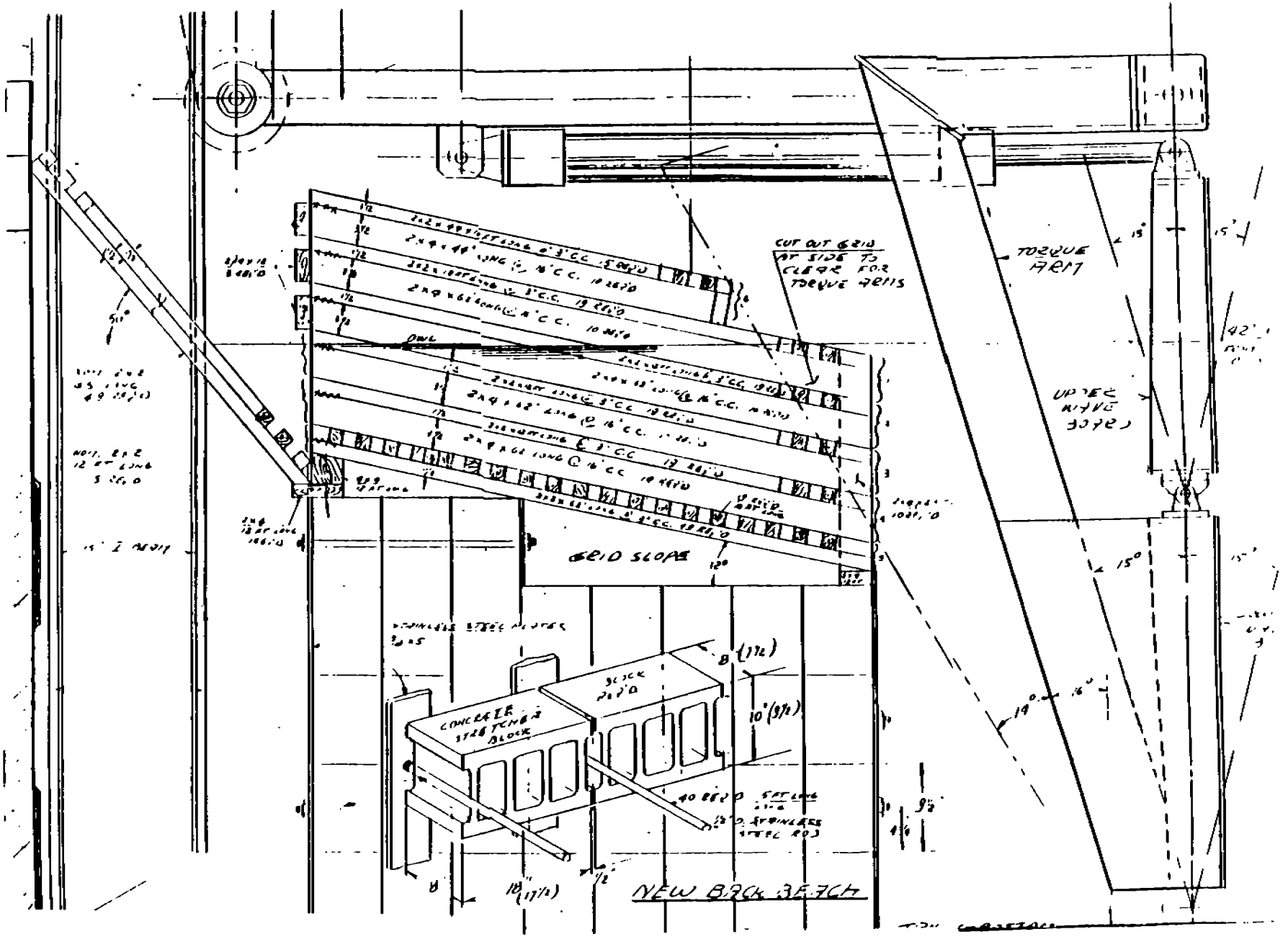

FIGURE 11 BACKBEACH

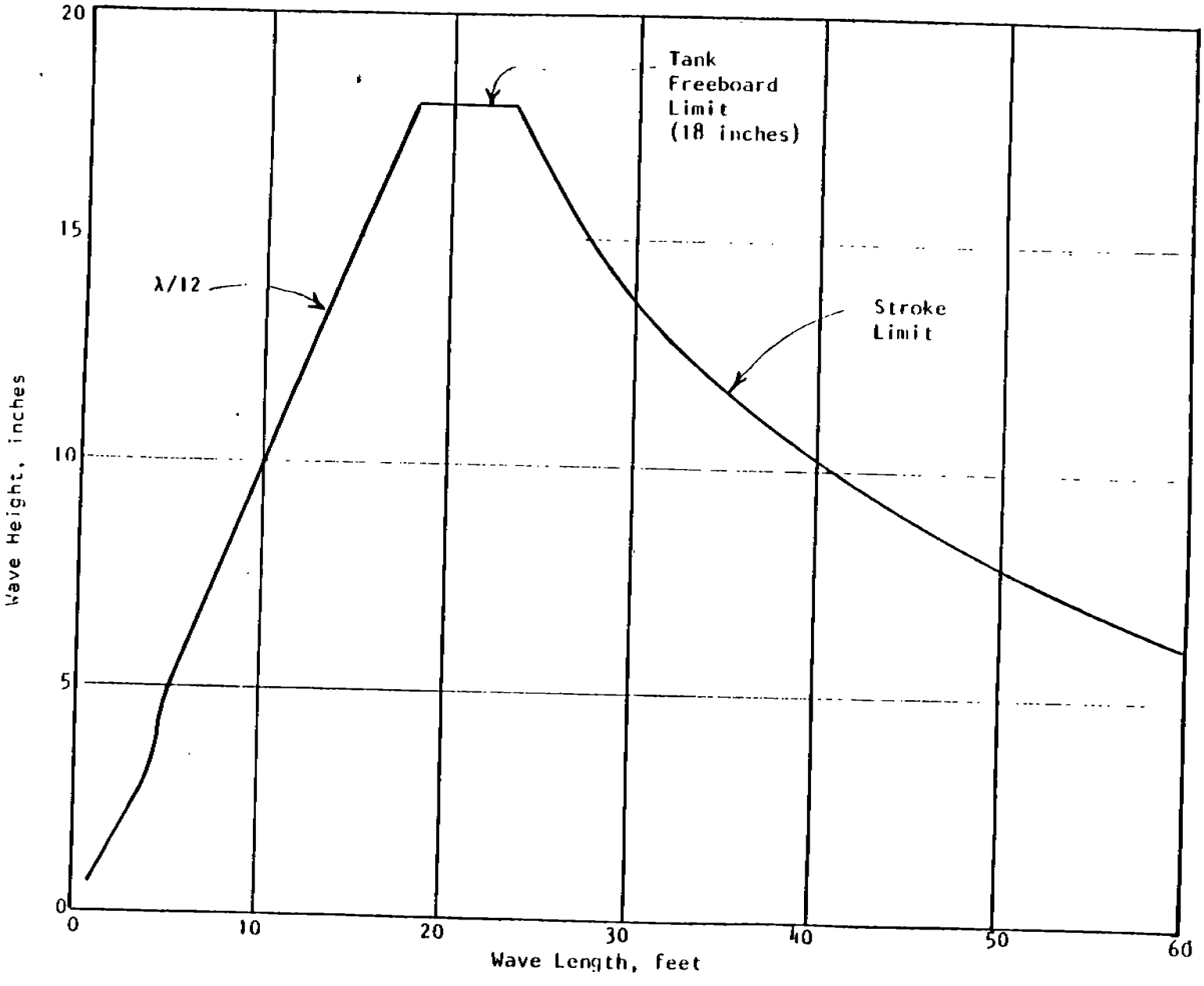

FIGURE III REGULAR WAVE CAPACITY, NORMAL OPERATING DEPTH, LIMITED LINEAR REGRESSION APPORTIONMENT

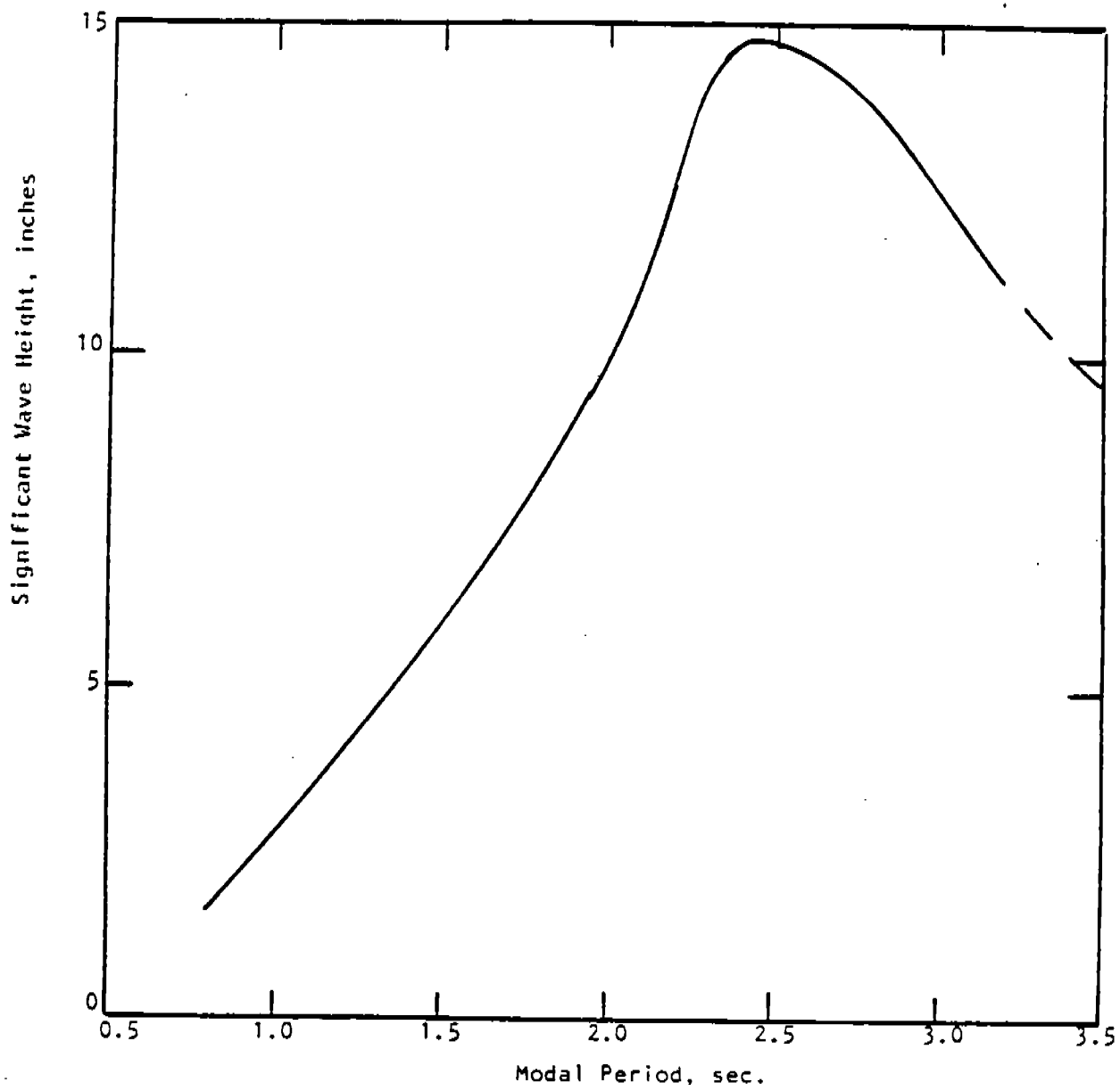

FIGURE IV IRREGULAR WAVE CAPACITY,

(APPENDIX B)

A PSUEDO-RANDOM WAVE GENERATOR SYSTEM

As presently developed, the random wave generator system is a three step process:

1. Define the desired spectral shape.
2. Generate a particular realization of a Guassian random wave process having the desired spectral shape and having a one inch significant height. Apply the wave machine calibration to this process to produce sequences of required angles for upper and lower flap. Finally, store this result in a (binary) program file which will be used at run time.
3. Read the program file from disk and scale the angles from 1 inch significant height to those for the desired significant height. Compute actuator positions for each flap and scale the results to bits into the D/A converters. This result is stored in virtual memory, and as now programmed is a periodic sequence 128 seconds in length. The starting point of the periodic sequence output may be specified and once this is done the stored sequences are loaded into low memory and output upon receipt of external trigger pulse by subroutine RUNOUT just as in the regular wave program.

The reasons for making an essentially two step process into three steps are: a) memory requirements for Step 2 are approaching that available, and b) a significant increase in flexibility is achieved. The increase in flexibility is because the output of Step 1 is an ASCII file which defines the specturm shape numerically. This file may be created by hand so that any half-way reasonable spectrum shape may be specified (for example analytical spectra not built into the program to be described, or observed spectra).

Three programs, SPTGEN, RANGEN, and RANWAV constitute the system. Source and SAV versions are on Disk 19.

SPTGEN

This program automates the first step of the process and eliminates the hand generation of files containing numerically defined spectra so ong as what is wanted is a spectrum having one of the following five analytical forms:

1. A Exp $[-B/\omega^4]/\omega^5$ (ITTC, ISSC, Pierson-Moskowitz, Bretschneider, etc.)
2. JONSWAP
3. NEUMANN
4. A Exp $[-B/\omega^4]/\omega^6$ (Voznesenski-Netsvetayev; the form used in the USSR.)
5. A band pass filter form, which, with reasonable selection of bandwidth, should simulate swell.

The program will in addition superimpose any two of the above forms to create "sea and swell" spectra. The details of each spectral form are built into a subroutine library, SPCTLB in such a way that the addition of new analytical forms should not be a difficult job.

RANGEN

This program automates Step 2 of the process using the FFT fast convolution technique. Required input besides the spectrum form file is the tank water depth, the desired flap apportionment scheme, and the random sample number. Since each sample produces 2 minutes of simulation, there is the theoretical possibility of about 18 hours of statistically independent time history realizations for each spectral form. Generation of the program requires about 3 minutes of computation.

RANWAV

This program is the run-time step. Once the program file is specified and the contents of the file are documented, the program asks for a significant height. Making the non-linear corrections to required angles to get to actuator positions and D/A bits requires about 1 2/3 minutes of computation. Once this is done, loading and running sequences for any starting point, or repeating runs takes no appreciable time.

APPENDIX E
NUMERICAL MODEL OF A NONLINEAR RANDOM SEAWAY

by
John F. Dalzell

Introduction

The basic objective of Task 3 of the present work was to see if the trends in half-cycle counts of the maxima of observed severe wave time histories could be quantitatively and/or qualitatively represented by a functional model of the second degree; that is, by a second order mathematical model. The purpose of this Appendix is to summarize the mathematical background and procedures which were utilized in order to arrive at the second order model described in Section 6 of the report.

Prior Work

The basic formulation of a wave field as a modified functional polynomial of the second degree is due to Hasselmann[21]*, and an early, if not first, utilization of this formulation in the simulation of nonlinear wave time series was by Hineno[22]. The approach used in the present instance is in essence that of Hineno[22], though some elements are derived from the somewhat more general derivation of Dalzell[23].

The general wave field model includes spatial as well as time dependence for the short-crested case. If $\bar{\mathcal{X}}$ denotes a position vector and t denotes time, the true wave field to second order, $\zeta_T(\bar{\mathcal{X}},t)$, is written as the sum of two terms:

$$\zeta_T(\bar{\mathcal{X}},t) = \zeta_1(\bar{\mathcal{X}},t) + \zeta_2(\bar{\mathcal{X}},t),$$

where $\zeta_1(\bar{\mathcal{X}},t)$ is a first order (linear) field which may be short-crested, and $\zeta_2(\bar{\mathcal{X}},t)$ is a second order contribution. The form of Hasselmann's[21] functional formulation of the nonlinear wave field to second order arises from the properties of the second order Stokes expansion of progressive gravity waves. Broadly, what happens in the second order Stokes expansion is that all the second order nonlinearities in the wave field arise from self interactions and interactions between pairs of first order wave components. Thus, if the first order components are specified, the second order components may be derived. The relationship between the first and second order components of the field is a rather complicated space-time convolution, and is given in Dalzell[23].

Simplifying Assumptions

The ultimate comparisons of interest were to be with wave time histories observed at one fixed point as a function of time. Thus, nothing was to be gained by simulating the spatial "field", especially as setting $\bar{\mathcal{X}} = 0$ greatly simplifies matters. Within the general formulation, if a short crested simulation is desired, a first estimate at least of the directional spread of the variance spectrum of the observations is required in order to define $\zeta_1(\bar{\mathcal{X}},t)$ as an essential prerequisite to the determination of $\zeta_2(\bar{\mathcal{X}},t)$. For the wave data of interest we do not know the directional spread. There consequently seemed no point in attempting a short-crested simulation in the present exploratory project. Finally, there is a considerable simplification of the results of hydrodynamic theory if mathematically deep water is assumed.

To summarize the principal simplifying assumptions, the simulation was assumed to be for the wave elevations at a fixed point of a long-crested, deep water random wave system. It might

* References appear on page 71

be noted that the target full scale wave data finally adopted is not too likely to have been exactly long-crested or free from the influence of finite water depth. The simplifications were accepted for a first approximation because they have the beneficial effect of making the final functional model almost the same as that discussed in Appendix B.

Second Order Wave-wave Interaction Theory

The second order wave-wave interaction theory of interest here may be derived from the theory by Longuet-Higgins[24], summarized in Dalzell[23]. To first order, the potential solutions for small amplitude gravity waves superimpose. The waves propagate independently and without interaction — this is one of the primary assumptions in contemporary seakeeping practice. To second order the waves interact, and the interaction produces a small, bounded modification to the wave motion. To define these nonlinear modifications it is sufficient to consider the interactions between pairs of waves. Thus, the theory postulates two first order harmonic gravity waves propagating in arbitrary directions. By means of a systematic perturbation analysis, a solution for the total velocity potential (correct to second order for deep water) is obtained, and this result in turn determines the wave elevations (correct to second order) corresponding to an assumed pair of first order wave trains.

The results pertinent to the present work were specialized from those presented in Dalzell[23]. In particular, two first order deep water harmonic waves of different wave frequencies, σ_1 and σ_2, are assumed to propagate in the same direction in an earth fixed coordinate system. If the elevations are evaluated at the origin of the coordinate system, the superimposed first order waves may be represented by:

$$\tilde{\zeta}_1(t) = a_1 \cos(\epsilon_1 - \sigma_1 t) + a_2 \cos(\epsilon_2 - \sigma_2 t)\,, \qquad (E.1)$$

where a_1 and a_2 are arbitrary amplitudes, and the ϵ_j are arbitrary phases.

The result for the total wave elevation to second order given in Dalzell[23] may easily be specialized to the corresponding total wave elevation at the origin, $\tilde{\zeta}_T(t)$, for the deep-water, long-crested case, with the following result:

$$\begin{aligned}\tilde{\zeta}_T(t) = {} & a_1 \cos(\epsilon_1 - \sigma_1 t) + a_2 \cos(\epsilon_2 - \sigma_2 t) \\ & + a_1^2 \frac{\sigma_1^2}{2g} \cos(2\epsilon_1 - 2\sigma_1 t) + a_2^2 \frac{\sigma_2^2}{2g} \cos(2\epsilon_2 - 2\sigma_2 t) \\ & + a_1 a_2 \frac{(\sigma_1^2 + \sigma_2^2)}{2g} \cos(\epsilon_1 + \epsilon_2 - \{\sigma_1 + \sigma_2\} t) \\ & - a_1 a_2 \frac{|\sigma_1^2 - \sigma_2^2|}{2g} \cos(\epsilon_1 - \epsilon_2 - \{\sigma_1 - \sigma_2\} t)\,, \end{aligned} \qquad (E.2)$$

where only the gravitational constant, g, is a new parameter.

An important thing to note about Equation E.2 is that the first two terms on the right hand side are identical to the right hand side of the assumed first order waves, Equation E.1. The last four terms on the right hand side are the second order "corrections", and involve second harmonics of the input wave frequencies as well as sum and difference frequencies. If the result is viewed in the context of input-output theory, the input, Equation E.1, appears in the output unchanged; that is, the only determiner of the amplitudes of the components of frequencies σ_1 and σ_2 is the assumed first order wave "input".

Functional Polynomial Expansion

The form of Equation E.2, which results from the physics of the problem, is that of the response of a degree two functional polynomial to dual frequency excitation. This similarity suggests the expansion of the "true" wave elevations as a Volterra functional series in the first order wave elevation, which may be written:

$$\zeta_T(t) = g_0 + \sum_{j=1}^{\infty} \left[\int \cdots \int g_j(\tau_1, \ldots \tau_j)\, \zeta_1(t-\tau_1) \ldots \zeta_1(t-\tau_j)\, d\tau_1 \ldots d\tau_j \right] , \qquad (E.3)$$

where the various kernels are not yet defined. The series is truncated at both ends on physical grounds. First, there can be no "true" wave in the absence of first order waves, so that g_0 is set equal to zero. Next, the present problem involves only second order corrections to the first order waves, and with the encouragement of the last section, all terms resulting from $j > 2$ in Equation E.3 are dropped. The result is a functional polynomial containing only linear and quadratic terms:

$$\zeta_T(t) = \int g_1(\tau_1)\, \zeta_1(t-\tau_1)\, d\tau_1 + \int \int g_2(\tau_1, \tau_2)\, \zeta_1(t-\tau_1)\, \zeta_1(t-\tau_2)\, d\tau_1\, d\tau_2 . \qquad (E.4)$$

To use the model in a simulation, the linear and quadratic impulse responses, $g_1(\tau)$, and $g_2(\tau_1, \tau_2)$, must be obtained. The strategy employed is similar to that discussed in Appendix B; that is, to first obtain the corresponding linear and quadratic frequency responses, $G_1(\omega)$ and $G_2(\omega_1, \omega_2)$, and then employ the inverse Fourier transform, Equation B.3, to derive the impulse responses.

The frequency responses are conveniently identified from the theoretical result for the output, $\zeta_T(t)$, when the input, $\zeta_1(t)$, is composed of two harmonic waves. In particular, set

$$\tilde{\zeta}_1(t) = a_1 \cos(\epsilon_1 - \omega_1 t) + a_2 \cos(\epsilon_2 - \omega_2 t) , \qquad (E.5)$$

where the only difference between Equations E.5 and E.1 is the ω_j notation for wave frequency. Then the resulting output, $\tilde{\zeta}_T(t)$ becomes Dalzell[3]:

$$\begin{aligned}
\tilde{\zeta}_T(t) = {} & a_1\, \Re e\{G_1^*(\omega_1) \exp[i\epsilon_1 - i\omega_1 t]\} + a_2\, \Re e\{G_1^*(\omega_2) \exp[i\epsilon_2 - i\omega_2 t]\} \\
& + \frac{1}{2} a_1^2\, G_2(\omega_1, -\omega_1) + \frac{1}{2} a_2^2\, G_2(\omega_2, -\omega_2) \\
& + \frac{1}{2} a_1^2\, \Re e\{G_2^*(\omega_1, \omega_1) \exp[i2\epsilon_1 - i2\omega_1 t]\} + \frac{1}{2} a_2^2\, \Re e\{G_2^*(\omega_2, \omega_2) \exp[i2\epsilon_2 - i2\omega_2 t]\} \\
& + a_1 a_2\, \Re e\{G_2^*(\omega_1, \omega_2) \exp[i(\epsilon_1 + \epsilon_2) - i(\omega_1 + \omega_2)t]\} \\
& + a_1 a_2\, \Re e\{G_2^*(\omega_1, -\omega_2) \exp[i(\epsilon_1 - \epsilon_2) - i(\omega_1 - \omega_2)t]\}
\end{aligned} \qquad (E.6)$$

where the general frequency response functions are complex, the asterisks denote complex conjugates, and the frequency domain extends to negative frequencies.

Frequency Response Functions for the Simulation

For the present problem the required frequency response functions are obtained by comparing the general Equation E.6 with the similar equation which defines the physics, Equation E.2 . The "σ" notation was used for wave frequencies in Equations E.1 and E.2 because essentially positive wave frequencies enter the physical problem. The "ω" notation for frequencies in Equation E.5

and E.6 is used because the frequency domain required by the Fourier transform pairs, Equation B.3, is symmetric about zero frequency. However, for purposes of interpreting Equations E.5 and E.6 the σ_j's and ω_j's may be considered equal. The absence of "sin(...)" terms in Equation E.2 requires that the frequency response functions for the present problem be purely real. With this observation it is clear from a comparison of the first two terms in Equations E.2 and E.6 that $G_1(\omega)$ must be unity. It is also clear that $G_2(\omega_1,\omega_2)$ will be proportional to sums and differences of the squares of wave frequency. As far as the overall simulation strategy is concerned, this last produces a potentially serious problem, which is, that as either or both wave frequencies tend to ∞, the value of the quadratic frequency response function will also. Under such circumstances the required Fourier transform can not be calculated numerically.

The problem just noted is gotten around by redefining the system in such a way that the required Fourier transforms can be carried out. It is useful to summarize the polynomial model of Equation E.4 in a simple input-output diagram, Figure E.1, in which the "true" or corrected wave elevation, $\zeta_t(t)$, results from a linear and quadratic transformation of the "input" or first order wave elevation, $\zeta_1(t)$.

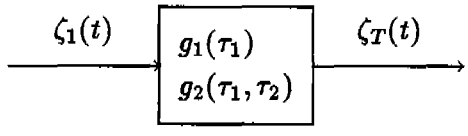

Figure E.1 Input-Output Diagram

In order to proceed, a linear "window" is inserted between the input, $\zeta_1(t)$, and the linear plus quadratic physical system. The relationships are summarized in a cascade diagram, Figure E.2, in which the "window" transformation $f_1(\tau)$, produces an intermediate function, $\zeta_{1W}(t)$, which is then input to the physical system now denoted by linear and quadratic impulse response functions, $h_1(\tau_1)$ and $h_2(\tau_1,\tau_2)$.

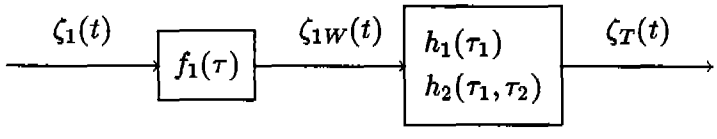

Figure E.2 Cascade Diagram

Now if the cascaded system of Figure E.2 is excited by a dual harmonic wave system, the resulting expression for $\tilde{\zeta}_T(t)$ is the same as Equation E.6 with the linear and quadratic frequency response functions replaced by:

$$\begin{aligned} G_1(\omega_1) &= H_1(\omega_1)\,F_1(\omega_1) \\ G_2(\omega_1,\omega_2) &= H_2(\omega_1,\omega_2)\,F_1(\omega_1)\,F_1(\omega_2)\,. \end{aligned} \qquad (E.7)$$

where $F_1(\omega_1)$,$H_1(\omega_1)$, and $H_2(\omega_1,\omega_2)$ are the frequency response functions corresponding to the impulse responses indicated in Figure E.2. Since the "window" transformation is an analytical artifice, $F_1(\omega)$ will be assumed real.

The input to the physical problem, Equation E.1, was not "windowed" in any way, so that by assuming $F_1(\omega)$ to be unity in Equation E.6 as modified by Equation E.7, the linear and quadratic

frequency responses relating first order wave input and the corrected wave may be identified:

$$
\begin{aligned}
G_1(\omega_1) &= F_1(\omega_1) \\
G_2(\omega_1,\omega_2) &= \frac{(\omega_1^2+\omega_2^2)}{2g} F_1(\omega_1) F_1(\omega_2) && \text{If the signs of } \omega_1 \text{ and } \omega_2 \text{ are the same,} \\
&= -\frac{|\omega_1^2-\omega_2^2|}{2g} F_1(\omega_1) F_1(\omega_2) && \text{If the signs of } \omega_1 \text{ and } \omega_2 \text{ are different,} \\
&= 0 && \text{If either } \omega_1 \text{ or } \omega_2 \text{ is zero.} \qquad (E.8)
\end{aligned}
$$

The explicit functions of ω_j in Equation E.8 arise from the physical wave-wave interaction problem. As noted, the window function is an analytical artifice which has so-far been assumed only to be real. A choice of window frequency response function useful for the present simulation is shown in Figure E.3. The function, $F_1(\omega)$, is assumed to be real and symmetric about $\omega = 0$ as is required by the Fourier transform conventions. For frequencies between $-\omega_I$ and ω_I it is taken to be unity. For $|\omega| > \omega_{II}$ it is exactly zero, and in-between the breakpoints a linear variation is assumed. With $F_1(\omega)$ defined in this way, the frequency response functions defined by Equation E.8 are different from zero in a finite domain of frequency, and thus the required Fourier inversion may be carried out without trouble. What this window does is allow the physical wave-wave interactions to work as theoretically required only for interactions involving frequencies whose absolute values are less than ω_I. If the first order wave input is band limited, and the maximum frequency in the band is well below ω_I, the window will have no influence upon the the validity of a simulation of $\zeta_T(t)$ because the window will distort the first order wave elevations only at frequencies where there is no energy present in the first place. Similarly, under this circumstance the wave-wave interactions will be valid according to the physical theory for all interactions involving non-zero energy — we are not interested in interactions between nonexistent wave components.

Thus if the breakpoints in the window are chosen appropriately, the linear impulse response, $g_1(\tau)$, in Equation E.4 approaches a delta function, and the quadratic impulse response function, $g_2(\tau_1,\tau_2)$, may be calculated as the (numerical) Fourier transform of the second of Equations E.8. The effect is that the time domain model for the simulation of $\zeta_T(t)$ becomes:

$$\zeta_T(t) \Rightarrow \zeta_1(t) + \int\int g_2(\tau_1,\tau_2)\,\zeta_1(t-\tau_1)\,\zeta_1(t-\tau_2)\,d\tau_1\,d\tau_2\,, \qquad (E.9)$$

which is the same as Hasselmann's theoretical model[21].

Determination of "First Order" Wave Spectra

An arbitrary observed wave variance spectrum is what was to be simulated in the present work. The preceeding sections indicate that the first ingredient in the required simulation is a time domain simulation of the "first order" wave elevations, $\zeta_1(t)$. To accomplish this in the conventional way it is necessary to have an estimate of the variance spectrum of the "first order" component of the observation.

Specializing some results in Dalzell[3], the functional polynomial model for the wave elevations, Equation E.9, implies that the "true" wave variance spectrum corrected for second order wave-wave interactions, $S_T(\omega)$, is related to the spectrum of the first order component, $S_1(\omega)$, as follows:

$$S_T(\omega) = S_1(\omega) + \int_0^\infty \left|G_2[(\omega-v)/2\,,(\omega+v)/2]\right|^2 S_1(|\omega-v|/2)\,S_1(|\omega+v|/2)\,dv\,, \qquad E.10)$$

where the quadratic frequency response function is defined in the second of Equations E.8. If the significant nonlinearities in a given wave observation are second order, and the simplifying assumptions noted earlier in this Appendix are in order, Equation E.10 defines the variance spectrum which would be observed.

There is a clear problem if the spectrum of the first order component , $S_1(\omega)$, is solved for in a "nice" way. For the present exploratory investigation solving the problem "nicely" did not seem worth the effort, and a "dirty" trial and error solution was attempted. Equation E.10 was programmed to combine the selected quadratic frequency response function with an assumed numerical definition of $S_1(\omega)$. With this tool a semi-manual iteration was carried out in which assumed $S_1(\omega)$'s were successively modified until $S_T(\omega)$ as computed by Equation E.10 agreed reasonably well with the observed spectrum to be simulated.

For the present work the wave spectrum observed for "Hurricane Camille, 1500-1530 hours", as given in Section 5.0 was adopted as the target for the simulation. As matters turned out the procedure just outlined was not too time consuming because the quadratic contribution to the total mostly influences the high frequency tail of the observed spectrum. Figure E.4 compares the observed target spectrum with the approximated linear (first order) spectrum, $S_1(\omega)$, and the linear plus quadratic ("true") spectrum, $S_T(\omega)$, on the conventional linear scales. Figure E.5 shows the same results on a semi-log basis. For practical purposes, this exercise was almost not necessary except to show that the quadratic component contributes a relatively insignificant amount to the high frequency tail of the spectrum. In the semi-log plot, Figure E.5, above $\omega \approx 1.5$, the correspondence between observation and $S_T(\omega)$ is poor. However, the significance of the full scale observation in the high frequency range is influenced by quite a number of extraneous things — it is suspected that the truth could be almost any small number in the high frequency range.

Numerical Simulation Details

The first of the details of the numerical simulation was to define the window frequency response, $F_1(\omega)$. Inspection of the observed Camille spectrum, Figure E.4, indicates no appreciable or believable energy content above a frequency of about 1.5 radians/second. Accordingly, the window breakpoints were set at $\omega_I = 3.$ radians/second and $\omega_{II} = 6.$ radians/second. (These values were also used in the development of the first order spectrum discussed in the last section.) Once this selection is made, the quadratic frequency response function of Equation E.8 is defined, and the Fourier transform defined by Equation B.3 may be carried out numerically so as to generate a numerically defined impulse response, $g_2(\tau_1, \tau_2)$. As in the work summarized in Appendix B, the time domain simulation equation (Equation E.9 in this case) is turned into a summation, so that the impulse response "function" must be evaluated at uniform intervals of τ_1 and τ_2. For the present simulation an interval, $\Delta\tau$, of 0.25 seconds adequately defined the impulse response.

The starting point of the simulation of the first order wave time series was the numerically defined first order ("linear") wave spectrum, $S_1(\omega)$, shown in Figures E.4 and E.5. The simulation method employed is often called "fast convolution". In this recipe a time series containing band limited white Gaussian noise is first generated. The complex FFT spectrum of the noise is then computed. A non-realizable frequency domain filter corresponding to the desired variance spectrum is formed by simply square-rooting the spectrum, and this is applied to the FFT noise spectrum to produce a complex FFT spectrum of the process. The final step is an FFT inverse transform, which produces a time series realization of the desired process.

The time series simulations of $\zeta_1(t)$ were generated in "handy size" realizations of about 1000 seconds duration at a Δt of 0.25 seconds to conform to the evaluation interval of the quadratic impulse response function. Ten such statistically independent realizations were generated in order

to achieve a data base containing about as many half-cycles as were involved in the simulations described in Appendix B.

Once the convolutions were carried out and the time series results inspected it became clear that a Δt of 0.25 seconds was not really required to resolve the data, and for convenience in the subsequent processing the time series were decimated by retaining every other point. As in the simulations of Appendix B, the first and second order components of the simulated $\zeta_T(t)$ were stored separately.

One of the important things to do in qualifying the final realizations was to compute the mean variance spectrum and compare with the original full scale observation. This was done and the results are shown in Figure E.6. In the Figure $S_T(\omega)$ is the "Spectrum of Simulation" of the legend. The analysis was done by frequency smoothing an FFT spectrum of each realization, and then averaging over the ten-realization ensemble. The frequency spacing of the result is nearly the same as that of the full-scale observation. The results shown for the simulation involve spectral density estimates with 160 degrees of freedom each — which translates to 90% confidence bounds on the spectral estimates of plus 21% and minus 16%. Thus the agreement between the original and the simulated spectra is acceptable. The ten-sample "wave" elevation variance was computed as 104.1 Ft^2, with a 90% confidence interval of $\pm 6\%$.

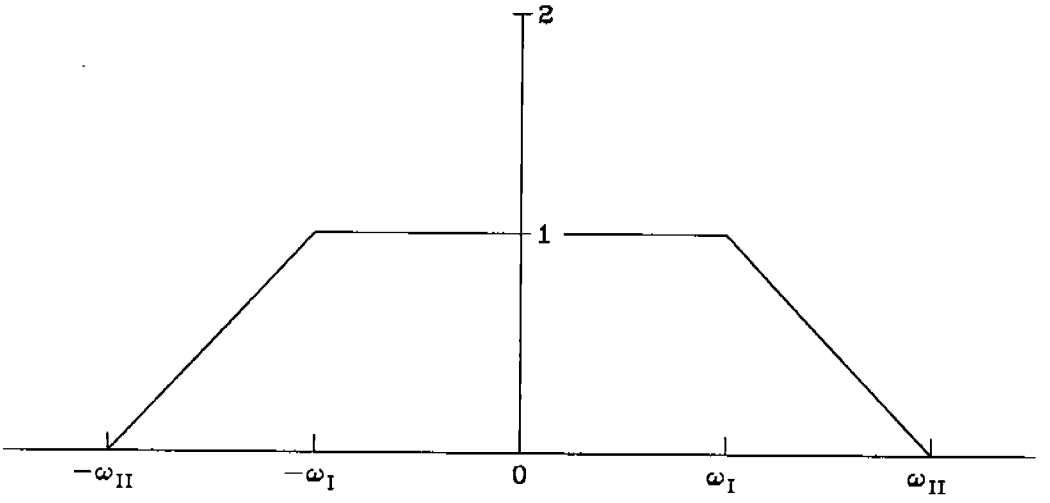

FIGURE C.3 WINDOW FREQUENCY RESPONSE FUNCTION, $F_1(\omega)$

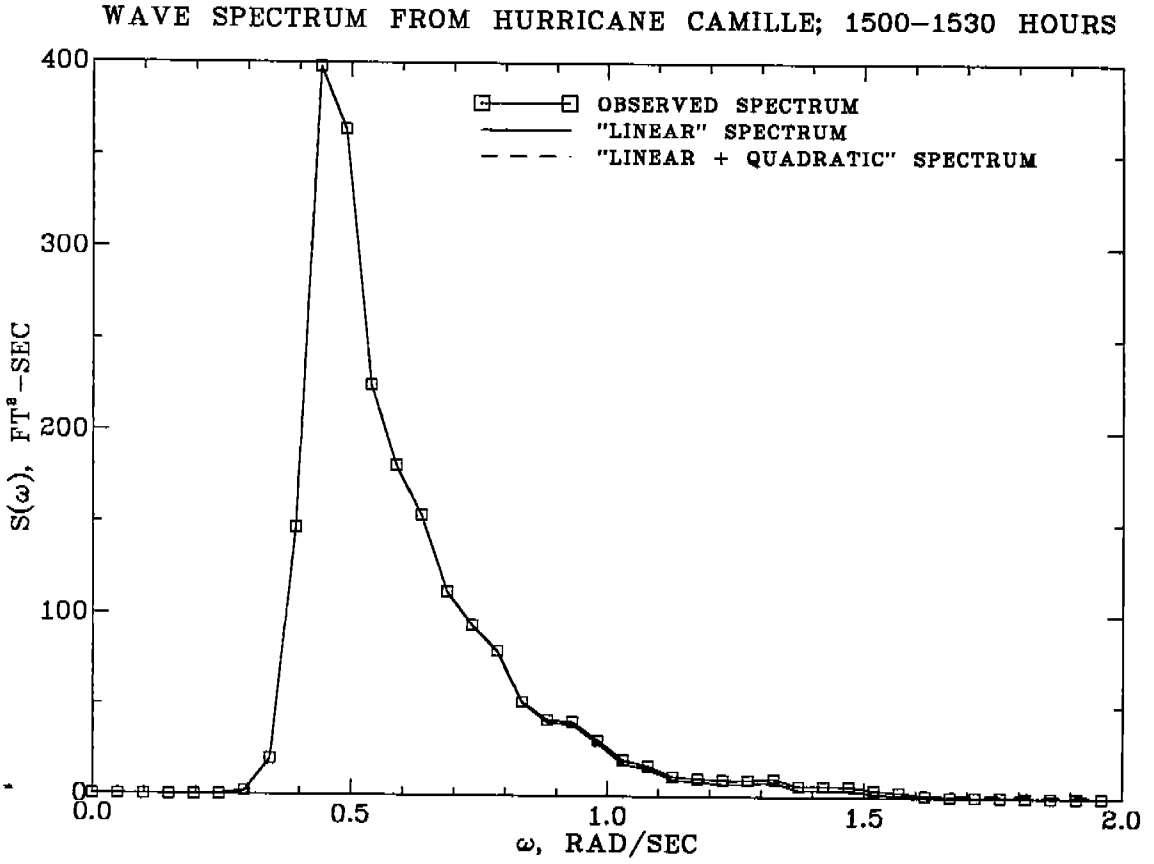

FIGURE C.4 "OBSERVED", "LINEAR" AND "LINEAR PLUS QUADRATIC" SPECTRA

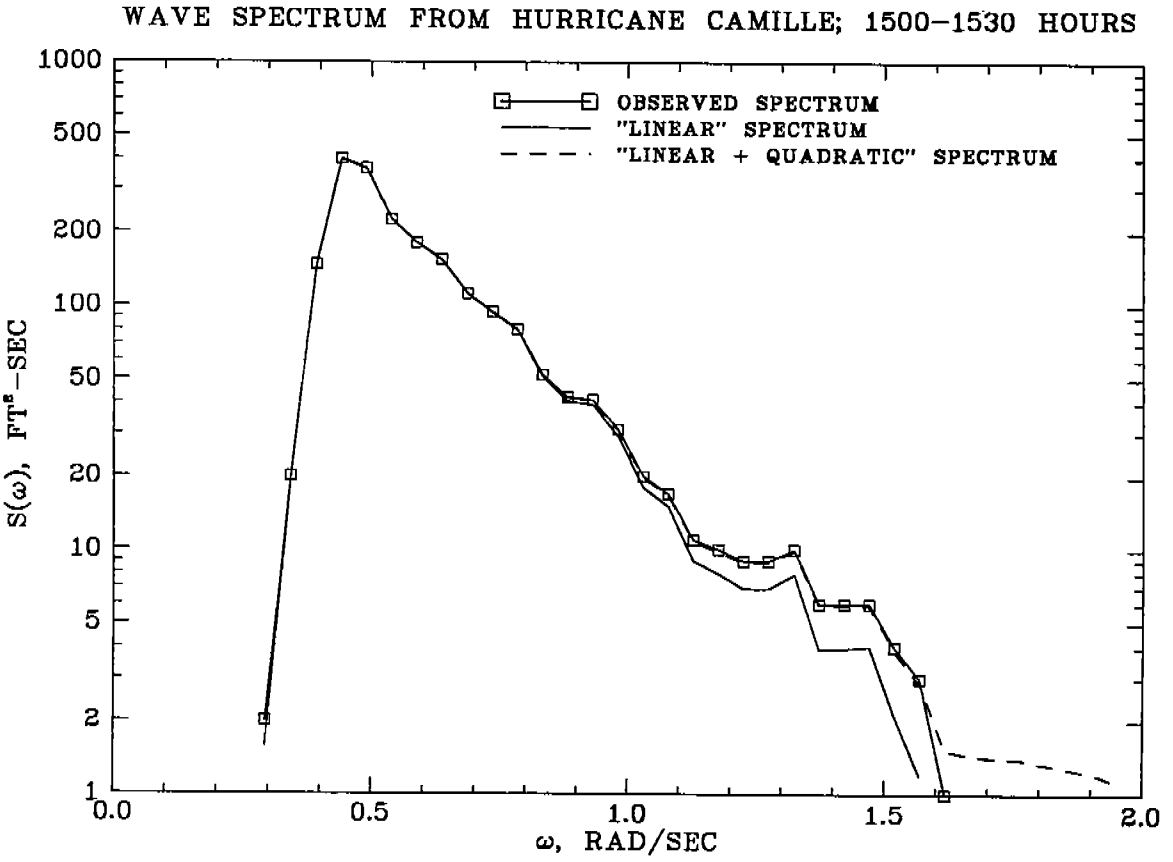

FIGURE C.5 "OBSERVED", "LINEAR" AND "LINEAR PLUS QUADRATIC" SPECTRA

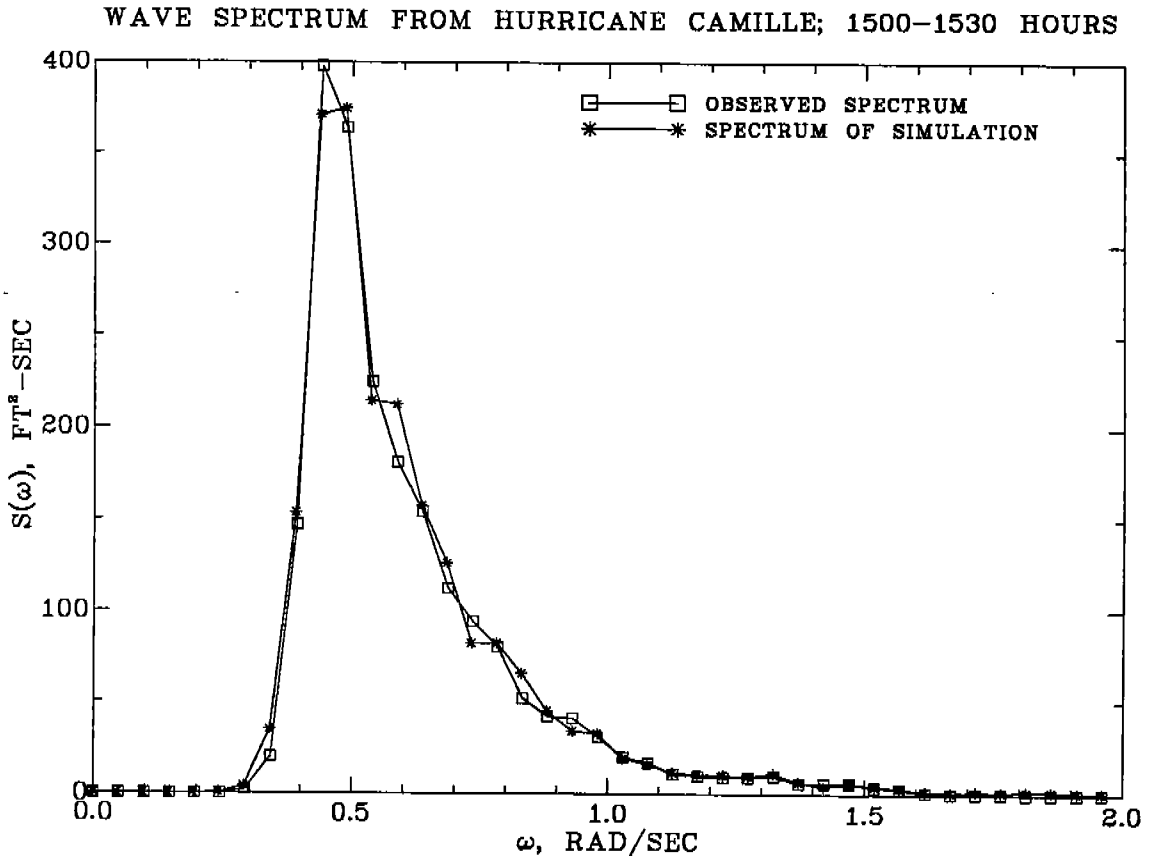

FIGURE C.6 COMPARISON OF SPECTRA OF SIMULATION AND OBSERVATION

COMMITTEE ON MARINE STRUCTURES

Commission on Engineering and Technical Systems

National Academy of Sciences - National Research Council

The COMMITTEE ON MARINE STRUCTURES has technical cognizance over the interagency Ship Structure Committee's research program.

Stanley G. Stiansen (Chairman), Riverhead, NY
Mark Y. Berman, Amoco Production Company, Tulsa, OK
Peter A. Gale, Webb Institute of Naval Architecture, Glen Cove, NY
Rolf D. Glasfeld, General Dynamics Corporation, Groton, CT
William H. Hartt, Florida Atlantic University, Boca Raton, FL
Paul H. Wirsching, University of Arizona, Tucson, AZ
Alexander B. Stavovy, National Research Council, Washington, DC
Michael K. Parmelee, Ship Structure Committee, Washington, DC

LOADS WORK GROUP

Paul H. Wirsching (Chairman), University of Arizona, Tucson, AZ
Subrata K. Chakrabarti, Chicago Bridge and Iron Company, Plainfield, IL
Keith D. Hjelmstad, University of Illinois, Urbana, IL
Hsien Yun Jan, Martech Incorporated, Neshanic Station, NJ
Jack Y. K. Lou, Texas A & M University, College Station, TX
Naresh Maniar, M. Rosenblatt & Son, Incorporated, New York, NY
Solomon C. S. Yim, Oregon State University, Corvallis, OR

MATERIALS WORK GROUP

William H. Hartt (Chairman), Florida Atlantic University, Boca Raton, FL
Fereshteh Ebrahimi, University of Florida, Gainesville, FL
Santiago Ibarra, Jr., Amoco Corporation, Naperville, IL
Paul A. Lagace, Massachusetts Institute of Technology, Cambridge, MA
John Landes, University of Tennessee, Knoxville, TN
Mamdouh M. Salama, Conoco Incorporated, Ponca City, OK
James M. Sawhill, Jr., Newport News Shipbuilding, Newport News, VA

SHIP STRUCTURE COMMITTEE PUBLICATIONS

SSC-338 Fatigue Prediction Analysis Validation from SL-7 Hatch Corner Strain Data by Jen-Wen Chiou and Yung-Kuang Chen 1985

SSC-339 Ice Loads and Ship Response to Ice - A Second Season by C. Daley, J. W. St. John, R. Brown, J. Meyer, and I. Glen 1990

SSC-340 Ice Forces and Ship Response to Ice - Consolidation Report by C. Daley, J. W. St. John, R. Brown, and I. Glen 1990

SSC-341 Global Ice Forces and Ship Response to Ice by P. Minnick, J. W. St. John, B. Cowper, and M. Edgecomb 1990

SSC-342 Global Ice Forces and Ship Response to Ice - Analysis of Ice Ramming Forces by Yung-Kuang Chen, Alfred L. Tunik, and Albert P-Y Chen 1990

SSC-343 Global Ice Forces and Ship Response to Ice - A Second Season by P. Minnick and J. W. St. John 1990

SSC-344 Development of an Onboard Strain Recorder by Eric Greene and William A. Wood 1987

SSC-345 Elastic-Plastic Fracture Mechanics by T. L. Anderson 1990

SSC-346 Fatigue Characterization of Fabricated Ship Details - Phase 2 by K. K. Park and F. V. Lawrence, Jr. 1988

SSC-347 Strategies for Nonlinear Analysis of Marine Structures by Subrata K. Chakrabarti 1988

SSC-348 Corrosion Experience Data Requirements by Karl A. Stambaugh and John C. Knecht 1988

SSC-349 Development of a Generalized Onboard Response Monitoring System (Phase I) by F. W. DeBord, Jr. and B. Hennessy 1987

SSC-350 Ship Vibration Design Guide by Edward F. Noonan 1989

SSC-351 An Introduction to Structural Reliability Theory by Alaa E. Mansour 1990

SSC-352 Marine Structural Steel Toughness Data Bank by J. G. Kaufman and M. Prager 1990

None Ship Structure Committee Publications - A Special Bibliography 1983